N-I/28091--061

Pahute Mesa Well Development and Testing Analyses for Wells ER-20-8 and ER-20-4, Nevada National Security Site, Nye County, Nevada

Final

Revision No.: 0

September 2012

Prepared for U.S. Department of Energy under Contract No. DE-AC52-09NA28091.

Approved for public release; further dissemination unlimited.

Available for sale to the public from:

U.S. Department of Commerce
National Technical Information Service
5301 Shawnee Road
Alexandria, VA 22312
Telephone: 800.553.6847
Fax: 703.605.6900
E-mail: *orders@ntis.gov*
Online Ordering: *http://www.ntis.gov/help/ordermethods.aspx*

Available electronically at *http://www.osti.gov/bridge*

Available for a processing fee to U.S. Department of Energy and its contractors, in paper, from:

U.S. Department of Energy
Office of Scientific and Technical Information
P.O. Box 62
Oak Ridge, TN 37831-0062
Phone: 865.576.8401
Fax: 865.576.5728
Email: *reports@adonis.osti.gov*

Reference herein to any specific commercial product, process, or service by trade name, trademark, manufacturer, or otherwise, does not necessarily constitute or imply its endorsement, recommendation, or favoring by the United States Government or any agency thereof or its contractors or subcontractors.

N-I/28091--061

Navarro-Intera

PAHUTE MESA WELL DEVELOPMENT AND TESTING ANALYSES FOR WELLS ER-20-8 AND ER-20-4, NEVADA NATIONAL SECURITY SITE, NYE COUNTY, NEVADA

Final
Revision No.: 0
September 2012
Navarro-Intera, LLC
c/o U.S. DOE
P.O. Box 98952
Las Vegas, NV 89193-8952

Reviewed and determined to be UNCLASSIFIED.
Derivative Classifier: Joseph P. Johnston/N-I CO
(Name/personal identifier and position title)
Signature: /s/ Joseph P. Johnston
Date: 9/26/2012

Prepared for U.S. Department of Energy under Contract No. DE-AC52-09NA28091.

Approved for public release; further dissemination unlimited.

PAHUTE MESA WELL DEVELOPMENT AND TESTING ANALYSES FOR WELLS ER-20-8 AND ER-20-4, NEVADA NATIONAL SECURITY SITE, NYE COUNTY, NEVADA

Approved by: /S/ Sam Marutzky Date: 9-20-12

Sam Marutzky, UGTA Project Manager
Navarro-Intera, LLC

TABLE OF CONTENTS

TABLE OF CONTENTS (CONTINUED)

LIST OF FIGURES

LIST OF FIGURES (CONTINUED)

LIST OF FIGURES (CONTINUED)

LIST OF FIGURES (CONTINUED)

LIST OF TABLES

LIST OF ACRONYMS AND ABBREVIATIONS

General Acronyms and Abbreviations

Al	Aluminum
Am	Americium
amsl	Above mean sea level
Ba	Barium
bgs	Below ground surface
BN	Bechtel Nevada
Br	Bromide
C	Carbon
Ca	Calcium
$CaCO_3$	Calcium carbonate
CAIP	Corrective action investigation plan
CAU	Corrective action unit
CD-ROM	Compact disc-read only memory
Cl	Chlorine
CO_3	Carbonate
Cs	Cesium
CS	Carbon steel
D	Deuterium
day/ft^2	Days per square foot
DO	Dissolved oxygen
DOE	U.S. Department of Energy
DRI	Desert Research Institute
EPA	U.S. Environmental Protection Agency
ER	Environmental restoration
ET	Earth tide
Eu	Europium
F	Fluorine
FFACO	*Federal Facility Agreement and Consent Order*
ft	Foot
ft/day	Feet per day
ft/min	Feet per minute
ft^2/day	Square feet per day
FY	Fiscal year
gal	Gallon

LIST OF ACRONYMS AND ABBREVIATIONS (CONTINUED)

GMWL	Global meteoric water line
gpm	Gallons per minute
H	Hydrogen
HCO_3	Bicarbonate
HFM	Hydrostratigraphic framework model
Ho	Holmium
HSU	Hydrostratigraphic unit
I	Iodine
in.	Inch
K	Potassium
LANL	Los Alamos National Laboratory
LiBr	Lithium bromide
LLNL	Lawrence Livermore National Laboratory
LMWL	Local meteoric water line
LTWLM	Long-term water-level monitoring
m	Meter
m^2	Square meter
m^2/s^2	Square meters per square second
m/day	Meters per day
MCL	Maximum contaminant level
Mg	Magnesium
mg/L	Milligrams per liter
mmhos/cm	Millimhos per centimeter
Na	Sodium
N/A	Not applicable
NAD	North American Datum
Nb	Niobium
ND	Not detected
NDEP	Nevada Division of Environmental Protection
N-I	Navarro-Intera, LLC
NNES	Navarro Nevada Environmental Services, LLC
NNSA/NSO	U.S. Department of Energy, National Nuclear Security Administration Nevada Site Office
NNSS	Nevada National Security Site
Np	Neptunium
NSPC	Nevada State Plane Coordinate
NSTec	National Security Technologies, LLC

LIST OF ACRONYMS AND ABBREVIATIONS (CONTINUED)

NTU	Nephelometric turbidity unit
O	Oxygen
pCi/L	Picocuries per liter
PM	Pahute Mesa
pmc	Percent modern carbon
psia	Pounds per square inch absolute
PST	Pacific Standard Time
Pu	Plutonium
PXD	Pressure transducer
QC	Quality control
RPS	Revolutions per second
S	Sulfur
SEC	Specific electrical conductivity
Sn	Tin
SO_4	Sulfate
Sr	Strontium
S_S	Specific storage
SS	Stainless steel
SWL	Static water level
Tc	Technetium
TD	Total depth
Th	Thorium
TiO_2	Titanium dioxide
UDI	United Drilling, Inc.
UGTA	Underground Test Area
USGS	U.S. Geological Survey
UTC	Coordinated Universal Time
UTM	Universal Transverse Mercator
WDT	Well development and testing
WL	Water level
Zr	Zirconium
°C	Degrees Celsius
°F	Degrees Fahrenheit
%meq/L	Percent milliequivalents per liter
µg/L	Micrograms per liter

LIST OF ACRONYMS AND ABBREVIATIONS (CONTINUED)

List of Stratigraphic, Geologic, Hydrostratigraphic, and Hydrogeologic Unit Abbreviations and Symbols

AA	Alluvial aquifer
BA	Benham aquifer
BFCU	Bullfrog confining unit
BRA	Belted Range aquifer
CFCM	Crater Flat composite unit
CFCU	Crater Flat confining unit
CHCU	Calico Hills confining unit
CHZCM	Calico Hills zeolitic composite unit
CPA	Comb Peak aquifer
DWT	Densely welded ash-flow tuff
FCCM	Fortymile Canyon composite unit
FCCU	Fortymile Canyon confining unit
IA	Inlet aquifer
LCA	Lower carbonate aquifer
LFA	Lava-flow aquifer
LPCU	Lower Paintbrush confining unit
MPCU	Middle Paintbrush confining unit
MWT	Moderately welded ash-flow tuff
NTMMSZ	Northern Timber Mountain moat structural zone
NWT	Nonwelded ash-flow tuff
PBRCM	Pre-belted range composite unit
PLFA	Paintbrush lava-flow aquifer
PVTA	Paintbrush vitric-tuff aquifer
PWT	Partially welded ash-flow tuff
Qay	Young alluvial deposits
SCCC	Silent Canyon caldera complex
SPA	Scrugham Peak aquifer
SPLFA	Scrugham Peak lava-flow aquifer
TCA	Tiva Canyon aquifer
Tcpj	Tuff of Jorum
Tcps	Rhyolite of Sled
TCU	Tuff confining unit
TCVA	Thirsty Canyon volcanic aquifer
Th	Calico Hills Formation

LIST OF ACRONYMS AND ABBREVIATIONS (CONTINUED)

THCM	Tannenbaum Hill composite unit
THLFA	Tannenbaum Hill lava-flow aquifer
Thp	Mafic-poor Calico Hills formation
TMA	Timber Mountain aquifer
Tmap	Mafic-poor Ammonia Tanks tuff
Tmar	Mafic-rich Ammonia Tanks tuff
Tmat	Rhyolite of Tannenbaum Hill
TMCC	Timber Mountain caldera complex
TMLVTA	Timber Mountain lower vitric-tuff aquifer
Tmrf	Rhyolite of Fluorspar Canyon
Tmrp	Mafic-poor Rainier Mesa tuff
TMWTA	Timber Mountain welded-tuff aquifer
Tp	Paintbrush Group, undivided
Tpb	Rhyolite of Benham
Tpc	Tiva Canyon tuff
Tpcm	Pahute Mesa lobe of Tiva canyon tuff
Tpcy	Tuff of Pinyon Pass
Tpd	Rhyolite of Delirium Canyon
Tpk	Rhyolite of Comb Peak
Tps	Rhyolite of Scrugham Peak
Tpt	Topopah Spring tuff
Tptm	Pahute Mesa lobe of Topopah Spring tuff
TSA	Topopah Spring aquifer
UPCU	Upper Paintbrush confining unit
VTA	Vitric-tuff aquifer
WTA	Welded-tuff aquifer

1.0 INTRODUCTION

In 2009, the *Phase II Corrective Action Investigation Plan* (CAIP) *for Corrective Action Units 101 and 102: Central and Western Pahute Mesa, Nevada Test Site, Nye County, Nevada* (NNSA/NSO, 2009) was published. This plan describes activities governed by the *Federal Facility Agreement and Consent Order* (FFACO) Underground Test Area (UGTA) strategy (FFACO, 1996; as amended 2010) and forms an essential part of corrective action unit (CAU) compliance overseen by the Nevada Division of Environmental Protection (NDEP). Characterization activities described in this plan were initiated for the U.S. Department of Energy (DOE), National Nuclear Security Administration Nevada Site Office's (NNSA/NSO) UGTA Activity.

Wells ER-20-4 and ER-20-8 were drilled during fiscal year (FY) 2009 and FY 2010 (NNSA/NSO, 2011a and b). The closest underground nuclear test detonations to the area of investigation are TYBO (U-20y), BELMONT (U-20as), MOLBO (U-20ag), BENHAM (U-20c), and HOYA (U-20 be) (Figure 1-1). The TYBO, MOLBO, and BENHAM detonations had working points located below the regional water table. The BELMONT and HOYA detonation working points were located just above the water table, and the cavity for these detonations are calculated to extend below the water table (Pawloski et al., 2002). The broad purpose of Wells ER-20-4 and ER-20-8 is to determine the extent of radionuclide-contaminated groundwater, the geologic formations, groundwater geochemistry as an indicator of age and origin, and the water-bearing properties and hydraulic conditions that influence radionuclide migration. Well development and testing is performed to determine the hydraulic properties at the well and between other wells, and to obtain groundwater samples at the well that are representative of the formation at the well. The area location, wells, underground nuclear detonations, and other features are shown in Figure 1-1. Hydrostratigraphic cross sections A-A', B-B', C-C', and D-D' are shown in Figures 1-2 through 1-5, respectively.

A striking feature of the area is its structural complexity. Some faulting is due to Basin-and-Range tectonic activity, and some is due to multiple stages of caldera collapse associated with the coalesced Silent Canyon caldera complex (SCCC) (Warren et al., 2000; BN, 2002). The Northern Timber Mountain moat structural zone (NTMMSZ) has between 1,000 and 2,200 feet (ft) of displacement (Figures 1-3 and 1-5), with other major faults having displacement of hundreds of feet (Figures 1-2

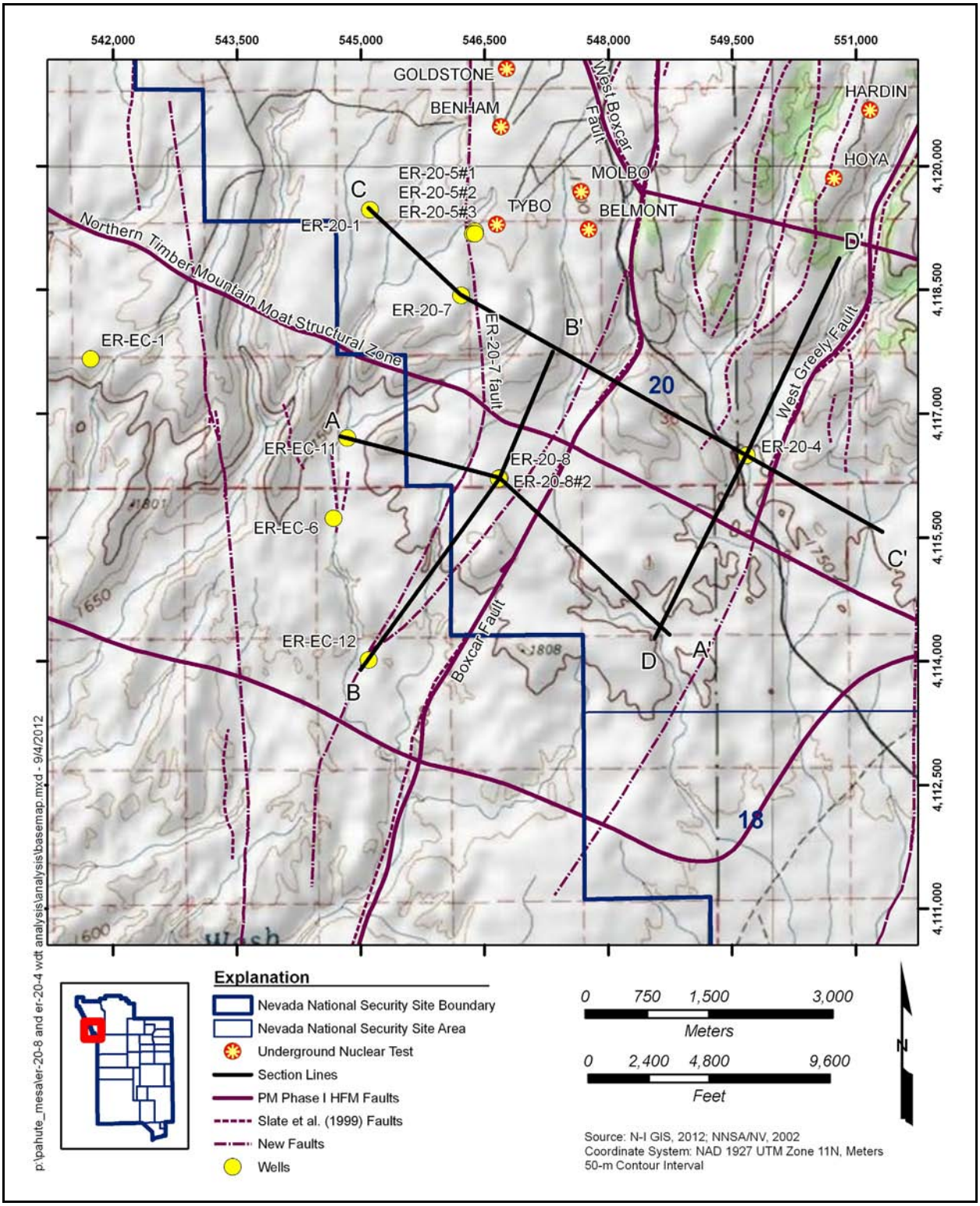

Figure 1-1
Study Area Base Map

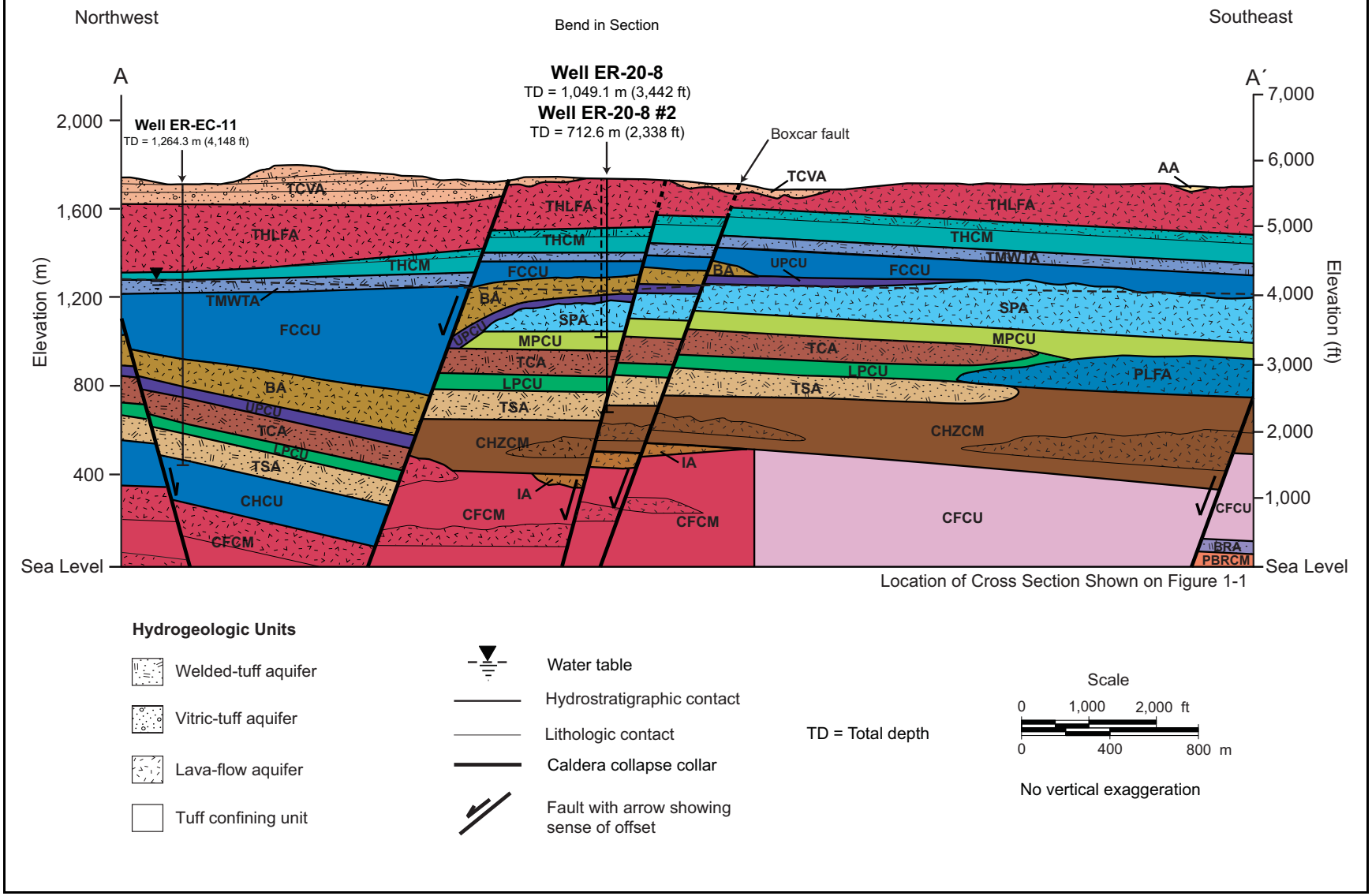

Figure 1-2
Northwest–Southeast Hydrostratigraphic Cross Section A-A' through Wells ER-20-8 and ER-20-8 #2

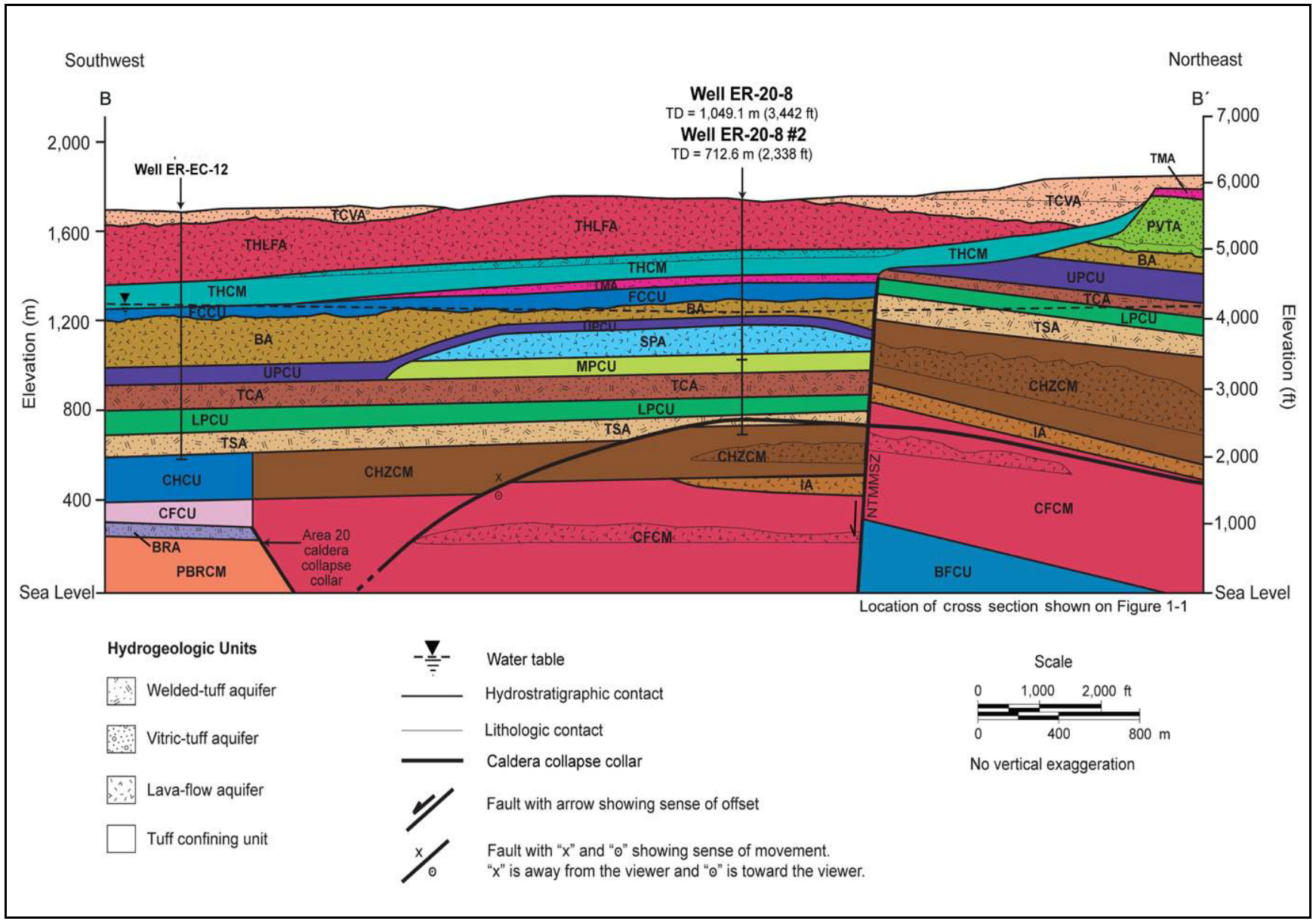

Figure 1-3
Southwest–Northeast Hydrostratigraphic Cross Section B-B' through Wells ER-20-8 and ER-20-8 #2

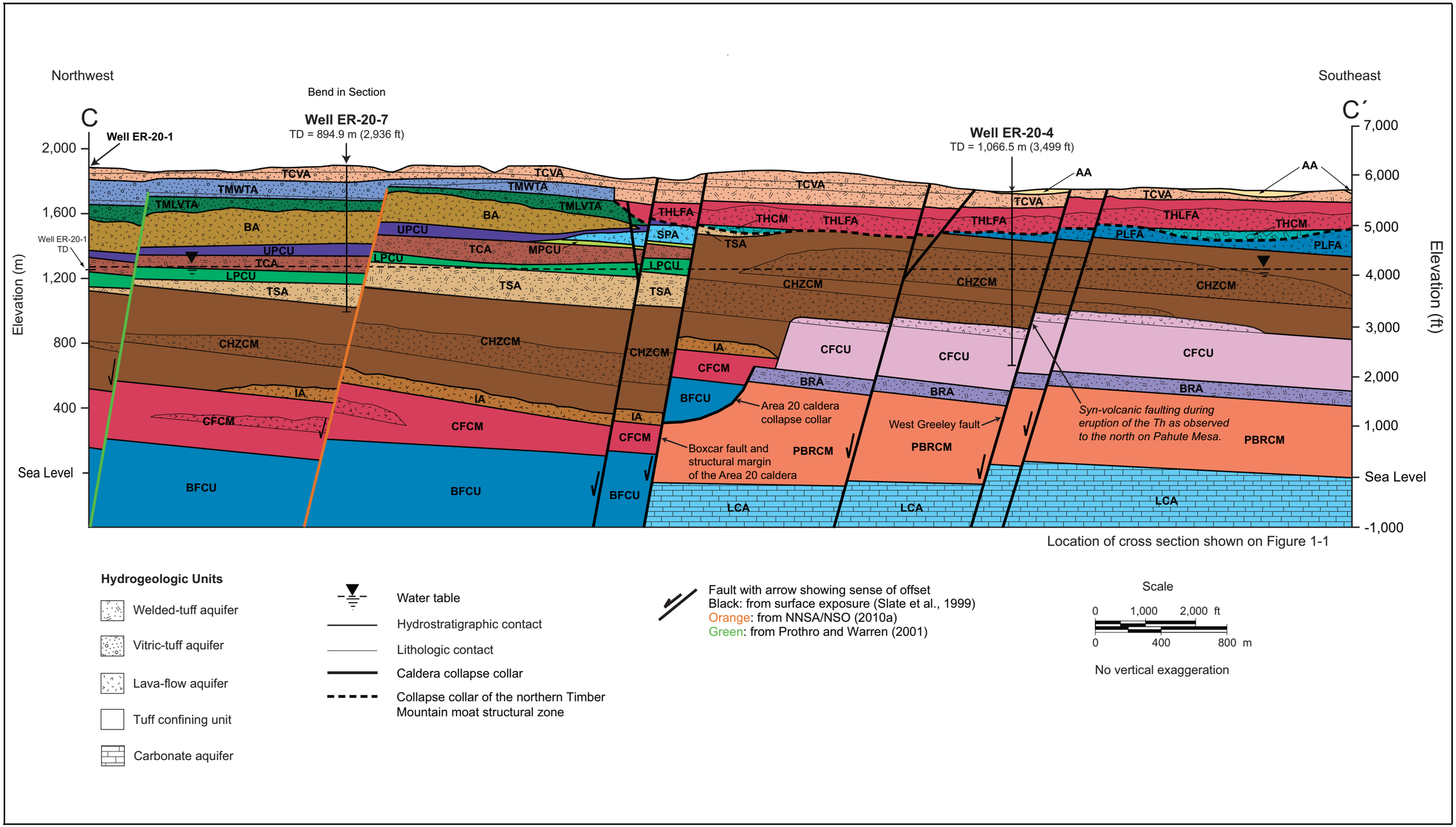

Figure 1-4
Northwest–Southeast Hydrostratigraphic Cross Section C-C' through Wells ER-20-7 and ER-20-4

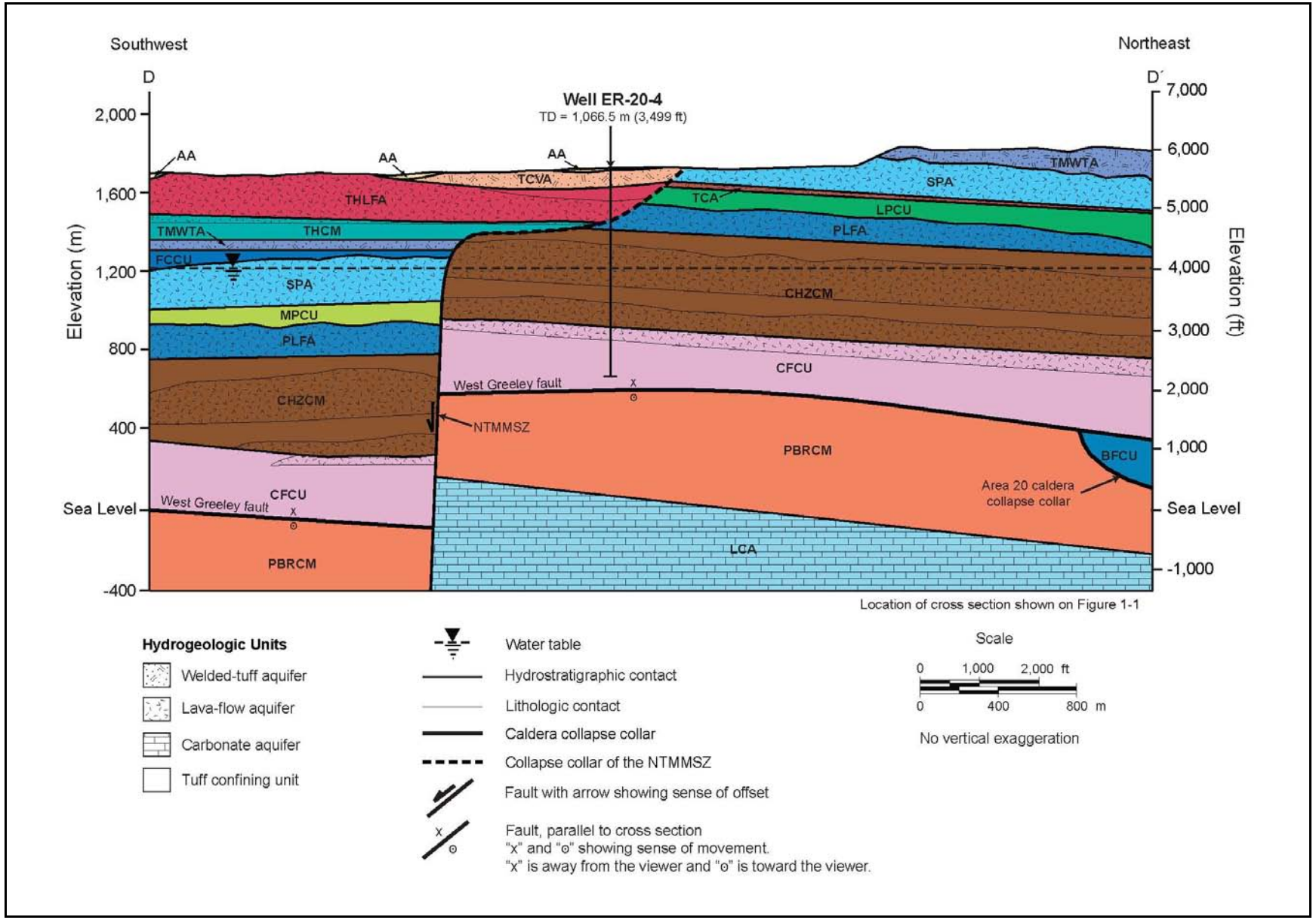

Figure 1-5
Southwest–Northeast Hydrostratigraphic Cross Section D-D' through Well ER-20-4

through 1-5). Fracture density may increase with proximity to faults; however, the hydrologic properties, if any, of faults themselves in the area are not well known. Limited data suggest that the full spectrum of hydraulic properties, from barrier to conduit, may be possible (Blankennagel and Weir, 1973; Faunt, 1997). In the area of interest, it may be that the major influence of faults is to juxtapose formations creating complex flow paths, as generally suggested by Faunt (1997). The area known as the Bench, a structural region between the northern NTMMSZ and the Timber Mountain caldera complex (TMCC), is of interest because radionuclide-contaminated groundwater has been observed to migrate through the NTMMSZ and off the Nevada National Security Site (NNSS) through this area (NNSA/NSO, 2011a and b).

Well ER-20-4 (NNSA/NSO, 2011a), located on southern Pahute Mesa in southern operational Area 20, was drilled and constructed between August 21 and September 12, 2010. Its primary objective was to investigate transport paths from central Pahute Mesa along the West Greeley fault and off of Pahute Mesa. It is completed in a section of stony rhyolite lava and flow breccia at the bottom of the Calico Hills zeolitic composite unit (CHZCM) and top of the Crater Flat confining unit (CFCU) (Figure 1-6). Well development and testing (WDT) operations occurred between August 10 and October 1, 2011, and are described in the Navarro-Intera, LLC (N-I), report (N-I, 2012a).

The Well ER-20-8 pad is located just south of the southern topographical margin of Pahute Mesa in NNSS operational Area 20. Well ER-20-8 (NNSA/NSO, 2011b) is located on the Well ER-20-8 pad in the southwestern portion of Area 20 with Well ER-20-8 #2. Drilling and construction of Well ER-20-8 occurred between June 15 and August 15, 2009. The well was completed in the Tiva Canyon aquifer (TCA) and the Topopah Spring aquifer (TSA) (Figures 1-7 and 1-8). Packers and bridge plugs were used in the well to develop and test the two aquifer units separately. WDT operations occurred in the TCA at ER-20-8 between May 10 and July 12, 2011. The well was then reconfigured, and development and testing operations occurred in the TSA between July 15 and August 11, 2011. These operations are described in N-I (2012b).

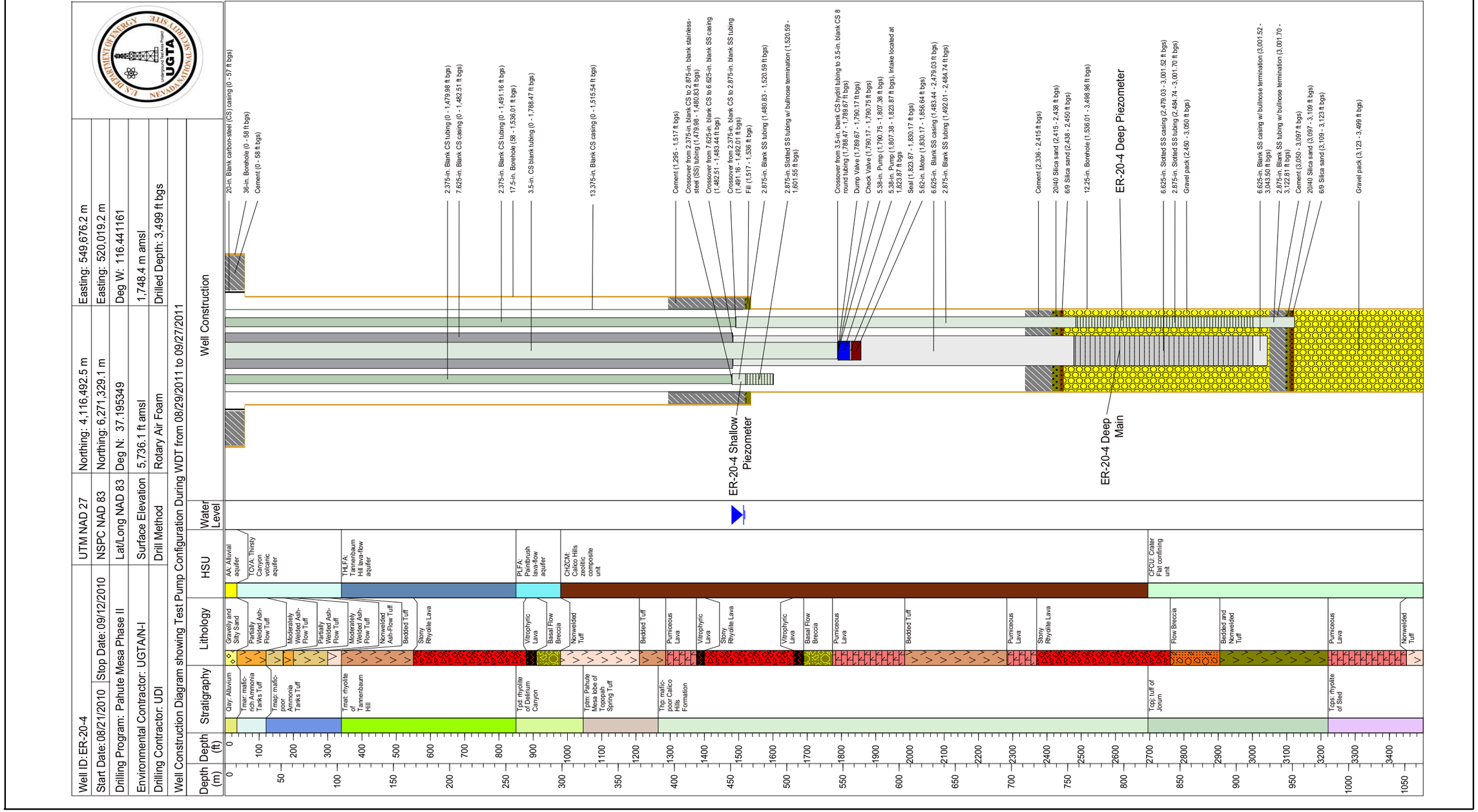

Figure 1-6
Well Completion Diagram for Well ER-20-4 during WDT

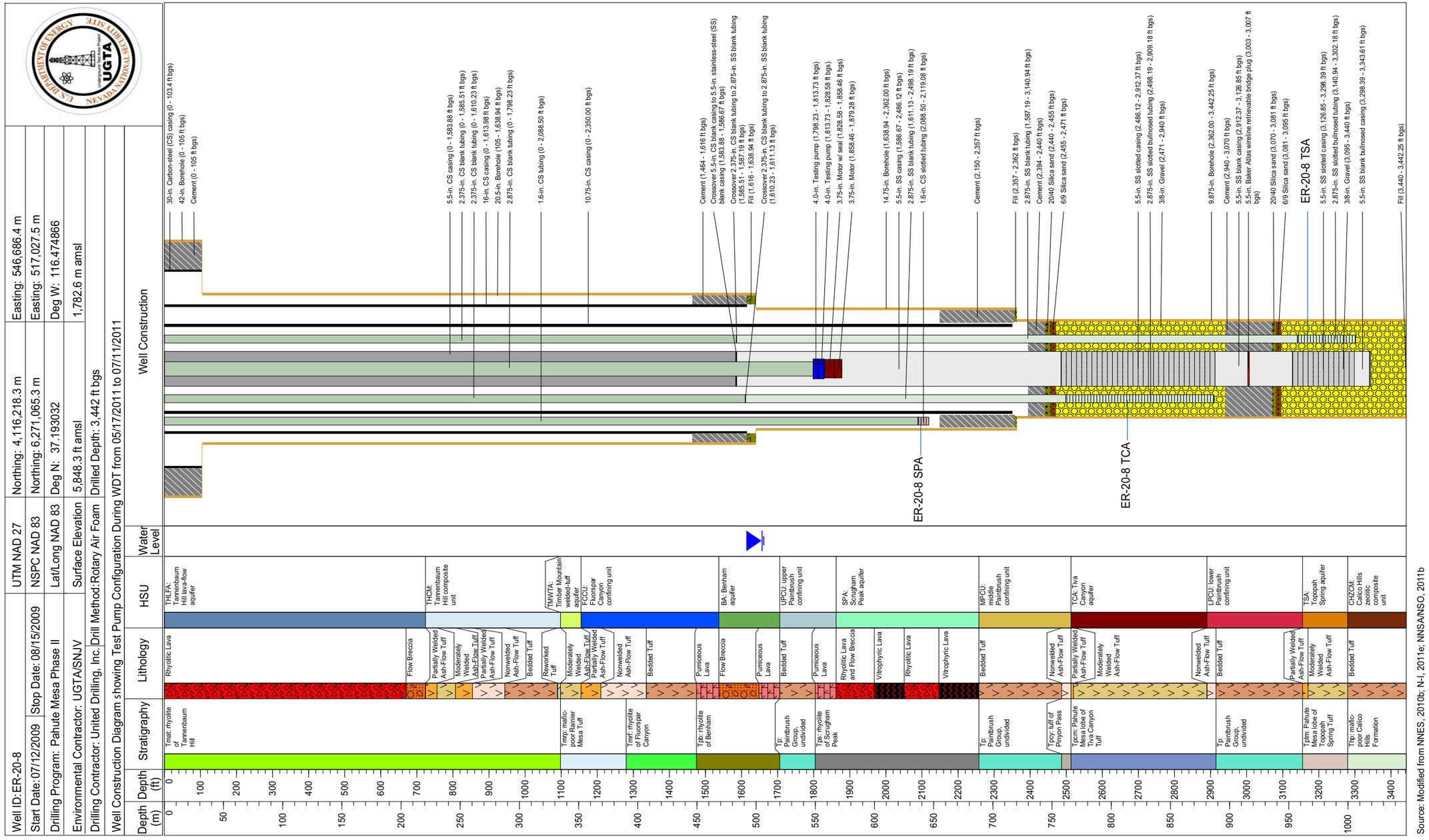

Source: Modified from NNES, 2010b; N-I, 2011e; NNSA/NSO, 2011b

Figure 1-7
Well Completion Diagram for Well ER-20-8 during TCA WDT

Well ID: ER-20-8		UTM NAD 27	Northing: 4,116,218.3 m	Easting: 546,686.4 m
Start Date: 07/12/2009	Stop Date: 08/15/2009	NSPC NAD 83	Northing: 6,271,065.3 m	Easting: 517,027.5 m
Drilling Program: Pahute Mesa Phase II		Lat/Long NAD 83	Deg N: 37.193032	Deg W: 116.474866
Environmental Contractor: UGTA/SNJV		Surface Elevation	5,848.3 ft amsl	1,782.6 m amsl
Drilling Contractor: United Drilling, Inc.	Drill Method: Rotary Air Foam		Drilled Depth: 3,442 ft bgs	

Well Construction Diagram showing Test Pump Configuration During WDT from 07/14/2011 to 08/17/2011

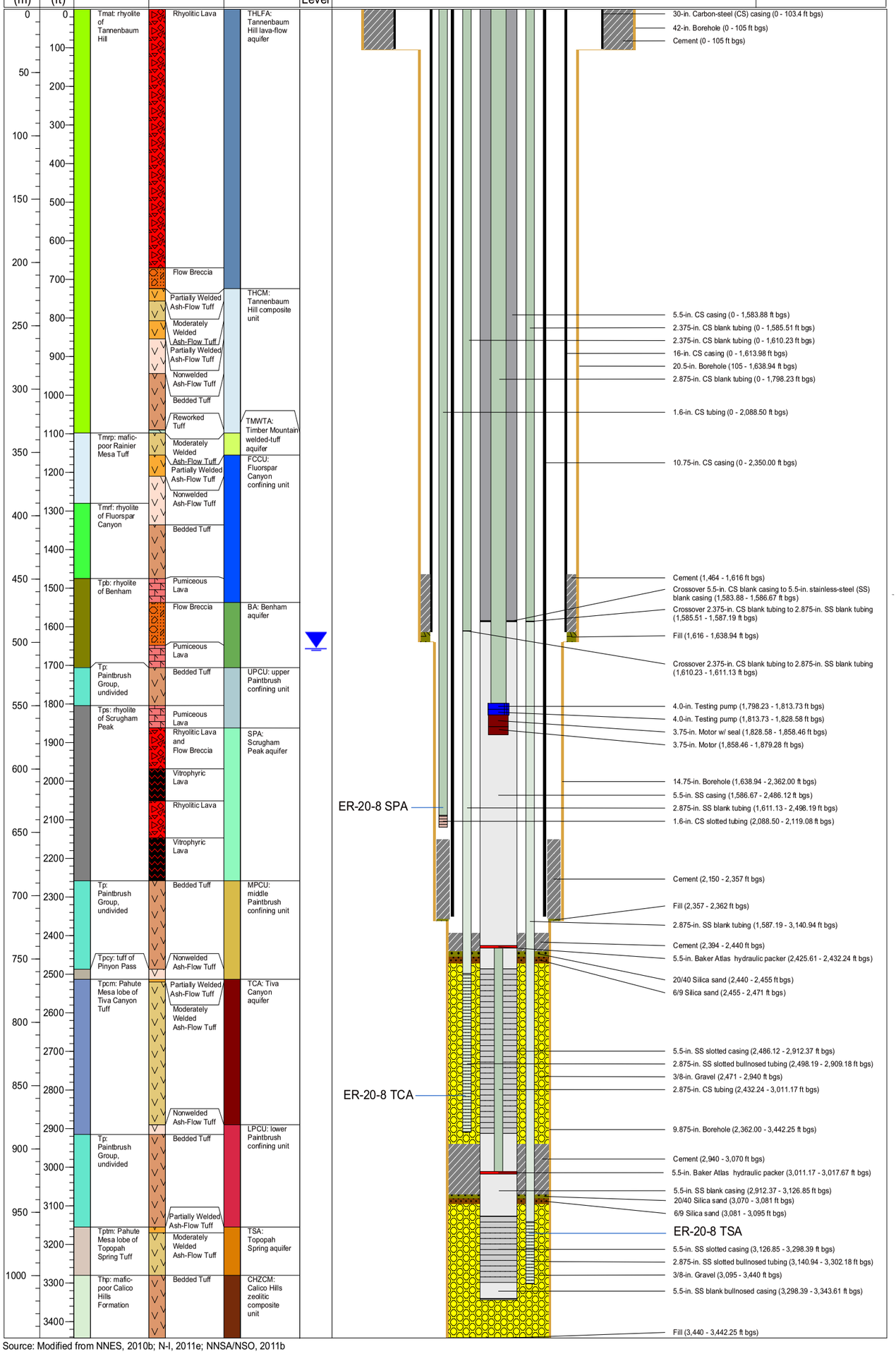

Source: Modified from NNES, 2010b; N-I, 2011e; NNSA/NSO, 2011b

Figure 1-8
Well Completion Diagram for Well ER-20-8 during TSA WDT

This report analyzes the following data collected from Wells ER-20-8 and ER-20-4 during WDT operations:

- Chemical indicators of well development (Section 2.0)
- Static hydraulic head (Section 3.0)
- Radiochemistry and geochemistry (Section 4.0)
- Drawdown observed at locations distal to the pumping well (Section 5.0)
- Drilling water production, flow logs, and temperature logs (Section 6.0)

The new data are further considered with respect to existing data as to how they enhance or change interpretations of groundwater flow and transport, and an interim small-scale conceptual model is also developed and compared to Phase I concepts (Section 7.0).

2.0 WELL DEVELOPMENT

The purpose of well development is to remove drilling fluids and drilling-associated fines from the formation adjacent to a well so samples reflecting ambient groundwater water quality can be collected, and to restore hydraulic properties near the well bore. Drilling fluids can contaminate environmental samples from the well, resulting in nonrepresentative measurements. Both drilling fluids and drilling-associated fines in the formation adjacent to the well can impede the flow of water from the formation to the well, creating artifacts in hydraulic response data measured in the well.

Well development can be monitored by measuring several water-quality indicators during pumping. Dissolved oxygen (DO), pH, turbidity (nephelometric turbidity unit [NTU]), and specific conductivity (SEC) stabilize as fluid introduced during drilling is removed (EPA, 2001). This stabilization is an indication that water produced from the well is representative of the formation. Changes in the connection of the well to the formation also should cause an increase in the specific capacity of the well.

UGTA wells are developed and step tested concurrently. Step testing is pumping the well at increasing production rates for short, adjacent periods. The time series plot of the discharge rate looks like steps. This is done to help determine changes in specific capacity and to determine the pumping rate that will be used for constant rate testing.

UGTA wells are drilled with an air-foam/polymer drilling fluid. Drilling fluids in UGTA wells are tagged with lithium bromide (LiBr) in order to estimate groundwater production during drilling, and to aid in determining well development. Bromide (Br) is typically found in low concentrations in NNSS groundwater, so the tagging allows removal of drilling fluid to be monitored. Br levels in non-environmental restoration (ER) wells are variable but samples generally indicate concentrations less than 0.1 milligrams per liter (mg/L) in Area 20 wells (N-I, 2011a). Br concentration in the drilling fluid varies with the amount of groundwater inflow but is generally 30 to 100 mg/L for the injected fluid. Detailed logs of the concentrations in the injected fluid and the discharge during drilling can be found in the drilling data report for each well (e.g., N-I, 2010b and 2011c).

Br concentrations are also monitored during WDT to gauge the removal of drilling fluid. Grab samples are collected every two hours (or as needed) from the discharge line while personnel are on site. The Br concentration is measured with a HORIBA F-53 meter equipped with an 8005-10C Br electrode. The measurement range of the 8005-10C electrode is 0.8 to 80,000 mg/L (HORIBA, 2003). During WDT, the instrument is calibrated daily at 0.5, 1, and 5 mg/L. Readings below the measurement range for the Br electrode do not follow Nernst's equation (HORIBA, 2003), so the measurements are not strictly quantitative. Such measurements indicate that the actual values are below the measurement range, but any measurements and trends in measurements should be treated as approximations.

The cement slurry used to fix casing in the well and isolate completion intervals is alkaline and, in most groundwater, this slurry raises the pH of fluid it mixes with before it cures. As the well is cleaned out during development, residual cement-tainted fluids will be removed, and pH from produced water should stabilize to a representative level for the water in the formation.

Turbidity is an indication of fines suspended in the water, and the trend and absolute values of turbidity indicate whether fines are still being removed from the well. As drilling fluid and sediment are removed from the well, clarity improves and turbidity drops. Wells tend to show spikes in turbidity when the pump is turned on initially. The U.S. Environmental Protection Agency (EPA) standard operating procedure for well development recommends that wells be developed until the water has a turbidity of less than 50 NTU (EPA, 2001).

The SEC is a measure of the capacity of water produced from the well to conduct an electrical current. Electrical conductance of water is a function of the types and quantities of dissolved substances in water, so there is no universal linear relation between total dissolved substances and conductivity (USGS, 2011).

Specific capacity is the ratio of discharge rate to drawdown in a well. It is a rough measurement, and is specific to a given well configuration and sensitive to changes in discharge rate. As a well is developed, drilling fines are removed and the well becomes better connected to the surrounding formation, so the amount of drawdown for a given discharge rate should decrease, increasing the specific capacity. As the discharge rate increases, turbulent well losses increase and the amount of

drawdown will increase faster than the discharge rate, so only specific capacities at the same discharge rate are directly comparable.

To frame the discussion of well development in the new wells, it is useful to look at water-quality samples from a previously developed well. Well ER-EC-6 was drilled and developed as part of Phase I Pahute Mesa activities. For WDT, 1.7 million gallons (gal) of water were produced from the well between January 14 and February 11, 2000 (IT, 2000b). Observations from thermal flow logging in 2000 indicate 0.58 gallons per minute (gpm) downward flow within the upper flow completion under static conditions. This flow could allow as much as 2.7 million gal to flow through the well over the nine years the well was open, although this estimate should be treated as an upper bound because the gradient between the sections of the well—and, therefore, the flow—will decrease with time.

Well ER-EC-6 was pumped from April 7 to April 12, 2009, so groundwater samples could be obtained (SNJV, 2009b). Water-quality data from the 2009 sampling are provided in Figure 2-1 to allow comparison of the new wells to a previously developed well.

2.1 Well ER-20-8 TCA Completion

WDT operations for the Well ER-20-8 TCA completion produced a total of 3.1 million gal of water from May 18 to June 27, 2011. Of this total, 1.2 million gal were produced during the formal development operations (May 18 to June 3, 2011). Figure 2-2 shows production rates and water-quality measurements for the WDT period. The time that samples for laboratory analysis (further described in Section 4.0) were taken is also shown.

The turbidity measurement for the first sample taken from the well on May 18, 2011, is 46 NTU after approximately 6,000 gal had been produced from the well. The next measurement was not taken until about 16,000 gal were produced from the well and is within the 5 to 15 NTU range of measurements that predominates for most of the rest of the well development. This is consistent with the expectation that the leftover drilling fluid in the well will be turbid and the surrounding groundwater clear. During the constant rate test, the turbidity measurements appear to have a consistent downward trend. The overall range of measurements during the constant rate test is similar to the range of scatter in measurements late in the well development period.

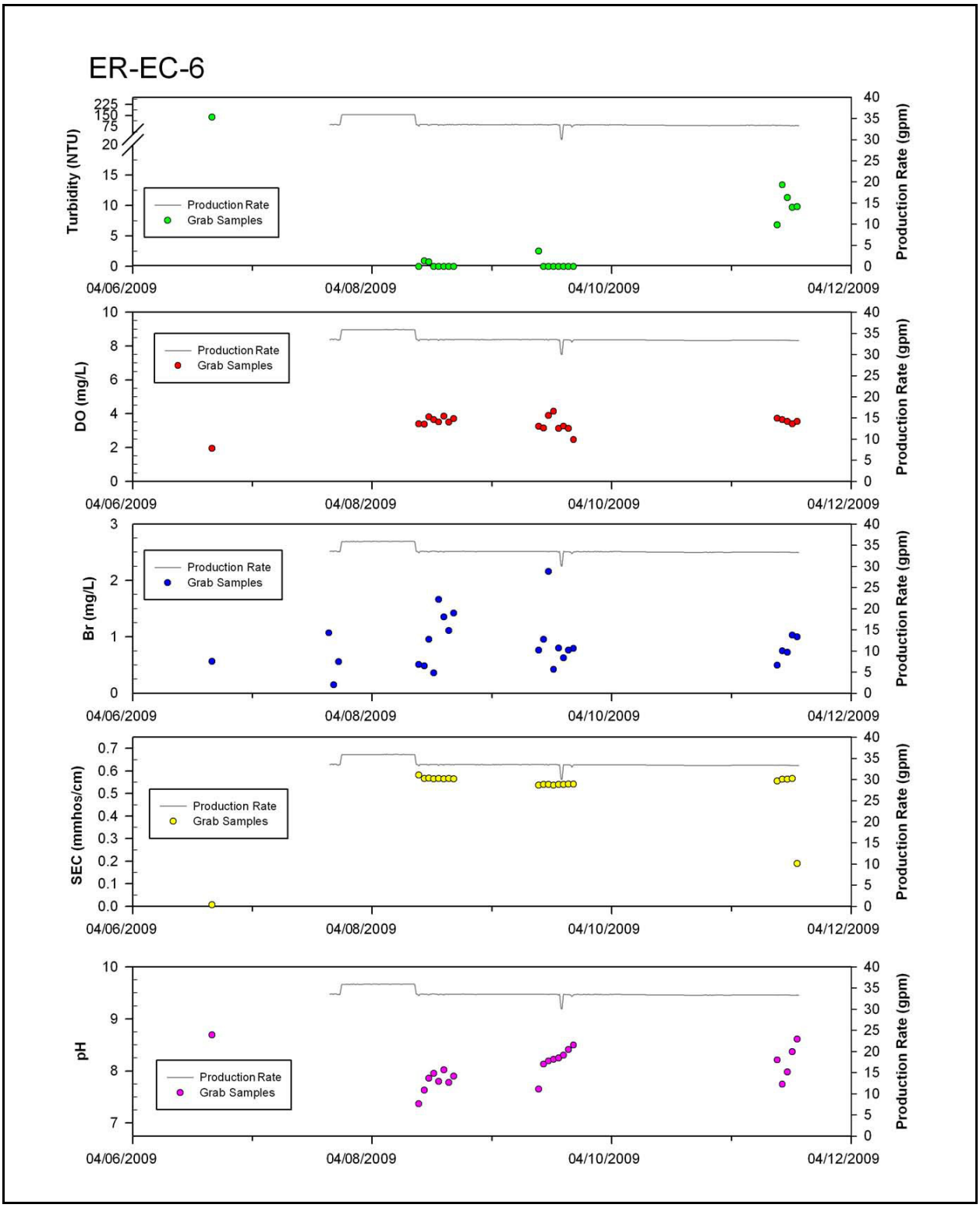

Figure 2-1
Well ER-EC-6 Water-Quality Monitoring Values

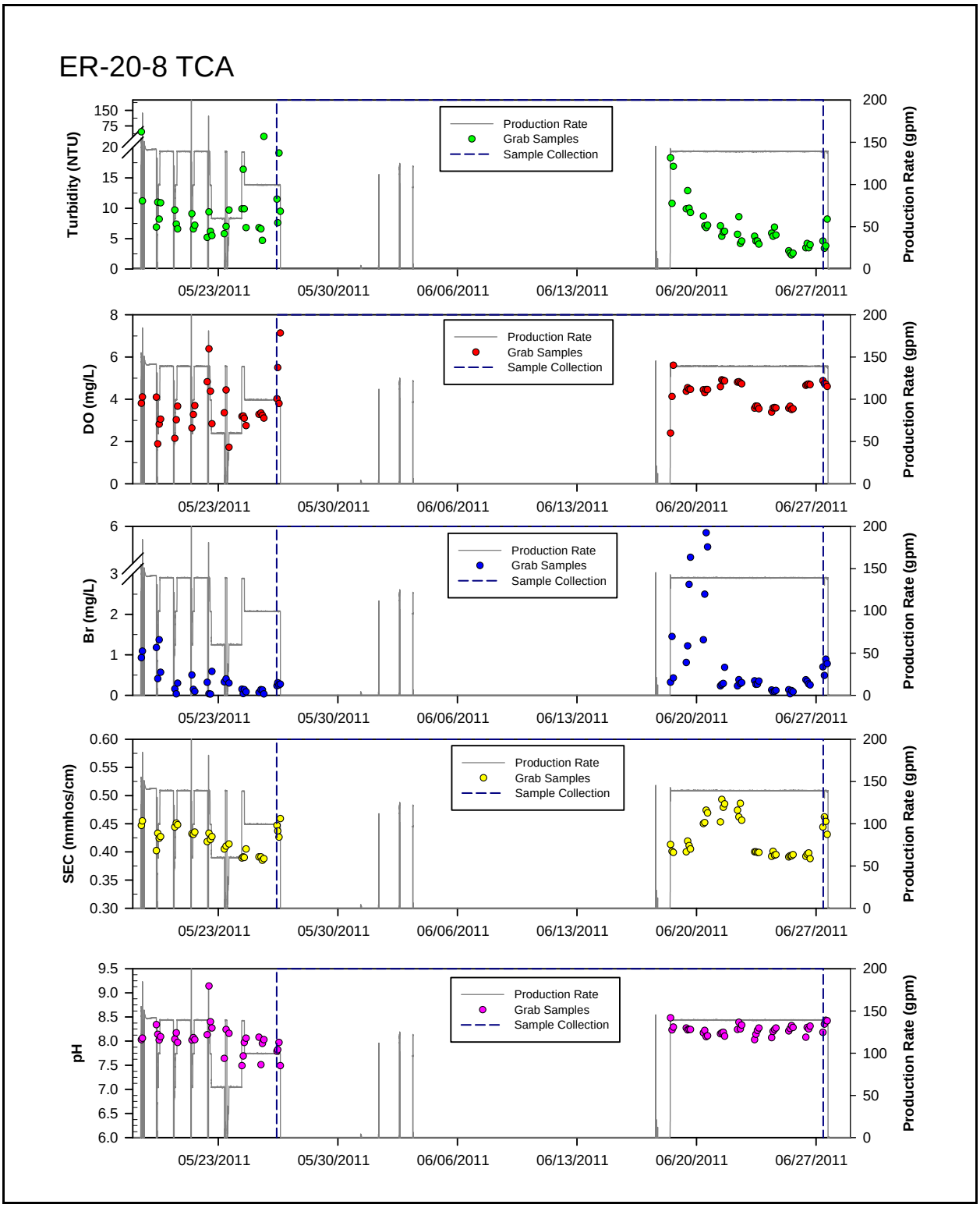

Figure 2-2
Well ER-20-8 TCA Water-Quality Monitoring Values

There is a spike in the Br measurements during the first several days constant rate test; however, there is a great deal of scatter, and some measurements are below the calibration range of the Br probe interspersed with these higher measurements. The remainder of the monitored geochemical parameters are stable during both the development and testing periods.

Specific capacity appears to stay stable during well development operations. A slight increase in specific capacity was calculated in the WDT data report (N-I, 2012b), but the amount of increase seems to be within the uncertainty of the calculations. Specific capacity is sensitive to production rate, elapsed time from the start of pumping, and recovery of the well from previous pumping cycles.

It appears that Well ER-20-8 TCA was sufficiently developed. The stability of the water-quality measurements over the large volume of water produced from the well is the strongest argument for this.

2.2 Well ER-20-8 TSA Completion

WDT operations for the Well ER-20-8 TSA completion produced a total of 1.9 million gal of water from July 15 to August 8, 2011. Of this total, 1.2 million gal were produced during the formal development operations (July 15 to July 27, 2011). Figure 2-3 shows production rates and water-quality measurements for the WDT period. The time that samples for laboratory analysis (further described in Section 4.0) were taken is also shown.

The turbidity measurement for the first sample taken from the well on July 15, 2011, is 150 NTU after less than 1,000 gal had been produced from the completion. The next turbidity measurement did not occur until 83,000 gal had been produced, and it is consistent with the range of measurements present during the rest of development and testing. There are no discernible trends in the turbidity measurements for the rest of the WDT.

The remainder of the monitored geochemical parameters are stable during both the development and testing periods. Scatter in the measurements is greater than any trends.

Specific capacity appears to stay stable during well development operations. A slight increase in specific capacity was calculated in the WDT data report (N-I, 2012b), but the amount of increase

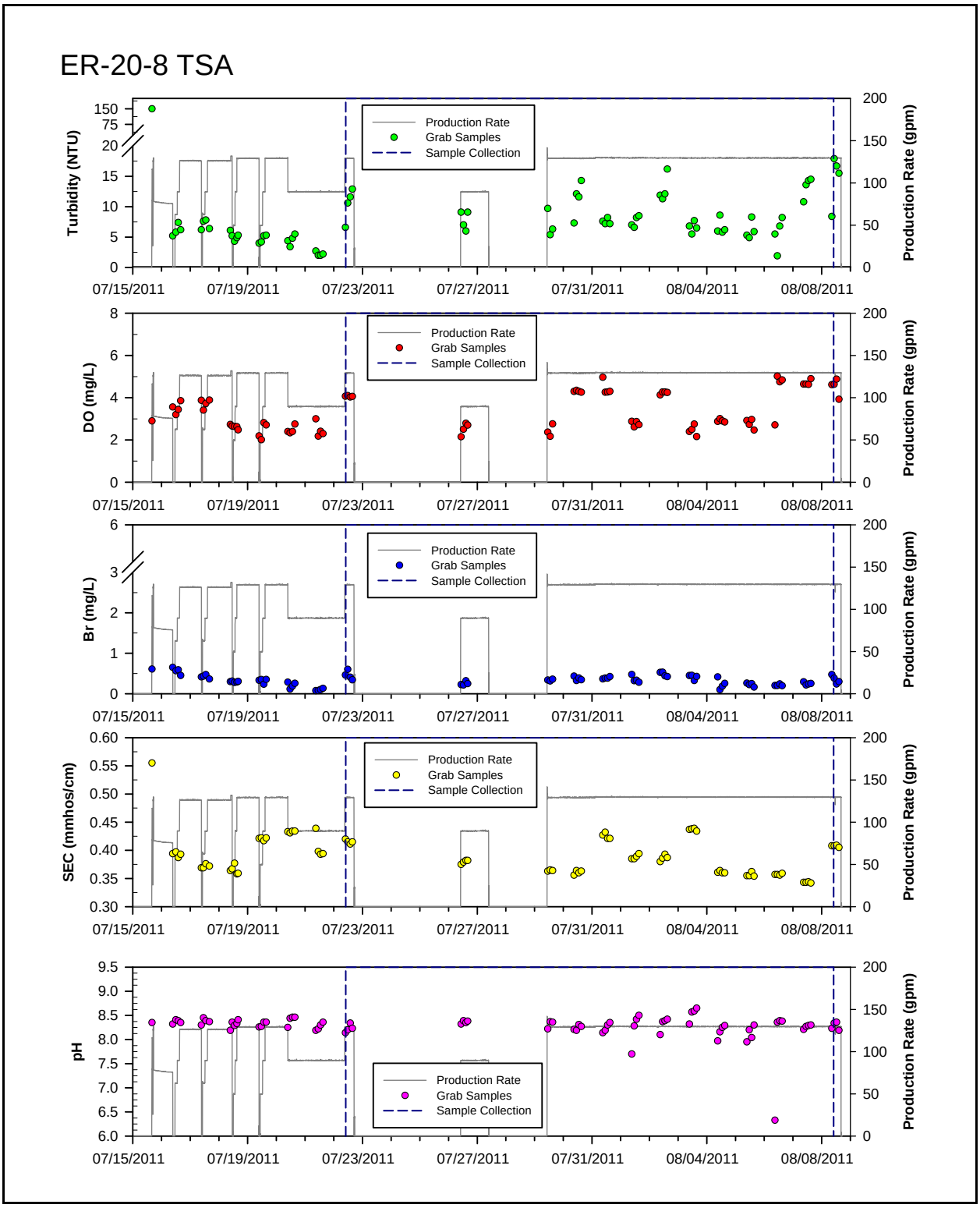

Figure 2-3
Well ER-20-8 TSA Water-Quality Monitoring Values

seems to be within the uncertainty of the calculations. Specific capacity is sensitive to production rate, elapsed time from the start of pumping, and recovery of the well from previous pumping cycles.

It appears that Well ER-20-8 TSA was sufficiently developed. The stability of the water-quality measurements over the large volume of water produced from the well is the strongest argument for this. Consistently low Br concentrations throughout WDT support this argument.

2.3 Well ER-20-4

WDT operations for Well ER-20-4 produced a total of 5.2 million gal of water from August 27 to September 21, 2011. Of this total, 1.9 million gal were produced during the formal development operations (August 27 to September 9, 2011). Figure 2-4 shows production rates and water-quality measurements for the WDT period. The time that samples for laboratory analysis (further described in Section 4.0) were taken is also shown.

There are few trends in the geochemical grab sample data. Br measurements are all below the calibration range for the Br probe, and the scatter of the measurements is greater than any trends.

Several calculated specific capacities are presented in Table 3-3 of N-I (2012a). These specific capacities are calculated at a range of different production rates and cannot be directly compared.

It appears that Well ER-20-4 was sufficiently developed. The stability of the water-quality measurements over the large volume of water produced from the well is the strongest argument for this. Consistently low Br concentrations throughout WDT support this argument.

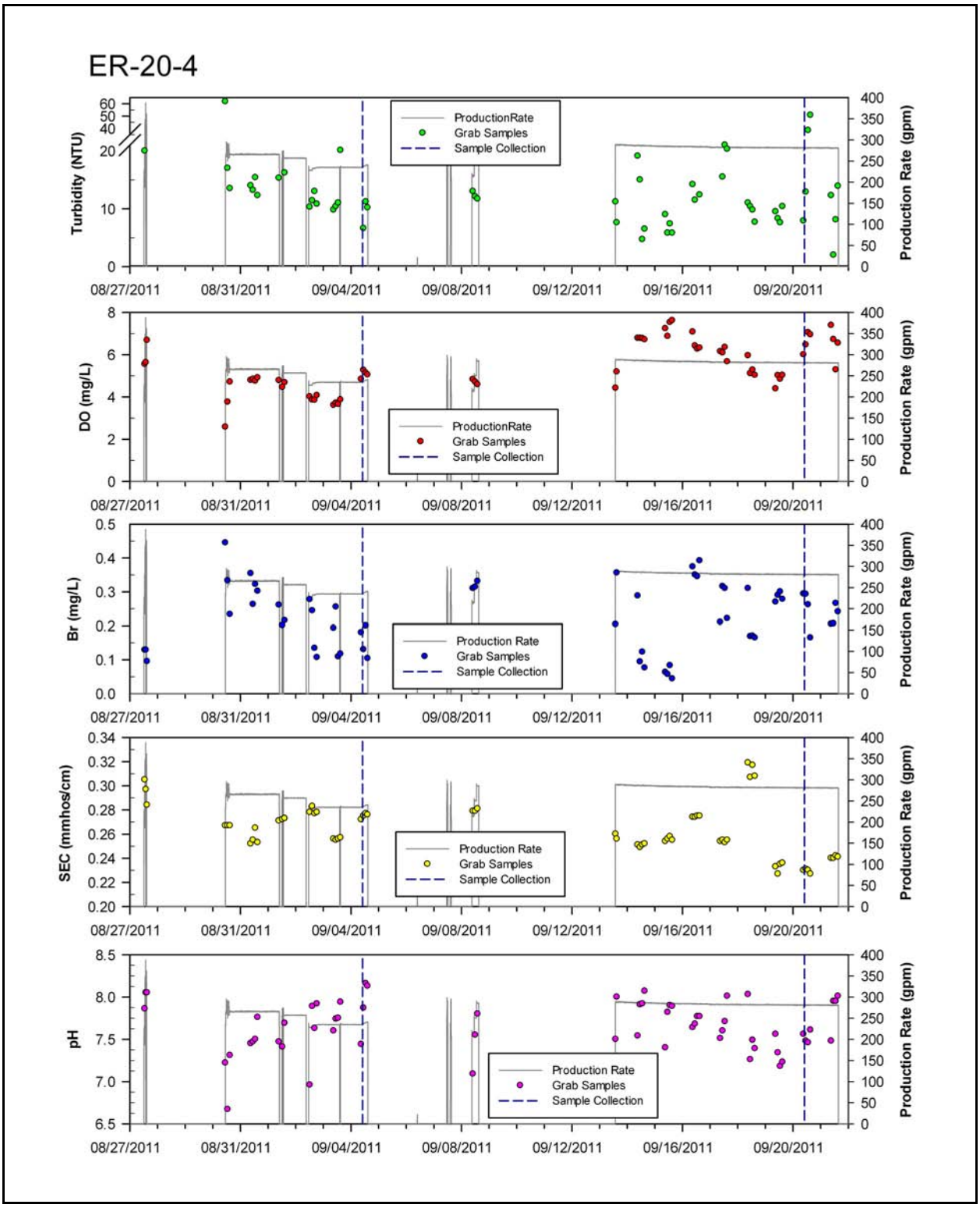

Figure 2-4
Well ER-20-4 Water-Quality Monitoring Values

3.0 STATIC HEAD

Static head data from wells provide information about potentiometric gradients and groundwater flow. Fenelon et al. (2010) conducted a broad study of wells across the NNSS that covers the area surrounding Wells ER-20-4 and ER-20-8. The contours developed and locations of data used in Fenelon et al. (2010) are shown in Figure 3-1. These contours provide a good overview of the general direction of flow that is consistent with the interpretations of radionuclide transport data in the vicinity of southwest Area 20.

To better understand smaller-scale variations and the degree that the data support interpretations of local flow direction and the potentiometric gradient, the data and interpretation from Fenelon et al. (2010) have been combined with new water levels acquired during Pahute Mesa Phase II characterization operations (ER-20-4 and ER-20-8) and the detailed geologic model. Table 3-1 shows the wells, water levels, and hydrostratigraphic units (HSUs) discussed in this section. The complexity of the geology makes it difficult to develop a clear picture of smaller-scale phenomena; however, a discussion of the data with respect to flow directions and the geologic framework is still instructive, particularly in understanding the effects of the many faults and structures in the area.

Figure 3-2 shows water levels that have been separated out by aquifer HSU as defined by Bechtel Nevada (BN) (2002) in the Phase I hydrostratigraphic framework model (HFM) along with contours from Fenelon et al. (2010). Well ER-EC-1 was not considered because all the completions are open, and the water levels cannot be attributed to a single HSU. As Figure 3-2 shows, water levels can vary between aquifer units at the same well. The clearest instance of this is in U-20y. The average of water levels in the TCA in U-20y is 1,340.8 meters (m) above mean sea level (amsl), while those in the deeper TSA in the same well are 1,277.1 m amsl. The TCA and TSA are separated by a 60-m section of the lower Paintbrush confining unit (LPCU) composed of zeolitized tuffs. In this case, it is likely that the well samples an isolated portion of the TCA and the higher water level is caused by local recharge, held above a larger flow system by the limited permeability of the LPCU. Fenelon et al. (2010) calls these water levels perched or semiperched.

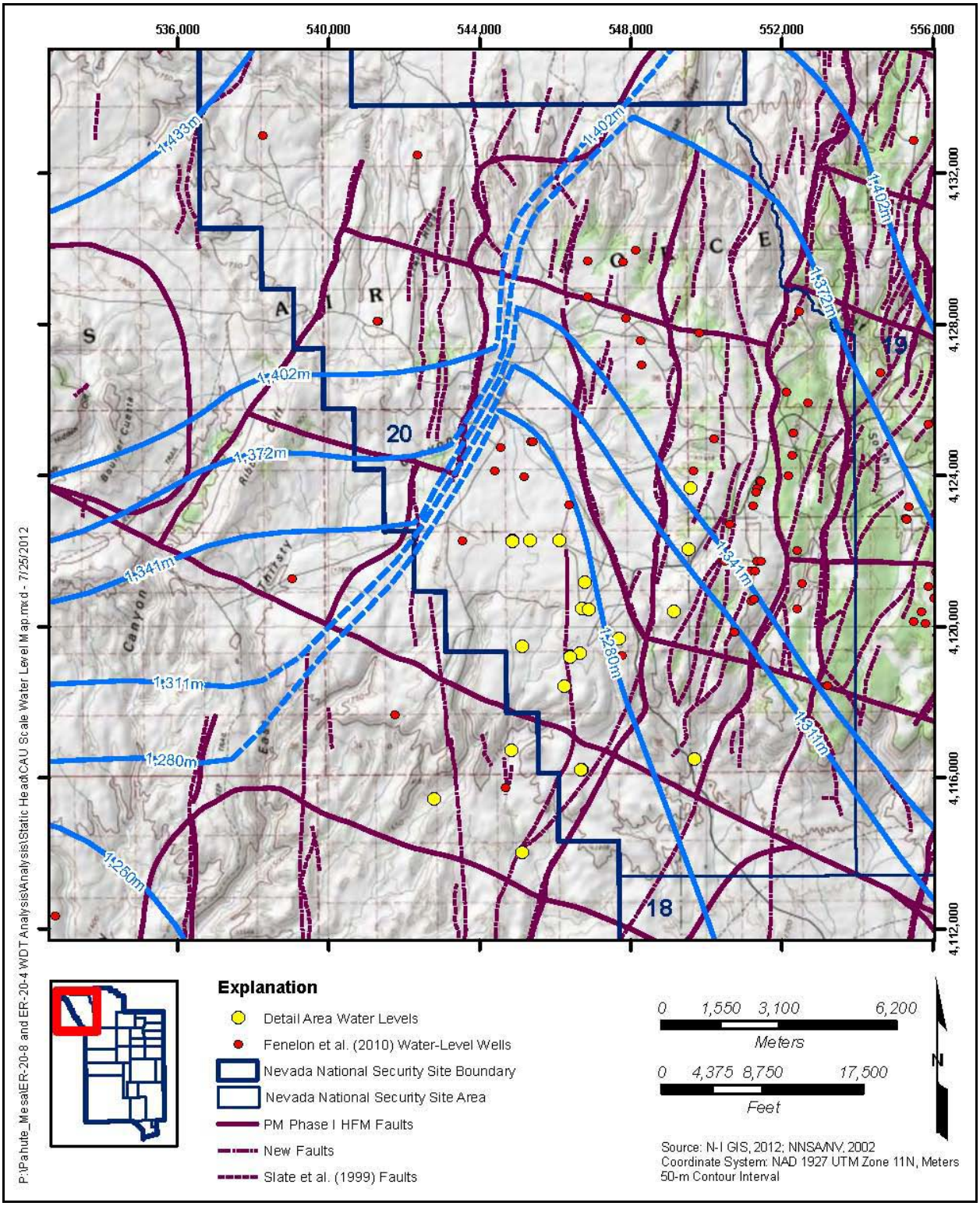

Figure 3-1
Southwest Area 20 and Vicinity Water-Level Contours

Table 3-1
Water Levels

Well Name	Water Level (m amsl)	HSU	Source
ER-20-1	1,277.7	TCA	Fenelon et al., 2010
ER-20-5 #1	1,276.5	TSA	Fenelon et al., 2010
U-20ag	1,285.6	BA	Fenelon et al., 2010
U-20ak	1,278.3	BA	Fenelon et al., 2010
U-20ao	1,317.7	BA	Fenelon et al., 2010 [a]
U-20ax	1,329.8	CHZCM	Fenelon et al., 2010 [a]
U-20ay	1,360.9	CHZCM	Fenelon et al., 2010
U-20bb	<1,272.8	BA	Fenelon et al., 2010
U-20bb #1	1,279.6	BA	Fenelon et al., 2010
U-20bf	≥1,339.0	CHZCM	Fenelon et al., 2010
U-20c	1,273.5	CHZCM	Fenelon et al., 2010
U-20y	1,340.8	TCA	Fenelon et al., 2010 [a]
U-20y	1,277.1	TSA	Fenelon et al., 2010
UE-20c	≥1,266.7	TCA, TSA	Fenelon et al., 2010
UE-20d	1,273.8	TSA	Fenelon et al., 2010
UE-20d	1,272.5	TCA	Fenelon et al., 2010
UE-20d	≤1,295.4	CHZCM	Fenelon et al., 2010 [a]
ER-20-7	1,276.0	TSA	N-I, 2011b
ER-20-8 Deep	1,274.6	TSA	N-I, 2011b
ER-20-8 Intermediate	1,274.7	TCA	N-I, 2011b
ER-20-8 #2	1,274.5	BA	N-I, 2011b
ER-EC-11 Deep (Tptm)	1,274.2	TSA	N-I, 2011b
ER-EC-11 Intermediate (Tpcm)	1,274.0	TCA	N-I, 2011b
ER-EC-11 Main	1,274.1	TCA, TSA	N-I, 2011b
ER-EC-11 Shallow (Tpb)	1,273.9	BA	N-I, 2011b
ER-20-5 #3	1,275.4	CHZCM	N-I, 2011b
ER-20-4 Shallow	1,284.8	CHZCM	N-I, 2011b
ER-20-4 Deep	1,284.7	CHZCM	N-I, 2011b
ER-EC-12 Shallow	1,271.9	TCA	N-I, 2011b
ER-EC-12 Intermediate	1,271.5	TSA	N-I, 2011b
ER-EC-15 Intermediate	1,272.9	TCA	N-I, 2012c
ER-EC-15 Deep	1,273.5	TSA	N-I, 2012c

[a] Water level marked as "anomalously high" in Fenelon et al. (2010). Not used in contouring.

BA = Benham aquifer
Tpb = Rhyolite of Benham
Tpcm = Pahute Mesa lobe of Tiva canyon tuff
Tptm = Pahute Mesa lobe of Topopah Spring tuff

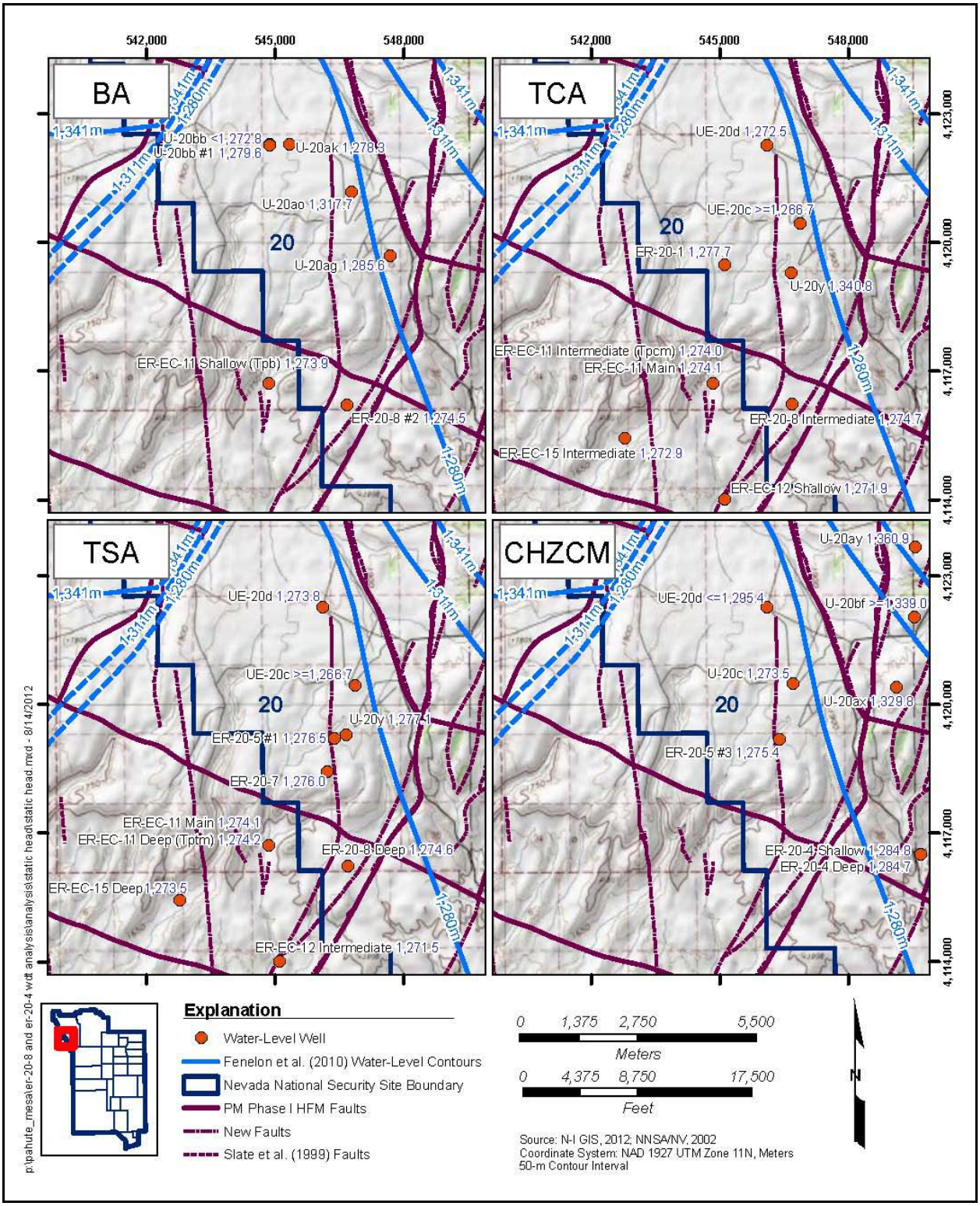

Figure 3-2
Water Levels by Aquifer

With the exceptions of U-20ao and U-20ag, there is only a modest amount of variation in the water levels of wells completed in the BA in southwestern Pahute Mesa. Both U-20ao and U-20ag are close to the West Boxcar fault. The elevated water levels in the two wells reflect the higher water levels found in the CHZCM wells across the fault. The range of water levels in the rest of the BA wells is 1,272.8 to 1,279.6 m. This entire range is expressed in two different wells (U-20bb and U-20bb 1, respectively) that are very close to each other, illustrating the amount of noise in the water-level data.

There are several anomalous water levels in wells in the TCA. The water level in the TCA/TSA in UE-20c is only 1,266.7 m amsl. The water level is the last measurement in a recovery test that recovered about 15 m in 1 hour 40 minutes. The recovery rate over the last 40 minutes was 2 m per hour, so it appears the last water level is within a few meters of recovery. It is difficult to reconcile this water-level measurement with the surrounding wells. The measurement is a local minimum at a point where there is no known discharge sink. The water level in U-20y is anomalously high compared to the surrounding wells. There is only a 13-m column of water at the bottom of the TCA above a section of zeolitized tuff in the well. This water is likely local recharge retarded by the zeolitized tuff. There is only a modest difference (about 3 m) between Wells ER-EC-11 and ER-20-8 and the wells on the other side of the NTMMSZ. Water levels in Wells ER-EC-11 and ER-20-8 differ by only 0.6 m in the TCA.

There is little variation in the water levels in the TSA in southwestern Pahute Mesa. Excluding the anomalously low level in the TCA/TSA in UE-20c, the range is 1,271.5 to 1,277.1 m expressed in Wells ER-EC-12 and U-20y, respectively. If UE-20d and UE-20c are removed from the set of TSA wells, a plane can be used to obtain a good fit to the water levels in the rest of the set using multiple regression. The plane dips 183° (due south) with a gradient of 1m/1.06km, and the R square of the fit is 0.96.

In the CHZCM east of the Boxcar fault, three wells (U-20ay, U-20bf, and U-20ax) have water levels of 1,360.9, 1,339.0, and 1,329.8 m, respectively. Well U-20ay is completed in the upper lava-flow aquifer (LFA) portion of the HSU and should be representative of an extended portion of the aquifer. Wells U-20bf and U-20ax are both completed in zeolitized tuffs below the upper LFA and may be less representative. Across the Boxcar and West Boxcar faults, water levels in the CHZCM are significantly lower. A plane can be used to obtain a good fit to the water levels in the CHZCM wells

using multiple regression. The plane dips 234° (southwest) with a gradient of 1m/55m, and the R squared of the fit is 0.96.

Over southwest Area 20, a large number of wells have water levels between 1,271.5 and 1,279.5 m. This supports the current (Fenelon et al., 2010) and past (DOE/NV, 1997; O'Hagan and Laczniak, 1996; Blankennagel and Weir, 1973) characterization of southwest Area 20 as a flatter valley in the potentiometric surface. New characterization data do not suggest that an abrupt change in this interpretation is necessary (at least for the BA/Scrugham Peak aquifer [SPA], TCA, and TSA), even with the NTMMSZ present in a configuration most likely to make the effects of the fault detectable (Faunt, 1997). The presence of tritiated groundwater at Wells ER-20-7, ER-20-8 #2, and ER-EC-11 is an unambiguous indication that groundwater is flowing from southwest Area 20.

3.1 Vertical Head Differences

Water levels between completions are very close to each other, and it is difficult to determine whether there is a small vertical gradient between the aquifer HSUs in Wells ER-20-4 and ER-20-8. Temperature dependent density effects can make a meter or two of difference in water levels in wells with steep temperature gradients and deep aquifers. To tease out small head differences between aquifers, it is necessary to correct for these temperature effects. Water levels are measured as depth to water within a string of piezometer tubing below a fixed point at the well head on the surface. The aquifer is usually several hundred meters below the water levels, leaving a large water column that is affected by temperature. The corrections were performed by methods discussed in Post et al. (2007).

To determine the potentiometric differences between the aquifers, it is necessary to calculate the pressure head at the elevation of the aquifer using a temperature log. The wells in this report are fresh water wells, so water density is calculated from temperature using the Thiesen-Scheel-Diesselhorst equation (McCutcheon et al., 1993). The pressure head at the midpoint of the aquifer is calculated as follows:

$$P_{aq} = \rho_T(z_{wl} - z_{midpoint}) \qquad (3\text{-}1)$$

where

P_{aq} = the water pressure at the midpoint of the aquifer
ρ_T = the average water density calculated from the average water temperature between z_{wl} and $z_{midpoint}$
z_{wl} = the elevation of the water level measured in the piezometer tube
$z_{midpoint}$ = the elevation of the midpoint of the aquifer

Once pressures are calculated in multiple aquifers, it is necessary to compare the difference in pressures at the midpoints to the hydrostatic pressure difference that would be expected given the natural temperature/density profile between the aquifers. Density is calculated from temperature and the resulting average density between the midpoints of the two aquifers is used to calculate the expected hydrostatic pressure difference as follows:

$$P_{hydrostatic} = \rho_T(z_{midpoint1} - z_{midpoint2}) \quad (3\text{-}2)$$

where

$P_{hydrostatic}$ = the pressure difference between two aquifers due to hydrostatic pressure
ρ_T = the average density calculated from average temperature between $z_{midpoint1}$ and $z_{midpoint2}$
$z_{midpoint1}$ = the elevation of the midpoint of aquifer 1
$z_{midpoint2}$ = the elevation of the midpoint of aquifer 2

If $P_{hydrostatic} > P_{aq1} - P_{aq2}$, then the hydraulic gradient slopes down from aquifer 1 to aquifer 2.
If $P_{hydrostatic} < P_{aq1} - P_{aq2}$, then the hydraulic gradient slopes up from aquifer 1 to aquifer 2.

This makes the assumption that the temperatures measured in the well are representative of the natural aquifer system. This assumption introduces some error into the calculations performed in this report, as the temperature logs available are generally taken immediately after drilling or well testing. This error is discussed further for each well examined.

3.1.1 Well ER-20-8 Vertical Gradient

Figure 3-3 shows water levels, temperature log dates, and pumping dates for Well ER-20-8. Temperature logs were taken in the well immediately after drilling (July and August 2009) and during WDT operations (June through September 2011). A pair of Desert Research Institute (DRI) logs (Figure 3-4) were run on September 27, 2011, in the TSA and TCA piezometer tubing, and water levels were measured in both completions on September 26 and September 29, 2011. These are the best data available with which to perform a temperature corrected static head calculation. Water levels fluctuate during WDT, but they appear to have largely recovered by September 26, 2011.

The temperatures in the well had not reached ambient conditions on September 29, 2011. The temperature from 500 to 600 m bgs (coincident with the UPCU and SPA units) is distinctively warmer than expected (about 49 degrees Celsius [°C]), presumably due to residual heat, generated by the pump used in development and testing. There is a sharp dip in temperature in the TCA section of

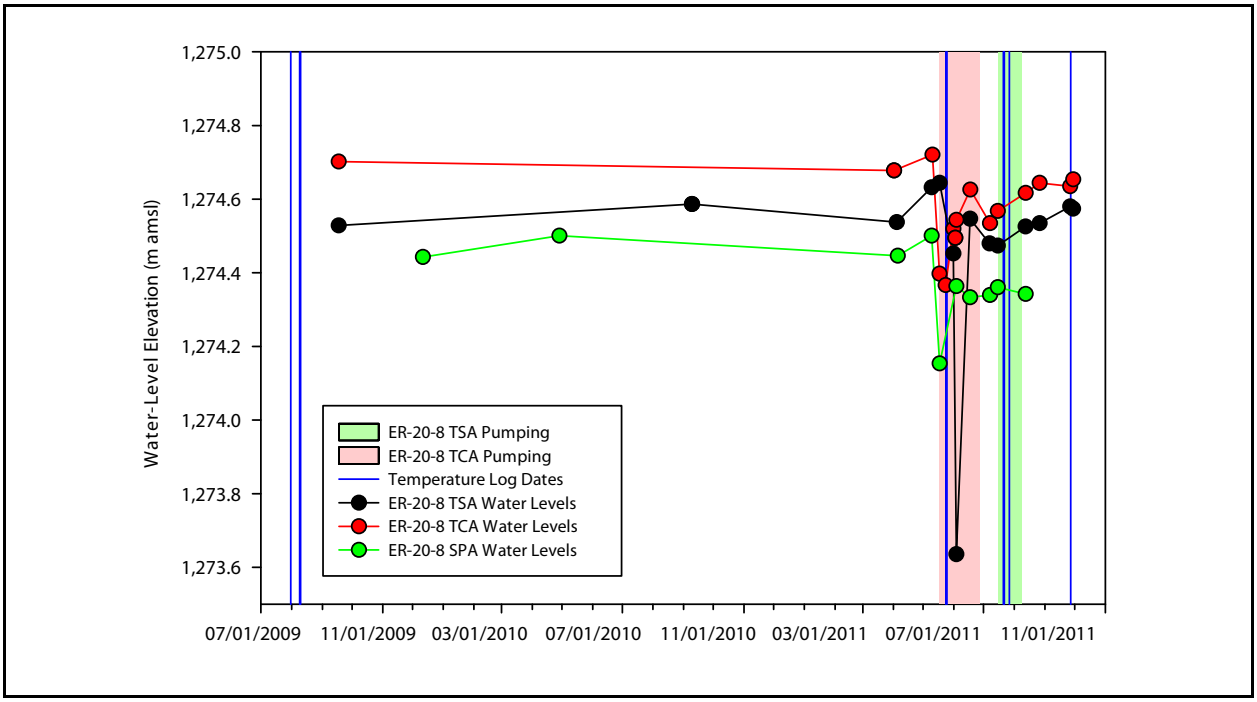

Figure 3-3
Water-Level Measurements and Temperature Log Dates in Well ER-20-8

the well to about 42 °C followed by a steady increase to about 46 °C in the TSA section. Water temperatures above the upper aquifer (the TCA in this case) matter for the calculation of the pressure at the aquifer midpoints; however, it is only important that they are accurate when the water levels are measured, not that they represent natural conditions. In this case, the close temporal proximity of the temperature log to the water-level measurements indicates that the logs can be used for the correction. The temperature profile between the two aquifers, however, needs to represent natural conditions because it is used to calculate the hydrostatic gradient. It is expected that temperature profiles will be fairly constant in the sections of aquifer where advection moves heat around freely, and there will be gradients in confining units, where conduction is the dominant heat transfer mechanism. With the exception of a slight, unnatural drop in temperature from 823 to about 850 m bgs, the log generally follows a natural, monotonically increasing temperature profile between the midpoints of the TCA and TSA (823 m bgs and 975 m bgs).

The uncorrected water level on September 29, 2011, in the TSA is 0.079 m lower than the water level in the TCA. When the temperature correction is performed, the TSA water level is 0.113 m higher than water level in the TCA. This result is slightly above the measurement error, and the measurements occurred very close to the end of the WDT pumping. It is difficult to draw a firm

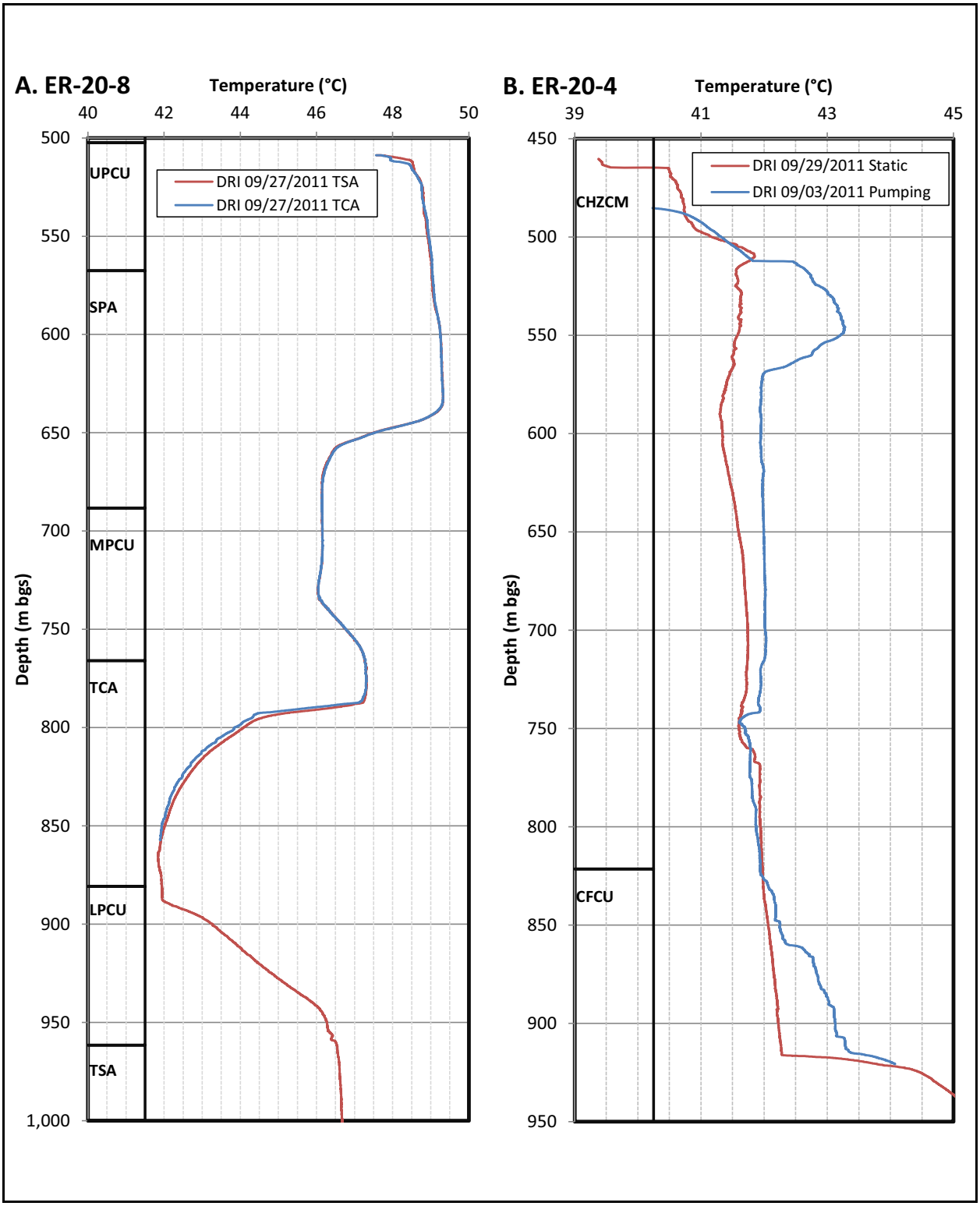

Figure 3-4
Temperature Logs in Wells ER-20-8 and ER-20-4

conclusion using the available data, but higher head in the deeper TSA would indicate that the TSA is better connected to the recharge zone upgradient to the northeast or that the TCA is better connected to the discharge zone downgradient to the southwest.

Water levels for the SPA could not be corrected because no temperature logs reflecting the natural temperature gradient between the SPA and the TCA are available, and the closest water level from the SPA to the September 29, 2011, DRI log is August 12, 2011, immediately after pumping when pump-related heating of the water column was greatest. The nonrepresentative temperature log would cause error in the calculation of pressure at the midpoint of the SPA.

3.1.2 Well ER-20-4 Vertical Gradient

Figure 3-5 shows water levels, temperature log dates, and pumping dates for Well ER-20-4. The total variation in water levels is only about 0.3 m. The maximum difference between any pair of water levels measured in the two completions on the same day is 0.06 m, but sometimes Well ER-20-4 deep is higher, and sometimes Well ER-20-4 shallow is higher. When the differences between same-day pairs of water levels are averaged, Well ER-20-4 deep is 0.002 m higher than Well ER-20-4 shallow, a result that is insignificant compared to the uncertainty in individual measurements and normal variability in the water levels.

Temperature corrections were performed using the DRI temperature log from September 29, 2011 (Figure 3-4), and water levels from September 26 and October 3, 2011. In this temperature log, there is little temperature gradient between the midpoints of the two wells, and the temperature correction makes no significant difference in the hydraulic head (less than ± 0.0002 m). The two logs in Figure 3-4 are the only two logs readily available for Well ER-20-4, and the degree to which the logs reflect the temperature of the surrounding aquifer is uncertain.

It appears that there is little vertical hydraulic gradient in the CHZCM at Well ER-20-4. The water levels between the two completions in the well are close to each other, and the average difference in water levels is very small.

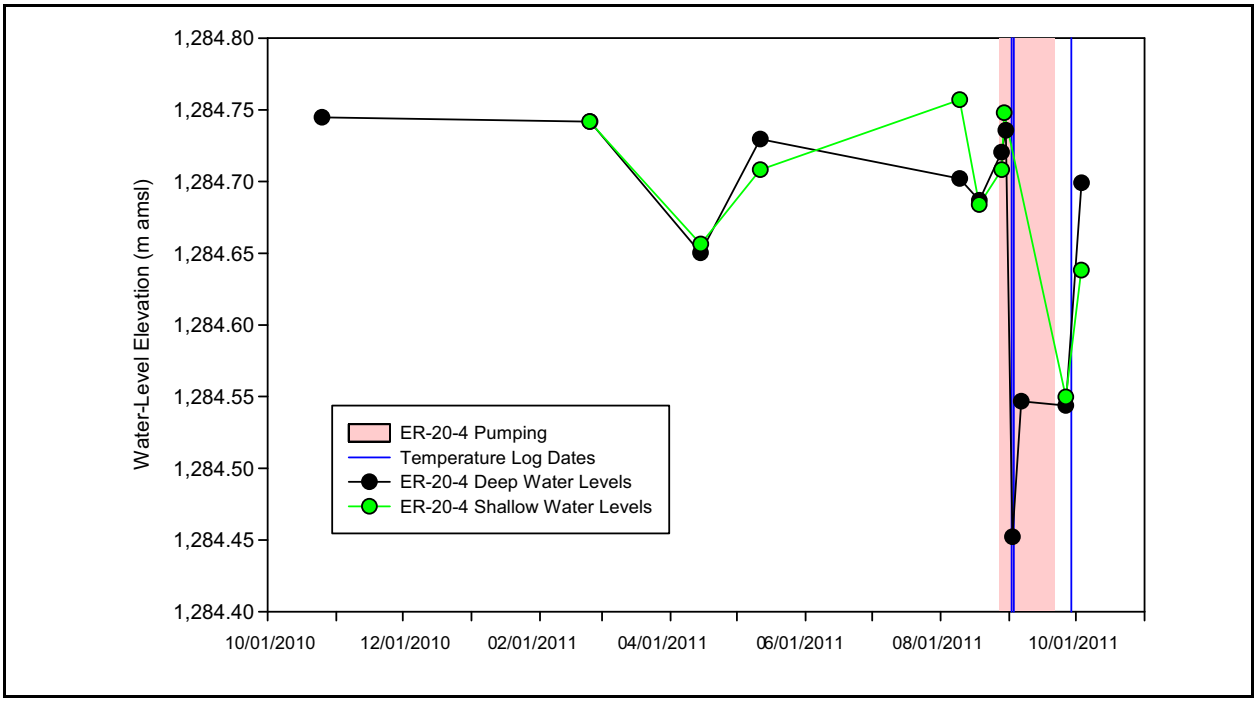

Figure 3-5
Water-Level Measurements and Temperature Log Dates in Well ER-20-4

4.0 GROUNDWATER CHEMISTRY

This section presents an evaluation of groundwater chemistry data for Wells ER-20-4 and ER-20-8, and other wells in their vicinity. Comprehensive groundwater chemistry evaluations for Pahute Mesa are presented in Thomas et al. (2002), Kwicklis et al. (2005), Rose et al. (2006), and Kwicklis (2009). This section integrates the new data with these earlier investigations in a qualitative manner. The wells included in this evaluation, along with the primary HSU sampled within each well, are presented in Figure 4-1. In general, the primary HSU is the HSU that extends the largest length within the effective open interval. For Wells ER-EC-1 and ER-EC-6, the primary HSU is specified as the BA because flow logs show that production in these wells was derived from the upper completions when initially sampled (IT, 2000a and b), and these wells have not been resampled under different configurations.

Chemistry data for Wells ER-20-4 and ER-20-8 are presented in Appendix A. In addition, Appendix A presents chemistry data for Wells ER-20-7, ER-20-8 #2, and ER-EC-11 WDT samples, including results reported subsequent to N-I (2011a).

4.1 Sample Collection

During drilling, fluid-discharge samples were collected for onsite and/or laboratory analysis of tritium. Samples were also collected at the end of drilling using a depth-discrete wireline bailer and analyzed for a limited number of parameters. Both depth-discrete bailer and pumped wellhead groundwater samples were collected during WDT. Details of the sampling activities associated with drilling operations are presented in N-I (2010b and 2011c), and those associated with WDT operations are presented in N-I (2012a and b).

Depth-discrete samples were analyzed by ALS Laboratory Group, whereas the samples collected at the end of WDT operations were analyzed by ALS Laboratory Group, DRI, Lawrence Livermore National Laboratory (LLNL), Los Alamos National Laboratory (LANL), and the U.S. Geological Survey (USGS) for a larger suite of parameters (see Appendix A). The commercial laboratory, ALS Laboratory Group, is certified by the State of Nevada; the other laboratories provide state-of-the-art

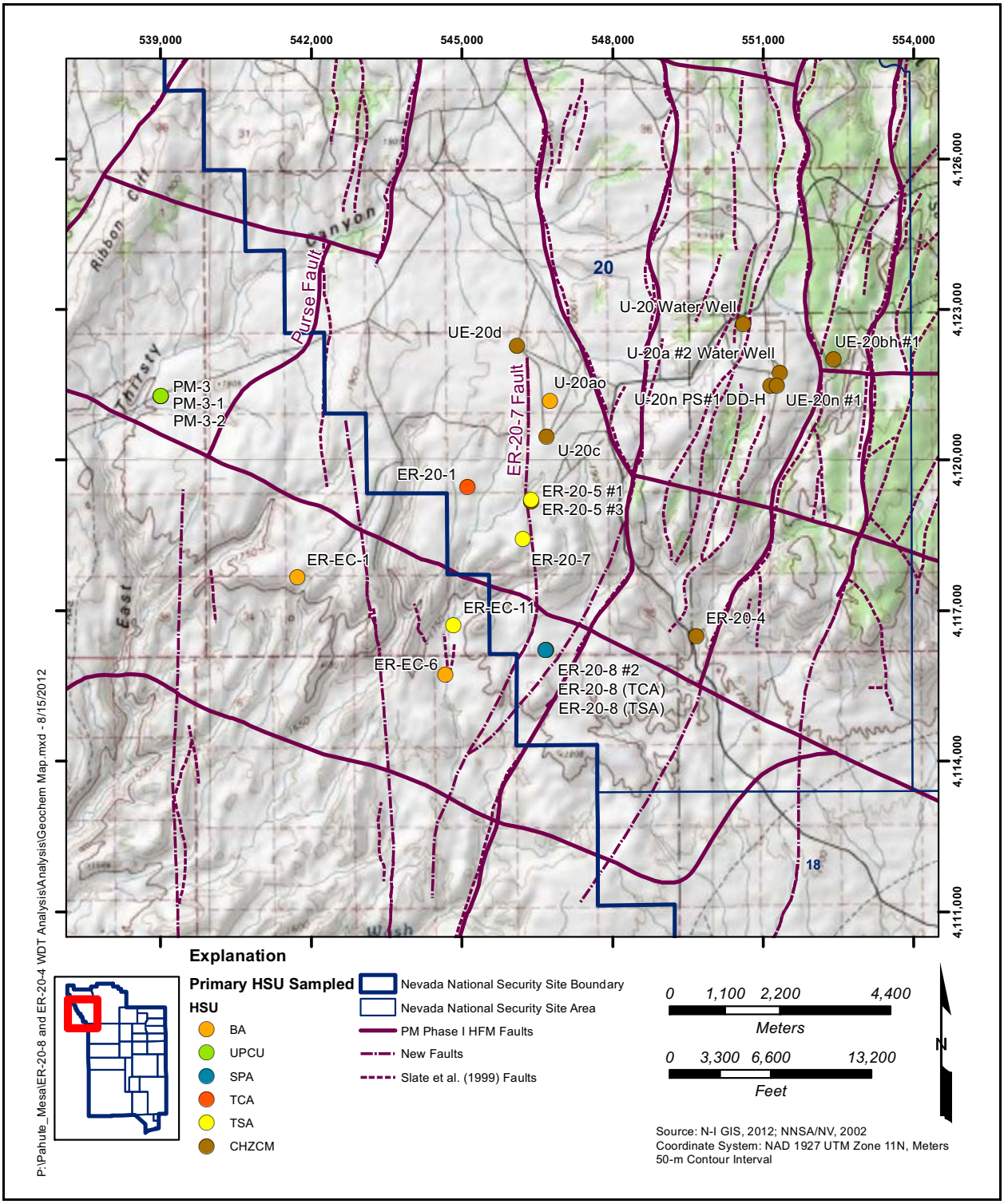

Figure 4-1
Wells Included in the Groundwater-Chemistry Evaluation

Note: The primary HSUs are as follows for wells that sample multiple completions: PM-3-1 (TCA), PM-3-2 (UPCU), ER-20-5 #1 (TSA), ER-20-5 #3 (CHZCM), ER-20-8 (SPA).

analyses not available from commercial laboratories in addition to analyses used to corroborate commercial laboratory results.

Water-quality measurements (temperature, pH, SEC, DO, and turbidity) were made on grab samples collected throughout WDT operations to ensure sufficient well development to obtain samples representative of the formation water (Section 2.0). Figures 2-2 through 2-4 demonstrate stabilization of the water-quality parameters before samples were collected for laboratory analysis. This stabilization, along with the low Br concentrations measured in the field and laboratory (0.048 to 0.26 mg/L), and the large purge volume, suggest the samples likely represent formation waters.

4.1.1 Well ER-20-8 TCA Completion

Depth-discrete bailer samples were collected from Well ER-20-8 within the TCA at depths of 2,700 ft bgs (August 11, 2009) and 2,800 ft bgs (May 26, 2011). The May 26, 2011, sample and duplicate were collected at the end of the step-drawdown test while the TCA was under production at 99 gpm and after pumping approximately 1.2 million gal. Wellhead samples were collected in duplicate on June 27, 2011, after pumping approximately 3.0 million gal (N-I, 2012b). The results for these analyses are presented in Table A.1-1 of Appendix A.

4.1.2 Well ER-20-8 TSA Completion

Depth-discrete bailer samples were collected from Well ER-20-8 within the TSA at depths of 3,160 ft bgs (August 11, 2009) and 3,170 ft bgs (July 22, 2011). The July 22, 2011, sample and duplicate were collected at the end of the step-drawdown test while the TSA was under production at 129 gpm and after pumping approximately 1.0 million gal (N-I, 2012b). Wellhead samples were collected in duplicate on August 8, 2011, after pumping approximately 1.9 million gal (N-I, 2012b). The results for these analyses are presented in Table A.1-2 of Appendix A.

4.1.3 Well ER-20-4

Depth-discrete bailer samples were collected from Well ER-20-4 within the CHZCM (1,870 ft bgs) and the CFCU (3,000 ft bgs) on September 7, 2010, and within the CFCU (2,750 ft bgs) on September 4, 2011. The September 4, 2011, sample and duplicate were collected at the end of the step-drawdown test while pumping at 234 gpm and after pumping more than 1.7 million gal. Wellhead samples were collected from deepest screened zone (CHZCM) in duplicate on September

20 and 21, 2011, after pumping more than 4.7 million gal (N-I, 2012a). The results for these analyses are presented in Table A.1-3 of Appendix A.

4.2 Results

The following section presents major-ion, stable-isotope, and radionuclide data for the samples collected from Wells ER-20-4 and ER-20-8 and from other wells in the vicinity. Depth-discrete and pumped wellhead samples from Wells ER-20-4 and ER-20-8 are included in the evaluation. The evaluation is limited to pumped wellhead samples collected during WDT operations for the rest of the UGTA wells (ER-EC-1, ER-EC-6, ER-EC-11, ER-20-7, and ER-20-8 #2); these samples are considered most representative of the formation water. The data included in this evaluation are presented in Appendix A. Tables A.1-1 through A.1-3 present results for Wells ER-20-4 and ER-20-8; Table A.1-4 presents results for Wells ER-20-7, ER-20-8 #2, and ER-EC-11; and Tables A.1-5 and A.1-6 presents all major-ion and stable isotope data used for this evaluation. The mean concentrations are reported for the wells with multiple samples available.

4.2.1 Major Ions

The dissolved constituents in groundwater provide a record of the minerals encountered as water moves through an aquifer; therefore, the major-ion characteristics of groundwater can provide insight on groundwater source areas and flow directions. A Piper diagram—illustrating the relative major-ion concentrations in groundwater from Wells ER-20-4 and ER-20-8 and from other wells in the vicinity—is presented in Figure 4-2. The major ions consist of calcium (Ca^{2+}), potassium (K^{+}), magnesium (Mg^{2+}), sodium (Na^{+}), chloride (Cl^{-}), sulfate (SO_4^{2-}), bicarbonate (HCO_3^{-}), and carbonate (CO_3^{2-}). The Piper diagram presents relative concentrations in percent milliequivalents per liter (%meq/L) and is used to classify various groundwater chemistry types, or facies, and illustrate the relationships that may exist between water samples. The relative concentrations of cations and anions are presented in the left and right triangles, respectively, and are projected onto the central diamond to present the combined major-ion chemistry (Figure 4-2).

The Piper diagram shows that Na+K dominates the cations in the study area groundwaters. The relative concentrations of anions are substantially more variable (Figure 4-2); the dominant anion in most samples is HCO_3, but significant relative concentrations of Cl^{-} and SO_4^{2-} also exist in many of the samples. The groundwaters vary from a Na+K-HCO_3 type (greater than 50 percent HCO_3^{-} as the

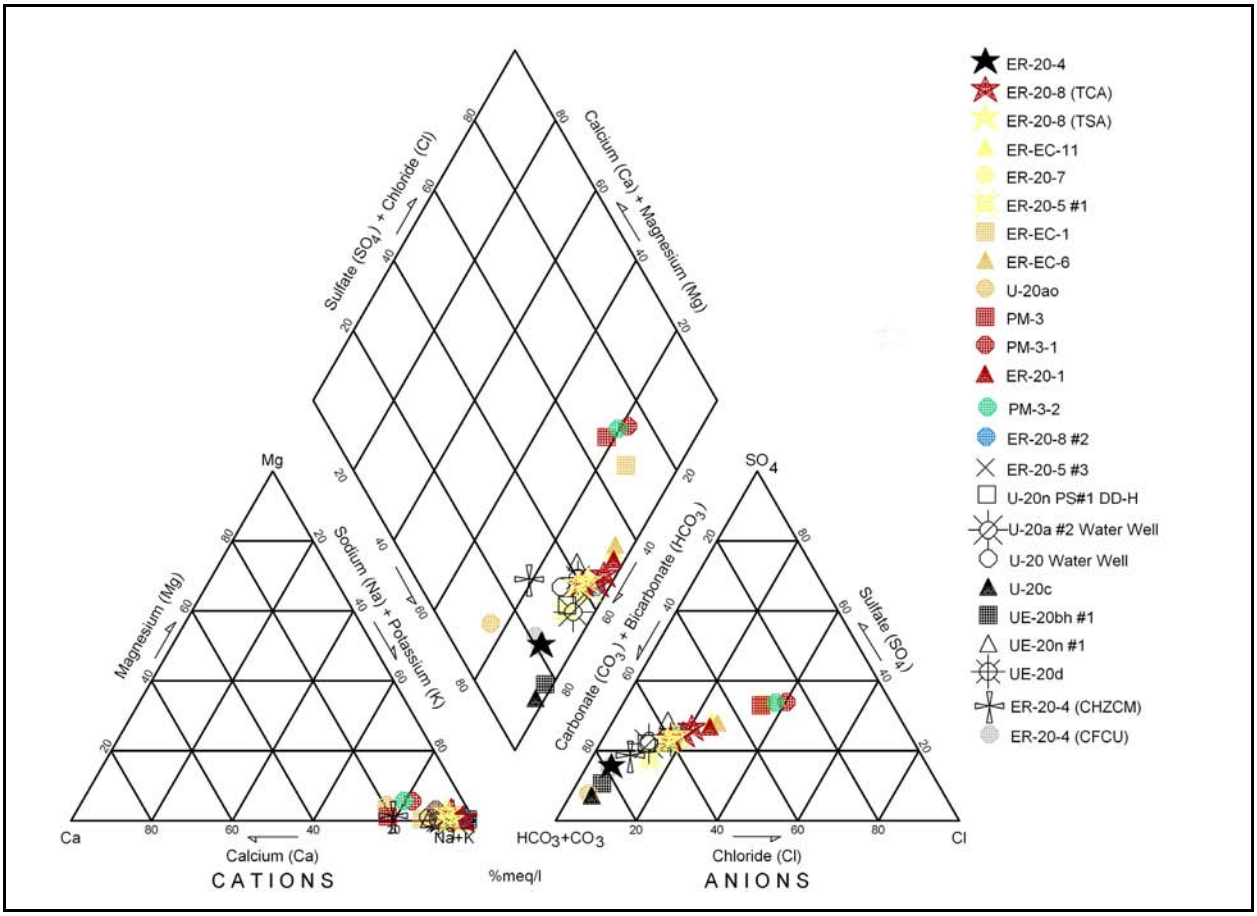

Figure 4-2
Piper Diagram Illustrating Groundwater Major-Ion Chemistry of Wells ER-20-4 and ER-20-8 and Wells in Their Vicinity

Note: Symbol colors represent the primary HSU: blue (TSA), yellow (SPA), orange (BA), green (UPCU), red (TCA), and black (CHZCM)

dominant anion) to a Na+K-HCO_3/SO_4/Cl type (relatively equal concentrations of the three anions are present). These groundwater types are characteristic of waters that have dissolved volcanic rhyolitic lava, ash-fall and ash-flow tuffs, and associated volcanic alluvium. The elevated levels of Cl and SO_4 are thought to result from interaction with hydrothermally altered zones; drill core and cuttings from wells in the area show evidence of hydrothermal alteration (NNSA/NSO, 2011a, b, and c).

The Well ER-20-8 depth-discrete and pumped wellhead samples (both TCA and TSA samples) plot quite similarly on the Piper diagram; the pumped wellhead samples are symbolized by stars in Figure 4-2. With the exception of the sample collected during drilling from the CHZCM, the ER-20-4 depth-discrete and pumped wellhead samples (both CHZCM and CFCU samples) plot quite similarly on the Piper diagram. An elevated Ca concentration is observed in the ER-20-4 sample collected

during drilling from the CHZCM, which is likely a result of the presence of cement and not representative of the formation. The high Br in this sample (7.9 to 8.0 mg/L) also indicates the presence of drilling fluids.

The Wells ER-20-4 and ER-20-8 groundwaters are a Na+K-HCO_3 type and lie within a rough trend line connecting the Na+K-HCO_3 and Na+K-HCO_3/SO_4/Cl type waters. The end members of this trend line consist of samples collected from the cluster of wells in the northeastern portion of the study area including UE-20bh#1, U-20ao, and U-20c (Na+K-HCO_3 type) and samples collected from the wells located west of the Purse fault, including Wells ER-EC-1 and PM-3 (Na+K-HCO_3/SO_4/Cl type).

Cl typically behaves conservatively in groundwater; it is highly soluble and does not participate in any common geochemical reactions at concentrations typical of NNSS groundwaters. Therefore, preliminary flow paths can be evaluated based on Cl concentrations. The Cl concentration in Well ER-20-8 samples ranges from 23 to 33 mg/L (TCA samples) and from 23 to 24 mg/L (TSA samples). The Cl concentrations are lower in the Well ER-20-4 groundwaters (4.6 to 9.0 mg/L); the Cl concentrations in the samples collected during drilling from the CHZCM are greater (8.9 to 9.0 mg/L) than other samples from this well (4.6 to 4.7 mg/L).

Figure 4-3 presents a spatial representation of Cl concentrations along with the primary HSU sampled. From Figure 4-3, some trends are apparent. For instance, the lowest Cl concentrations, ranging from 3 to 13 mg/L, are observed in wells located in the northeastern portion of the study area (i.e., east of the Well ER-20-7 fault) that sample the CHCZM HSU. This low Cl concentration is also observed in the Well ER-20-4 samples. The highest Cl concentrations, ranging from 84 to 112 mg/L, are observed in Wells ER-EC-1 and PM-3 located in Thirsty Canyon. Groundwater samples from the remaining wells (including Well ER-20-8) exhibit a range in Cl concentrations intermediate to these values and are potentially a mixture of groundwater from these two areas. These trends were described in the earlier investigations (Thomas et al., 2002; Kwicklis et al., 2005; and Rose et al., 2006). The inference from these results was that the relatively dilute groundwater from Pahute Mesa flows southwest toward Thirsty Canyon, where it mixes with more concentrated groundwater flowing from the north and west of the Purse fault. The results are consistent with the water-level gradients presented in Figure 3-1.

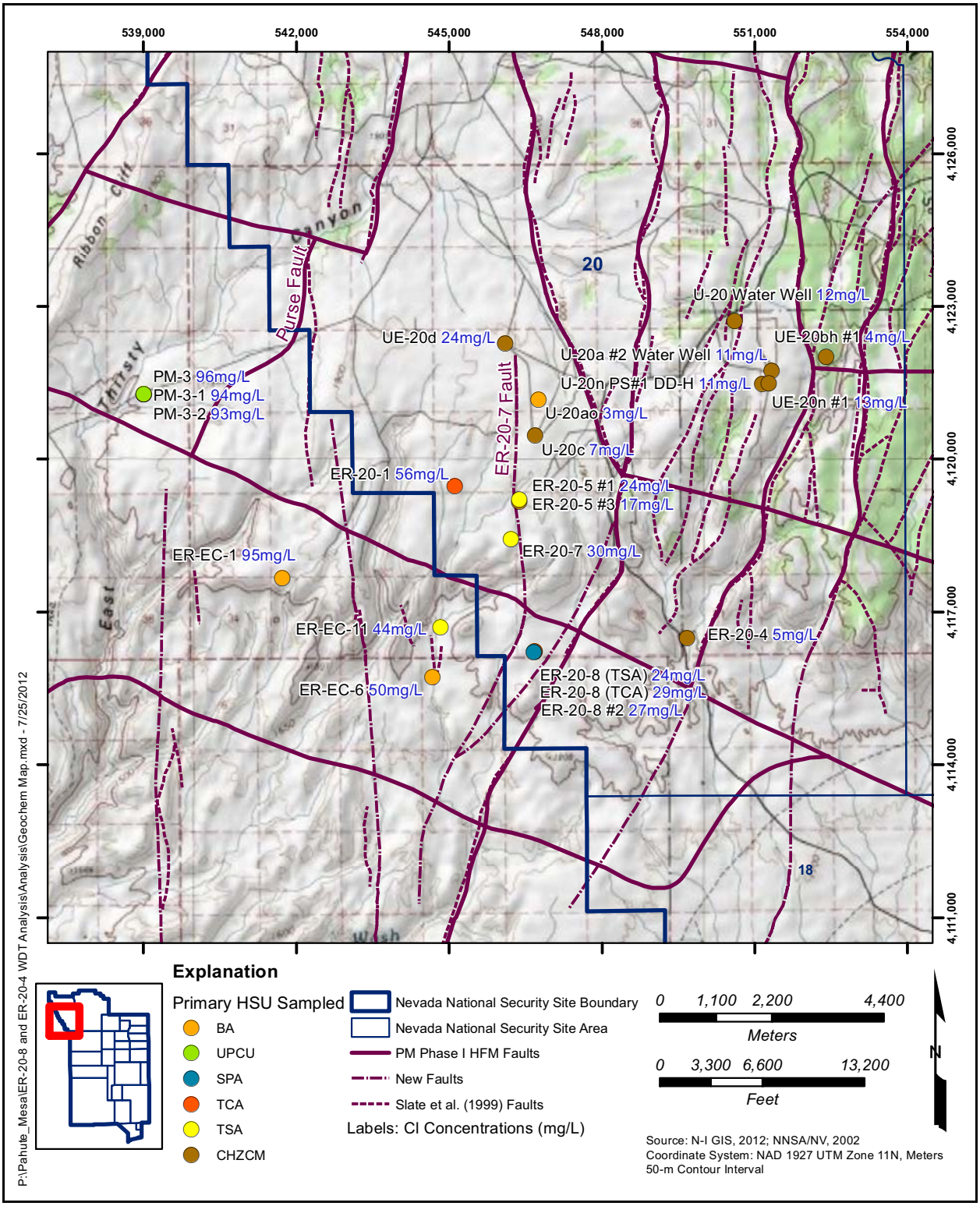

Figure 4-3
Spatial Distribution of Cl within the Study Area

Note: The primary HSUs are as follows for wells that sample multiple completions: PM-3-1 (TCA), PM-3-2 (UPCU), ER-20-5 #1 (TSA), ER-20-5 #3 (CHZCM), ER-20-8 (SPA).

4.2.2 Stable Isotopes

The stable isotopes of hydrogen ($^{2}H/^{1}H$ or $D/^{1}H$) and oxygen ($^{18}O/^{16}O$) are intrinsic to the water molecule and therefore behave conservatively in most groundwater systems. In the water cycle, these isotopes are fractionated (partitioned) between the liquid and vapor phases during evaporation and condensation processes. Once precipitation has infiltrated to the water table, the stable isotope values are unaffected by water-rock interaction at temperatures below approximately 100 °C (Criss, 1999). These isotopes are therefore used along with Cl as conservative tracers for evaluating groundwater origin and flow paths. Hydrogen and oxygen isotopes are conventionally reported as delta (δ) values representing permil (‰) variations in the isotope ratio of the sample relative to a reference standard.

Samples were analyzed for δD, $\delta^{13}C$, and $\delta^{18}O$ by DRI and LLNL (see Appendix A). In general, LLNL analyses tend to produce lighter δD and $\delta^{18}O$ values (deviating by as much as 3 ‰ for δD and 0.4 ‰ for $\delta^{18}O$) and heavier $\delta^{13}C$ values (deviating by almost 5 ‰). This is presently being evaluated by the respective laboratories. The accepted uncertainty is generally 2, 1, and 0.2 ‰ for δD, $\delta^{13}C$, and $\delta^{18}O$, respectively.

Plots of δD versus $\delta^{18}O$ and δD versus Cl are presented in Figures 4-4 and 4-5, respectively. The three data points for Wells ER-EC-1 and ER-EC-6 represent averages of the multiple samples collected for each of the three sampling events. Unfortunately, the number of wells with isotope data is less than those with major-ion data. For reference, the global meteoric water line (GMWL) defined by Craig (1961) and the local meteoric water line (LMWL) defined by Ingraham et al. (1990) are included (Figure 4-4). The meteoric water lines represent the observed correlations in $\delta^{18}O$-δD values of precipitation samples from around the world and from the NNSS, respectively. The GMWL is defined by the equation $\delta D = 8\delta^{18}O + 10$ (Craig, 1961), while the LMWL is defined by the equation $\delta D = 6.87\delta^{18}O - 6.5$ (Ingraham et al., 1990). All samples (except Well ER-20-7) plot well below the present-day global or local meteoric water lines, suggesting that the groundwater is mostly fossil groundwater unrelated to present precipitation (Merlivat and Jouzel, 1979).

No trend in $\delta^{18}O$ with HSU is apparent from Figure 4-4. A rough trend in δD and Cl with HSU, consistent with that observed in the Piper diagram, does exist (Figure 4-5). The samples collected from the northeastern portion of the study area (U-20a #2 Water Well, UE-20bh #1, U-20n PS#1 DDH, and UE-20n #1) tend to have the most enriched δD values (ranging from -115 to -110 ‰) and the lowest Cl concentrations (4 to 17 mg/L). Conversely, the lightest $\delta^{18}D$ and greatest

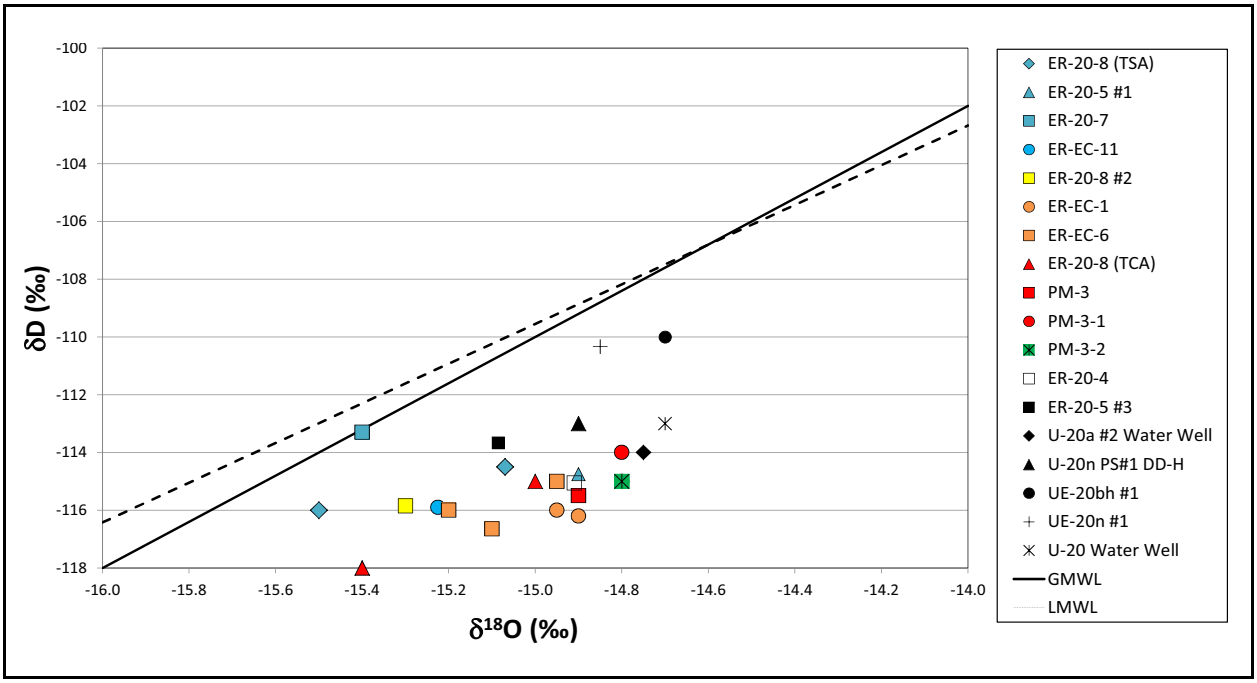

Figure 4-4
Plot of δD versus δ18O

Note: Symbol colors represent the primary HSU: blue (TSA), yellow (SPA), orange (BA), green (UPCU), red (TCA), and black (CHZCM).

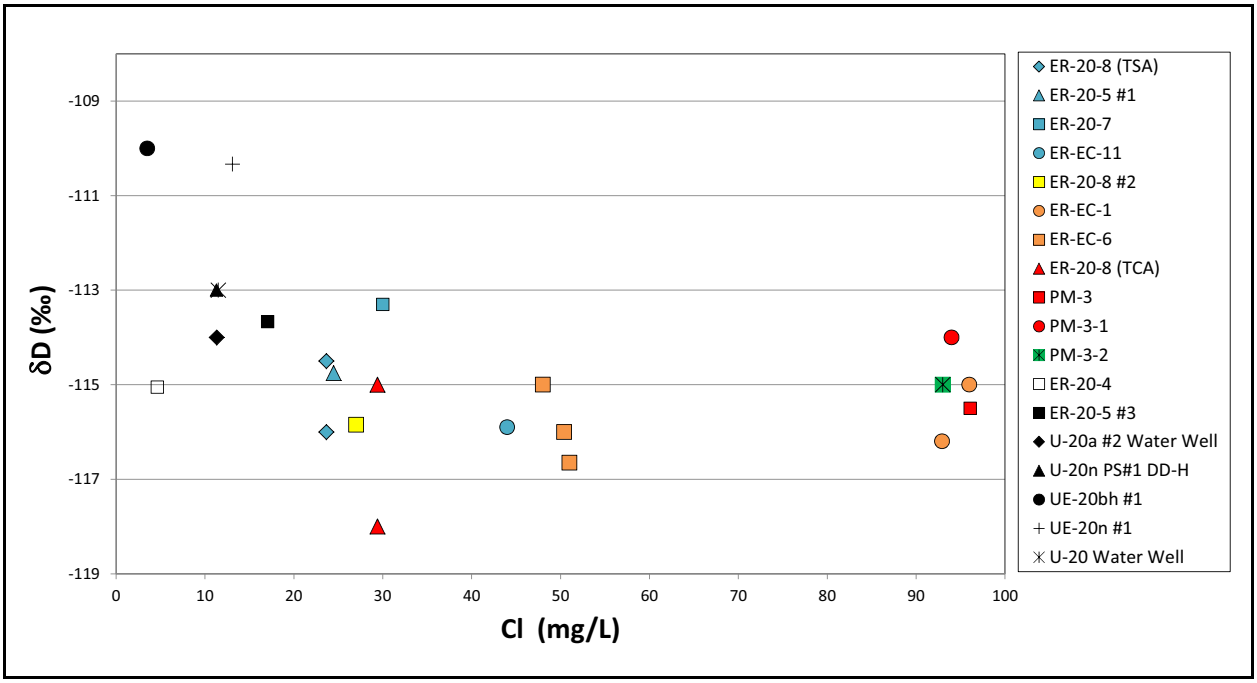

Figure 4-5
Plot of δD versus Cl

Note: Symbol colors represent the primary HSU: blue (TSA), yellow (SPA), orange (BA), green (UPCU), red (TCA), and black (CHZCM).

Cl concentrations are observed in the Thirsty Canyon wells located west of the Purse fault. The difference in the groundwater conservative tracer compositions on either side of the Purse fault suggests two distinct water masses occur in this area. Intermediate δD and Cl values immediately downgradient from this water-level discontinuity imply the two water masses are mixing.

The groundwater in the eastern portion of the investigation area may have a larger proportion of modern recharge, given that these samples are closer to the GMWL (Figure 4-4) and heavier in δD (Figures 4-4 and 4-5). This is consistent with higher recharge in the eastern portion of the Mesa compared with the western, and downward gradients in the eastern area (Blankennagel and Weir, 1973). It therefore appears that there may be some long-term climatic influences on the stable isotope data.

Kwicklis et al. (2005) applied the geochemical modeling code, PHREEQC, to groundwater chemistry data of Pahute Mesa to develop mixing models based on the conservative (Cl, SO_4, δD, and $\delta^{18}O$) and reactive (cations, dissolved silica, pH, alkalinity, and carbon isotopes [$\delta^{13}C$ and ^{14}C]) components in groundwater. Based on the PHREEQC models, Kwicklis et al. (2005) determined that groundwater at ER-EC-6 is composed of roughly equal amounts of groundwater from Well ER-EC-1 and U-20 Water Well, with a possible minor contribution of groundwater from the vicinity of UE-19h (located northeast of U-20 Water Well).

4.2.3 Radionuclides

Samples collected during WDT were analyzed for a suite of radionuclides included in the radiologic source term (Bowen et al., 2001). The radionuclides and their respective maximum contaminant levels (MCLs) are presented in Table 4-1 (CFR, 2012). This section presents the radionuclide data available to date for Wells ER-20-4 and ER-20-8. In addition, this section presents the radionuclide data for Wells ER-20-7, ER-20-8 #2, and ER-EC-11 WDT samples, including results reported subsequent to N-I (2011a).

In some cases, radionuclide analyses are performed using different methods, and analytical detection limits may vary considerably depending on the method. For instance, LLNL uses an accelerator mass spectrometer for ^{14}C, ^{129}I, and ^{36}Cl analysis that provides detection limits several orders of magnitude below the traditional methods of the commercial laboratory. Also, LANL reports results from a gamma spectrometer that provides simultaneous analysis of several radionuclides (^{40}K, ^{94}Nb, ^{99}Tc,

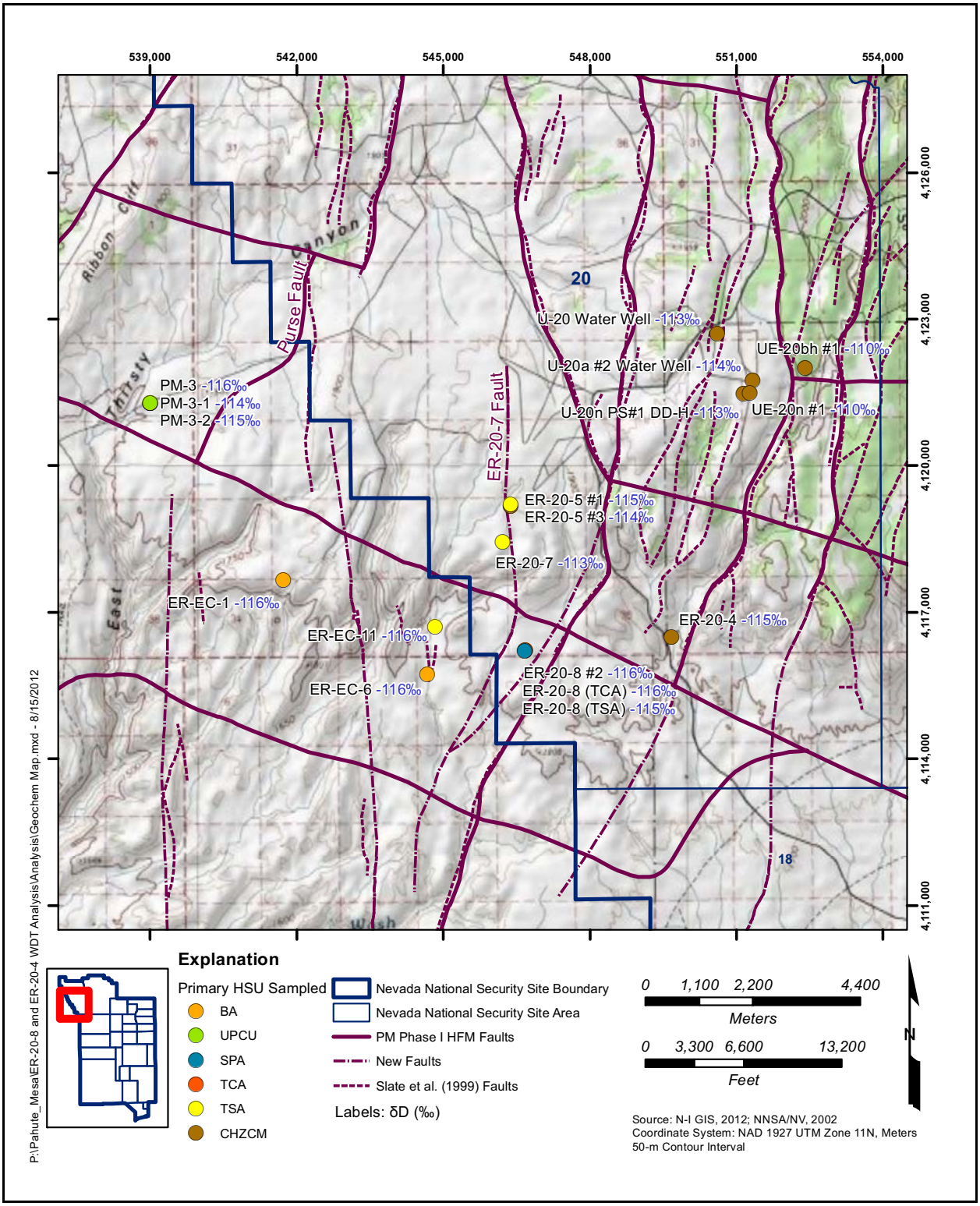

Figure 4-6
Spatial Distribution of δD within the Study Area

Note: The primary HSUs are as follows for wells that sample multiple completions: PM-3-1 (TCA), PM-3-2 (UPCU), ER-20-5 #1 (TSA), ER-20-5 #3 (CHZCM), ER-20-8 (SPA).

Table 4-1
Maximum Contaminant Levels

Radionuclide	MCL [a] (pCi/L)
Americium-241,243 (^{241,243}Am)	15
Carbon-14 (^{14}C)	2,000
Cesium-137 (^{137}Cs)	200
Chlorine-36 (^{36}Cl)	700
Curium-244 (^{244}Cm)	15
Europium-152 (^{152}Eu)	200
Europium-154 (^{154}Eu)	60
Iodine-129 (^{129}I)	1
Plutonium-239,240, 242 ($^{239,240,\ 242}$Pu)	15
Plutonium-241 (^{241}Pu)	300
Strontium-90 (^{90}Sr)	8
Technetium-99 (^{99}Tc)	900
Tritium	20,000

[a] Source: CFR, 2012

pCi/L = Picocuries per liter

Note: No *Safe Drinking Water Act* activity to dose factor is available for some radionuclides (e.g., niobium-94 [^{94}Nb], tin-121m [^{121m}Sn], ^{126}Sn, ^{150}Eu, holmium-166 [^{166}Ho], thorium-232 [^{232}Th], and neptunium-237 [^{237}Np]) included by Bowen et al. (2001) in the radiologic source term.

^{121m,126}Sn, ^{129}I, ^{137}Cs, ^{150,152,154,155}Eu, ^{166m}Ho, ^{232}Th, ^{233,234,236}U, ^{237}Np, $^{241,\ 242}$Pu, ^{241,243}Am, and ^{244}Cm) included in the radiologic source term (Bowen et al., 2001). Although their detection limits are often superior because of a sample concentrating method applied to their analysis, their detection limits for ^{129}I (30 to 40 pCi/L) and ^{99}Tc (20,000 pCi/L) are greater than those of the commercial laboratory, and LLNL methods designed specifically for their analysis. Although these detection limits are greater than the MCL for these radionuclides, the results are presented in Appendix A. Four radionuclides (^{237}Np, ^{241}Pu, ^{242}Pu, and ^{244}Cm) reported below a detection limit (80, 6 x 10^4, 600, and 1,000 pCi/L, respectively) greater than the MCL (Table 4-1) by LANL are not presented in Appendix A.

4.2.3.1 Well ER-20-8

Tritium was encountered in the fluid discharge samples collected while drilling the BA and SPA (N-I, 2010b). Because field tritium analysis was problematic, LLNL analyzed three samples (collected at depths of 2,270, 2,294, and 2,362 ft bgs) for tritium and anions. In addition, a composite sample containing equal parts from each sampling interval was analyzed for Pu using two methods (Zavarin, 2009). The tritium activities were reported to be 1,220 pCi/L (2,270 ft), 1,170 pCi/L

(2,294 ft), and 1,160 pCi/L (2,362 ft) and are attributed to the SPA HSU. Pu was not detected in the composite sample using either analytical method (detection limits were 0.01 and 0.002 pCi/L). The drilling fluids had relatively low Br concentrations (less the 0.1 to 2.1 mg/L), indicating that they were predominantly formation waters (Zavarin, 2009).

TCA Completion

Well ER-20-8 (TCA completion) tritium activities reported by the ALS Laboratory Group ranged from less than 240 to 3,020 pCi/L. Tritium activities were the greatest in the WDT samples (2,650 and 3,020 pCi/L) and the least in the depth-discrete samples collected at 2,700 ft bgs during drilling operations (less than 240 and 250 pCi/L). With the exception of $^{239, 240}$Pu in a single sample, all other radionuclides were reported as below the detection limit by ALS. Although a low $^{239, 240}$Pu activity (0.020 pCi/L) was reported in the sample collected on May 26, 2011, the value is less than the detection limit (0.008 pCi/L) plus the error (0.015 pCi/L), and is highly uncertain (i.e., it is likely that the result is an analytical artifact). Gross alpha activities ranged from 2.6 to 4.8 pCi/L, and gross beta activities ranged from less than 2.8 to 5.7 pCi/L (see Table A.1-1 of Appendix A).

LLNL reported a tritium activity of 2,813 pCi/L, indicating contaminant transport from underground nuclear testing. The ^{14}C activity, 0.197 pCi/L, is greater than observed in non-contaminated wells in this area but four orders of magnitude less than the MCL. Although present, the ^{129}I activity is low (2.06×10^{-4} pCi/L), and also over four orders of magnitude below the MCL. LANL reported that the majority of the gamma emitters were below their respective detection limits. ^{137}Cs was detected by LANL at a low level (0.17 and 0.10 pCi/L) in these samples. None of the analyzed radionuclides exceeded their MCL.

TSA Completion

Radionuclide activities for all Well ER-20-8 (TSA completion) samples were reported below their method detection limit by the ALS Laboratory Group. Gross alpha activities ranged from 1.7 to 7.4 pCi/L, and gross beta activities ranged from less than 2.3 to 6.9 pCi/L. These activities decreased as well development progressed (see Table A.1-1 of Appendix A). LLNL reported tritium, ^{14}C, and ^{129}I activities of 267, 0.0636, and 3.53×10^{-5} pCi/L, respectively, which are greater than observed in non-contaminated wells. LANL reported all gamma emitters below their detection limit.

4.2.3.2 Well ER-20-4

Tritium levels of discharged fluids at Well ER-20-4 were generally below the detection limits (N-I, 2011c). Radionuclide activities for all Well ER-20-4 depth-discrete and pumped wellhead samples were reported below their method detection limits by the ALS Laboratory Group. Gross alpha activities ranged from 2.0 to 10.1 pCi/L, and gross beta activities ranged from less than 2.3 pCi/L to 12.7 pCi/L. The gross alpha and beta activities decreased as well development progressed (see Table A.1-4 of Appendix A). LLNL reported tritium below a 142-pCi/L detection limit and a very low ^{129}I activity of 1.14×10^{-6} pCi/L. LANL reported all gamma emitters below their detection limit.

4.2.3.3 Well ER-20-7

Tritium activities in the Well ER-20-7 samples collected at the end of WDT, measured by ALS Laboratory Group and LLNL, ranged from 17.7 million to 19.1 million pCi/L. $^{239,240}Pu$ activities were reported as 0.062 and 0.070 pCi/L by ALS Laboratory Group, and as 0.10 pCi/L by LLNL. LLNL determined that the majority of the Pu (0.095 pCi/L) was associated with colloids. ^{99}Tc was reported by the ALS Laboratory Group as 13.4 and 16.4 pCi/L for the duplicate samples; detection limits were reported as 6.1 and 6.0 pCi/L, respectively (LLNL did not report a ^{99}Tc activity). ^{90}Sr was reported by the ALS Laboratory Group as 1.47 ± 0.43 pCi/L and 1.52 ± 0.45 pCi/L for the duplicate samples; detection limits were reported as 0.31 and 0.32 pCi/L, respectively. The presence of ^{90}Sr is presently being verified by LLNL; the low values are near the detection limit and are considered highly uncertain.

LLNL reported ^{129}I, ^{14}C, and ^{36}Cl as 0.132, 165, and 2.41 pCi/L, respectively. Although these elevated activities indicate transport of these radionuclides (^{14}C, ^{36}Cl, ^{99}Tc, ^{129}I, and Pu) away from the underground test, tritium is the only radionuclide that exceeded the MCL in these samples (Table 4-1). The Pu isotope measurements of LLNL suggest that the Pu contamination is attributed at least in part to the BENHAM test (N-I, 2011a).

4.2.3.4 Well ER-20-8 #2

Tritium activities in the Well ER-20-8 #2 samples collected at the end of WDT, measured by ALS Laboratory Group and LLNL, ranged from 880 to 1,280 pCi/L. No other radionuclides were detected by the ALS Laboratory Group. LLNL reported activities of ^{129}I, ^{14}C, and ^{36}Cl above background levels

(9.27 x 10^{-5}, 0.134, and 2.09 x 10^{-3} pCi/L, respectively), indicating transport away from the underground test site (see Table A.1-4 of Appendix A). ^{99}Tc was not detected above a 0.1 pCi/L detection limit. No radioisotopes exceeded the MCL in these samples (Table 4-1).

Zavarin (2012a) points out that ^{14}C is enriched relative to tritium (relative to the Bowen et al. [2001] inventory) at leading edges of plumes (Wells ER-20-8, ER-20-8 #2, and ER-20-5#3) while they are depleted in locations with high tritium (Wells ER-20-5#1 and ER-20-7). He also states that this is consistent with the evolving conceptual model of a broader redistribution of ^{14}C relative to tritium due to hydrothermal test-related effects and possible gas-phase redistribution.

4.2.3.5 Well ER-EC-11

No radionuclides, including tritium, were detected by the commercial laboratory (ALS Laboratory Group) in the Well ER-EC-11 WDT samples. The majority of radionuclides analyzed by LLNL, including tritium, were reported below the detection limit (see Table A.1-4 of Appendix A). The ^{14}C and ^{36}Cl activities reported by LLNL (0.043 and 8.1 x 10^{-4} pCi/L, respectively) were consistent with background levels.

While no tritium was observed in the TCA or TSA (formations sampled during WDT) at this location, tritium activities ranging from 9,800 to 10,100 pCi/L were reported for depth-discrete samples collected from the FCCU, BA, and UPCU (i.e., 2,450, 2,750, and 3,150 ft bgs) after drilling was complete. Tritium was below the detection limits in similar depth-discrete samples collected from the TCA and TSA (i.e., 3,285 and 3,755 ft bgs).

5.0 DRAWDOWN ANALYSIS

5.1 Geological Conceptual Model

During WDT activities at Wells ER-20-4 and ER-20-8, hydraulic responses were observed at and water samples taken from wells in welded ash-flow tuffs and rhyolitic lavas (i.e., welded tuff aquifers [WTAs] and LFAs) in southwestern Pahute Mesa and the Bench (Figure 1-1). In order to provide a unifying interpretative framework, a geologic conceptual model was developed. The lavas and ash-flow tuffs were laid down by sequential volcanic eruptions. The distribution of permeability in these aquifer units reflects a complex history of eruptive and cooling processes that have been overprinted by regional tectonic activity. The fractured volcanic aquifers are separated by layers of tuff confining units that are typically low-permeability ash-fall tuffs that have become zeolitic in the saturated zone, and whose properties can be altered by faulting (BN, 2002; Prothro et al., 2009; Sweetkind and Drake, 2007; Fenelon et al., 2010).

LFAs in the Bench area are composed of rhyolitic lavas. These are highly viscous, silicic lava flows that erupt from local vents or fissures and form relatively thick steep-sided flows that typically have thickness to lateral extent ratios considerably greater than more fluid volcanic deposits such as ash-flow tuffs and basalt. Phase II drill-hole data have refined the extent of Paintbrush lava flows in the area (NNSA/NSO, 2010a and b; and 2011a) to differentiate three separate, overlapping rhyolitic lava flows that increase in age from west to east. Stratigraphically, from oldest to youngest, these rhyolitic lava flows are the rhyolite of Scrugham Peak (Tps), rhyolite of Benham (Tpb), and rhyolite of Comb Peak (Tpk). Interim interpretation of the extents of the lavas is shown in Figure 5-1; they are conceptualized as disrupted at the NTMMSZ margin. The three rhyolitic lava flows have been designated hydrostratigraphically as the Comb Peak aquifer (CPA), BA, and SPA and, as mentioned above, are separated from one another by layers of tuff confining unit. The three LFAs are thought to have similar hydrologic properties because they are related to the same eruptive cycle, are very similar mineralogically, and exhibit the same basic internal architecture consisting of five distinct lithofacies. Figure 5-2 illustrates the general conceptual model of a rhyolitic lava, and the relation

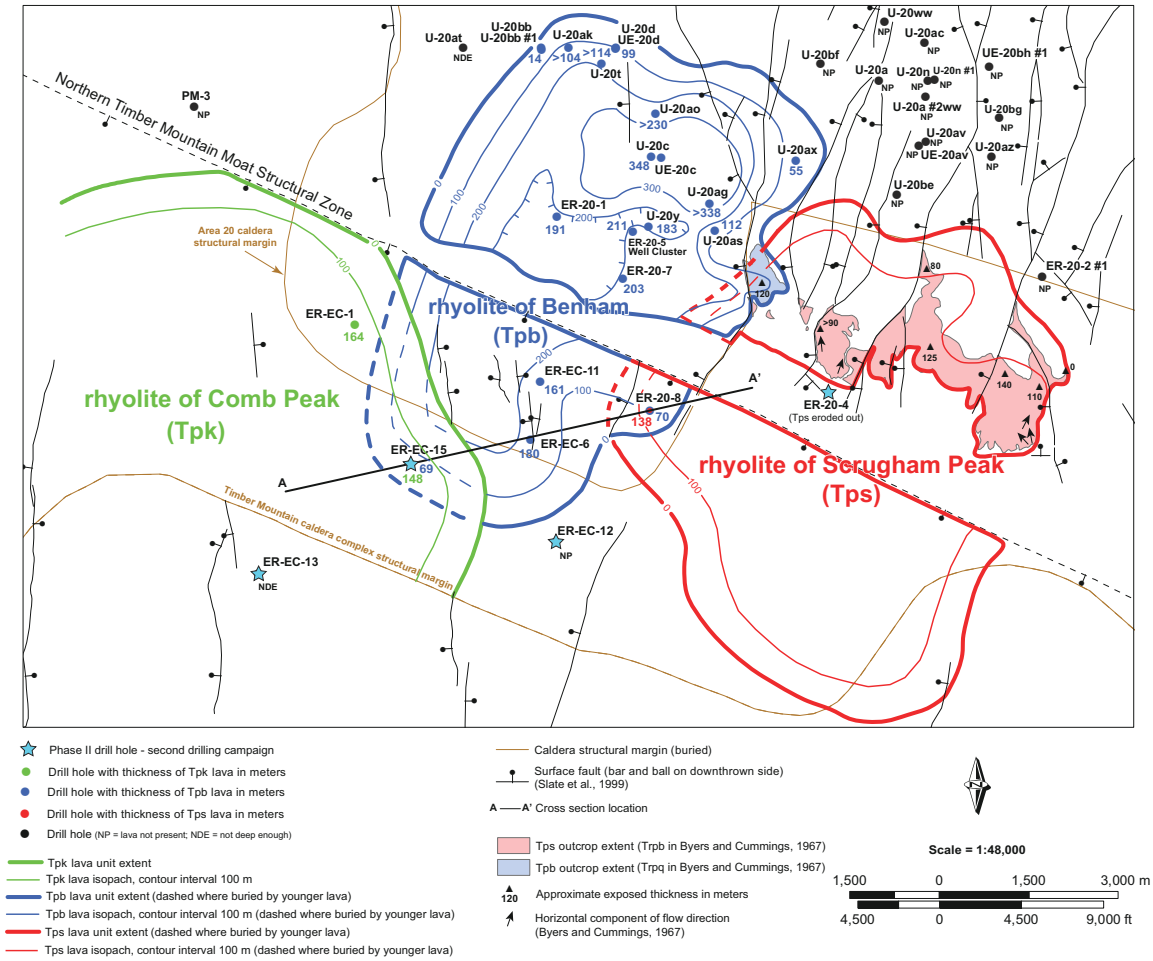

Isopach Maps of Post-Tpc Paintbrush Group Lavas, Southwestern Pahute Mesa
(NSTec, 04/27/2012)

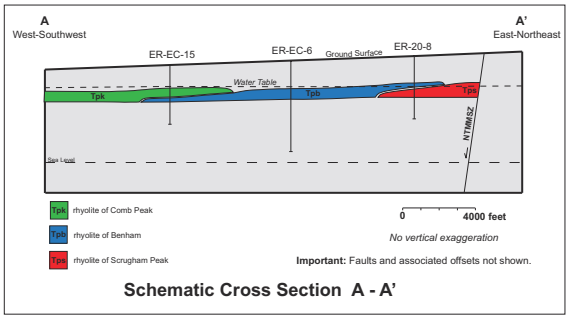

Schematic Cross Section A - A'

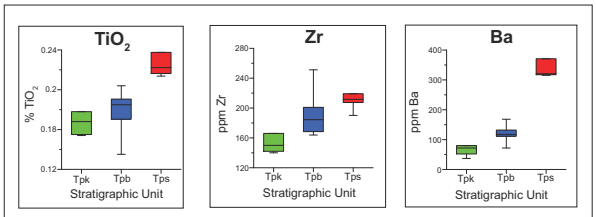

Trace Element Analyses for Post-Tpc Lavas in Southwestern Pahute Mesa Showing Chemical Differences between the Three Lava Flows

Figure 5-1
Extent of LFAs in Southwest Area 20
Source: Modified from Drellack, 2011a

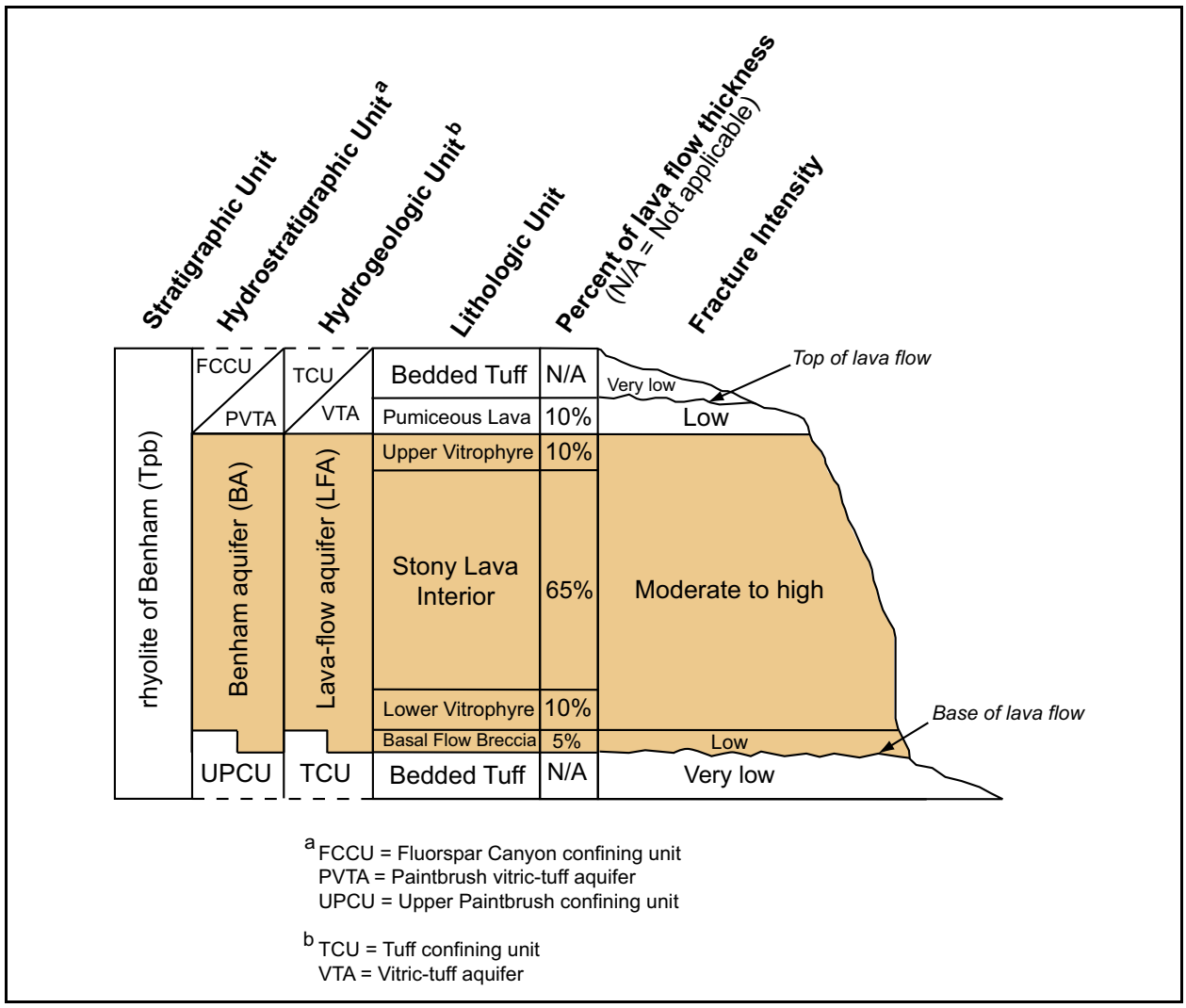

Figure 5-2
Conceptual Hydrologic Model of a Rhyolitic LFA
Source: Modified from Drellack, 2010a

between lithology and hydrologic conceptual model. From top to bottom, these lava lithofacies are as follows:

1. *Pumiceous lava cap.* Porous and poorly fractured; included in the overlying tuff confining layer where zeolitic.

2. *Upper vitrophyre.* Fractured with very low primary porosity.

3. *Stony lava interior.* Fractured with double porosity.

4. *Lower vitrophyre.* Fractured with very low primary porosity.

5. *Basal flow breccia.* Porous with lower fracture intensity than seen in the vitrophyre or stony interior. Depending on degree of alteration, this may or may not be included within lava-flow aquifer.

The Calico Hills formation (Th) (named the CHZCM in the Phase I HFM [BN, 2002]), in which Well ER-20-4 is completed, is a complex distribution of zeolitized bedded and nonwelded tuff and rhyolitic lava deposits. There appears to be at least three intervals of LFAs separated by zeolitic aquitards. The overall percentage of the Calico Hills that is lava averages about 50 percent, and can range from 20 to 70 percent (by thickness) (Prothro and Drellack, 1997). Blankennagel and Weir (1973) make the following hydrogeologic observations about the Calico Hills formation (Th):

> In most of the drill holes in the eastern part of the caldera, where Paintbrush rhyolitic lava flows comprise 90 to 100 percent of the rock section in the saturated zone, heads are relatively stable through depths ranging to 2,500 feet below the top of the saturated zone; heads decrease, or probably decrease, below these relatively stable intervals to total drilled depth.
>
> Where the percentage of rhyolitic lava flows decreases, head changes with depth in drill holes are less pronounced, and a transition zone between decreasing heads with depth and increasing head with depth is approached. A reduction in vertical permeability occurs where lava flows interfinger with tuffs. Hence, vertical permeability is a major factor controlling the pattern of head changes with depth beneath Pahute Mesa.
>
> The rhyolitic lavas in the western and central parts of the caldera are lenticular bodies of variable thickness. These lava flows are separated by thick sections of ash-fall and ash-flow tuffs that have low permeabilities. The tuffs are relatively incompetent and, hence, are more sensitive than the rhyolitic lavas to compression by weight of rock overburden. Fractures are more likely to be resealed, volume and porosity are reduced, and pressures are increased. Vertical permeability in some areas may be low enough to create confined aquifers.
>
> In holes drilled in the western and central parts of the caldera, heads usually are variable from the top of the saturated zone through intervals of rhyolitic lava flows that have high permeabilities and then increase with depth to the total drilled depth. Ground-water flow is essentially lateral with upward leakage.

These observations imply a system where the discontinuous lavas refract and concentrate groundwater flow along the flow path, with the lower permeability, more continuous encapsulating zeolitic tuffs (i.e. TCU) controlling the flow and transport between lavas laterally and vertically. The Calico Hills lavas are not from the same source as those on the Bench, but the same conceptual model is believed to hold.

In contrast to rhyolitic lavas, ash-flow tuffs are highly fluid pyroclastic deposits emplaced very quickly as the eruption column of a large volcanic eruption collapses. The resulting high-temperature density currents consisting of ash, pumice, mineral crystals, and rock fragments flow out at high rates away from the volcano. Many large-volume ash-flow tuffs are related to caldera formation, when the land surface around the erupting volcano collapses rapidly as the underlying magma chamber is depleted. Caldera-forming ash-flow tuffs can accumulate to great thicknesses within the subsiding portions of calderas. Outside the caldera, the same large-volume, caldera-forming ash-flow tuff is typically much thinner, with thickness to lateral extent ratios considerably less than more viscous volcanic deposits like rhyolitic lavas.

Ash-flow tuffs typically have an internal architecture defined by zones of varying degrees of welding with welding typically increasing inward toward the interior of the ash flow. This welding process occurs as the flow cools and compresses after emplacement. Thermal contraction during the cooling and welding processes results in the formation of cooling joints within the welded portions of the flow, particularly at the top and bottom. This forms the initial fracture network from which the permeability of the rock is derived—the permeability of the matrix is orders of magnitude lower because of the welding. Figure 5-3 illustrates the general conceptual model of a non-lithophysal ash-flow tuff; the initial basis for this conceptual model is the work of Winograd (1971). Lithophysae, small cavities caused by expanding gases before solidification, form if gas is entrapped in the center portion of the unit.

Two saturated welded ash-flow tuffs, the Tiva Canyon tuff (Tpc) and older Topopah Spring tuff (Tpt), are present in drill holes in southwestern Pahute Mesa and the Bench. Both represent outflow sheets from caldera sources located south of the Bench. These two welded ash-flow tuffs form WTAs and have been designated hydrostratigraphically as the TCA and TSA. Although both are WTAs, they differ in internal architecture, particularly with regards to the distribution of fractures and lithophysae. The TCA contains prominent and well-developed lithophysal zones within its interior, resulting in fractures concentrated at the top and bottom of the flow and few fractures in the lithophysal interior (Prothro et al., 2009; Prothro, 2009 and 2010a). The TSA lacks well-developed lithophysal zones at Pahute Mesa, and borehole image logs indicate that fractures are distributed more evenly throughout the aquifer (Prothro et al., 2009; Prothro, 2009 and 2010a).

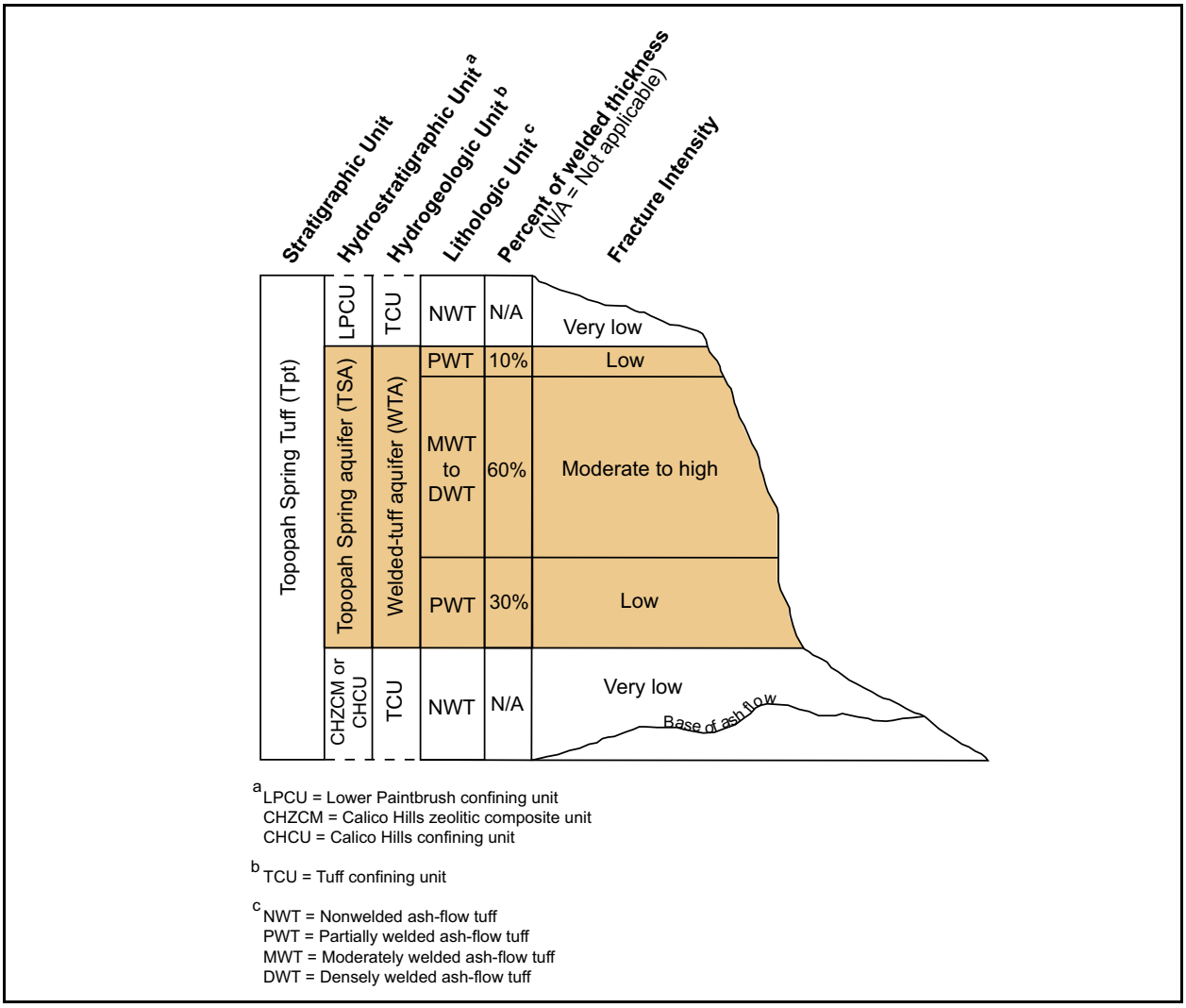

Figure 5-3
Preliminary Conceptual Model of the TSA in Southwestern Pahute Mesa Area
Source: Modified from Drellack, 2010b

For hydrologic purposes, rocks are categorized by their ability to transmit water (e.g., aquifer or aquitard) rather than stratigraphically as shown in Figures 5-2 and 5-3. As a result, the nonwelded and pumiceous portions of ash-flow tuffs that undergo zeolitic alteration in the presence of water are included in adjacent tuff confining units. This results in the interleaved sequence of aquifers and aquitards seen in cross section (BN, 2002; Fenelon et al., 2010).

Blankennagel and Weir (1973) summarized results of 297 hydraulic, mostly drill stem (slug) tests, performed on various volcanic rocks on Pahute Mesa. The zeolitized bedded tuff had the consistently lowest hydraulic conductivity (relative specific capacity), followed by the welded tuff, and then rhyolitic lava, which had considerable scatter in values.

The presence of aquitards between aquifers would conceptually restrict vertical communication resulting in vertical head changes through the geologic section, a feature noted by Blankennagel and Weir (1973). However, one of the striking features of this area is the presence of faults and other large structures. Caine and Forster (1999) proposed a fault conceptual model that includes fault gouge and damage zones of altered permeability that result in a range, depending on the proportions of each component, of hydraulic behavior. Sweetkind and Drake (2007) noted that damage zones tend to scale with fault offset in volcanic rocks in Yucca Flat, and damage zones associated with large-offset faults (greater than 100 m) are many tens of meters wide, whereas damage zones associated with smaller offset faults are generally only a meter or two wide. They also noted that zeolitized tuff develops moderate-sized (on the scale of meters) damage zones. Prothro et al. (2009) also studied faults at the NNSS and observed the following: (1) faults often form discrete zones; (2) more recently active faults probably form permeable fault zones where they cut stronger rocks such as welded tuff and lava; (3) faults that intersect TCU form zones of enhanced permeability, relative to TCU protolith, although of less absolute permeability than those in welded tuff and lava; (4) fault cores were observed to be relatively thin, and thus are unlikely to form a complete and continuous barrier everywhere along the fault; and (5) any enhanced fault-zone permeability will be generally controlled by fractures that will be subparallel to the strike of the fault resulting in anisotropic permeability. Blankennagel and Weir (1973) suggested that well yields could be enhanced in rocks otherwise unfavorable for pumping near large structures because of fault damage zone enhanced permeability. Geldon (2004) notes that, at Yucca Mountain, faults that cut tuffaceous rocks tend to locally enhance permeability. Due to the structural complexity, one of the goals of the Phase II characterization work is to better inform the geologic model of the area by incorporating feedback from hydrologic data. *That is, are the geology and hydrology consistent?* Figure 5-4 shows a preliminary fault distribution interpretation that will be considered in the analysis of well-test interference data that follows.

In summary, an initial flow system conceptual model would have the following features:

- Multiple flow systems revealed by clear vertical head differences—because the mineralogy of the rocks is quite similar, natural geochemical differences may not be distinguishable.
- Areally extensive drawdown responses in the laterally extensive welded tuffs, potentially even when formations are completely offset by faults (if the faults themselves are conduits).

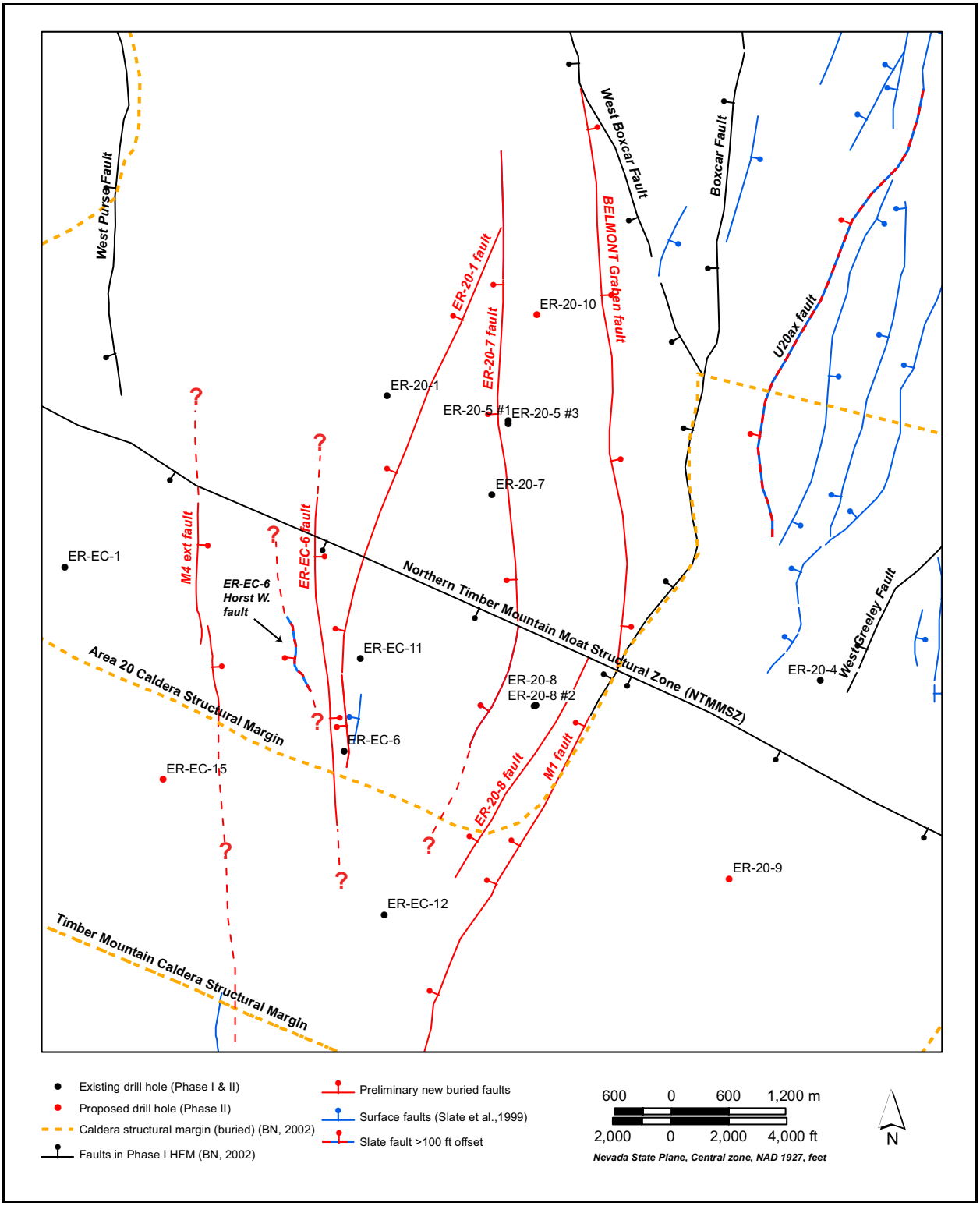

Figure 5-4
Preliminary Structure Map for Southwest Pahute Mesa
Source: Modified from Drellack, 2011b

- Localized responses in the limited extent LFAs, unless otherwise connected by permeable faults or offset to other permeable rocks to rupture the zeolitic tuffs that tend to encase the lavas.

- Fault structures through aquitards allowing vertical connections between otherwise laterally and vertically separated aquifers.

5.2 Single-Well Test Analysis

The response of wells to pumping provides key information about formation properties and flow regime. The analysis of drawdown transient data begins by reviewing the data with the log-log drawdown and drawdown derivative diagnostic plot in order to identify responses that are characteristic of certain types of flow regimes, and also to identify how changes over time further refine conceptual understanding (Horne, 1995). These changes are evaluated in the context of the geologic conceptual model.

5.2.1 Well ER-20-8 TCA Pumping

The TCA completion of Well ER-20-8 was pumped at about 140 gpm from June 18 to June 27, 2011. The check valve malfunctioned when the pump was turned off, and water levels rebounded as the water in the production casing (up to a 1,600-ft water column above static water level [SWL]) reentered the formation. Thus, the recovery data were not analyzed.

The log-log diagnostic plot (Figure 5-5) shows the ending of the wellbore storage period with some oscillatory behavior between 0.0001 and 0.001 days. Using the “1.5-cycle” rule (Horne, 1995), the beginning of infinite acting radial flow would begin at approximately 0.005 days—the data recording rate was not fast enough to make this determination, but it is clear that by 0.01 days the rate of drawdown is approximately constant. Beginning at about 0.2 days, the rate of drawdown increases to a new plateau at about 0.4 days, followed by another change in slope beginning at about 1.5 days and continuing through the end of pumping. There was some slight upward drift in pumping rate between about 0.15 and 0.3 days that reasonably accounts for the first break in slope and the resulting plateau. No obvious operational issues were discovered that account for the increase in the rate of drawdown after 1.5 days, and it was concluded that this effect was geologic in nature. An initial fit with Barker’s (1988) interpretative model incorporated wellbore storage, skin, and radial flow illustrates the sparse data for diagnosing the end of wellbore storage and the systematic misfit resulting from the assumption of purely radial flow after 1 day (Figure 5-5). An impermeable linear feature causes the

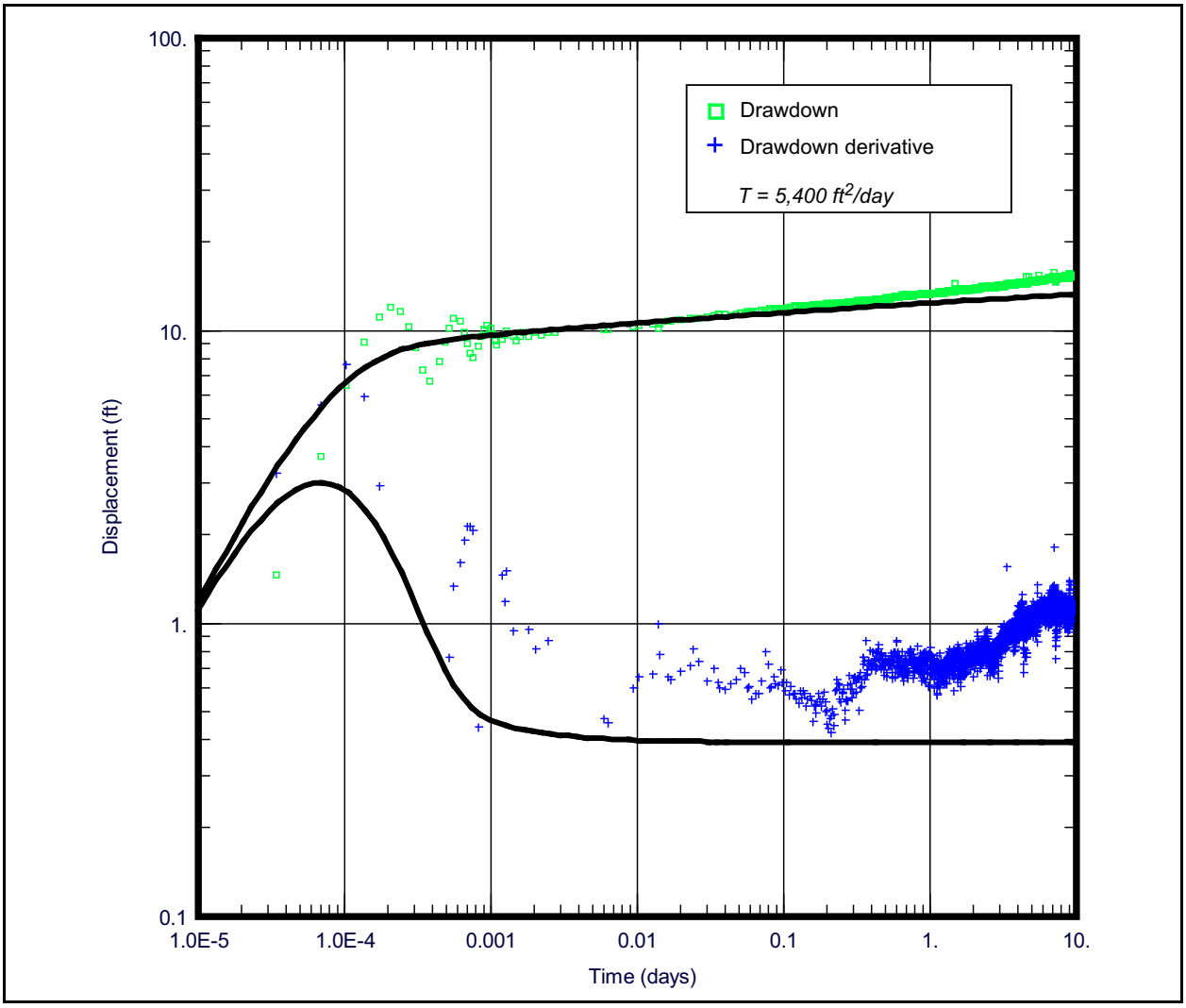

Figure 5-5
Initial Log-Log Diagnostic Plot of Well ER-20-8 TCA Constant-Rate Test

slope of drawdown to double (Horne, 1995). A doubling of the slope is not observed, but the effect (if real) may not have been fully revealed by the end of the test.

To refine the initial transmissivity estimate (5,400 square feet per day [ft^2/day]) a Cooper-Jacob analysis was performed on the data between 0.3 and 2 days, when the flow regime could reasonably be interpreted to be infinite acting and radial, and is shown in Figure 5-6.

The systematic deviation after about 3 days can be clearly seen. To further investigate, a linear impermeable boundary was added to the solution. The results of the fit with a boundary at 6,000 ft from Well ER-20-8 are shown in Figure 5-7—clearly with an extra parameter, the fit is improved at

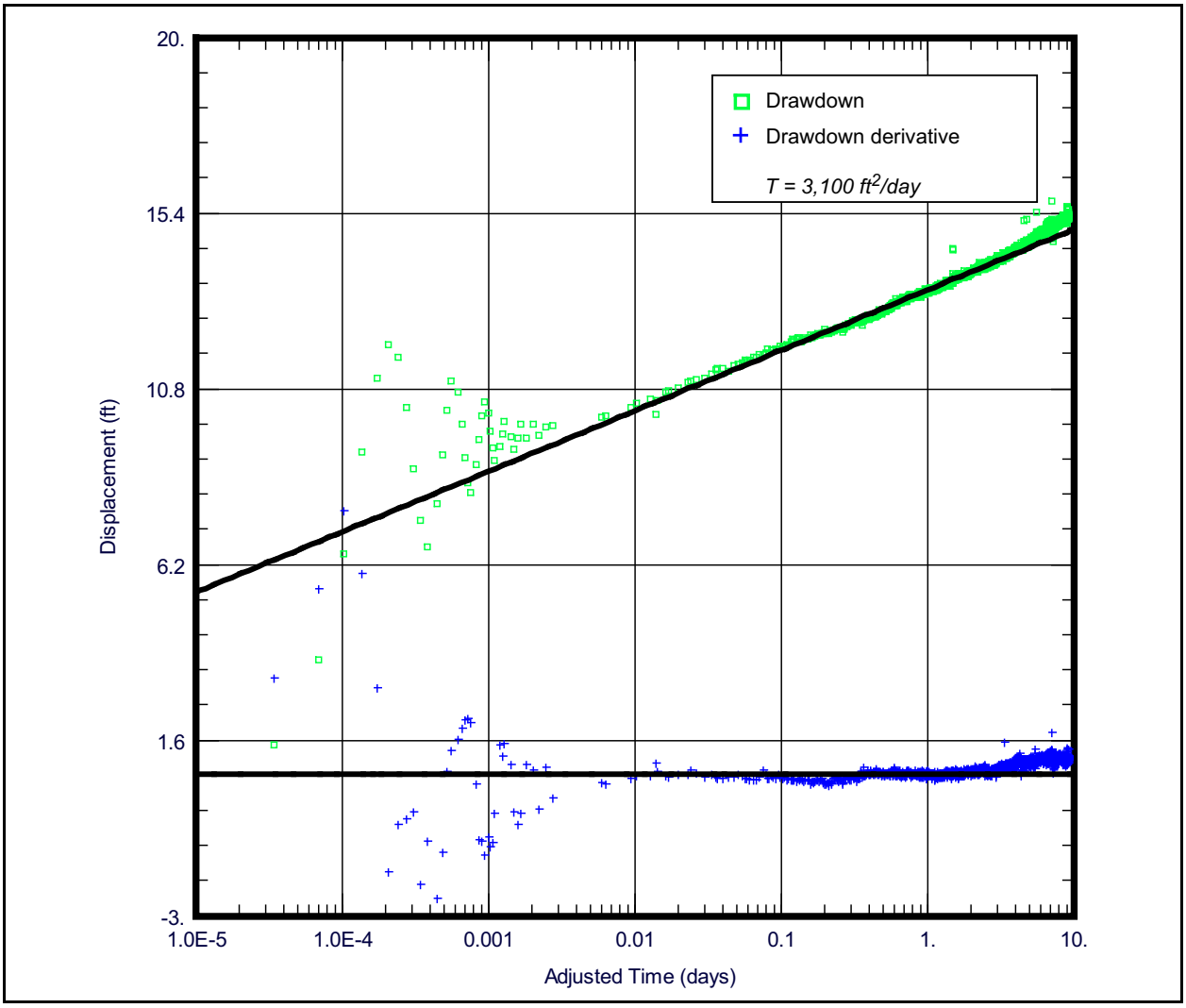

Figure 5-6
Cooper-Jacob Interpretation of Well ER-20-8 TCA Constant-Rate Test

all but the earliest times (this model does not incorporate wellbore storage); the difficulty lies in deciding on the geologic plausibility. The radii of investigation of a pumping test are

$$r_{inner} = \sqrt{0.1Tt/S} \qquad (5\text{-}1)$$

and

$$r_{outer} = \sqrt{14.8Tt/S} \qquad (5\text{-}2)$$

where

T = transmissivity (L^2/T)
S = storativity (-)
t = elapsed time (Streltsova, 1988)

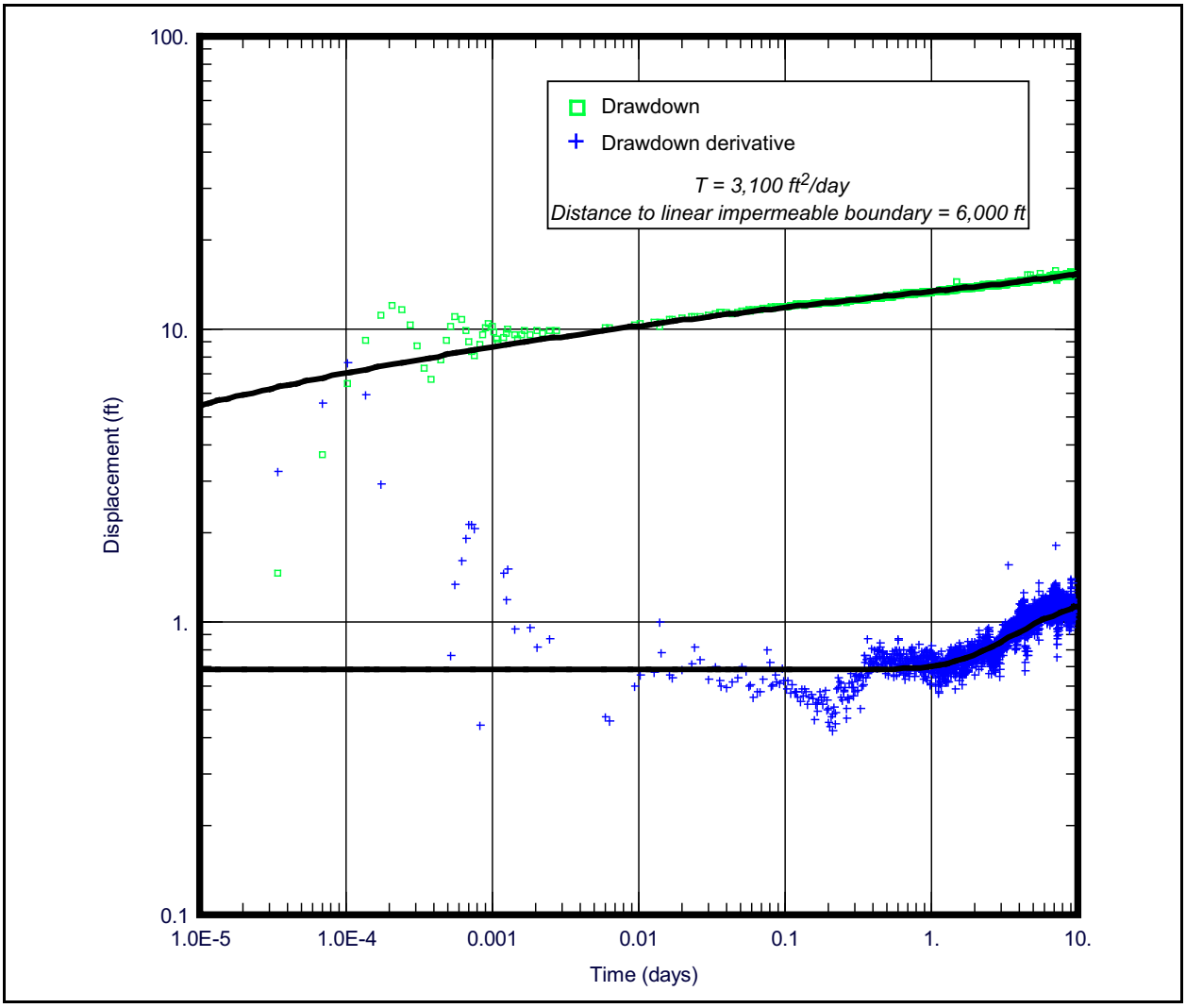

Figure 5-7
Theis with a Linear No-Flow Boundary Interpretation of Well ER-20-8
TCA Constant-Rate Test

Storativity is not reliably estimated from single-well tests (Horne, 1995); thus, other data are needed to estimate the radii of investigation. Halford et al. (2010) assumed a specific storage (S_s) of 2×10^{-6} 1/ft, which gives an S of 9×10^{-4} for the tested interval. IT (1998) estimated S_s from about 5.6×10^{-7} 1/m (1.7×10^{-7} 1/ft) to 2.8×10^{-6} 1/m (8.5×10^{-7} 1/ft). Using 5×10^{-7} 1/ft (S of 2.3×10^{-4}), r_{inner} and r_{outer} are 1,900 and 23,000 ft, respectively. For reference, the NTMMSZ is about 2,000 ft from ER-20-8. As shown in Figure 5-4, there are numerous faults within 6,000 ft. However, to date most interpretations of fault behavior are that they form connections for drawdown via juxtaposition (Halford et al., 2010), or may be conduits for flow (N-I, 2011a), not barriers. Alternatively, any strong change in aquifer properties would give the appearance of a no-flow boundary. This change may not

be located at 6,000 ft from the well; it is just that the assumption of a no-flow creates the proper effect when located at this distance—more geologic information is required to identify the cause of this feature, and its presence should be considered tentative. Cooling of the fluid column would also cause an apparent rise in the rate of drawdown. No temperature logs from this period exist to evaluate this possibility, but it seems unlikely. These data and interpretation are considered of medium-high quality because the pumping test duration was past the wellbore storage period, there were minimal fluctuations in pumping, and there is an adequate match of the theoretical model to the data.

5.2.2 Well ER-20-8 TSA Pumping

The TSA completion of Well ER-20-8 was pumped at about 130 gpm from July 29 to August 8, 2011. The check valve malfunctioned when the pump was turned off, and water levels rebounded as the water in the production casing (up to a 1,600-ft water column above SWL) reentered the formation. Thus, the recovery data were not analyzed.

The log-log diagnostic plot (Figure 5-8) shows the ending of the wellbore storage period between 0.0001 and 0.001 days. The drawdown data and drawdown derivative quickly become very flat, actually recovering after 0.1 day, which generally implies a source of water other than the release of storage with radial distance. Operationally, leakage induced through the straddle packers used to isolate the TCA completion could cause such an effect, as could thermal expansion of the piezometer water where the transducer is located near the top of the tubing—no obvious indications of leakage were observed, and the data required to perform the time varying adjustments to the piezometer water column do not exist (temperature was observed to increase at the piezometer transducer). Geologically, given the presence of a fault through Well ER-20-8 (NNSA/NSO, 2011b), a leaky aquitard interpretation does not seem unreasonable, and the Moench (1985) solution for a well with wellbore storage, skin, and a leaky aquifer with constant head aquifers on either side of the aquitards was selected—as long as at least one constant head on either side of the aquitard was assumed, the results remained unaffected.

Problems with the interpretative model fit include the wellbore storage period offset, which can only be corrected by increasing the casing radius more than the actual casing dimensions, and the noise in the data and apparent recovery (from thermal expansion of the piezometer water) after 0.1 day. These data and interpretation are considered of low quality because while the pumping test duration was past the wellbore storage period and there were minimal fluctuations in pumping, there also was an

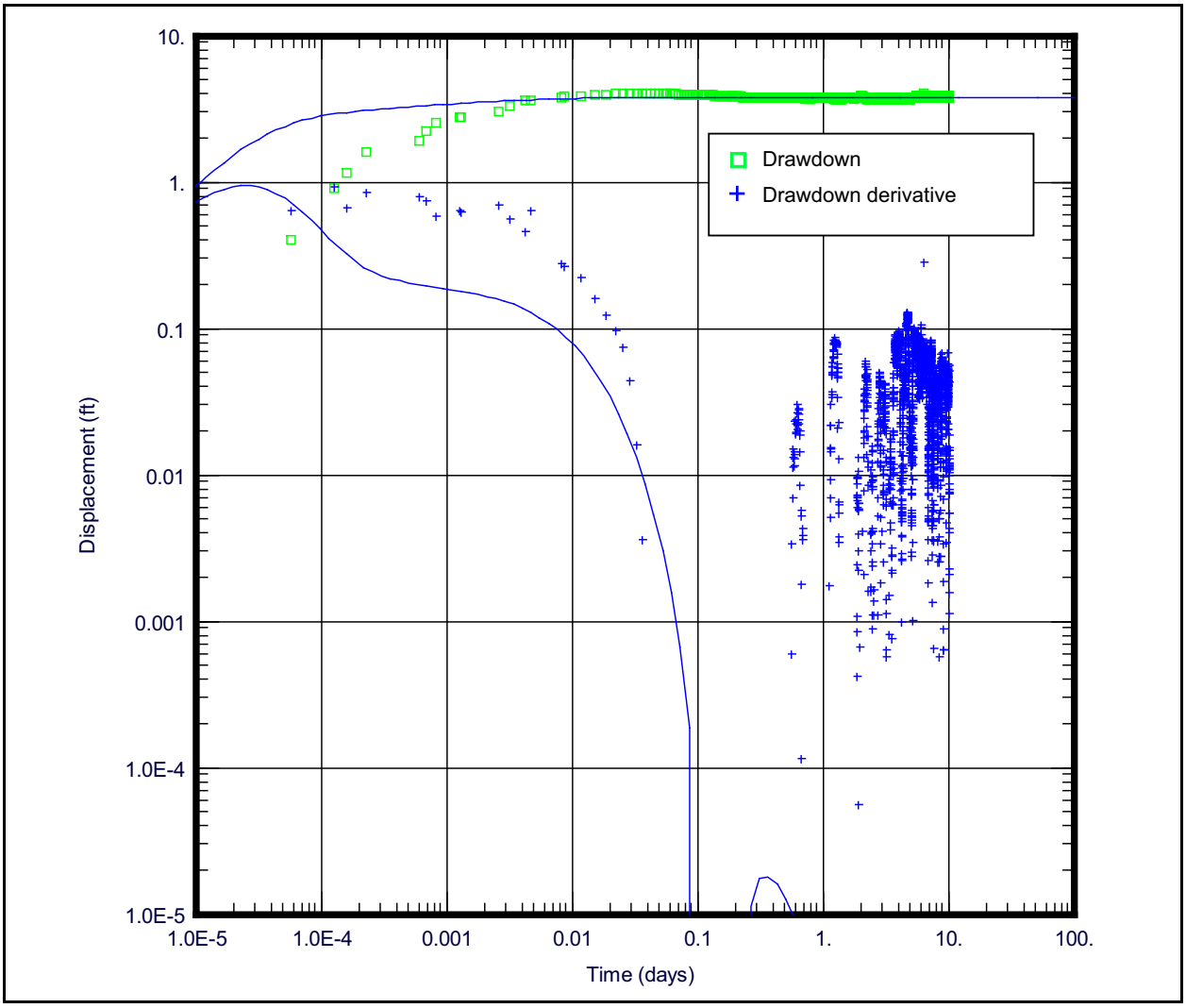

Figure 5-8
Log-Log Diagnostic Plot of Well ER-20-8 TSA Constant-Rate Test

adequate match of the theoretical model to only a part of the data, and there were thermal expansion effects. Thus, no aquifer parameters are reported. These data, if used, should be considered with these effects in mind.

5.2.3 Well ER-20-4 Calico Hills Pumping

Well ER-20-4 was pumped at about 285 gpm from September 9 to September 21, 2011. Initial production was about 289 gpm and gradually declined to about 281 gpm. A stepped production rate was developed to approximate this decline as shown Table 5-1. Piezometers accessing the main completion and near the water table were monitored during the test.

Table 5-1
Stepwise Approximation of the Well ER-20-4 Constant-Rate Test Pumping

Date-Time	Production Rate (gpm)	Elapsed Time (days)
09/14/2011 7:12:00	286.0	0.730
09/16/2011 1:05:00	282.3	2.475
09/20/2011 8:25:00	279.7	6.781
09/20/2011 9:12:30	273.3	6.814
09/20/2011 9:27:30	281.0	6.824
09/21/2011 15:25:30	0	8.073

The log-log diagnostic plot (Figure 5-9) shows the ending of the wellbore storage period near 0.001 days—the entire period from wellbore storage into radial flow at about 0.03 days is clearly developed. Temperature was observed to rise from about 40.8 to 42.2 °C by the end of the test, and the slight recovery near 0.1 day may be from this effect. Barker's (1988) interpretative model incorporating wellbore storage, skin, and radial flow agrees reasonably well with the data to properly interpret changes in the log-log diagnostic plot. The transmissivity is about 4,400 ft^2/day, and it is notable that the wellbore skin is about 30; this well is not especially efficient. As a check, the period from about 0.01 to 0.1 days was evaluated with a Cooper-Jacob approach, giving transmissivity of about 3,000 ft^2/day—Butler (1990) notes that the log-log and semilog analyses emphasize different portions of the response, which accounts for some of the difference. The recovery period evaluated with Barker's model is shown in Figure 5-10.

Note that the lava at Well ER-20-4 is thought to be similar to other lavas in the Calico Hills formation (Th), which has been tested at Wells ER-20-6 and U-20WW. Interference data between Wells ER-20-6#1 and ER-20-6 #2 gave a hydraulic conductivity of 1.65 meters per day (m/day) (IT, 1998). Single well test results at Well ER-20-6 #1 were 2.07 m/day, and at Well ER-20-6#2 were 1.28 m/day. The hydraulic conductivity, 7.3 feet per day (ft/day) (2.22 m/day), estimated from Well ER-20-4 WDT is not greatly different from that at ER-20-6. Garcia et al. (2011) obtained an average hydraulic conductivity of 4.8 ft/day for Calico Hills lavas several miles northwest of Well ER-20-4. The hydraulic conductivity estimates are based on the gravel pack length. It is possible, because of faulting and fracturing observed by Prothro (2011), more thickness contributed to the response. In particular, a zone about 100 ft below the screen was observed to contribute inflow to the well even though in bedded tuff; Prothro (2011) attributes this flow—conceptually inconsistent with bedded tuff acting as aquitards, not aquifers—to a fault. This zone, and possibly

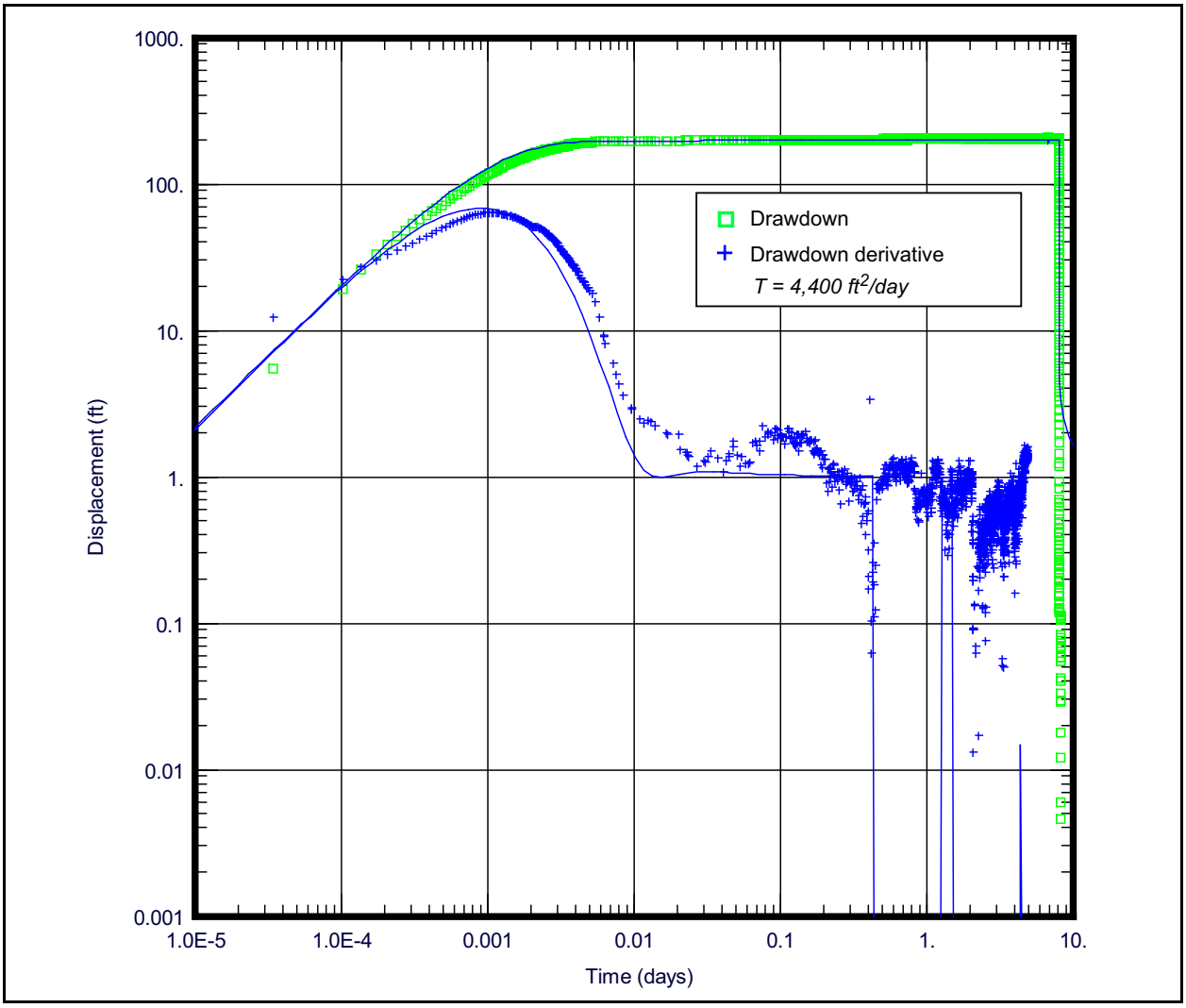

Figure 5-9
Log-Log Diagnostic Plot of Well ER-20-4 Constant-Rate Test

others, may increase the formation thickness actually tested to be greater than the gravel pack assumed in this analysis.

These data and interpretation are considered of medium-high quality because the pumping test duration was past the wellbore storage period, there were minimal fluctuations in pumping, and there is a good match of the theoretical model to most of the data. There may be thermal effects, but the identification of the same interpretive model as at BULLION (IT, 1998) gives some confidence that the effects are not extreme.

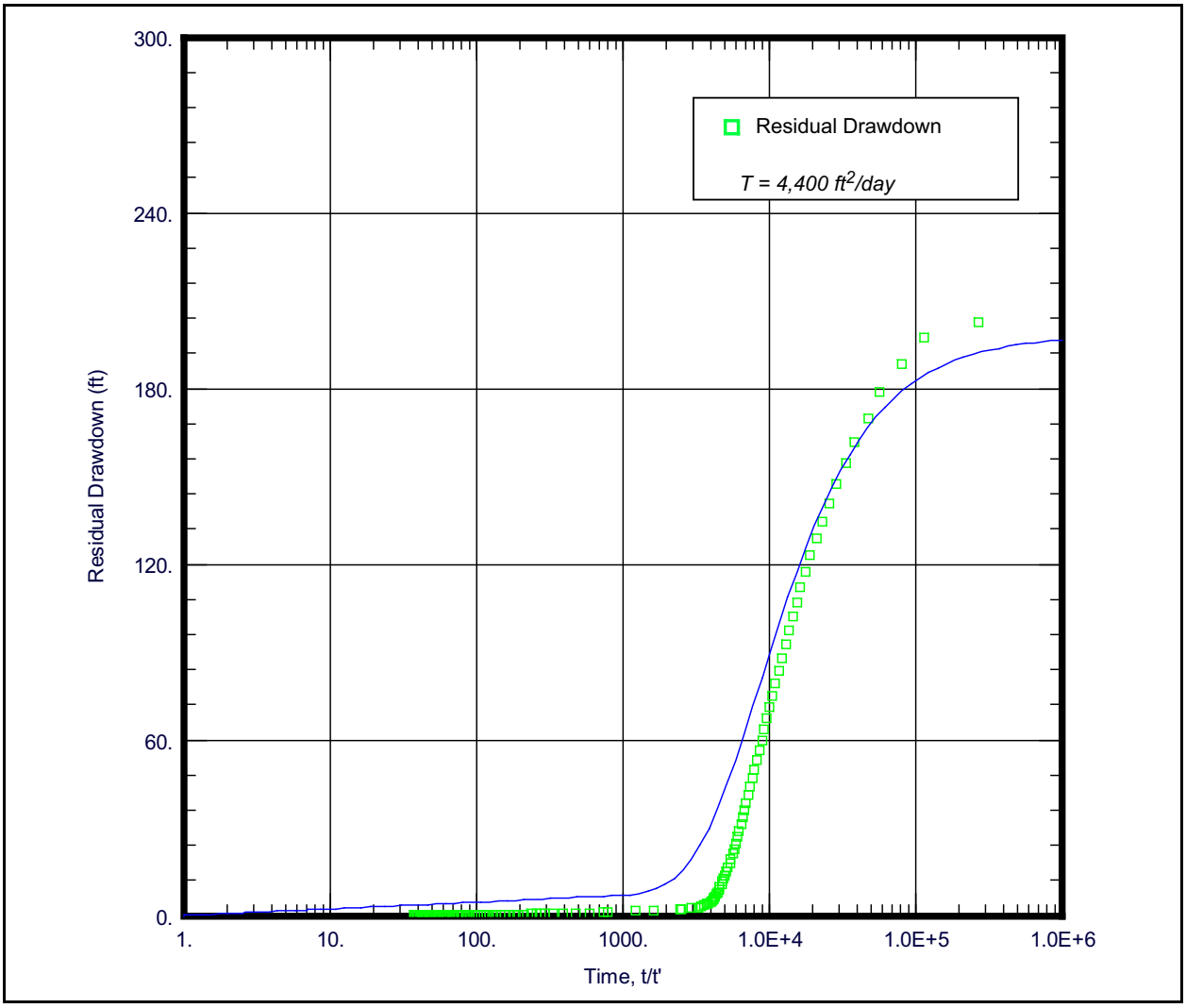

Figure 5-10
Semilog Plot of Well ER-20-4 Constant-Rate Test Recovery

5.3 Interference Data Analysis

Additional insight into aquifer connections can be provided through distance-drawdown analysis. This approach examines the total drawdown (displacement) as a function of distance from the pumping well at a specific time. Deviations from the theoretical Theis solution provide guidance for determining whether specific hydraulic pathway connections are enhanced or attenuated compared to an anticipated response.

In the complexly faulted geology at Pahute Mesa, the assumptions inherent in prototypical conceptual models that are tractable with semianalytic methods are violated. Additionally, the assumption that the drawdown response seen by an observation well is due to the full discharge from the pumping

well is violated in fractured rock—a small response at a distal well may result from a poor connection to the fracture system that is being pumped, rather than a high transmissivity. However, while it is true that properties may not be reliably estimated in very complex settings with simple solutions, they are still useful for comparing and contrasting the observed response to gain conceptual insight into what is actually occurring. Streltsova (1988) defines the radius of investigation as $r = \sqrt{2\eta t}$, where η (transmissivity divided by storativity for a single aquifer or fracture) is hydraulic diffusivity (L^2/T) and *t* is elapsed time. When data are normalized by t/r^2, different diffusivity flow paths can be distinguished because if the diffusivity is the same, all the curves will plot on top of one another. Knudby and Carrera (2006) show that this approximate measure can be useful in mapping fracture connectivity; Beauheim (2007) illustrates such an analysis. To examine the relationships among hydraulic responses and geologic structure, each set of test data was examined to determine trends in well behavior. This type of plot is termed a "composite" plot in AQTESOLV (Duffield, 2007).

An analysis was performed using data N-I and USGS collected in 2011 as part of N-I's WDT operations and Long-Term Head Monitoring Program to examine potential hydraulic responses at wells distal to Wells ER-20-4 and ER-20-8. These data were examined for relative hydraulic diffusivity, potential conceptual interpretations of the aquifer system, and the presence and absence of flow barriers or high-flow features such as faults. The approach was applied at the local (well pad) and distant (hundreds of meters or more from the pumping well) observation wells.

5.3.1 Local Hydraulic Responses from Well ER-20-8 TCA Pumping

During WDT operations hydraulic interference was noticed at nearby Well ER-20-8#2 (completed in the BA/SPA) and the SPA and TSA piezometers. The raw drawdown from these wells is shown on the composite plot (Figure 5-11)—a Theis curve is shown to aid in contrasting the data with ideal response, not for property estimation. The distance was taken as the Euclidean distance from the center of each well screen; the actual paths of drawdown transmission could be quite different because of geologic heterogeneity. The path from the TCA to the TSA has the highest diffusivity, followed by the SPA, and then Well ER-20-8#2—no barometric or other corrections were applied, and this is likely the source of the trough in the Well ER-20-8#2 data near 1×10^{-5} (days per square foot [day/ft^2]). It is interesting to note that the early time slope (from about 5×10^{-9} to 1×10^{-8} day/ft^2) of both the TSA and SPA piezometer data is near unity—the wellbore storage diagnostic not typically seen in observation wells. This could imply that the observation wells are

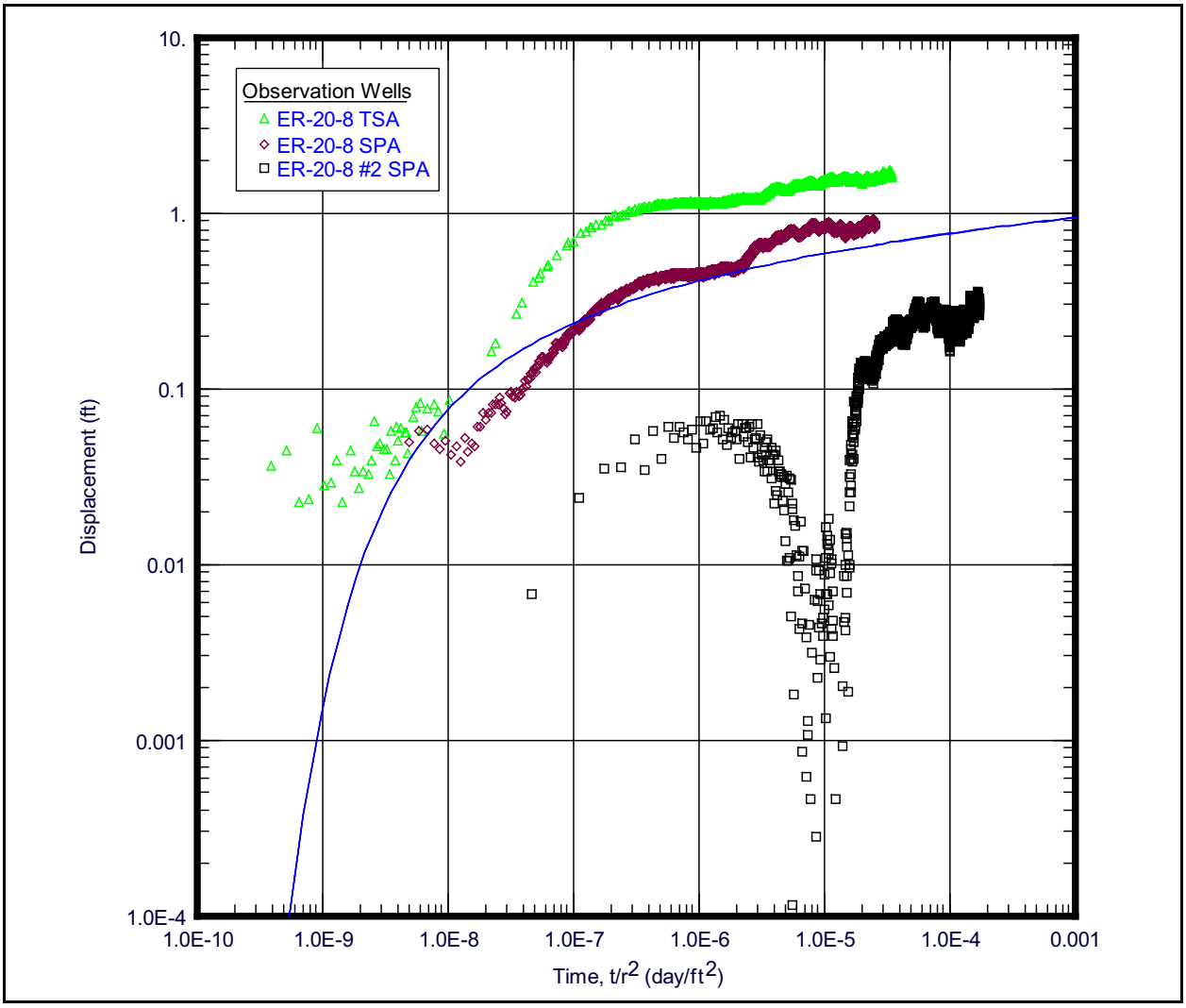

Figure 5-11
Composite Plot of Well ER-20-8 Piezometers and Completions during Well ER-20-8 TCA Constant-Rate Test

well connected to the pumping zone, possibly from the fault at Well ER-20-8. Beauheim (1987) noticed this effect in observation wells in a highly fractured dolomite. Alternatively, leakage in the borehole between zones could explain the data, but that would require all the cement plugs in the well to be bad—a very unlikely possibility because the cement jobs are checked with a nuclear annulus investigation log to confirm the quality of the seal during well construction.

NNSA/NSO (2011b) notes the following:

> The Topopah Spring Tuff in Well ER-20-8 is 88.4 to 110.6 m (290 to 363 ft) thinner than in other holes in the area such as Wells ER-EC-6 (DOE/NV, 2000), ER-20-7 (NNSA/NSO, 2010a), ER-EC-11 (NNSA/NSO, 2010b), and ER-20-5#3

> (DOE/NV, 1997). The proximity of these wells to Well ER-20-8 suggests that the thinning is not related to depositional processes (i.e., stratigraphic thinning) but instead to faulting (i.e., structural thinning). This means that the Well ER-20-8 borehole intercepted a fault that effectively cuts out approximately 91.4 m (300 ft) of Topopah Spring Tuff in the well. Detailed analyses of data from the well…indicate that the fault is within the Topopah Spring Tuff and not at the top or base of the unit.

The pathway, which incorporates the fault and the aquifer, from the TCA to the TSA has the highest diffusivity. Given that the conceptual model of a WTA holds that the densely welded portion is most likely to be fractured, and yet that is the interval removed by the fault, it initially seems that the fault must be more permeable between the TSA and TCA than between the TCA and SPA. However, given that the TSA is most affected by the fault, it is also possible that the damage to the remaining TSA (not conceptually especially permeable) has increased the permeability of the remaining TSA. In any event, because of the similar response times and magnitudes to pumping (in contrast to delayed or no responses that might be expected from a confined system), it is clear that the fault acts to connect the three aquifers at Well ER-20-8.

5.3.2 Local Hydraulic Responses from Well ER-20-8 TSA Pumping

During WDT operations, hydraulic interference was noticed at Wells ER-20-8#2 and the BA/SPA and TCA piezometers. The TCA piezometer showed a rising water level from thermal expansion—no data exist to correct for this effect, followed by drawdown as the thermal effect was overcome. No further evaluation of these data was conducted.

5.3.3 Local Hydraulic Responses from Well ER-20-4 Calico Hills Pumping

During WDT operations, drawdown was observed in the shallow piezometer completed in rhyolitic lava straddling the water table, and separated from the main completion by about 300 ft of zeolitic bedded tuff and zeolitic pumiceous lava (300 ft)—effectively, 600 ft of aquitard.

Data for the Well ER-20-4 shallow piezometer from N-I's Long-Term Head Monitoring beginning May 11 and ending August 9, 2011, were combined with WDT operations data beginning August 18, 2011, to develop corrections for barometric and earth tide effects to clean the response observed during pumping of the main completion using the approach of Halford (2006). The quiescent record was about 3.5 months long, and the record for which detrending applied about 1.5 months. Figure 5-12 shows the processed drawdown and recovery on a log-log diagnostic plot—a

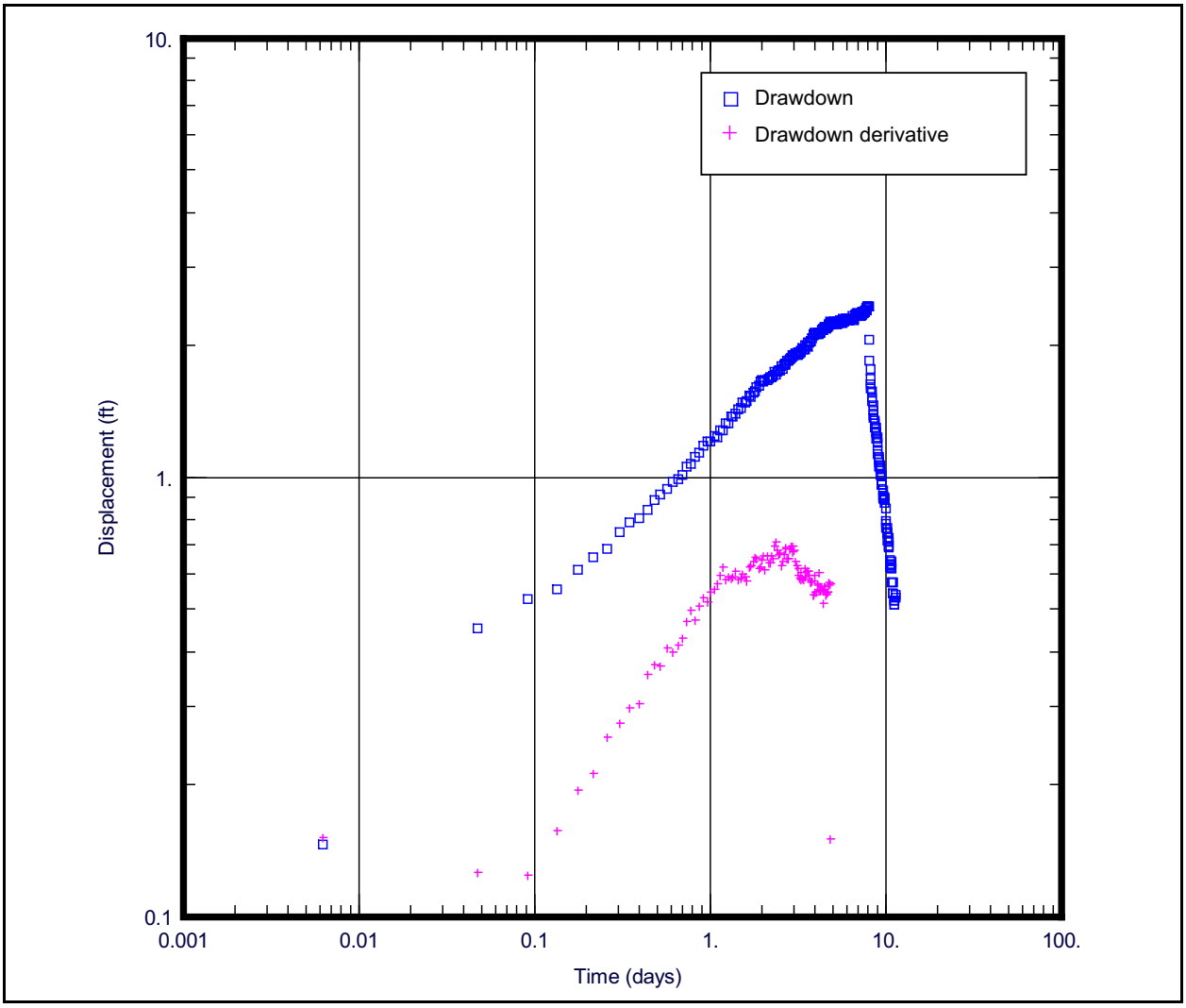

Figure 5-12
Log-Log Diagnostic Plot of Well ER-20-4 Shallow Piezometer Response to Well ER-20-4 Constant-Rate Test

well-defined infinite acting radial flow period does not appear, but it unambiguous that some hydraulic response has occurred. Appendix C presents a numerical model analysis of the piezometer response. The hydraulic conductivity of the zeolitic bedded tuff and pumiceous lava is orders of magnitude higher than expected from core-scale measurements, attributed to faulting and fracturing (Prothro, 2011).

5.4 Drawdown at Distal Wells from WDT Operations

Data collected at distal wells by N-I and the USGS as part of long-term monitoring were evaluated using the approach and software developed by Halford (2006). In this approach, environmental water-level fluctuations are computed by summing the effects of barometric pressure, earth tides, and background undisturbed water levels in a synthetic water-level series and comparing the effects to measured data. An initial quiescent (with respect to pumping, at least) calibration period is used to develop the proper combination of data series to adequately explain the natural fluctuations. The relationships are assumed to hold during a period where it is suspected pumping may influence water levels, and the deviation of the synthetic and actual data assessed with respect to magnitude and timing of pumping. When possible, a fitting period three times or more that of the pumping period was used, as suggested by Halford (2006). The numerical criteria developed by Halford et al. (2010) were used to assess the certainty that a pumping response occurred. Deviations of 0.2 ft or more were considered large, and 0.03 to 0.08 ft small. Relative certainty that the signal is significantly different than background noise is ranked as low or high. A well with low relative certainty indicates drawdown may or may not have occurred, and if it occurred it is poorly constrained and probably has a magnitude that is equal to or less than the estimated maximum drawdown. Closer wells were considered, until such a distance as no influence was detected and then analysis ceased.

Figure 5-13 shows an example of the results of the synthetic water-level modeling process for Well ER-EC-6. The curves plotted are the residuals of the measured water levels minus the modeled synthetic water levels. The level of noise in the fitting period is typical of the wells analyzed for this report. In this case, a clear response at Well ER-EC-6 can be seen in all three completions in response to pumping in both the TCA and TSA at Well ER-20-8.

5.4.1 Well ER-20-8

WDT operations at Well ER-20-8 in the TCA and TSA zones occurred nearly continuously from roughly May 18 through August 8, 2011. This period was analyzed as one response period rather than attempting to consider each interval's step and constant-rate testing individually. Table 5-2 shows the wells with available data, their distance, completion interval, and estimated maximum drawdown.

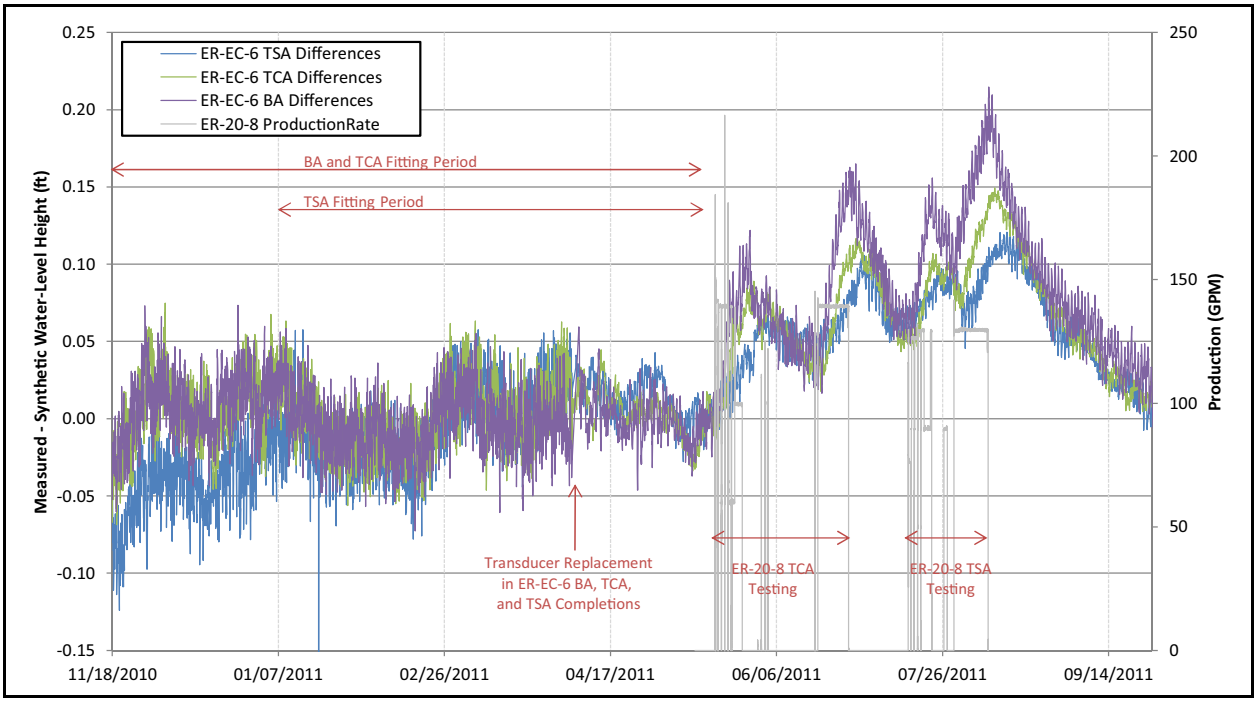

Figure 5-13
Results of the Synthetic Water-Level Modeling Process for Well ER-EC-6

Figure 5-14 shows a composite plot of the smoothed response at Wells ER-20-7, ER-EC-11, and ER-EC-6 to both the Well ER-20-8 TCA and TSA pumping. The first peak at all the wells is from the effects of Well ER-20-8 TCA step testing. Well ER-20-7 has the most delay, about three weeks, from the start of pumping to the peak. In contrast, Well ER-EC-11 BA has the fastest response, reaching a peak within about a week of the start of pumping. The data show that the two BA completions on the NTMMSZ hanging wall respond the fastest to TCA pumping, followed by the TCA, and then the TSA completions. The trough in the data at about 6 x 10^{-7} day/ft^2 is the period between the end of step and beginning of constant-rate testing at Well ER-20-8 TCA. The response to renewed TCA pumping is in all the data but very muted at Well ER-20-7. The second peak in the data, near 1 x 10^{-6} day/ft^2, is from Well ER-20-8 TCA constant-rate testing. The final peak, near 2 x 10^{-6} day/ft^2, is from Well ER-20-8 TSA constant-rate testing. The general descending order of connection is the BA, TCA, and TSA.

Table 5-2
Estimated Maximum Drawdown in Observation Wells from Pumping in Well ER-20-8 TCA and TSA Completion

Well Name	HSU	Estimated Maximum Drawdown (ft)	Distance from Well ER-20-8 (ft)	Relative Certainty Response Occurred
ER-20-1	TCA	Not estimated	11,844.6	N/A
ER-20-2 #1	CHZCM	Not estimated	22,619.7	N/A
ER-20-4	CHZCM	Not estimated	9,850.3	N/A
	CFCU	Not estimated	9,850.3	N/A
ER-20-5 #1	TSA	Not estimated	9,859.0	N/A
ER-20-5 #3	CHZCM	Not estimated	9,757.2	N/A
ER-20-7	TSA	0.06	7,416.1	Low
ER-20-8 #2	BA/SPA	0.37	50.4	High
ER-EC-1	Composite of BA/TCA/TSA/CFCM	Not estimated	16,935.3	N/A
ER-EC-2A	FCCM	Not estimated	32,351.3	N/A
ER-EC-6	BA	0.2	6,796.1	High
	TCA	0.15	6,796.1	High
	TSA	0.11	6,796.1	High
ER-EC-11	BA	0.16	6,266.3	High
	TCA	0.13	6,266.3	High
	TSA	0.11	6,266.3	High
ER-EC-12	TCA	0	8,912.9	N/A
	TSA	0	8,912.9	N/A
	CFCU	0	8,912.9	N/A
ER-EC-13	FCCM (S)	Not estimated	23,304.2	N/A
	FCCM (I)	Not estimated	23,304.2	N/A
	FCCM (D)	Not estimated	23,304.2	N/A
ER-EC-15	UPLFA	Not estimated	13,110.5	N/A
	TCA	Not estimated	13,110.5	N/A
	TSA	Not estimated	13,110.5	N/A
UE-20bh #1	CHZCM	Not estimated	26,690.7	N/A
UE-20n #1	CHZCM	Not estimated	22,910.7	N/A

Source: Modified from N-I, 2012b

Notes:
Estimated maximum drawdown: Maximum drawdown was estimated by matching measured water levels in the observation well to a synthetic curve of nonpumping and pumping responses.
Relative certainty that drawdown occurred: A relative scale indicating likelihood that estimated drawdown is large enough to be observed above background noise in data. High, very likely; Low, possible, but drawdown also could be zero; N/A, not applicable.

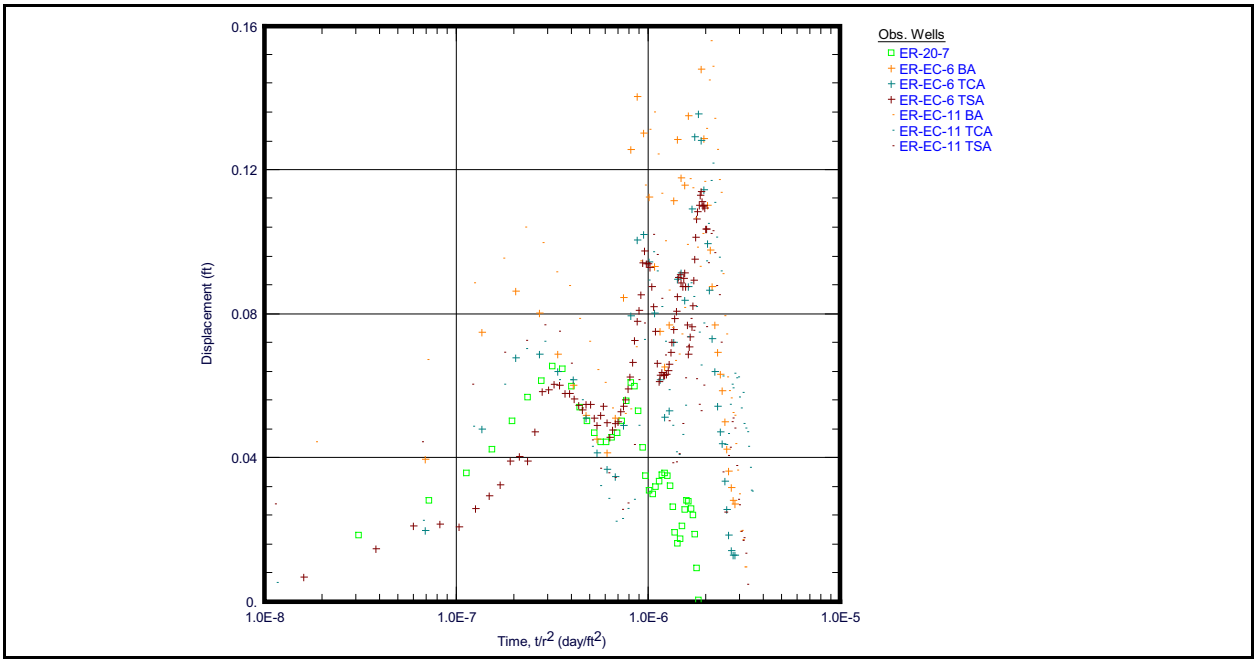

Figure 5-14
Composite Plot of Responses Observed from Well ER-20-8 TCA and TSA Pumping

5.4.2 Well ER-20-4

WDT operations at Well ER-20-4 occurred nearly continuously from roughly August 27 through September 21, 2011. This period was analyzed as one response period rather than attempting to consider each step rate and constant-rate testing separately. Table 5-3 shows the wells with available data, their distance, completion interval, estimated maximum drawdown, and the relative degree of certainty that the estimated drawdown occurred.

5.5 Observations and Conclusions

The following observations and conclusions were made from hydraulic testing:

- The NTMMSZ appears to provide significant connections and enhancement in hydraulic responses across the structure, consistent with static water levels shown in Figure 3-1, and pumping responses in Well ER-20-7 from Wells ER-EC-11 and ER-20-8.
- Similar drawdown response times and magnitudes at wells in the three aquifers of the Bench (BA/SPA, TCA, and TSA) from pumping in different horizons, coupled with approximate knowledge of fault locations, suggests that faults provide vertical connections. These observations are consistent with the very flat static water level surface in the area.
- Responses to pumping at Well ER-20-8 are consistent with those previously observed from Wells ER-20-8 # 2 and ER-EC-11.

Table 5-3
Estimated Maximum Drawdown in Observation Wells from Pumping in Well ER-20-4
(Page 1 of 2)

Well Name	HSU [a]	Estimated Drawdown (ft)	Distance from Well ER-20-4 (ft)	Relative Certainty Response Occurred
ER-20-1	TCA	Not estimated	17,872.0	N/A
ER-20-2 #1	CHZCM	0	13,251.1	N/A
ER-20-5 #1	TSA/CHZCM	Not estimated	13,997.2	N/A
ER-20-5 #3	CHZCM	Not estimated	13,935.1	N/A
ER-20-6 #3	CHZCM	Not estimated	23,848.7	N/A
ER-20-7	TSA/CHZCM	Not estimated	13,003.5	N/A
ER-20-8	BA/SPA	Not estimated	9,850.3	N/A
	TCA	Not estimated	9,850.3	N/A
	TSA	Not estimated	9,850.3	N/A
ER-20-8 #2	BA/SPA	Not estimated	9,897.1	N/A
ER-EC-1	Composite of CPA/TCA/TSA/CFCM	Not estimated	26,350.6	N/A
ER-EC-2A	FCCM	Not estimated	41,320.4	N/A
ER-EC-6	BA	Not estimated	16,602.8	N/A
	TCA	Not estimated	16,602.8	N/A
	TSA	Not estimated	16,602.8	N/A
ER-EC-11	BA	Not estimated	15,885.3	N/A
	TCA	Not estimated	15,885.3	N/A
	TSA	Not estimated	15,885.3	N/A
ER-EC-12	TCA	Not estimated	17,077.4	N/A
	TSA	Not estimated	17,077.4	N/A
	CHCU/CFCU	Not estimated	17,077.4	N/A
ER-EC-13	FCCM (S)	Not estimated	32,857.7	N/A
	FCCM (I)	Not estimated	32,857.7	N/A
	FCCM (D)	Not estimated	32,857.7	N/A
ER-EC-15	CPA	Not estimated	22,928.0	N/A
	TCA	Not estimated	22,928.0	N/A
	TSA	Not estimated	22,928.0	N/A

Table 5-3
Estimated Maximum Drawdown in Observation Wells from Pumping in Well ER-20-4
(Page 2 of 2)

Well Name	HSU [a]	Estimated Drawdown (ft)	Distance from Well ER-20-4 (ft)	Relative Certainty Response Occurred
PM-3 #1	TCA	Not estimated	38,862.0	N/A
U-20bg #1	CHZCM	Not estimated	17,860.0	N/A
UE-20bh #1	CHZCM	Not estimated	20,183.2	N/A
UE-20n #1	CHZCM	0	17,193.7	N/A

Source: Modified from N-I, 2012a

S = Shallow
I = Intermediate
D = Deep

Notes:
Estimated maximum drawdown: Maximum drawdown was estimated by matching measured water levels in the observation well to a synthetic curve of nonpumping and pumping responses.
Relative certainty that drawdown occurred: A relative scale indicating likelihood that estimated drawdown is large enough to be observed above background noise in data. High, very likely; Low, possible, but drawdown also could be zero; N/A, not applicable.

6.0 OTHER SUPPORTING INFORMATION

During the drilling and testing of Wells ER-20-8 and ER-20-4, a large amount of information was collected, some of which can be used to support flow system interpretation. That information is summarized here.

6.1 Water Production during Drilling

The drilling method used for ER wells under saturated conditions is rotary tool with underbalanced air-foam and conventional circulation. This approach limits the amount of water and other drilling fluids that need to be introduced to the formations during drilling. As mentioned in Section 2.0, LiBr is added to drilling fluid to help estimate water production volumes during drilling and the efficacy of well development. During drilling operations, the bit advances down the hole, and the water inflow from the formation that reaches the bit is circulated up to the surface using pumps and hydraulic lines. This water quantity is shown in Figures 6-1 and 6-2 as estimated water production profiles for Wells ER-20-4 (N-I, 2011c) and ER-20-8 (N-I, 2010a). The relative change in flow can be considered a qualitative indicator of the formation hydraulic conductivity in the saturated zone. This information is qualitative and dependent on many unmeasured, down hole conditions including pump pressures, formation pressures, and other items.

During drilling at Well ER-20-4, water production increased steadily, but without any strong pattern. The most striking observation is that flow increased near the top of the CFCU, which conceptually should have little or no flow, where Prothro (2011) interpreted the presence of a fault. Conceptually, flow could occur anywhere in the interior stony lava, but the presence of flow throughout further corroborates Prothro's interpretation.

Water production during drilling of Well ER-20-8, as estimated by Br injection and dilution, is shown in Figure 6-2. Strong inflow began near the middle of the SPA, generally consistent with the geologic conceptual model that fractures would tend to occur in stony lava interior (Figure 5-2). Water production diminished (injected Br concentrations were not diluted) in the Middle Paintbrush confining unit (MPCU), recurred in the TCA near the bottom third where colonnade cooling joints occur, diminished slightly in the LPCU, and increased in the TSA. Reduced, but not eliminated, water

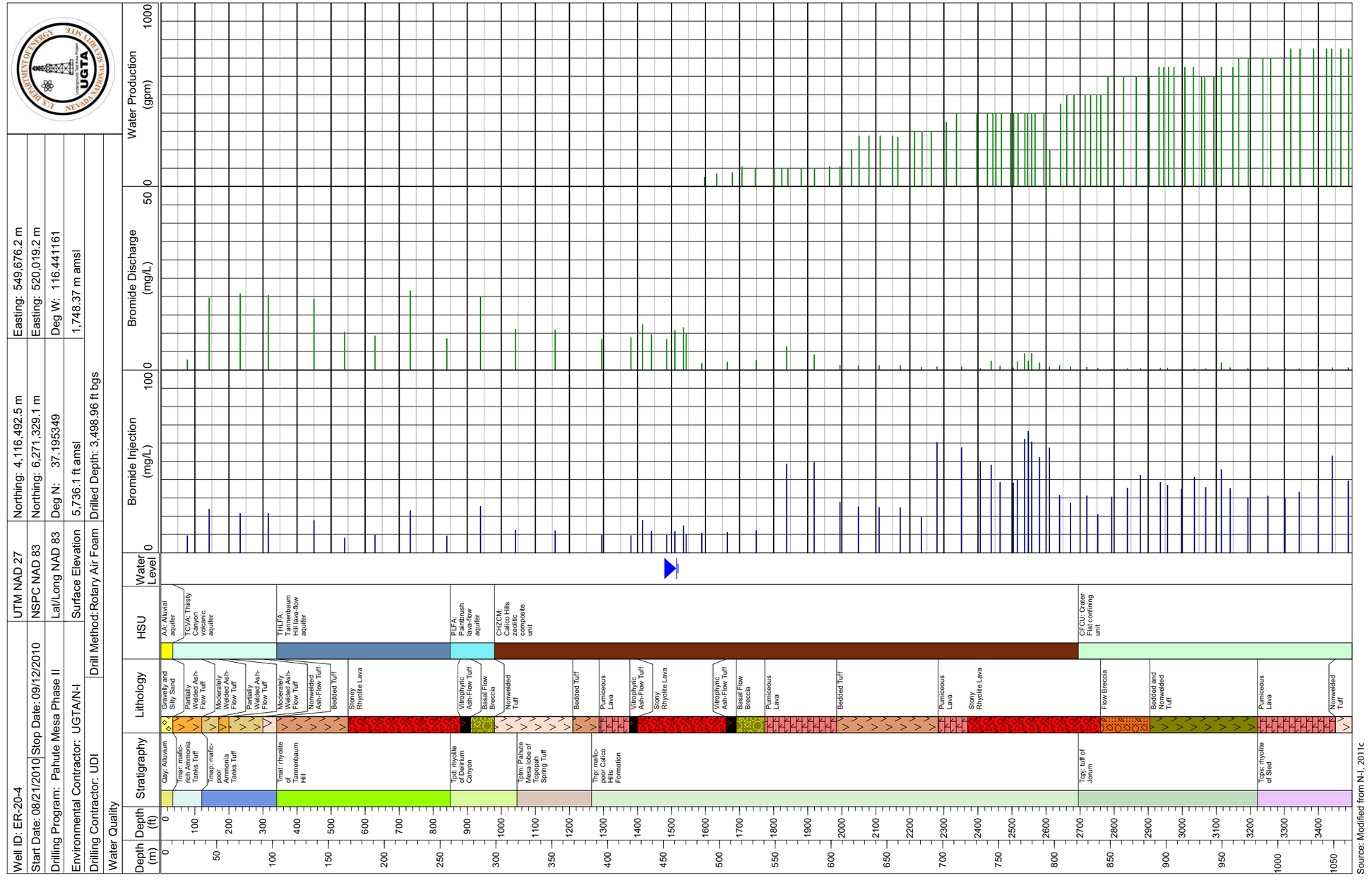

Figure 6-1
Well ER-20-4 Br Tracer Monitoring versus Water Production during Drilling

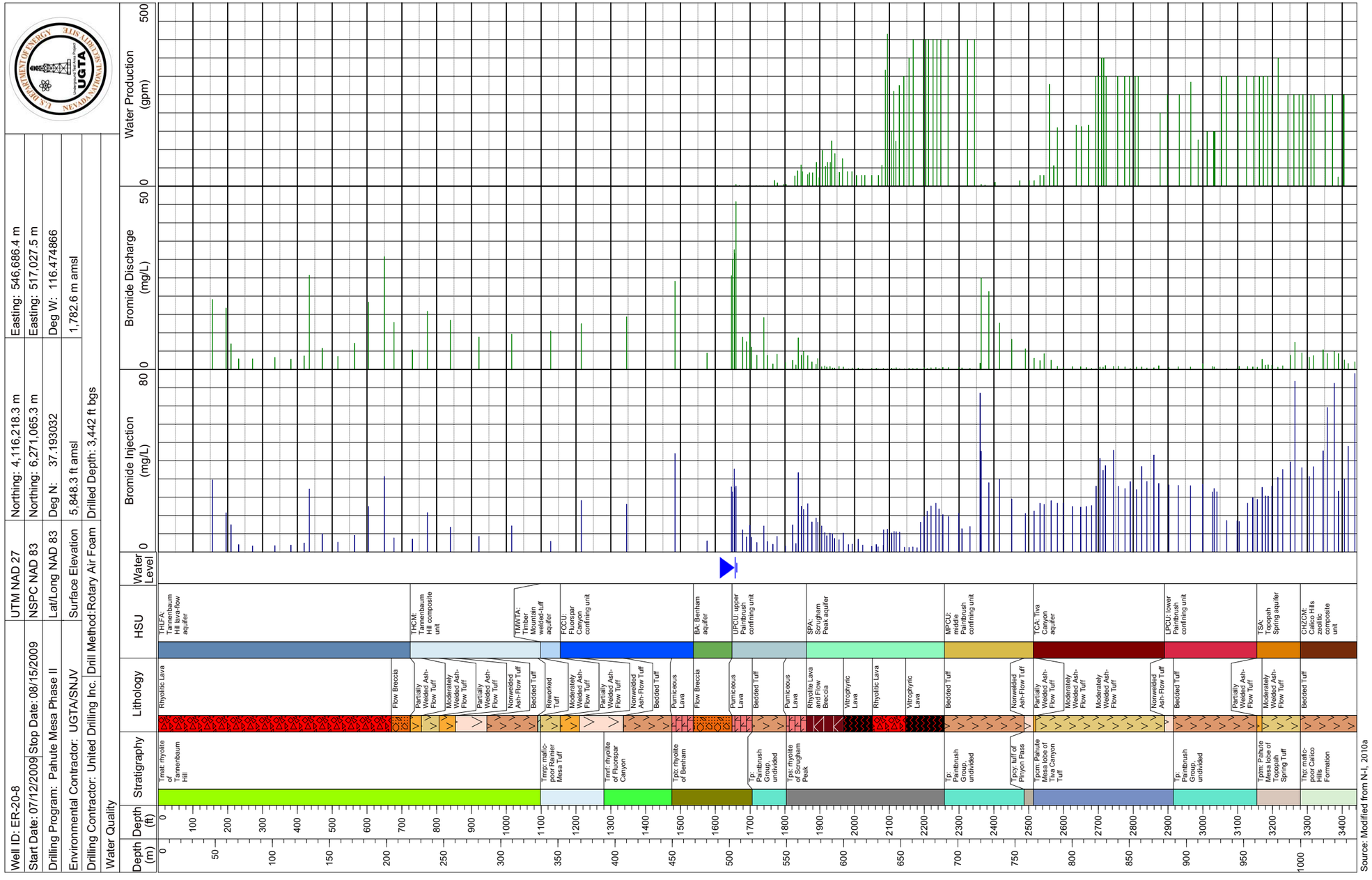

Figure 6-2
Well ER-20-8 Br Tracer Monitoring versus Water Production during Drilling

production in the LPCU could be interpreted to be the result of the fault running through Well ER-20-8.

6.2 Flow Logging

Flow logging can be useful for determining the hydrologic significance of geologic features and, when run under static borehole conditions, for directly evaluating formation potential differences.

Flow logging during pumping at Well ER-20-4 was conducted by Baker Atlas as shown in Figure 6-3. Little flow was observed in the upper 200 ft and lower 250 ft of the screened interval. The spinner log shows substantial flow increase near the top of the flow breccia and into the bottom of the stony lava. This flow is not in general agreement with the conceptual model and may reflect the fault Prothro (2011) has suggested exists in the CFCU.

Flow and temperature logging was conducted for the TCA and TSA in Well ER-20-8 as shown in Figures 6-4 and 6-5. Flow increased gradually through the bottom half of the TCA, consistent with the conceptual model of colonnade cooling joints providing flow in the top or bottom portions of a lithophysal WTA. The TSA log (Figure 6-5) shows flow increasing in the upper half of the formation and into the lower portion of the LPCU, consistent with the interpretation of a fault in the TSA, with the influence of a damage zone extending upward into the LPCU. Data show high temperatures in the TSA production zone (Figure 6-5), suggesting that during pumping, water is being pulled up from a greater depth.

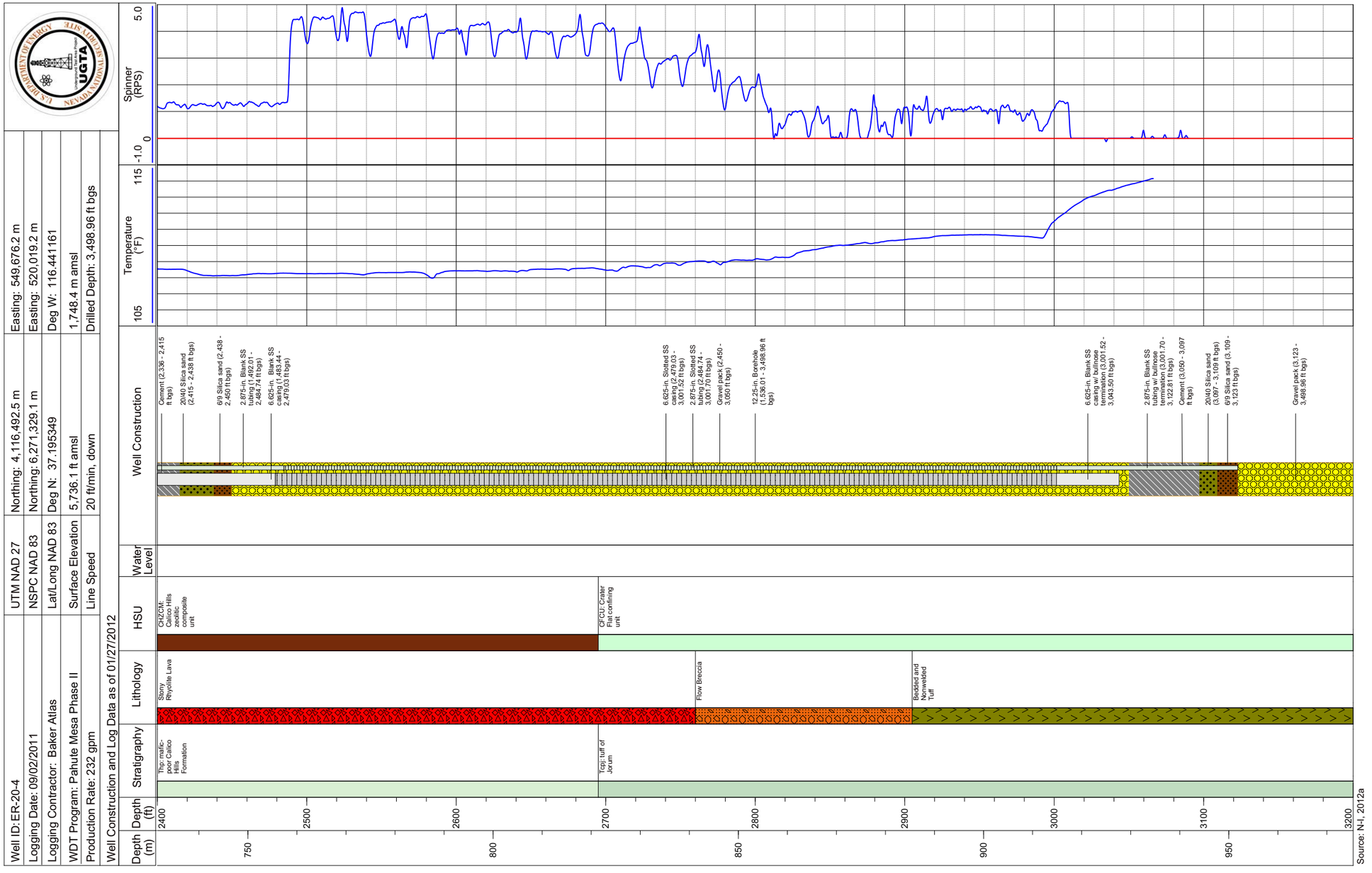

Figure 6-3
Well ER-20-4 Baker Atlas Temperature and Spinner Logs under Stressed Conditions (232 gpm)

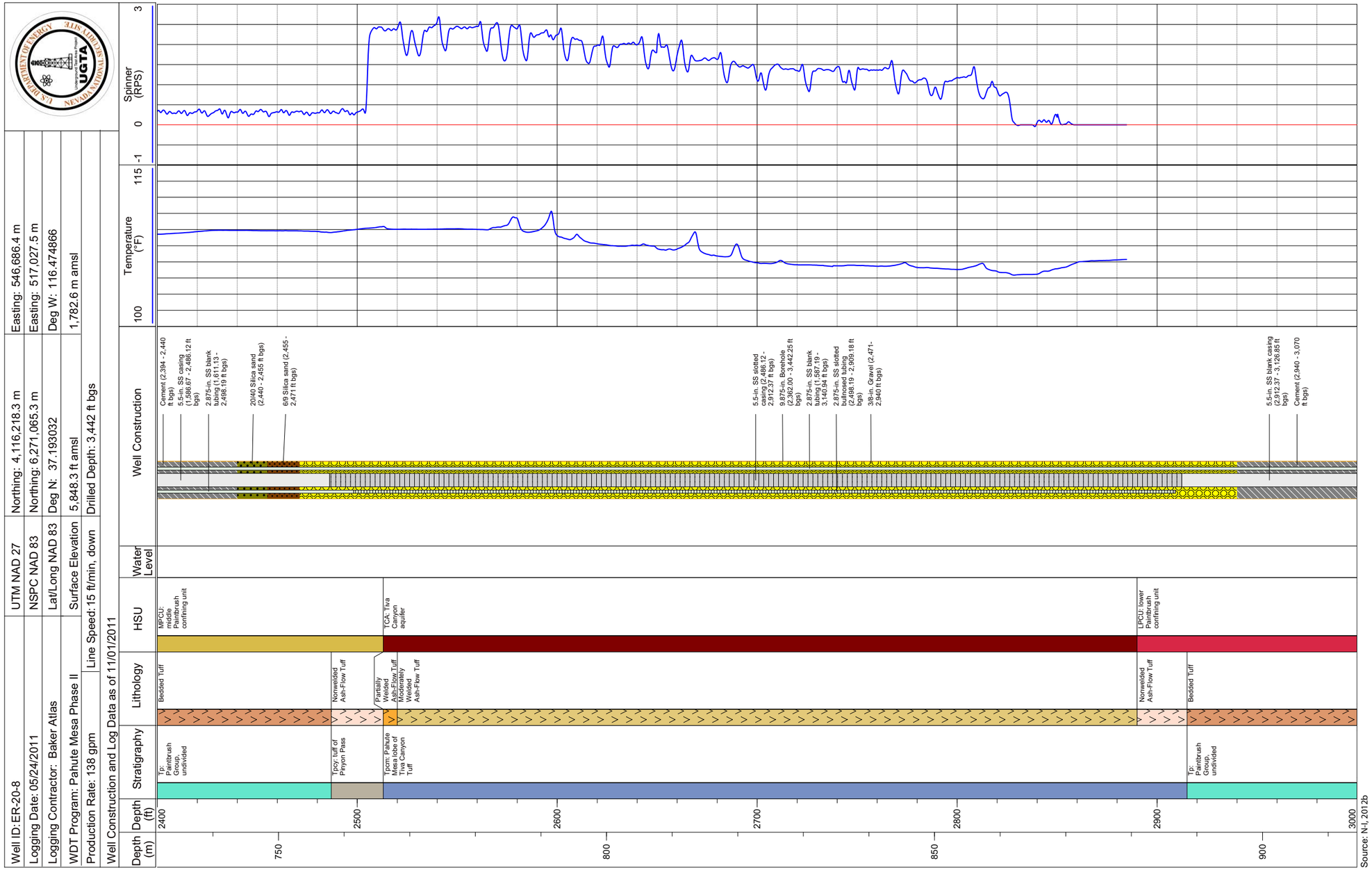

Figure 6-4
Well ER-20-8 Baker Atlas Spinner and Temperature Logs under Stressed Conditions (138 gpm)

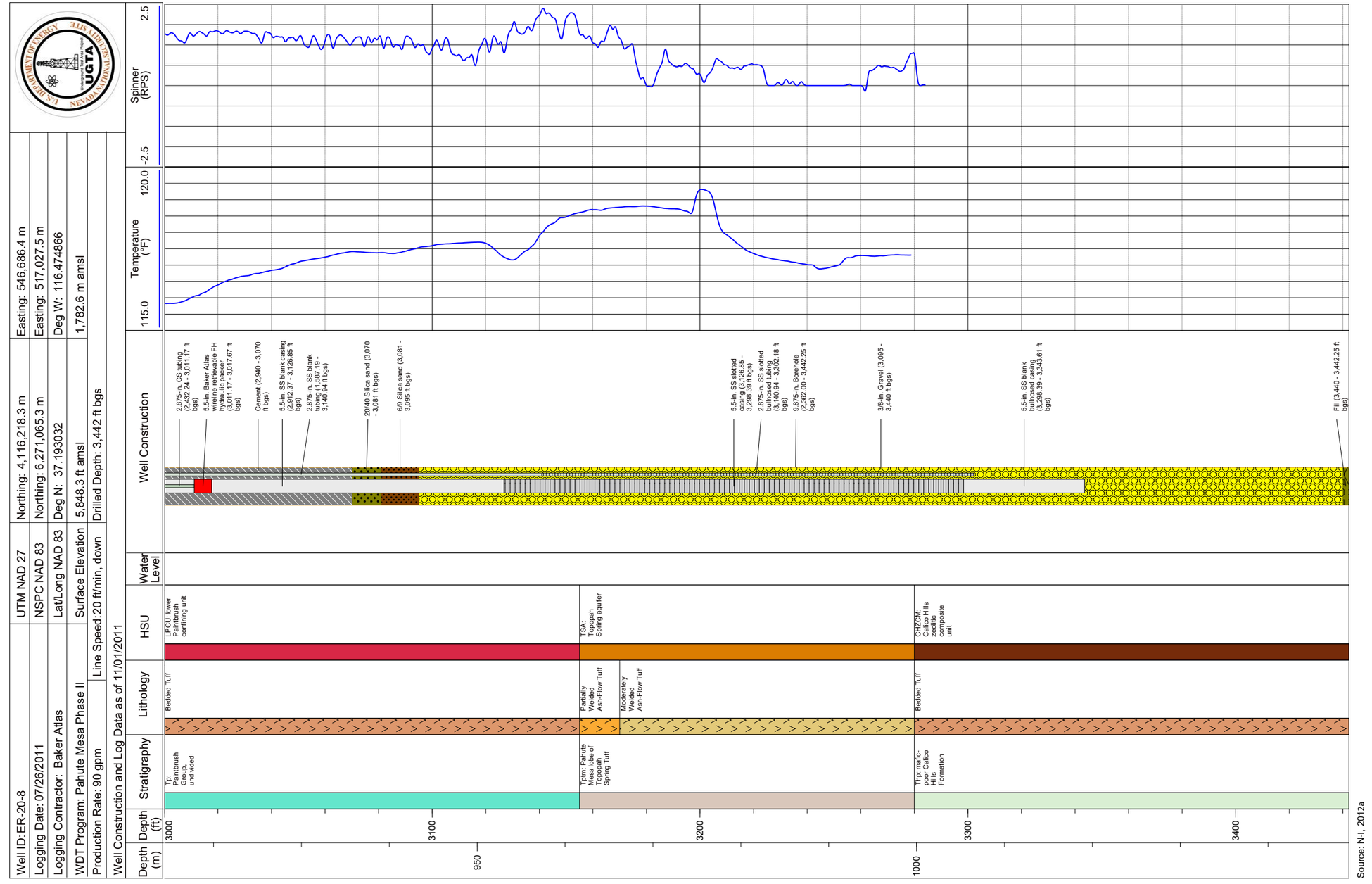

Figure 6-5
Well ER-20-8 Baker Atlas Spinner and Temperature Logs in the TSA under Stressed Conditions (90 gpm)

7.0 CONCEPTUAL MODEL

The Phase II corrective action investigation for Pahute Mesa emphasizes the importance of understanding the flow path from southwest Area 20 to Oasis Valley. Of particular interest is the area between the SCCC and the Timber Mountain caldera structural margin where the rocks present in southwest Area 20 have been down-dropped up to 2,200 ft along the east–west trending NTMMSZ in an area known as the Bench (Section 1.0). The NTMMSZ is crisscrossed by north–south trending basin-and-range-like dip-slip faults. Furthermore, the rocks in the area are reasonably permeable with an extent of several kilometers, circumstances that are favorable for radioactive groundwater to migrate from underground tests. Conceptually, it is anticipated that fault zone width, fault offset, depth of burial, type of rock, secondary mineralization, and current stress conditions may influence the hydraulic behavior of these large structures. Radionuclide migration may further elucidate the role these features play. As part of the Phase II characterization effort, Wells ER-20-7, ER-20-8#2, ER-EC-11, ER-20-8, and ER-20-4 have been pumped for the purpose of development and sampling, HSU transmissivity estimation, and drawdown observations at distal wells in this critical area.

Sweetkind and Drake (2007) examined volcanic rock basin-and-range fault architecture at various scales in Yucca Flat—their observations should apply to Pahute Mesa basin-and-range-like faults as well. They observed the following:

> Field observations in these rocks utilized generally accepted zonation of fault-related rocks into (1) a fault core that is adjacent to the slip plane and composed of clay-rich gouge or matrix-supported breccia; (2) a damage zone of brecciated and fractured rock surrounding the fault core; and (3) a protolith of relatively undamaged rock at some distance from the fault (Caine and others, 1996; Kim and others, 2004). Volcanic rocks near Yucca Flat display differences in the nature and width of these zones that are related to degree of welding, alteration, and amount of fault offset. Damage zones tend to scale with fault offset; damage zones associated with large-offset faults (>100 m) are many tens of meters wide, whereas damage zones associated with smaller offset faults are generally only a meter or two wide. Zeolitized tuff develops moderate-sized damage zones whereas vitric nonwelded, bedded and air fall tuff have very minor damage zones, often consisting of the fault zone itself as a deformation band, with minor fault effect to the surrounding rock mass.

Prothro et al. (2009) make observations of NNSS faults in a similar vein:

> Faults at the [NNSS] form relatively narrow (less than 100 m [300 ft]), yet discrete, tabular fault zones that have flow properties that vary from fault to fault as well as along individual faults. The most recently active faults, such as strike-slip faults and normal faults in the more extended terrains of the eastern and southern portions of the NTS, probably form the most permeable fault zones, but only where they cut the stronger and more consolidated HGUs such as WTA, LFA, CA, Precambrian CCU, IICU, and GCU. Where these faults intersect TCU, they likely form zones of enhanced fracture permeability significantly less than those formed in the stronger HGUs, but possibly still significantly enhanced relative to TCU protolith. Within weaker HGUs, such as AA, PCU, and VTA, these faults will typically not form zones of enhanced permeability, and may actually form zones of slightly reduced permeability relative to the protolith. Enhancement of fault zone permeability is generally controlled by fractures, and will tend to be anisotropic, with greater permeability values parallel to the strike of the fault. Fault segments oriented N25°–40°E will likely have the greatest amounts of permeability enhancement. Zones of enhanced fracturing between overlapping fault segments can effectively link fault zones and create long continuous zones of enhanced permeability.

Interference data from Wells ER-20-8#2 and ER-20-8 clearly show the north–south trending fault at Well ER-20-8 has locally increased the hydraulic conductivity of the aquitards separating the volcanic aquifers. From the data of Sweetkind and Drake (2007), the fault at Well ER-20-8 (about 100-m displacement) might have a damage zone of about 5 m. Prothro et al. (2009) present data from a fault with about 400 ft of displacement that had an estimated 6-ft fault core, fractured footwall TCU with an undetermined thickness, and a 30-ft damaged zone in the hanging wall WTA.

Gray et al. (2005) identify four different classes of genetically linked faults observed in ash flow units at Yucca Mountain. In the largest-scale structures, with 10 to hundreds of meters of displacement, faults are likely to have fault parallel flow with reduced flow normal to the fault and act as a conduit-barrier system. Any of the structures may be laterally gradational with different fault classes resulting in discontinuities in the hydrologic responses across of along structures.

Another fault conceptual element is anisotropic permeability associated with the damage zones. For instance, Bredehoeft et al. (1992) used a fault model with low permeability normal to the fault in the direction of the flow and enhanced vertical permeability within the fault to simultaneously explain nearly hydrostatic conditions over the depth of the faults, with the faults also acting as barriers to horizontal flow with significant head drop across individual faults. At the NNSS, Prothro (2011)

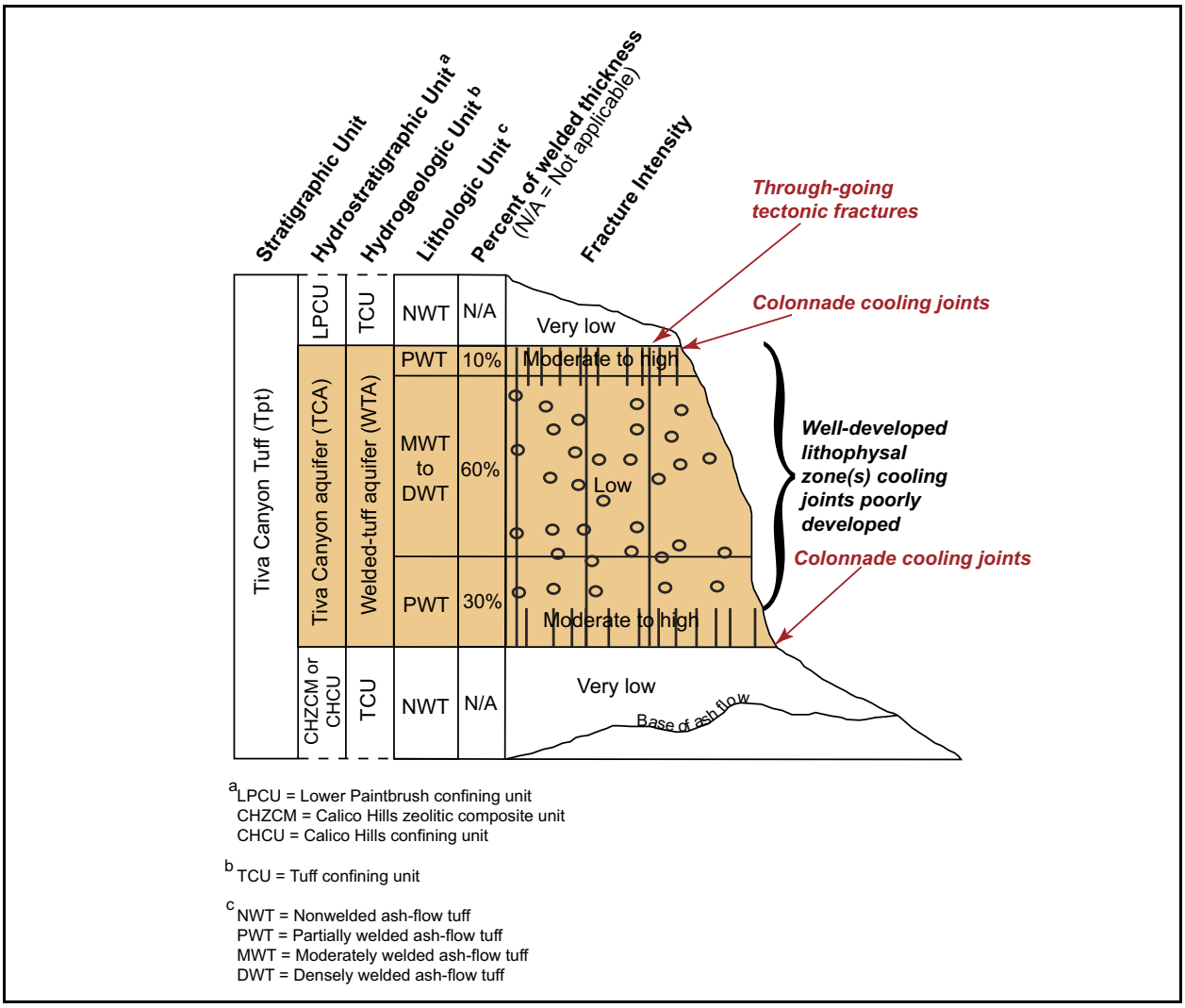

Figure 7-1
Preliminary Conceptual Model of the TCA in Southwestern Pahute Mesa Area
Source: Modified from Drellack, 2010b

observed that most fractures in welded tuffs and lava at Well ER-20-4 have the same northeast strike as the nearby West Greeley fault, which is aligned with the large-scale basin-and-range-like structural fabric of Pahute Mesa. Also observed at Well ER-20-4 were a small fraction of TCU fractures striking northwest parallel to the NTMMSZ; these were interpreted as a small fault related to the catastrophic collapse that formed the NTMMSZ.

FY 2010 and 2011 testing at Wells ER-20-8#2 and ER-20-8 clearly show that the LFAs, TSA, and TCA communicate hydraulically throughout the Bench. This vertical connection between formations is further illustrated by the response to Well ER-EC-11 pumping at Wells ER-EC-6 and ER-20-7. The

postulated ER-20-1 fault (also roughly coincident with a fault segment identified at the surface by Slate et al. [1999] [Figure 5-4]), with either the fault-damage zone concept in zeolitic rocks or juxtaposition (the fault offset is not known accurately), provides a straightforward explanation of why all three horizons respond nearly identically, when pumping at Well ER-EC-11 is only from the bottom two HSUs.

Fault disruption of aquitards can range from sporadic to complete. In order to completely mechanically disrupt a zeolitic aquitard, it would require 100-m faults spaced every 5 to 10 m (based on the data of Sweetkind and Drake [2007] and Prothro et al. [2009])—so that the damage zones touch. Fault spacing from Slate et al. (1999) is on the order of 1,000 m, and ranges from 200 m to 2 kilometers (Drellack, 2012). The presence of these damage zones may have enhanced connectivity in areas where TCUs have been disrupted by antithetic and synthetic faults associated with large-scale structures resulting in increased aquitard hydraulic conductivity (Bredehoeft et al., 1983)—the responses at Well ER-20-8 are believed to be due to this effect.

The NTMMSZ is a west–northwest-striking structural feature that is at least partly related to the formation of the Timber Mountain caldera. The Rainier Mesa Tuff and older units in southwest Area 20 have been down-dropped along the south side of the NTMMSZ by as much as 2,200 ft. The NTMMSZ appears to represent a late-stage outer collapse of the Timber Mountain caldera during the later stages of, or shortly after, the eruption of the Rainier Mesa Tuff. The NTMMSZ is thus a major high-angle structural feature oriented generally perpendicular to north– to north–northeast-striking basin-and-range-style surface faults observed on Pahute Mesa. Static head measurements were examined to see whether the NTMMSZ affects the potentiometric surface (Section 3.0). Although the structure is orthogonal to groundwater flow, similar to the Purse Fault in Figure 3-1, the new data indicate no obvious resistance to groundwater flow through the NTMMSZ. The new data are consistent with the *de facto* NTMMSZ conceptual model implemented in the Phase I model, which had the alteration of permeability in the structural zone mostly neutral, and relied upon juxtaposition and HSU properties to direct flow through the structure. It could be interpreted, inspecting of the maps of Fenelon et al. (2010) in conjunction with the new SWLs, that hydraulic gradient decreases through the NTMMSZ. Upstream of the NTMMSZ, only the TCA and TSA are materially saturated; but downstream, the BA, TCA, and TSA are all saturated (Figure 5-3). Thus, the total transmissivity increases on the downstream side of the NTMMSZ in the Bench.

Previous conceptual interpretations of the NTMMSZ are as follows:

- There is enough juxtaposition to maintain sufficient connected transmissivity across the NTMMSZ to maintain the hydraulic gradient. This is the interpretation of Halford et al. (2010), which was able to replicate observed pumping responses across the NTMMSZ without explicitly representing faults.

- Based on the fault damage zone conceptual model, the damage zone of the NTMMSZ itself has a direct role in conducting groundwater flow through the area—conceptually acting as a manifold. In tension with this interpretation is Faunt's (1997) suggestion that, because of the observed NNSS regional stress field, faults that strike northwest–southeast are not optimally oriented to be open and transmissive. Given the up to 2,200 ft (approximately 670 m) displacement, damage zones could be tens of meters wide and would provide an easy mechanism for water levels to equilibrate. However, there appears to be little head loss through the NTMMSZ, which in the presence of anisotropic permeability striking along the structure is inconsistent with the general fault conceptual model. A third possibility is that near the NTMMSZ, aquitards are sufficiently damaged by faulting to locally act more like aquifers, and these damage zones are equilibrating hydraulic potential and allowing for cross formation radionuclide migration

Drawdown response data at wells distal from the pumping wells have provided insight into the role of structure and stratigraphy (N-I, 2011a; Section 5.2). Overall, the most striking result from these data is how well connected hydraulically the formations are vertically (through multiple aquitards) as discussed previously and laterally through faults and the NTMMSZ. Of special note is that Well ER-20-7, completed in the TSA on the upside of the NTMMSZ, responded as fast to pumping at Well ER-EC-11 as Well ER-EC-6, which is closer to Well ER-EC-11 and on the down-dropped side of the NTMMSZ (Figure 5-4). These data confirm the concept that the NTMMSZ is more or less transparent to groundwater flow, but not how this transparency occurs. An alternative concept is that the northeast–southwest striking faults themselves (geologically younger than the NTMMSZ) provide a preferred direction for drawdown propagation, independent of the NTMMSZ— these faults would be more optimally oriented to be open in the present-day stress field.

Although the flow paths and hydraulic responses give a large-scale view of potential connectivity, direct evidence of contaminant transport provides further insight into the key flow paths for radionuclide migration. The Pahute Mesa Phase I (SNJV, 2009a) and Frenchman Flat Phase II transport model (NNES, 2010a) results suggested that tritium, ^{14}C, ^{36}Cl, ^{99}Tc, and ^{129}I would be the

radionuclides most likely encountered in groundwater away from underground nuclear tests. With the analysis of FY 2011 samples, radionuclide data currently include the following observations:

- Well ER-20-5#1, in the TSA, is contaminated by tritium at tens of millions pCi/L; ^{14}C, ^{99}Tc, ^{129}I; and colloidal plutonium from BENHAM.
- Well ER-20-5#3, completed in lava in the Calico Hills formation, is contaminated with tritium above the MCL; and ^{99}Tc, ^{129}I, and ^{14}C.
- Well ER-20-7, in the TSA, is contaminated by tritium, ^{14}C, ^{36}Cl, ^{99}Tc, and ^{129}I. Colloidal $^{239,240}Pu$ from BENHAM has also been detected. All detected radionuclides, with the exception of tritium, are greatly below their MCL (Section 4.2.3). ^{90}Sr has nominally been detected, but the result is currently considered suspect and is being evaluated with alternative analyses.
- Well ER-20-8#2 (BA/SPA) is contaminated by tritium, ^{14}C, ^{36}Cl, and ^{129}I, all orders of magnitude below their MCL (Section 4.2.3).
- The Well ER-20-8 TCA completion is contaminated by tritium, ^{14}C, and ^{129}I, all orders of magnitude below their MCL (Section 4.2.3). The activities are generally similar (within a factor of 3) to those at Well ER-20-8#2.
- The Well ER-20-8 TSA completion is contaminated by tritium (about 10 times less than the TCA completion); and ^{14}C, ^{36}Cl, and ^{129}I, all orders of magnitude below their MCL (Section 4.2.3).
- The Well ER-EC-11 TCA and TSA completions are uncontaminated. Tritium was encountered in drilling through the lava (N-I, 2011a).
- The BA at Well ER-EC-6 is contaminated with a trace (1.7 pCi/L) of tritium, thought to be the leading edge of a plume (Zavarin, 2012c).
- Well ER-20-4 is uncontaminated.
- Well ER-EC-1 is uncontaminated (Zavarin, 2012b).

At Wells ER-20-8 and ER-20-8#2, contamination is similar in the BA/SPA and TCA, but is clearly lower in the TSA. Analysis of the new static head data suggests a local flow direction nearly due south from Well ER-20-7. The presence of more contamination and radionuclides at Wells ER-20-8 and ER-20-8#2 relative to Well ER-EC-11 suggests that locally contaminated groundwater is not moving southwest but southerly, along the trajectory of the basin-and-range-like faults and vertically through the NTMMSZ. Radionuclide migration shows that the contamination is highest in the

shallowest aquifer and decreases with depth. Clearly, the BA/SPA, the topmost saturated aquifer in the down-dropped block of the NTMMSZ, is receiving water from the TSA but is unable to completely accommodate the flow from the northeast, which is redistributed vertically until equilibrium is reached, resulting in varying degrees of contamination vertically. Additionally, with another saturated aquifer, the total cross-sectional area for flow is increased downstream of the NTMMSZ, and migration velocities may be slower.

Preferred open fracture directions are imparted by the regional stress field (Faunt, 1997; IT, 1998; Prothro, 2009, 2010a and b, 2011). Fracture data collected and reviewed in Phase I showed a general strike to the north–northeast (Drellack et al., 1997; IT, 2001). More recent data confirm (Prothro, 2009, 2010a and b, 2011) that open fractures in welded tuff and lava tend to strike, often strongly, north to northeast consistent with the preferred orientation of the basin-and-range-like faults. This preferred orientation results in an anisotropic permeability (NRC, 1996), which directs flow and transport along the structural fabric of the rocks and is no longer strictly orthogonal to the potentiometric surface, which may not reflect the large-scale flow paths.

In summary, a working conceptual model of the area has the following features and uncertainties:

1. The relatively large-scale connections are a reflection of the juxtaposition of aquifers and of fault structures, and may not be solely reflective of the initial extent of fracturing. Radionuclide concentration data show some vertical connections exist, but it is unknown whether they are ubiquitous and/or homogeneous.

   Uncertainty. The fault damage zone is the mechanism that creates the pathway. How ubiquitous are these zones? Halford et al. (2010) did not simulate the effect of individual faults on the test interference data, but more broadly changed the TCU properties. Conceptually, this would allow diffuse leakage, rather than concentrated leakage, between aquifers.

2. The distribution of secondary porosity (fracturing) influences groundwater flow pathways and the distribution of radionuclides within HSUs. The conceptual fracture distributions shown in Figures 7-1 and 5-3 for the TCA and TSA, respectively, indicate that the rock is not ubiquitously fractured through the entire HSU. Observations of tritium concentrations that are higher in the central portion of the TSA and the top of the TCA support this conclusion.

   Uncertainty. The heterogeneity of the system is large, the permeability of the aquifer units is high, and the faulted TCU provides for leakage among the units. Vertical variations of

radionuclide concentration within HSUs are only a reflection of local variations of vertical leakage.

3. The hydraulic responses throughout the Bench, indicating that diffusivity of the TSA is higher than the TCA, support the more fractured nature of the TSA and the hypothesis that the presence of lithophysae in the TCA has disrupted the development of cooling fractures in the center of the unit as conceptualized in Figure 7-1. Sweetkind and Williams-Stroud (1996) observed that lower joint frequencies and connectivities occurred in the lithophysal zones of the Tiva Canyon tuff (Tpc) and Topopah Spring tuff (Tpt) at Yucca Mountain.

   Uncertainty. The large-scale diffusivity and apparent hydraulic responses in the ash-flow aquifers are a reflection of fault connection and the juxtaposition of the aquifer units and may not be reflective of the extent of fracturing within the unit.

4. The presence of only tritium, ^{14}C, ^{36}Cl, ^{99}Tc, and ^{129}I at Well ER-20-8 suggests that conclusions drawn from previous calculations about the radionuclides of concern are supported by data.

   Uncertainty. The radiological source term, both unclassified and classified, has only general estimates of inventory uncertainty. Additionally, there may be other physical processes that influence the availability of the inventory to groundwater, such as gas-phase transport of ^{14}C. Zavarin (2012a) has suggested an evolving source-term conceptual model that has thermal effects and gas-phase redistribution as explanatory factors.

5. The NTMMSZ is not a significant barrier to flow at the scale of the Bench.

   Uncertainty. Whether the connections are formed by juxtaposition of transmissive units, or by the fault itself as a conduit, is unknown.

6. The overall transmissivity of the Paintbrush HSU stack (CPA, BA, SPA, TCA, and TSA) where it is saturated west of the Boxcar fault appears to be higher than the Calico Hills formation that dominates the saturated zone east of the Boxcar fault.

   Uncertainty. The Boxcar fault may have properties itself that confound the observation.

8.0 REFERENCES

BN, see Bechtel Nevada.

Barker, J.A., 1988. "A Generalized Radial Flow Model for Hydraulic Tests in Fractured Rock." In *Water Resources Research*, Vol. 24(10): pp. 1796–1804. Washington, DC: American Geophysical Union.

Beauheim, R.L. 1987. *Analysis of Pumping Tests of the Culebra Dolomite Conducted at the H-3 Hydropad at the Waste Isolation Pilot Plant (WIPP) Site*, SAND86-2311, Albuquerque, NM: Sandia National Laboratories.

Beauheim, R.L. 2007. "Diffusivity Mapping of Fracture Interconnections." In *Proceedings of the 2007 U.S. EPA/NGWA Fractured Rock Conference*, pp. 235–249. Westerville, OH: U.S. Environmental Protection Agency and National Ground Water Association.

Bechtel Nevada. 2002. *A Hydrostratigraphic Model and Alternatives for the Groundwater Flow and Contaminant Transport Model of Corrective Action Units 101 and 102: Central and Western Pahute Mesa, Nye County, Nevada*, DOE/NV/11718--706. Prepared for the U.S. Department of Energy, National Nuclear Security Administration Nevada Operations Office. Las Vegas, NV.

Blankennagel, R.K., and J.E. Weir, Jr. 1973. *Geohydrology of the Eastern Part of Pahute Mesa, Nevada Test Site, Nye County, Nevada*, Professional Paper 712-B. Denver, CO: U.S. Geological Survey.

Bowen, S.M., D.L. Finnegan, J.L. Thompson, C.M. Miller, P.L. Baca, L.F. Olivas, C.G. Geoffrion, D.K. Smith, W. Goishi, B.K. Esser, J.W. Meadows, N. Namboodiri, and J.F. Wild. 2001. *Nevada Test Site Radionuclide Inventory, 1951-1992*, LA-13859-MS. Los Alamos, NM: Los Alamos National Laboratory.

Bredehoeft, J.D., C.E. Neuzil, and P.C. Milly. 1983. *Regional Flow in the Dakota Aquifer; A Study of the Role of Confining Layers*, USGS Water-Supply Paper 2237. Washington, DC: U.S. Geological Survey.

Bredehoeft, J.D., K. Belitz, and S. Sharp-Hansen. 1992. "The Hydrodynamics of the Big Horn Basin; A Study of the Role of Faults." In *AAPG Bulletin*, Vol. 76(4): pp. 530–546.

Butler, J.J., Jr. 1990. "The Role of Pumping Tests in Site Characterization: Some Theoretical Considerations." In *Ground Water,* Vol. 28(3): pp. 394–402.

Byers, F.M., Jr., and D. Cummings. 1967. *Geologic Map of the Scrugham Peak Quadrangle, Nye County, Nevada*. U.S. Geological Survey, Geologic Quadrangle Map GQ-695, scale 1:24,000. Denver, CO: U.S. Geological Survey.

CFR, see *Code of Federal Regulations*.

Caine, J.S., and C.B. Forster. 1999. "Fault Zone Architecture and Fluid Flow: Insights from Field Data and Numerical Modeling." In *Faults and Subsurface Fluid Flow in the Shallow Crust*, Geophysical Monograph 113, pp. 101–127. W.C. Haneberg, P.S. Mozley, J. Casey Moore, and L.B. Goodwin eds. Washington, DC: American Geophysical Union.

Caine, J.S., J.P. Evans, and C.B. Forster. 1996. "Fault Zone Architecture and Permeability Structure." In *Geology*, Vol. 24(11): pp. 1025–1028.

Code of Federal Regulations. 2012. Title 40 CFR Part 141, "National Primary Drinking Water Regulations." Washington, DC: U.S. Government Printing Office.

Craig, H. 1961. "Isotopic Variations in Meteoric Waters." In *Science*, Vol. 133(3465): pp. 1702–1703. Washington, DC: American Association for the Advancement of Science.

Criss, R.E. 1999. *Principles of Stable Isotope Distribution*. New York, NY: Oxford University Press.

DOE/NV, see U.S. Department of Energy, Nevada Operations Office.

Drellack, S., National Security Technologies, LLC. 2010a. Personal communication to G. Ruskauff (N-I) and N. DeNovio (Golder Associates, Inc.) regarding the BA Conceptual Model, 15 September. Las Vegas, NV.

Drellack, S., National Security Technologies, LLC. 2010b. Personal communication to N. DeNovio and W. Dershowitz (Golder Associates, Inc.) regarding the TSA Conceptual Model, 26 August Las Vegas, NV.

Drellack, S., National Security Technologies, LLC. 2011a. Personal communication to T. Vogt (N-I) regarding the BA and SPA, 15 July. Las Vegas, NV.

Drellack, S., National Security Technologies, LLC. 2011b. Personal communication to G. Ruskauff (N-I) regarding new buried faults, 12 July. Las Vegas, NV.

Drellack, S., National Security Technologies, LLC. 2012. Personal communication to G. Ruskauff (N-I) regarding fault frequency at pahute Mesa, 14 August. Las Vegas, NV.

Drellack, S.L., Jr., L.B. Prothro, K.E. Roberson, B.A. Schier, and E.H. Price. 1997. *Analysis of Fractures in Volcanic Cores from Pahute Mesa, Nevada Test Site*, DOE/NV/11718-160. Las Vegas, NV: Bechtel Nevada.

Duffield, G.M. 2007. *AQTESOLV for Windows Version 4.5 User's Guide.* Reston, VA: HydroSOLVE, Inc.

EPA, see U.S. Environmental Protection Agency.

FFACO, see *Federal Facility Agreement and Consent Order.*

Faunt, C.C. 1997. *Effect of Faulting on Ground-Water Movement in the Death Valley Region, Nevada and California,* Water-Resources Investigations Report 95-4132. Denver, CO: U.S. Geological Survey.

Federal Facility Agreement and Consent Order. 1996 (as amended March 2010). Agreed to by the State of Nevada; U.S. Department of Energy, Environmental Management; U.S. Department of Defense; and U.S. Department of Energy, Legacy Management. Appendix VI, which contains the Underground Test Area Strategy, was last modified May 2011, Revision No. 4.

Fenelon, J.M., D.S. Sweetkind, and R.J. Laczniak. 2010. *Groundwater Flow Systems at the Nevada Test Site, Nevada: A Synthesis of Potentiometric Contours, Hydrostratigraphy, and Geologic Structures,* Professional Paper 1771. Reston, VA: U.S. Geological Survey.

Garcia, C.A., J.M. Fenelon, K.J. Halford, S.R. Reiner, and R.J. Laczniak. 2011. *Assessing Hydraulic Connections across a Complex Sequence of Volcanic Rocks—Analysis of U-20 WW Multiple-Well Aquifer Test, Pahute Mesa, Nevada National Security Site, Nevada,* U.S. Geological Survey Scientific Investigations Report 2011–5173. 24 p.

Geldon, A.L. 2004. *Hydraulic Tests of Miocene Volcanic Rocks at Yucca Mountain and Pahute Mesa and Implications for Groundwater Flow in the Southwest Nevada Volcanic Field, Nevada and California,* GSA Special Papers Vol. 381. 93 p. Boulder, CO: Geological Society of America.

Gray, M.B., J.A. Stamatakos, D.A. Ferrill, and M.A. Evans. 2005. "Fault-Zone Deformation in Welded Tuffs at Yucca Mountain, Nevada, USA." In *Journal of Structural Geology,* Vol. 27(10): pp. 1873–1891.

HORIBA, see HORIBA, Ltd.

Halford, K.J. 2006. *Documentation of a Spreadsheet for Time-Series Analysis and Drawdown Estimation,* Scientific Investigations Report 2006-5024. Carson City, NV: U.S. Geological Survey.

Halford, K., J. Fenelon, and S. Reiner, U.S. Geological Survey. 2010. Memorandum to D. Galloway (RSO–Western Region) titled "AQUIFER-TEST PACKAGE—Analysis of ER-20-8 #2 and ER-EC-11 Multi-well Aquifer Tests, Pahute Mesa, Nevada National Security Site," 27 September. Henderson, NV.

HORIBA, Ltd. 2003. *pH Meter F-52/F-53/F-54/F-55 Instruction Manual.* Kyoto, Japan.

Horne, R.N. 1995. *Modern Well Test Analysis: A Computer-Aided Approach*, Second Edition. Palo Alto, CA: Petroway, Inc.

IT, see IT Corporation.

Ingraham, N.L., R.L. Jacobson, J.W. Hess, and B.F. Lyles. 1990. *Stable Isotopic Study of Precipitation and Spring Discharge on the Nevada Test Site*, DOE/NV/10845--03; Publication No. 45078. Las Vegas, NV: Desert Research Institute.

IT Corporation. 1998. *Report and Analysis of the BULLION Forced-Gradient Experiment*, DOE/NV/13052-042; ITLV/13052-042; UC-700. Las Vegas, NV.

IT Corporation. 2000a. Written communication. Subject: *Western Pahute Mesa–Oasis Valley Well ER-EC-1 Data Report for Development and Hydraulic Testing*. May. Las Vegas, NV.

IT Corporation. 2000b. Written communication. Subject: *Western Pahute Mesa–Oasis Valley Well ER-EC-6 Data Report for Development and Hydraulic Testing*. May. Las Vegas, NV.

IT Corporation. 2001. *Underground Test Area Fracture Analysis Report: Analysis of Fractures in Volcanic Rocks of Western Pahute Mesa–Oasis Valley*, Rev. 0, ITLV/13052-150. Las Vegas, NV.

Kim, Y.-S., D.C.P. Peacock, and D.J. Sanderson. 2004. "Fault Damage Zones." In *Journal of Structural Geology*, Vol. 26(3): pp. 503–517.

Knudby, C., and J. Carrera. 2006. "On the Use of Apparent Hydraulic Diffusivity as an Indicator of Connectivity." In *Journal of Hydrology*, Vol. 329(3-4): pp. 377-389.

Kwicklis, E. 2009. "Appendix D: Evaluation of Groundwater Travel Times in the PM-OV Flow System from ^{14}C Data." In *Phase I Transport Model of Corrective Action Units 101 and 102: Central and Western Pahute Mesa, Nevada Test Site, Nye County, Nevada*, S-N/99205--111. Las Vegas, NV: Stoller-Navarro Joint Venture.

Kwicklis, E.M., T.P. Rose, and F.C. Benedict, Jr. 2005. *Evaluation of Groundwater Flow in the Pahute Mesa–Oasis Valley Flow System Using Groundwater Chemical and Isotopic Data*, LA-UR-05-4344. Los Alamos, NM: Los Alamos National Laboratory.

McCutcheon, S.C., J.L. Martin, and T.O. Barnwell, Jr. 1993. "Water Quality." In *Handbook of Hydrology*: pp. 11.2–11.6. D.R. Maidment ed. New York, McGraw-Hill, Inc.

Merlivat, L., and J. Jouzel. 1979. "Global Climatic Interpretation of the Deuterium Oxygen-18 Relationship for Precipitation." In *Journal of Geophysical Research*, Vol. 84(C8): pp. 5029–5033.

Moench, A.F., 1985. "Transient Flow to a Large-Diameter Well in an Aquifer with Storative Semiconfining Layers." In *Water Resources Research*, Vol. 21(8): pp. 1121-1131. Washington, DC: American Geophysical Union.

N-I, see Navarro-Intera, LLC.

N-I GIS, see Navarro-Intera Geographic Information Systems.

NNES, see Navarro Nevada Environmental Services, LLC.

NNSA/NSO, see U.S. Department of Energy, National Nuclear Security Administration Nevada Site Office.

NNSA/NV, see U.S. Department of Energy, National Nuclear Security Administration Nevada Operations Office.

NRC, see National Research Council.

National Research Council. 1996. *Rock Fractures and Fluid Flow. Contemporary Understanding and Applications.* Prepared by the Committee on Fracture Characterization and Fluid Flow. Washington DC: National Academy Press.

Navarro-Intera Geographic Information Systems. 2012. ESRI ArcGIS Software.

Navarro-Intera, LLC. 2010a. Written communication. Subject: *Pahute Mesa ER-20-8 Well Data Report.* April. Las Vegas, NV.

Navarro-Intera, LLC. 2010b. Written communication. Subject: *Pahute Mesa Phase II ER-EC-11 Well Development, Testing, and Sampling Data Report*. September. Las Vegas, NV.

Navarro-Intera, LLC. 2011a. *Pahute Mesa Well Development and Testing Analyses for Wells ER-20-7, ER-20-8 #2, and ER-EC-11*, N-I/28091--037. Las Vegas, NV.

Navarro-Intera, LLC. 2011b. Written communication. Subject: "Depth to water level" forms from Field Operations web page. Las Vegas, NV.

Navarro-Intera, LLC. 2011c. Written communication. Subject: *Pahute Mesa ER-20-4 Well Data Report*. May. Las Vegas, NV.

Navarro-Intera, LLC. 2011d. Written communication. Subject: *Pahute Mesa Fiscal Year 2010 Long-Term Head Monitoring Data Report*. February. Las Vegas, NV.

Navarro-Intera, LLC. 2011e. Written communication. Subject: "UGTA Field Operations SharePoint Web Page for Well ER-20-8 Well Construction Diagram," 1 November. Las Vegas, NV.

Navarro-Intera, LLC. 2012a. Written communication. Subject: *Pahute Mesa Phase II ER-20-4 Well Development, Testing, and Sampling Data Report.* July. Las Vegas, NV.

Navarro-Intera, LLC. 2012b. Written communication. Subject: *Pahute Mesa Phase II ER-20-8 Well Development, Testing, and Sampling Data Report.* June. Las Vegas, NV.

Navarro-Intera, LLC. 2012c. Written communication. Subject: "UGTA Water Levels Database," UGTA Technical Data Repository Database Identification Number UGTA-4-137. Las Vegas, NV. As accessed on 3 July.

Navarro Nevada Environmental Services, LLC. 2010a. *Phase II Transport Model of Corrective Action Unit 98: Frenchman Flat, Nevada Test Site, Nye County, Nevada*, Rev. 1, N-I/28091--004, S-N/99205--122. Las Vegas, NV.

Navarro Nevada Environmental Services, LLC. 2010b. Written communication. Subject: *Pahute Mesa ER-20-8#2 Well Data Report*. April. Las Vegas, NV.

O'Hagan, M.D., and R.J. Laczniak. 1996. *Ground-Water Levels beneath Eastern Pahute Mesa and Vicinity, Nevada Test Site, Nye County, Nevada,* Water-Resources Investigations Report 96-4042. Denver, CO: U.S. Geological Survey.

Pawloski, G.A., T.P. Rose, J.W. Meadows, B.J. Deshler, and J. Watrus. 2002. *Categorization of Underground Nuclear Tests on Pahute Mesa, Nevada Test Site, for Use in Radionuclide Transport Models*, UCRL-TR-208347. Livermore, CA: Lawrence Livermore National Laboratory.

Post, V., H. Kooi, and C. Simmons. 2007. "Using Hydraulic Head Measurements in Variable-Density Ground Water Flow Analyses." In *Ground Water,* Vol. 45(6): pp. 664-671.

Prothro, L.B. 2009. Written communication. Subject: *Analysis and Interpretation of Borehole Image Logs from Well ER-20-7*. October. Las Vegas, NV: National Security Technologies, LLC.

Prothro, L.B. 2010a. Written communication. Subject: *Analysis and Interpretation of Borehole Image Logs from Well ER-20-8*. January. Las Vegas, NV: National Security Technologies, LLC.

Prothro, L.B. 2010b. Written communication. Subject: *Analysis and Interpretation of Borehole Image Logs from Well ER-EC-11*. May. Las Vegas, NV: National Security Technologies, LLC.

Prothro, L.B. 2011. Written communication. Subject: *Analysis and Interpretation of Borehole Image Logs from Well ER-20-4*. June. Las Vegas, NV: National Security Technologies, LLC.

Prothro, L.B., and S.L. Drellack. 1997. *Nature and Extent of Lava-Flow Aquifers Beneath Pahute Mesa, Nevada Test Site*, DOE/NV/11718-156. Las Vegas, NV: Bechtel Nevada.

Prothro, L.B., and R.G. Warren. 2001. *Geology in the Vicinity of the TYBO and BENHAM Underground Nuclear Tests, Pahute Mesa, Nevada Test Site,* DOE/NV/11718-305. Las Vegas, NV: Bechtel Nevada.

Prothro, L.B., S.L. Drellack, D.N. Haugstad, H.E. Huckins-Gang, and M.J. Townsend. 2009. *Observations on Faults and Associated Permeability Structures in Hydrogeologic Units at the Nevada Test Site*, DOE/NV/25946--690. Las Vegas, NV: National Security Technologies, LLC.

Rose, T.P., F.C. Benedict, Jr., J.M. Thomas, W.S. Sicke, R.L. Hershey, J.B. Paces, I.M. Farnham, and Z.E. Peterman. 2006. *Geochemical Data Analysis and Interpretation of the Pahute Mesa.Oasis Valley Groundwater Flow System, Nye County, Nevada, August 2002,* UCRL-TR-224559. Livermore, CA: Lawrence Livermore National Laboratory; Reno, NV: GeoTrans, Inc., and Desert Research Institute; Denver, CO: U.S. Geological Survey; and Las Vegas, NV: Harry Reid Center for Environmental Studies.

SNJV, see Stoller-Navarro Joint Venture.

Slate, J.L., M.E. Berry, P.D. Rowley, C.J. Fridrich, K.S. Morgan, J.B. Workman, O.D. Young, G.L. Dixon, V.S. Williams, E.H. McKee, D.A. Ponce, T.G. Hildenbrand, W.C. Swadley, S.C. Lundstrom, E.B. Ekren, R.G. Warren, J.C. Cole, R.J. Fleck, M.A. Lanphere, D.A. Sawyer, S.A. Minor, D.J. Grunwald, R.J. Laczniak, C.M. Menges, J.C. Yount, and A.S. Jayko. 1999. *Part A. Digital Geologic Map of the Nevada Test Site and Vicinity, Nye, Lincoln, and Clark Counties, Nevada, and Inyo County, California, Revision 4*, Open-File Report 99-554-A, scale 1:120,000. Denver, CO: U.S. Geological Survey.

Streltsova, T.D. 1988. *Well Testing in Heterogeneous Formations,* Exxon Monographs Series #5. New York, NY: John Wiley & Sons, Inc.

Stoller-Navarro Joint Venture. 2009a. *Phase I Transport Model of Corrective Action Units 101 and 102: Central and Western Pahute Mesa, Nevada Test Site, Nye County, Nevada*, Rev. 1, S-N/99205--111. Las Vegas, NV.

Stoller-Navarro Joint Venture. 2009b. Written communication. Subject: *Preliminary Data Report for Well ER-EC-6 Groundwater Characterization Sampling.* Las Vegas, NV.

Sweetkind, D.S., and R.M. Drake, II. 2007. *Characteristics of Fault Zones in Volcanic Rocks near Yucca Flat, Nevada Test Site, Nevada*, Open-File Report 2007-1293. Reston, VA: U.S. Geological Survey.

Sweetkind, D.S., and S.C. Williams-Stroud. 1996. Written communication. Subject: *Characteristics of Fractures at Yucca Mountain, Nevada: Synthesis Report.* Denver, CO: U.S. Geological Survey.

Thomas, J.M., F.C. Benedict, Jr., T.P. Rose, R.L. Hershey, J.B. Paces, Z.E. Peterman, I.M. Farnham, K.H. Johannesson, A.K. Singh, K.J. Stetzenbach, G.B. Hudson, J.M. Kenneally, G.F. Eaton, and D.K. Smith. 2002. *Geochemical and Isotopic Interpretations of Groundwater Flow in the Oasis Valley Flow System, Southern Nevada,* Water Resources Center, Publication 45190. Las Vegas, NV.

USGS, see U.S. Geological Survey.

U.S. Department of Energy, National Nuclear Security Administration Nevada Operations Office. 2002. *Nevada Test Site Orthophoto Site Atlas,* DOE/NV/11718--604. Aerial photos acquired Summer 1998. Prepared by Bechtel Nevada. Las Vegas, NV.

U.S. Department of Energy, National Nuclear Security Administration Nevada Site Office. 2009. *Phase II Corrective Action Investigation Plan for Corrective Action Units 101 and 102: Central and Western Pahute Mesa, Nevada Test Site, Nye County, Nevada,* DOE/NV--1312-Rev. 2. Las Vegas, NV.

U.S. Department of Energy, National Nuclear Security Administration Nevada Site Office. 2010a. *Completion Report for Well ER-20-7, Corrective Action Units 101 and 102: Central and Western Pahute Mesa,* DOE/NV--1386. Prepared by National Security Technologies, LLC. Las Vegas, NV.

U.S. Department of Energy, National Nuclear Security Administration Nevada Site Office. 2010b. *Completion Report for Well ER-EC-11, Corrective Action Units 101 and 102: Central and Western Pahute Mesa,* DOE/NV--1435. Prepared by National Security Technologies, LLC. Las Vegas, NV.

U.S. Department of Energy, National Nuclear Security Administration Nevada Site Office. 2011a. *Completion Report for Well ER-20-4, Corrective Action Units 101 and 102: Central and Western Pahute Mesa,* DOE/NV--1447. Prepared by National Security Technologies, LLC. Las Vegas, NV.

U.S. Department of Energy, National Nuclear Security Administration Nevada Site Office. 2011b. *Completion Report for Wells ER-20-8 and ER-20-8#2, Corrective Action Units 101 and 102: Central and Western Pahute Mesa,* DOE/NV--1440. Prepared by National Security Technologies, LLC. Las Vegas, NV.

U.S. Department of Energy, National Nuclear Security Administration Nevada Site Office. 2011c. *Underground Test Area Quality Assurance Project Plan, Nevada National Security Site, Nevada,* DOE/NV--1450. Las Vegas, NV.

U.S. Department of Energy, Nevada Operations Office. 1997. *Regional Groundwater Flow and Tritium Transport Modeling and Risk Assessment of the Underground Test Area, Nevada Test Site, Nevada,* DOE/NV--477. Las Vegas, NV.

U.S. Department of Energy, Nevada Operations Office. 2000. *Completion Report for Well ER-EC-6,* DOE/NV/11718--360. Prepared by Bechtel Nevada. Las Vegas, NV.

U.S. Environmental Protection Agency. 2001. *Monitor Well Development,* Standard Operating Procedure 2044, Rev. 0.1. 23 October. Washington, DC: Environmental Response Team.

U.S. Geological Survey. 2011. *National Field Manual for the Collection of Water-Quality Data: U.S. Geological Survey Techniques of Water-Resources Investigations, Book 9*. As accessed at http://water.usgs.gov/owq/Field Manual on 18 August.

Warren, R.G., G.L. Cole, and D. Walther. 2000. *A Structural Block Model for the Three-Dimensional Geology of the Southwestern Nevada Volcanic Field*, LA-UR-00-5866. Los Alamos, NM: Los Alamos National Laboratory.

Winograd, I.J. 1971. "Hydrogeology of Ash Flow Tuff: A Preliminary Statement." In *Water Resources Research*, Vol. 7(4): pp. 994-1006.Washington, DC: American Geophysical Union.

Zavarin, M., Lawrence Livermore National Laboratory. 2009. Memorandum to B. Wilborn (NNSA/NSO) titled "Isotopic Analyses: 2009 ER-20-8 #1 Drilling Fluids," 15 September.

Zavarin, M., Lawrence Livermore National Laboratory. 2012a. Memorandum to B. Wilborn (NNSA/NSO) titled "Isotopic Analyses: Environmental Monitoring Well ER-20-8 #2," 24 May.

Zavarin, M., Lawrence Livermore National Laboratory. 2012b. Memorandum to B. Wilborn (NNSA/NSO) titled "Isotopic Analyses: Environmental Monitoring Well ER-EC-1," 11 April.

Zavarin, M., Lawrence Livermore National Laboratory. 2012c. Memorandum to B. Wilborn (NNSA/NSO) titled "Isotopic Analyses: Environmental Monitoring Well ER-EC-6," 11 April.

Appendix A

Groundwater Chemistry Results

Table A.1-1
Water-Chemistry Data for Well ER-20-8 (TCA Completion)
(Page 1 of 4)

Analyte	Depth Discrete				Composite Wellhead				
	N-I				N-I		LLNL	USGS (LANL)*	DRI (LANL)*
	2,700 ft		2,800 ft						
	08/11/2009		05/26/2011		06/27/2011				
Miscellaneous and Field Measurements [a]									
Bromide (field) (mg/L)	--	--	0.2, 0.3, 0.3		0.5		0.9	0.5	0.8
DO (field) (mg/L)	--	--	4.0, 5.5, 3.8		4.7		4.7	4.7	4.6
pH (field)	--	--	7.79, 7.82, 7.97		8.35		8.43	8.35	8.42
pH (lab)	8.35 [b]	8.36 [b]	8.42 [b]	8.5 [b]	8.5 [b]	8.6 [b]	--	--	--
SEC (field) (mmhos/cm)	--	--	0.447, 0.437, 0.426		0.462		0.454	0.462	0.431
SEC (lab) (mmhos/cm)	0.409	0.419	0.435	0.432	0.430	0.430	--	--	--
Turbidity (NTU)	--	--	11.5, 7.6, 19.1		3.4		3.8	3.4	8.2
Temperature (°C)	--	--	45.5, 46.2		45.5		45.6	45.5	45.6
Major and Minor Constituents (mg/L)									
Bicarbonate as $CaCO_3$	120	110	110	110	100	100	--	--	--
Carbonate as $CaCO_3$	<20	<20	<20	<20	<10	<10	--	--	--
Bromide	0.26	0.22	0.10 [b]	0.11 [b]	0.098 [b]	0.11 [b]	<0.05	--	--
Chloride	23	23	26	28	33	28	28.3	--	--
Fluoride	4.0	4.0	3.7	3.5	3.8	3.8	4.3	--	--
Sulfate	43	42	47	45	49	50	50	--	--
Calcium	3.1 | 3.1	3.1 | 3.0	-- | 2.3	-- | 1.7	2.1 | 2.1	2.1 | 2.1	2.3	2.1	--
Magnesium	<1 [c] | <1 [c]	<1 [c] | <1 [c]	-- | 0.54 [d]	-- | <0.01	<1 [c] | <1 [c]	<1 [c] | <1 [c]	0.02	<0.4	--
Potassium	3.0 [c] | 2.2 [c]	2.5 [c] | 2.2 [c]	-- | 2.6	-- | 2.4	2.4 | 2.4	2.4 | 2.4	2.2	2.0	--
Sodium	72 | 71	72 | 71	-- | 81	-- | 82	79 [b] | 77 [b]	77 [b] | 78 [b]	88	89	--
Aluminum	1.3 [b] | 0.34 [c]	0.86 [b] | 0.34 [c]	0.6 [b] | 1.4 [b]	1.8 [b] | 0.017 [d]	<0.2 [c] | <0.2 [c]	<0.2 [c] | <0.2 [c]	0.06	0.04	R
Iron	38 | 7.6	35 | 7.6	1.7 [b] | 4.2 [b]	4.2 [b] | 0.038 [d]	<0.10 [c] | <0.10 [c]	<0.10 [c] | <0.10 [c]	<0.015	--	R
Silicon	26 | 22	23 | 21	28 | 29	29 | 26	25 [b] | 25 [b]	25 [b] | 25 [b]	--	24	--
Sulfide	<2.0	<2.0	<2.0	<2.0	<2.0	<2.0	--	--	--

Table A.1-1
Water-Chemistry Data for Well ER-20-8 (TCA Completion)
(Page 2 of 4)

Analyte	Depth Discrete				Composite Wellhead				
	N-I				N-I		LLNL	USGS (LANL)*	DRI (LANL)*
	2,700 ft		2,800 ft						
	08/11/2009		05/26/2011		06/27/2011				
Major and Minor Constituents (mg/L) continued									
Total Dissolved Solids	310	270	280	270	280	290	--	--	--
Total Inorganic Carbon	--	--	--	--	--	--	26	--	--
Total Organic Carbon	4.1	3.8	<1	<1	<1	<1	0.2	--	1.69
Trace Constituents (μg/L)									
Antimony	--	--	--	--	--	--	0.17	<2.5	--
Arsenic	<10 [c] | <3.4	<10 [c] | <3.4	7.1 [e] | 4.6 [e]	6.7 [e] | 5.3 [e]	7.3 [d] | 5.7 [d]	5.9 [d] | <3.9	7.1	6.6	--
Barium	<100 [c] | <100 [c]	<100 [c] | <100 [c]	3.8 [d] | 11 [d]	16 [d] | <0.19 [b]	<100 [c] | <100 [c]	<100 [c] | <100 [c]	0.67	<15	--
Beryllium	--	--	--	--	--	--	<0.09	<2.5	--
Boron	--	--	--	--	--	--	--	123	--
Cadmium	<0.38 | <0.38	<0.38 | <0.38	<0.33 | <0.33	<0.33 | <0.33	0.34 | <0.33	<0.33 | <0.33	<0.018	<2.5	--
Cesium	--	--	--	--	--	--	1.32	<0.5	--
Chromium	40 [b] | <10 [c]	10 [b] | <10 [c]	9.1 [d] | 17	13 | <0.51	0.95 | <0.51	<0.51 | 0.67	0.41	<1.3	--
Cobalt	--	--	--	--	--	--	<0.018	<1.3	--
Copper	--	--	--	--	--	--	0.3	<2.5	--
Lead	2.0 | <1.8	2.0 [b] | <1.8	<1.3 | <1.3	<1.3 | <1.3	1.5 | <1.3	<1.3 | <1.3	<0.03	<1.5	--
Lithium	110 [b] | 110	110 | 110	-- | 86 [b]	-- | 86 [b]	96 [b] | 95 [b]	95 [b] | 96 [b]	--	100	--
Manganese	340 | 210	320 | 210	25 | 63	71 | 1.1 [d]	<10 [c] | <10 [c]	<10 [c] | <10 [c]	3.8	3.6	--
Mercury	0.071 | 0.014	0.053 | <0.01	<0.01 | <0.01	<0.01 | <0.01	<0.01 | <0.01	<0.01 | <0.2	--	--	--
Molybdenum	--	--	--	--	--	--	4.9	5.5	--
Nickel	--	--	--	--	--	--	<0.57	<2.5	--
Rubidium	--	--	--	--	--	--	7.9	7.8	--
Selenium	<3.2 | <3.2	<3.2 | <3.2	<2.7 | <2.7	<2.7 | <2.7	<2.7 | <2.7	<2.7 | <2.7	<2.1	<2.5	--
Silver	<1.0 | <1.0	<1.0 | <1.0	<1.1 | <1.1	<1.1 | <1.1	<1.1 | <1.1	<1.1 | <1.1	<0.024	<2.5	--
Strontium	<10 [c] | <10 [c]	<10 [c] | <10 [c]	-- | 0.59 [d]	-- | <0.08	0.52 [d] | 0.22 [d]	0.26 [d] | 0.32 [d]	1.85	2.8	--

Table A.1-1
Water-Chemistry Data for Well ER-20-8 (TCA Completion)
(Page 3 of 4)

Analyte	Depth Discrete				Composite Wellhead				
	N-I				N-I		LLNL	USGS (LANL)*	DRI (LANL)*
	2,700 ft		2,800 ft						
	08/11/2009		05/26/2011		06/27/2011				
Trace Constituents (μg/L) continued									
Uranium	3.0 | 2.9	2.9 | 2.8	-- | 2.7	-- | 2.8	2.6 | 2.6	2.6 | 2.8	2.46	2.71 [f] | 2.85 [g]	--
Vanadium	--	--	--	--	--	--	1.86	1.7	--
Zinc	--	--	--	--	--	--	0.31	<50	--
Environmental Isotopes									
δD (‰)	--	--	--	--	--	--	-118	--	-115
$\delta^{18}O$ (%)	--	--	--	--	--	--	-15.4	--	-15.0
$\delta^{13}C$ (‰)	--	--	--	--	--	--	-2.7	--	-7.5
^{14}C (pmc)	--	--	--	--	--	--	122	--	--
$^{82}S/^{84}S$ (‰)	--	--	--	--	--	--	--	18.1	--
$^{87}Sr/^{86}Sr$ (Ratio)	--	--	--	--	--	--	--	0.71083	--
$^{234}U/^{238}U$ Activity Ratio	--	--	--	--	--	--	--	3.668	--
Radionuclides (pCi/L)									
Tritium	250 ± 150 (240 [h])	<240	2,110 ± 400 (320 [h])	2,070 ± 400 (320 [h])	3,020 ± 540 (350 [h])	2,650 ± 490 (350 [h])	2,813	2,800 *	3,000 *
Gross Alpha	4.8 ± 1.6 (1.3 [h])	4.3 ± 1.5 (1.4 [h])	2.6 ± 1.2 (1.5 [h])	4.7 ± 1.6 (1.3 [h])	4.1 ± 1.5 (1.3 [h])	3.2 ± 1.4 (1.6 [h])	--	--	--
Gross Beta	4.1 ± 1.8 (2.6 [h])	3.0 ± 2.0 (3.0 [h])	2.8 ± 1.5 (2.3 [h])	5.7 ± 1.9 (2.4 [h])	3.8 ± 1.7 (2.4 [h])	<2.8	--	--	--
^{14}C	<410	<410	<380	<390	<400	<400	0.197	--	--
^{26}Al	<7.4	<11	<4.1	<4.3	<4.7	<9.1	--	--	--
^{40}K	<130	<138	<82	<81	<111	<149	--	<2 *	<2 *
^{90}Sr	--	--	--	--	<0.46	<0.46	--	--	--
^{94}Nb	<7.0	<7.7	<3.6	<3.2	<4.0	<7.0	--	<0.2 *	<0.2 *
^{99}Tc	--	--	--	--	<7.4	<7.2	--	<2E+04 *	<2E+04 *
^{121m}Sn	--	--	--	--	--	--	--	<20 *	<20 *
^{126}Sn	--	--	--	--	--	--	--	<20 *	<20 *
^{129}I	--	--	--	--	<4.0 [b]	<3.4 [b]	2.06E-04	<40 *	<40 *

Table A.1-1
Water-Chemistry Data for Well ER-20-8 (TCA Completion)
(Page 4 of 4)

Analyte	Depth Discrete				Composite Wellhead				
	N-I				N-I		LLNL	USGS (LANL)*	DRI (LANL)*
	2,700 ft		2,800 ft						
	08/11/2009		05/26/2011		06/27/2011				
Radionuclides (pCi/L) continued									
^{137}Cs	<7.3	<8.0	<3.6	<3.1	<3.9	<7.4	--	0.17 ± 0.02 *	0.10 ± 0.02 *
^{150}Eu	--	--	--	--	--	--	--	<0.1 *	<0.1 *
^{152}Eu	<41	<48	<20	<20	<21	<38	--	<0.1 *	<0.1 *
^{154}Eu	<39	<48	<21	<19	<22	<44	--	<0.2 *	<0.2 *
^{166m}Ho	--	--	--	--	--	--	--	<0.2 *	<0.2 *
^{232}Th	--	--	--	--	--	--	--	<70 *	<70 *
^{233}U	--	--	--	--	--	--	--	<30 *	<30 *
^{234}U	--	--	--	--	--	--	--	<100 *	<100 *
^{235}U	<42	<39	<33	<25	<41	<41	--	--	--
^{236}U	--	--	--	--	--	--	--	<300 *	<300 *
^{239,240}Pu	<0.035	<0.031	0.020 ± 0.015 (0.008 [h]) [i]	<0.038	<0.025	<0.010	--	<0.001 *	<0.001 *
^{241}Am	<9.2	<7.6	<43	<25	<21	<46	--	<0.5 *	<0.5 *
^{243}Am	--	--	--	--	--	--	--	<0.3 *	<0.3 *

* All radionuclide data reported in these columns were reported by LANL; all other data are from USGS or DRI as specified by the column header. Field parameters reported for the LLNL sample were collected near the time of the LANL sample and are also considered representative of this sample.
[a] Field measurements were made by N-I and coincide as closely as possible to the collection time for the associated samples.
[b] Value is an estimate. Hold time was exceeded for pH measurements. Other results considered an estimate as a result of failure to meet specific QC criteria.
[c] Contamination was observed in the associated blank. The measured value is reported if greater than the contract required reporting limit; otherwise, the value is reported as less than the contract required reporting limit.
[d] Value is an estimate with a negative bias as a result of failure to meet specific QC criteria.
[e] Value is an estimate with a positive bias as a result of failure to meet specific QC criteria.
[f] Analyzed using thermal ionization mass spectrometry with isotope dilution.
[g] Analyzed using inductively coupled plasma mass spectrometry.
[h] Detection limit
[i] Reported value is less than the detection limit plus the error and thus highly uncertain.

-- = Not analyzed
R = Data were rejected.

Note: Values reported with a "|" indicate analysis results from unfiltered/filtered samples.

Al = Aluminum
$CaCO_3$ = Calcium carbonate
mmhos/cm = Millimhos per centimeter
NNES = Navarro Nevada Environmental Services, LLC

pmc = Percent modern carbon
QC = Quality control
S = Sulfur
µg/L = Micrograms per liter

Table A.1-2
Water-Chemistry Data for Well ER-20-8 (TSA Completion)
(Page 1 of 3)

Analyte	Depth Discrete		Composite Wellhead				
	N-I		N-I		LLNL	USGS (LANL)*	DRI (LANL)*
	3,160 ft	3,170 ft					
	08/11/2009	07/22/2011	08/08/2011				
Miscellaneous and Field Measurements [a]							
Bromide (field) (mg/L)	--	0.4, 0.3	0.2		0.5	0.2	0.4
DO (field) (mg/L)	--	4.0, 4.1	4.9		4.6	4.9	4.6
pH (field)	--	8.34, 8.23	8.36		8.23	8.36	8.34
pH (lab)	8.46 [b]	8.6 [b]	8.5 [b]	8.6 [b]	--	--	--
SEC (field) (mmhos/cm)	--	0.411, 0.415	0.409		0.408	0.409	0.408
SEC (lab) (mmhos/cm)	0.413	0.430	0.410	0.410	--	--	--
Turbidity (NTU)	--	11.6, 12.9	16.7		8.4	16.7	17.9
Temperature (°C)	--	49.7, 49.8	49.7		49.6	49.7	49.7
Major and Minor Constituents (mg/L)							
Bicarbonate as $CaCO_3$	120	110	110	110	--	--	--
Carbonate as $CaCO_3$	<20	<5	<10	<10	--	--	--
Bromide	0.24	0.081 [b]	0.081 [b]	0.081 [b]	<0.05	--	--
Chloride	23	24	23	24	24	--	--
Fluoride	4.1	4.2 [b]	4.2	4.1	4.7	--	--
Sulfate	43	44	43	42	44	--	--
Calcium	4.5 | 3.5	-- | 4.4	3.4 | 3.4	3.4 | 3.3	3.6	3.4	--
Magnesium	<1 [c] | <1 [c]	-- | <1 [c]	0.027 [d] | <1 [c]	<0.013 | <0.013	0.03	<0.4	--
Potassium	3.3 | 2.2 [c]	-- | 1.8	1.8 | 1.8	1.7 | 1.7	1.6	1.6	--
Sodium	74 | 72	-- | 77	79 [b] | 79 [b]	78 [b] | 78 [b]	93	86	--
Aluminum	3.0 [b] | 0.51	2.8 | <0.20 [c]	<0.20 [c] | <0.20 [c]	<0.20 [c] | <0.20 [c]	0.04	0.027	R
Iron	66 | 7.0	9.3 | <0.10 [c]	<0.10 [c] | <0.005	<0.10 [c] | <0.005	0.01	--	R
Silicon	28 | 22	28 | 23	24 | 24	24 | 24	22	26	--
Sulfide	<2	<2	<2	<2	--	--	--
Total Dissolved Solids	310	300	260	290	--	--	--
Total Inorganic Carbon	--	--	--	--	27.7	--	--
Total Organic Carbon	4.2	1.5	<1	<1	0.1	--	1.75
Trace Constituents (µg/L)							
Antimony	--	--	--	--	0.42	<2.5	--
Arsenic	11 [c] | <10 [c]	6.1 | <3.9	9.0 | 8.8	<3.9 | 5.0	6.7	6.6	--
Barium	100 | <100 [c]	23 [d] | 2.2 [d]	1.3 [d] | <100 [c]	<100 [c] | <0.19	0.31	<15	--
Beryllium	--	--	--	--	<0.18	<2.5	--
Boron	--	--	--	--	--	125	--
Cadmium	<5.0 [c] | <0.38	1.7 [d] | <0.33	<0.33 | <0.33	<0.33 | <0.33	<0.027	<2.5	--

Table A.1-2
Water-Chemistry Data for Well ER-20-8 (TSA Completion)
(Page 2 of 3)

Analyte	Depth Discrete		Composite Wellhead				
	N-I		N-I		LLNL	USGS (LANL)*	DRI (LANL)*
	3,160 ft	3,170 ft					
	08/11/2009	07/22/2011	08/08/2011				
Trace Constituents (μg/L) continued							
Cesium	--	--	--	--	1.75	<0.5	--
Chromium	35 [b] | <10 [c]	19 | <0.51	<0.51 | <0.51	<0.51 | <0.51	0.7	<1.3	--
Cobalt	--	--	--	--	0.072	<1.3	--
Copper	--	--	--	--	0.82	<2.5	--
Lead	5.2 [b] | 2.7	6.1 | <1.3	<1.3 | <1.3	<1.3 | <1.3	0.129	<0.9	--
Lithium	110 | 110	-- | <0.25 [b]	94 [b] | 94 [b]	94 [b] | 93 [b]	--	136	--
Manganese	720 | 260	170 | <10 [c]	<10 [c] | <10 [c]	<10 [c] | <10 [c]	3.37	3.1	--
Mercury	0.051 | 0.031	<0.003 | <0.003	<0.003 | <0.003	<0.003 | <0.003	--	--	--
Molybdenum	--	--	--	--	5.9	6.5	--
Nickel	--	--	--	--	0.46	<2.5	--
Rubidium	--	--	--	--	6.0	5.9	--
Selenium	<3.2 | <3.2	<2.7 | <2.7	3.7 | <2.7	<2.7 | 3.8	0.68	<2.5	--
Silver	<1.0 | <1.0	<1.1 | <1.1	<1.1 | <1.1	<1.1 | <1.1	<0.027	<2.5	--
Strontium	14 [b] | <10 [c]	-- | 5.9 [d]	3.4 [d] | 3.3 [d]	3.1 [d] | 3.0 [d]	6.1	7.4	--
Uranium	4.1 | 3.2	2.4	2.6 | 2.6	2.5 | 2.3	2.63	2.76 [e] | 2.77 [f]	--
Vanadium	--	--	--	--	1.68	<1.3	--
Zinc	--	--	--	--	<0.6	<50	--
Environmental Isotopes							
δD (‰)	--	--	--	--	-116	--	-115
$\delta^{18}O$ (‰)	--	--	--	--	-15.5	--	-15.1
$\delta^{13}C$ (Inorganic Carbon) (‰)	--	--	--	--	-2.6	--	-7.2
^{14}C (Inorganic Carbon) (pmc)	--	--	--	--	37.6	--	--
$^{82}S/^{84}S$ (‰)	--	--	--	--	--	17.8	--
$^{87}Sr/^{86}Sr$	--	--	--	--	--	0.71079	--
$^{234}U/^{238}U$ Activity Ratio	--	--	--	--	--	4.040	--
Radionuclides (pCi/L)							
Tritium	<240	<320	<350	<350	267	<500 *	<500 *
Gross Alpha	7.4 ± 2.2 (1.6 [g])	4.2 ± 1.2 (1.2 [g])	1.7 ± 1.1 (1.5 [g])	2.5 ± 1.1 (1.4 [g])	--	--	--
Gross Beta	6.9 ± 2.2 (2.8 [g])	4.0 ± 1.3 (1.7 [g])	3.1 ± 1.5 (2.2 [g])	<2.3	--	--	--
^{14}C	<410	<390	<380	<380	0.0636	--	--
^{26}Al	<11	<9.4	<9.2	<6.3	--	--	--

Table A.1-2
Water-Chemistry Data for Well ER-20-8 (TSA Completion)
(Page 3 of 3)

Analyte	Depth Discrete		Composite Wellhead				
	N-I		N-I		LLNL	USGS (LANL)*	DRI (LANL)*
	3,160 ft	3,170 ft					
	08/11/2009	07/22/2011	08/08/2011				
Radionuclides (pCi/L) continued							
^{40}K	<128	<168	<200	<127	--	<2 *	<2 *
^{90}Sr	--	--	<0.47	<0.48	--	--	--
^{94}Nb	<8.2	<6.3	<7.0	<6.1	--	<0.2 *	<0.2 *
^{99}Tc	--	--	<7.4	<7.1	--	<2E+04 *	<2E+04 *
^{121m}Sn	--	--	--	--	--	<20 *	<20 *
^{126}Sn	--	--	--	--	--	<20 *	<20 *
^{129}I	--	--	<14.3	<2.9	3.53E-05	<40 *	<40 *
^{137}Cs	<9.0	<6.8	<6.9	<5.6	--	<0.05 *	<0.06 *
^{150}Eu	--	--	--	--	--	<0.1 *	<0.1 *
^{152}Eu	<49	<31	<38	<29	--	<0.1 *	<0.1 *
^{154}Eu	<46	<31	<40	<39	--	<0.3 *	<0.3 *
^{166}Ho	--	--	--	--	--	<0.2 *	<0.2 *
^{232}Th	--	--	--	--	--	<70 *	<70 *
^{233}U	--	--	--	--	--	<30 *	<30 *
^{234}U	--	--	--	--	--	<100 *	<100 *
^{235}U	<47	<34	<42	<30	--	--	--
^{236}U	--	--	--	--	--	<300 *	<300 *
^{239,240}Pu	<0.023	<0.015	<0.043	<0.038	--	<0.001 *	<0.001 *
^{241}Am	<11.4	<7.5	<13.7	<137	--	<0.5 *	<0.5 *
^{243}Am	--	--	--	--	--	<0.3 *	<0.3 *

* All radionuclide data reported in these columns were reported by LANL; all other data are from USGS or DRI as specified by the column header. Field parameters reported for the N-I and USGS samples were collected near the time of the LANL sample and are also considered representative of this sample.
[a] Field measurements were made by N-I (formerly NNES) and coincide as closely as possible to the collection time for the associated samples.
[b] Value is an estimate. Hold time was exceeded for pH measurements. Other results considered an estimate as a result of failure to meet specific QC criteria.
[c] Contamination was observed in the associated blank. The measured value is reported if greater than the contract required reporting limit; otherwise, the value is reported as less than the contract required reporting limit.
[d] Value is an estimate with a negative bias as a result of failure to meet specific QC criteria.
[e] Analyzed using thermal ionization mass spectrometry with isotope dilution.
[f] Analyzed using inductively coupled plasma mass spectrometry.
[g] Detection limit

-- = Not analyzed
R = Data were rejected.

Note: Values reported with a "|" indicate analysis results from unfiltered/filtered samples.

Table A.1-3
Water-Chemistry Data for Well ER-20-4
(Page 1 of 5)

Analyte	Depth Discrete					Composite Wellhead (CHZCM)				
	N-I					N-I		LLNL	USGS (LANL)*	DRI (LANL)*
	1,870 ft bgs (CHZCM)		3,000 ft bgs (CFCU)	2,750 ft bgs (CFCU)						
	09/07/2010			09/04/2011		09/20/2011				09/21/2011
Miscellaneous and Field Measurements [a]										
Bromide (field) (mg/L)	--	--	--	0.2, 0.1		0.3		0.3		0.2, 0.2
DO (field) (mg/L)	--	--	--	4.8, 5.3		6.0		6.5		7.4, 6.7
pH (field)	--	--	--	7.44, 7.87		7.56		7.48		7.48, 7.95
pH (lab)	8.13 [b]	8.18 [b]	8.26 [b]	8.1 [b]	8.2 [b]	8.4 [b]	8.3 [b]	--		--
SEC (field) (mmhos/cm)	--	--	--	0.272, 0.275		0.230		0.231		0.240, 0.240
SEC (lab) (mmhos/cm)	0.484	0.496	0.313	0.280	0.280	0.250	0.250	--		--
Turbidity (NTU)	--	--	--	24.2, 6.6		7.9		12.9		12.3, 2.0
Temperature (°C)	--	--	--	43.6, 43.7		44.2		44.3		44.2, 44.3
Major and Minor Constituents (mg/L)										
Bicarbonate as $CaCO_3$	100	100	95	94	93	89	91	--	--	--
Carbonate as $CaCO_3$	<10	<10	<10	<10	<10	<10	<10	--	--	--
Bromide	7.9	8.0	0.067 [b]	0.048 [b]	0.053 [b]	<0.021	<0.021	--	--	--
Chloride	8.9	9.0	5.1	4.7	4.8	4.7	4.6	--	--	--
Fluoride	6.5	6.6	8.0	7.8	8.0	8.0	7.9	--	--	--
Sulfate	25	25	18	17	17	17	17	--	--	--
Calcium	21	21	4.0	4.2	4.2	4.3 | 4.3	4.2 | 4.2	4.5	3.8	--
Magnesium	<1 [c]	<1 [c]	<1 [c]	<1 [c]	<1 [c]	<1 [c] | <1 [c]	<0.01 | <0.01	0.05	<0.4	--
Potassium	4.1	4.3	1.9	1.3	1.3	1.2 | 1.2	1.2 | 1.2	1.3	1.0	--
Sodium	95	96	50	51	50	50 [b] | 49 [b]	49 | 49	62	53	--
Aluminum	2.8 | 0.22	2.7 | 0.41	0.76 | <0.20 [c]	<0.20 [c] | <0.02	0.22 | <0.02	<0.02 | <0.02	<0.02 | <0.02	0.005	0.005	--
Iron	1.7 [b] | 0.41 [b]	1.7 [b] | 0.58 [b]	0.46 [b] | 0.13 [c]	0.45 | <0.1 [c]	0.50 | <0.1 [c]	<0.005 | <0.1 [c]	<0.005 | <0.005	0.003	--	--

Table A.1-3
Water-Chemistry Data for Well ER-20-4
(Page 2 of 5)

Analyte	Depth Discrete					Composite Wellhead (CHZCM)				
	N-I					N-I		LLNL	USGS (LANL)*	DRI (LANL)*
	1,870 ft bgs (CHZCM)		3,000 ft bgs (CFCU)	2,750 ft bgs (CFCU)						
	09/07/2010			09/04/2011		09/20/2011				09/21/2011
Major and Minor Constituents (mg/L) continued										
Silicon	29 | 24	30 | 25	26 | 26	26 | 25	25 | 25	24 | 24	24 | 24	23	20	--
Sulfide	<2.0	<2.0	<2.0	<2.0 [b]	<2.0 [b]	<2.0	<2.0	--	--	--
Total Dissolved Solids	840 [b]	840 [b]	200 [b]	210 [b]	190 [b]	200	200	--	--	--
Total Inorganic Carbon	--	--	--	--	--	--	--	--	--	--
Total Organic Carbon	160	180	3.0	<1	<1	<1	<1	--	--	1.69
Trace Constituents (μg/L)										
Antimony	--	--	--	--	--	--	--	0.51	<2.5	--
Arsenic	7.2 | <3.9	9.5 | 6.0	6.2 | 4.2	5.9 [b] | <3.9	<3.9 | 5.1 [b]	<3.9 | 5.6 [b]	<3.9 | <3.9	4.9	4.6	--
Barium	48 [d] | 11 [d]	47 [d] | 19 [d]	150 [b] | 44 [d]	<100 [c] | <100 [c]	<100 [c] | <100 [c]	0.51 [d] | 1.9 [d]	0.55 [d] | 0.49 [d]	1.3	<15	--
Beryllium	--	--	--	--	--	--	--	<0.12	<2.5	--
Boron	--	--	--	--	--	--	--	--	87	--
Cadmium	1.5 | 0.43	1.0 | 0.76	<0.33 | 0.39	<0.33 | <0.33	<0.33 | <0.33	<0.33 | <0.33	<0.33 | <0.33	<0.06	<2.5	--
Cesium	--	--	--	--	--	--	--	1.03	<0.5	--
Chromium	<10 [c] | <10 [c]	<10 [c] | <10 [c]	<10 [c] | <10 [c]	<10 [c] | <0.51	<10 [c] | <0.51	<0.51 | <0.51	<0.51 | <0.51	0.08	<1.3	--
Cobalt	--	--	--	--	--	--	--	0.17	<1.3	--
Copper	--	--	--	--	--	--	--	0.88	<2.5	--
Lead	5.9 [d] | <1.3	6.9 [d] | <1.3	1.6 [d] | <1.3	<1.3 | <1.3	<1.3 | <1.3	<1.3 | <1.3	<1.3 | <1.3	0.32	<0.9	--
Lithium	-- | 620 [b]	-- | 630 [b]	-- | 70 [b]	-- | 69 [b]	-- | 67 [b]	63 [b] | 63 [b]	63 | 63	--	60.3	--
Manganese	110 | 52	120 | 66	40 | 6.0 [d]	14 | <10 [c]	13 | <10 [c]	1.7 [d] | 2.0 [d]	1.6 [d] | 1.6 [d]	2.58	2.3	--
Mercury	<0.01 | <0.01	<0.01 | <0.01	<0.2 [c] | <0.01	<0.003 | <0.003	<0.003 | <0.003	<0.003 | <0.003	<0.003 | <0.003	--	--	--
Molybdenum	--	--	--	--	--	--	--	9.6	9.7	--

Table A.1-3
Water-Chemistry Data for Well ER-20-4
(Page 3 of 5)

Analyte	Depth Discrete					Composite Wellhead (CHZCM)				
	N-I					N-I		LLNL	USGS (LANL)*	DRI (LANL)*
	1,870 ft bgs (CHZCM)		3,000 ft bgs (CFCU)	2,750 ft bgs (CFCU)						
	09/07/2010			09/04/2011		09/20/2011				09/21/2011
Trace Constituents (µg/L) continued										
Nickel	--	--	--	--	--	--	--	<0.27	<2.5	--
Rubidium	--	--	--	--	--	--	--	5.2	4.9	--
Selenium	11 | 6.5	14 | 6.5	<2.7 | <2.7	<2.7 | <2.7	<2.7 | <2.7	<2.7 | <2.7	<2.7 | <2.7	<0.3	<2.5	--
Silver	<1.1 | <1.1	<1.1 | <1.1	<1.1 | <1.1	<1.1 | <1.1	<1.1 | <1.1	<1.1 | <1.1	<1.1 | <1.1	<0.033	<2.5	--
Strontium	-- | 24 [b]	-- | 24 [b]	-- | 4.5 [d]	-- | 2.6 [d]	-- | 2.5 [d]	2.0 [d] | 2.3 [d]	2.0 [d] | 2.0 [d]	5.45	4.7	--
Uranium	-- | 1.3	-- | 1.4	-- | 1.5	-- | 1.5	-- | 1.6	1.7 | 1.6	1.6 | 1.7	1.61	1.72 [e] / 1.71 [f]	--
Vanadium	--	--	--	--	--	--	--	2.4	2.3	--
Zinc	--	--	--	--	--	--	--	0.65	<50	--
Environmental Isotopes										
δD (‰)	--	--	--	--	--	--	--	-116	--	-114
$\delta^{18}O$ (‰)	--	--	--	--	--	--	--	--	--	-14.9
$\delta^{13}C$ (DIC) (‰)	--	--	--	--	--	--	--	--	--	-8.6
$\delta^{13}C$ (DOC) (‰)	--	--	--	--	--	--	--	--	--	--
^{14}C (DOC) (‰)	--	--	--	--	--	--	--	--	--	--
$^{82}S/^{84}S$ (‰)	--	--	--	--	--	--	--	--	--	--
$^{87}Sr/^{86}Sr$ (Ratio)	--	--	--	--	--	--	--	--	0.71048	--
$^{234}U/^{238}U$ Activity Ratio	--	--	--	--	--	--	--	--	5.355	--

Table A.1-3
Water-Chemistry Data for Well ER-20-4
(Page 4 of 5)

Analyte	Depth Discrete					Composite Wellhead (CHZCM)				
	N-I					N-I		LLNL	USGS (LANL)*	DRI (LANL)*
	1,870 ft bgs (CHZCM)		3,000 ft bgs (CFCU)	2,750 ft bgs (CFCU)						
	09/07/2010			09/04/2011		09/20/2011				09/21/2011
Radionuclides (pCi/L)										
Tritium	<350	<350	<350	<290	<290	<300	<290	<142	<500 *	<500 *
Gross Alpha	10.1 ± 2.9 (1.9 g)	8.5 ± 2.2 (1.8 g)	4.1 ± 1.7 (1.6 g)	2.5 ± 1.5 (1.8 g)	3.7 ± 1.6 (1.5 g)	2.1 ± 1.5 (2.0 g)	2.0 ± 1.4 (1.8 g)	--	--	--
Gross Beta	12.7 ± 2.9 (2.7 g)	11.7 ± 2.5 (2.3 g)	4.0 ± 1.7 (2.2 g)	<2.7	<2.3	<2.6	<2.6	--	--	--
^{14}C	<370	<370	<370	<390 b	<390 b	<380	<380	--	--	--
^{26}Al	<7.8	<16	<9.7	<6.0	<6.5	<15	<11	--	--	--
^{40}K	<155	<180	<154	<128	<126	<182	<165	--	<2 *	<2 *
^{90}Sr	--	--	--	--	--	<0.44	<0.40	--	--	--
^{94}Nb	<7.5	<9.3	<8.3	<5.8	<5.6	<9.5	<11	--	<0.2 *	<0.1 *
^{99}Tc	--	--	--	--	--	<7.0	<7.2	--	<2E+04 *	<2E+04 *
^{121m}Sn	--	--	--	--	--	--	--	--	<15 *	<15 *
^{126}Sn	--	--	--	--	--	--	--	--	<15 *	<15 *
^{129}I	--	--	--	--	--	<3.6	<3.9	1.14E-06	<30 *	<30 *
^{137}Cs	<9.2	<9.0	<9.9	<5.7	<5.6	<10	<9.2	--	<0.4 *	<0.5 *
^{150}Eu	--	--	--	--	--	--	--	--	<10 *	<10 *
^{152}Eu	<45	<68	<48	<30	<34	<52	<45	--	<0.08 *	<0.08 *
^{154}Eu	<48	<55	<48	<33	<32	<55	<57	--	<0.2 *	<0.2 *
^{166m}Ho	--	--	--	--	--	--	--	--	<0.2 *	<0.2 *
^{232}Th	--	--	--	--	--	--	--	--	<60 *	<60 *
^{233}U	--	--	--	--	--	--	--	--	<20 *	<20 *
^{234}U	--	--	--	--	--	--	--	--	<100 *	<100 *
^{235}U	<52	<57	<55	<38	<24	<38	<55	--	--	--

Table A.1-3
Water-Chemistry Data for Well ER-20-4
(Page 5 of 5)

Analyte	Depth Discrete					Composite Wellhead (CHZCM)				
	N-I					N-I		LLNL	USGS (LANL)*	DRI (LANL)*
	1,870 ft bgs (CHZCM)		3,000 ft bgs (CFCU)	2,750 ft bgs (CFCU)						
	09/07/2010			09/04/2011		09/20/2011				09/21/2011
Radionuclides (pCi/L) continued										
^{236}U	--	--	--	--	--	--	--	--	<300 *	<300 *
$^{239,240}Pu$	<0.020	<0.019	<0.023	<0.020	<0.026	<0.009	<0.008	--	<0.001 *	<0.001 *
^{241}Am	<76	<54	<81	<6.9	<30	<18	<250	--	<0.4 *	<0.4 *
^{243}Am	--	--	--	--	--	--	--	--	<0.3 *	<0.3 *

* All radionuclide data reported in these columns were reported by LANL; all other data are from USGS or DRI as specified by the column header. Field parameters reported for the N-I sample were collected near the time of the LANL sample and are also considered representative of this sample.
[a] Field measurements were made by N-I (formerly NNES) and coincide as closely as possible to the collection time for the associated samples.
[b] Value is an estimate. Hold time was exceeded for pH, sulfide, and total dissolved solids measurements. Other measurements considered estimates as a result of failure to meet specific QC criteria.
[c] Contamination was observed in the associated blank. The measured value is reported if greater than the contract required reporting limit; otherwise, the value is reported as less than the contract required reporting limit.
[d] Value is an estimate with a negative bias as a result of failure to meet specific QC criteria.
[e] Analyzed using thermal ionization mass spectrometry with isotope dilution.
[f] Analyzed using inductively coupled plasma mass spectrometry.
[g] Detection limit

-- = Not analyzed

Note: Values reported with a "|" indicate analysis results from unfiltered/filtered samples.

Table A.1-4
Water-Chemistry Data for Wells ER-20-8 #2, ER-20-7, and ER-EC-11
(Page 1 of 4)

Analyte	ER-20-8 #2					ER-EC-11					ER-20-7				
	N-I		LLNL	DRI	USGS	N-I		LLNL	DRI	USGS	N-I		LLNL	USGS	
	12/18/2009				12/17/2009	05/18/2010					09/24/2010				
Miscellaneous and Field Measurements															
Bromide (field) (mg/L)	0.85 [a]	0.99 [a]	0.80 [a]	0.85 [a]	1.33 [a]	0.46 [a], 0.26 [a], 0.70 [a]					0.18 [a]			0.21 [a]	
DO (field) (mg/L)	2.66 [a]	3.26 [a]	3.15 [a]	2.66 [a]	2.74 [a]	3.2 [a], 3.4 [a], 3.4 [a]					5.99 [a]			3.54 [a]	
pH (field)	8.18 [a]	8.14 [a]	8.04 [a]	8.18 [a]	8.15 [a]	7.46 [a], 8.20 [a], 8.24 [a]					7.97 [a]			7.92 [a]	
pH (lab)	8.41 [b]	8.53 [b]	--	--	--	8.50 [b]	8.58 [b]	--	--	--	8.49 [b]	8.52 [b]	--	--	
SEC (field) (mmhos/cm)	0.436 [a]	0.437 [a]	0.437 [a]	0.436 [a]	0.383 [a]	0.519 [a], 0.517 [a], 0.512 [a]					0.522 [a]			0.500 [a]	
SEC (lab) (mmhos/cm)	0.448	0.449	--	--	--	0.538	0.545	--	--	--	0.502	0.500	--	--	
Turbidity (NTU)	1.6 [a]	2.9 [a]	2.1 [a]	1.6 [a]	2.3[a]	3.3 [a], 1.1 [a], 0.7 [a]					8.2 [a]			5.0 [a]	
Temperature (°C)	41.5 [a]	41.5 [a]	41.4 [a]	41.5 [a]	41.9 [a]	38.7 [a], 43.5 [a], 42.4 [a]					34.1 [a]			34.0 [a]	
Major and Minor Constituents (mg/L)															
Bicarbonate as $CaCO_3$	110	110	--	--	--	120	110	--	--	--	140	140	--	--	
Carbonate as $CaCO_3$	<10	<10	--	--	--	<10	<10	--	--	--	<20	<20	--	--	
Bromide	0.12 [b]	0.12 [b]	--	--	--	0.21	<0.023	--	--	--	0.15 [b]	0.15 [b]	<0.05	--	
Chloride	26	26	29	--	--	43	42	45	--	--	30	31	30	--	
Fluoride	4.5	4.5	5.4	--	--	3.1	3.0	3.3	--	--	6.3	6.3	6.4	--	
Sulfate	49	49	52	--	--	70	70	70	--	--	53	53	50	--	
Calcium	-- | 1.8	1.8 | 1.9	1.8	--	--	-- | 4.0	-- | 3.9	3.9	--	3.9	4.9	4.8	6.6	5.0	4.4
Magnesium	-- | <0.007	<0.007 | 0.011 [c]	0.034	--	--	-- | <0.013	-- | <0.013	0.009	--	--	<1 [d]	<1 [d]	0.18	<0.4	<0.4
Potassium	-- | 2.5	2.5 | 2.5	2.2	--	--	-- | 0.75 [c]	-- | 0.68 [c]	0.7	--	--	4.9	4.8	3.9	--	
Sodium	-- | 80	80 | 81	96	--	--	-- | 95	-- | 95	110	--	--	92	93	118	109	100
Aluminum	<0.2 [d] | <0.2 [d]	<0.2 [d] | <0.2 [d]	0.046	R	0.046	<0.2 [d] | <0.2 [d]	<0.2 [d] | <0.2 [d]	0.031	R	0.030	1.7 [b] | 1.5 [b]	1.7 [b] | 1.1 [b]	0.065	1.2	0.3
Iron	<0.1 [d] | <0.1[d]	<0.1 [d] | <0.1[d]	<0.03	R	--	0.05 [b] | 0.09 [b]	0.08 [b] | 0.07[b]	<0.045	R	--	0.16 [d] | 0.16 [d]	0.17 [d] | <0.10 [d]	0.007	--	--
Silicon	24 | 24	24 | 24	--	--	26	19 | 19	19 | 19	--	--	19	33 | 33	33 | 32	--	35	27
Sulfide	<2 [b]	<2 [b]	--	--	--	<2	<2	--	--	--	<2	<2	--	--	--
Total Dissolved Solids	300 [b]	290 [b]	--	--	--	330	340	--	--	--	350 [b]	360 [b]	--	--	--

Table A.1-4
Water-Chemistry Data for Wells ER-20-8 #2, ER-20-7, and ER-EC-11
(Page 2 of 4)

Analyte	ER-20-8 #2					ER-EC-11					ER-20-7				
	N-I		LLNL	DRI	USGS	N-I		LLNL	DRI	USGS	N-I		LLNL	USGS	
	12/18/2009				12/17/2009	05/18/2010					09/24/2010				
Major and Minor Constituents (mg/L) continued															
Total Inorganic Carbon	--	--	27.7	--	--	--	--	28.7	--	--	--	--	37.9	--	--
Total Organic Carbon	<1	<1	0.7	0.3	--	<0.12	<0.12	0.42	0.02	--	<0.1	<0.1	0.55	--	--
Trace Constituents (µg|L)															
Antimony	--	--	0.272	--	0.3	--	--	0.25	--	<1	--	--	0.26	<1	<1
Arsenic	6.9 | 6.8	6.9 | 8.4	--	--	7.5	9.8 | 7.2	9.4 | 11	8.8	--	8.4	7.2 | 5.0	5.8 | 7.6	5.2	4.1	4.3
Barium	2.1 [c] | 1.0 [c]	0.91 [c] | 1.3 [c]	1.5	--	<3	0.36 [c] | 0.50 [c]	1.2 [c] | 0.41 [c]	1.1	--	<15	1.9 [c] | 1.8 [c]	2.3 [c] | 1.3 [c]	7.1	<15	<15
Beryllium	--	--	<0.048	--	<0.2	--	--	<0.18	--	<1	--	--	<0.15	<2.5	<1
Boron	--	--	123	--	120	--	--		--	163	--	--	<48	203	192
Cadmium	<0.52 | <0.52	<0.52 | <0.52	<0.06	--	<0.2	<0.33 | <0.33	<0.33 | <0.33	<0.03	--	<1	<0.3 | <0.3	<0.3 | <0.3	<0.036	<1	<1
Cesium	--	--	1.12	--	--	--	--	3.9	--	3.9	--	--	1.12	<1	<1
Chromium	<10 [d] | <10 [d]	<10 [d] | <10 [d]	0.82	--	<0.9	<0.51 | <0.51	<0.51 | <0.51	0.84	--	<4.5	<10 [d] | <0.5	<0.5 | 0.85	0.54	<4.5	<4.5
Cobalt	--	--	<0.033	--	<0.25	--	--	<0.05	--	<1.3	--	--	<0.054	<1.3	<1.3
Copper	--	--	1.68	--	3.1	--	--	1.2	--	<2.5	--	--	0.78	<2.5	<2.5
Lead	2.3 | 1.2	1.3 | <1.1	0.419	--	0.62	3.2 [c] | 10	8.9 | 8.3	1.0	--	1.3	<1 | <1	2.2 [c] | <1	0.51	<0.9	<0.9
Lithium	-- | 110	110 | 110	--	--	107	-- | 170 [b]	-- | 170 [b]	--	--	163	-- | 95 [b]	-- | 95 [b]	--	89	87
Manganese	10 | 10	<10[d] | 10	9.2	--	11	2.2 [c] | 3.3 [c]	2.8 [c] | 2.7 [c]	2.0	--	2.1	12 | 12	12 | <10 [d]	4.32	11	4.0
Mercury	<0.02 [b] | <0.02 [b]	<0.02 [b] | <0.02 [b]	--	--	--	<0.0097 | <0.0097	<0.0097 | 0.016 [c]	--	--	--	0.023 [c] | <0.01	0.017 [c] | <0.01	--	--	--
Molybdenum	--	--	6.2	--	6.4	--	--	3.9	--	4.4	--	--	15.1	15.8	15.2
Nickel	--	--	0.52	--	<3 |	--	--	0.43	--	<15	--	--	0.36	<15	<15
Rubidium	--	--	8.5	--	8.4	--	--	5.5	--	5.4	--	--	12.4	7.5	5.2
Selenium	<5 [d] | <2.2	<2.2 | <2.2	<6.0	--	<1	<2.7 | <2.7	<2.7 | <2.7	<12	--	<5	<3 | <3	<3 | <3	2.4	<5	<5

Table A.1-4
Water-Chemistry Data for Wells ER-20-8 #2, ER-20-7, and ER-EC-11
(Page 3 of 4)

Analyte	ER-20-8 #2					ER-EC-11					ER-20-7				
	N-I		LLNL	DRI	USGS	N-I		LLNL	DRI	USGS	N-I		LLNL	USGS	
	12/18/2009				12/17/2009	05/18/2010					09/24/2010				
Trace Constituents (µg|L) continued															
Silver	<1.2 | <1.2	<1.2 | <1.2	<0.018	--	<0.7	<1.1 | <1.1	<1.1 | <1.1	<0.01	--	<3.5	<1.1 | <1.1	<1.1 | <1.1	<0.06	<3.5	<3.5
Strontium	-- | <0.08	<0.08 | <0.08	2.35	--	2.4	-- | 30 [b]	-- | 30 [b]	34.4	--	36	-- | 6.1 [c]	-- | 5.5 [c]	5.9	15.0	11.9
Uranium	-- | 2.4	2.6 | 2.4	2.36	--	2.52 [e], 2.41 [f]	-- | 1.6	-- | 1.6	1.64	--	1.756 [e], 1.82 [f]	-- | 8.0	-- | 7.7	7.5	8.2 [e], 7.7 [f]	8.1 [e], 7.6 [f]
Vanadium	--	--	2.24	--	1.7	--	--	2.6	--	1.6	--	--	1.8	1.9	1.9
Zinc	--	--	2.22	--	<3	--	--	0.8	--	<15	--	--	4.8	<15	<15
Environmental Isotopes															
δD (‰)	--	--	-117	-115	--	--	--	-117	-115	--	--	--	-113	--	--
$\delta^{18}O$ (%)	--	--	-15.4	-15.2	--	--	--	-15.3	-15.2	--	--	--	-15.4	--	--
$\delta^{13}C$ (DIC) (‰)	--	--	-2.0	-5.4	--	--	--	-2.5	-4.7	--	--	--	-3.1	--	--
$\delta^{13}C$ (DOC) (‰)	--	--	--	-26.7	--	--	--	--	-23.1	--	--	--	--	--	--
^{14}C (DIC) (pmc)	--	--	79.1	--	--	--	--	24.1	--	--	--	--	6.99E+04	--	--
^{14}C (DOC) (pmc)	--	--	--	28.9	--	--	--	--	52.2	--	--	--	--	--	--
$^{36}Cl/Cl$ (Ratio)	--	--	2.19E-12	--	--	--	--	5.55E-13	--	--	--	--	2.46E-09	--	--
$^{82}S/^{84}S$ (Ratio)	--	--	--	--	18.0	--	--	--	--	18.7	--	--	--	17.6	17.7
$^{87}Sr/^{86}Sr$ (Ratio)	--	--	0.70905	--	0.70968	--	--	0.70989	--	0.70987	--	--	0.71096	0.71100	0.71090
$^{234}U/^{238}U$ Activity Ratio	--	--	3.90	--	3.88	--	--	4.01	--	4.04	--	--	3.02	3.04	3.05
Radionuclides (pCi/L)															
Tritium	1,040 ± 270 (320) [g]	880 ± 250 (330) [g]	1,280 ± 70 (97) [g]	--	--	<270	<270	<134	--	--	1.91E+07 ± 0.29E+07	1.89E+07 ± 0.29E+07	1.77E+07	--	--
Gross Alpha	2.6 ± 1.8 (2.5) [g]	2.6 ± 1.8 (2.5) [g]	--	--	--	2.4 [b] ± 1.4 (1.8) [g]	3.4 ± 1.5 (1.6) [g]	--	--	--	8.5 ± 2.5 (1.9) [g]	8.8 ± 2.4 (1.7) [g]	--	--	--
Gross Beta	<2.5	<2.4	--	--	--	<2.2	<2.4	--	--	--	16.6 ± 3.4 (2.3) [g]	18.0 ± 3.4 (2.0) [g]	--	--	--
^{14}C	<420	<420	0.134	--	--	<390	<390	0.043	--	--	R	R	165	--	--
^{36}Cl	--	--	2.09E-03	--	--	--	--	8.1E-04	--	--	--	--	2.41	--	--

Table A.1-4
Water-Chemistry Data for Wells ER-20-8 #2, ER-20-7, and ER-EC-11
(Page 4 of 4)

Analyte	ER-20-8 #2					ER-EC-11					ER-20-7				
	N-I		LLNL	DRI	USGS	N-I		LLNL	DRI	USGS	N-I		LLNL	USGS	
	12/18/2009				12/17/2009	05/18/2010					09/24/2010				
Radionuclides (pCi/L) continued															
^{90}Sr	<0.49	<0.51	--	--	--	<0.59	<0.55	--	--	--	1.47 [h] ± 0.43 (0.31) [g]	1.52 [h] ± 0.45 (0.32) [g]	--	--	--
^{99}Tc	<6.9	<6.8	<0.1	--	--	<7.7	<8.1	--	--	--	13.4 ± 4.5 (6.1) [g]	16.4 ± 4.7 (6.0) [g]	--	--	--
^{129}I	<1.8 [b]	<7.1 [b]	9.27E-05	--	--	--	--	--	--	--	<3.0	<2.9	0.132	--	--
^{137}Cs	<9.7	<9.9	--	--	--	<8.6	<4.8	--	--	--	<8.8	<8.9	--	--	--
^{152}Eu	<48	<43	--	--	--	<53	<30	--	--	--	<52	<58	--	--	--
^{154}Eu	<59	<61	--	--	--	<55	<28	--	--	--	<51	<59	--	--	--
^{234}U	--	--	3.08	--	--	--	--	2.35	--	--	--	--	8.16	--	--
^{235}U	<33	<57	0.0366	--	--	<40	<36	0.0269	--	--	<76	<66	0.124	--	--
^{236}U	--	--	<2.3E-05	--	--	--	--	<1.7E-05	--	--	--	--	<2.31E-05	--	--
^{238}U	--	--	0.780	--	--	--	--	0.577	--	--	--	--	2.66	--	--
^{239,240}Pu	<0.026	<0.025	--	--	--	<0.027	<0.008	--	--	--	0.062 ± 0.032 (0.010) [g]	0.070 ± 0.040 (0.041) [g]	0.10 [i]	--	--
^{241}Am	<48	<86	--	--	--	<64	<44	--	--	--	<72	<55	--	--	--

[a] Field measurements were made by N-I (formerly NNES) and coincide as closely as possible to the collection time for the associated samples.
[b] Value is an estimate. Hold time was exceeded for pH, sulfide, and total dissolved solids measurements. Other results considered an estimate as a result of failure to meet specific QC criteria.
[c] Value is an estimate with a negative bias as a result of failure to meet specific QC criteria.
[d] Contamination was observed in the associated blank. The measured value is reported if greater than the contract required reporting limit; otherwise, the value is reported as less than the contract required reporting limit.
[e] Analyzed using thermal ionization mass spectrometry with isotope dilution.
[f] Analyzed using inductively coupled plasma mass spectrometry.
[g] Detection limit
[h] Value is near the detection limit and is considered uncertain. LLNL is presently analyzing the sample to verify these results.
[i] Total Pu is reported (0.095 pCi/L is associated with colloids and 0.006 pCi/L is in aqueous form).

-- = Not analyzed
R = Data were rejected. High tritium interfered with the ^{14}C analysis.

Note: Values reported with a "|" indicate analysis results from unfiltered/filtered samples.

Table A.1-5
Major-Ion Data for Wells in the Study Area
(Page 1 of 8)

Site ID	Date	Sample ID [a]	Depth (ft)	HCO_3 (mg/L)	CO_3 (mg/L)	Br (mg/L)	Cl (mg/L)	SO_4 (mg/L)	F (mg/L)	K (mg/L)	Mg (mg/L)	Na (mg/L)	Ca (mg/L)	Charge Balance	Ref_ID [b]
ER-20-1	07/02/2001	13365	--	--	--	--	--	--	--	3.7	0.1	155	3.7	--	481
	07/26/2005	14109	2,000 [c]	187	1.3		57	83	3.0	3.3	0.1 [d]	128	3.4	-6.2	519
	07/26/2005	14109	2,000 [c]	--	--	--	--	--	--	3.4	0.1 [d]	125	3.4	--	519
	10/31/2007	14831.5	2,000 [c]	185	<1.2	--	53	83	3.1	--	--	--	--	--	550
	10/31/2007	14831	2,000 [c]	185	<1.2	--	57	84	3.2	3.3	0.1	141	3.5	--	550
ER-20-4	09/07/2010	15386/15387	1,870	122 [e]	<6	7.9	8.9	25	6.5	4.1	<1.0	95	21	25	583
	09/07/2010	15389	1,870	122 [e]	<6	8.0	9.0	25	6.6	4.3	<1.0	96	21	25	583
	09/07/2010	15390/15391	3,000	116 [e]	<6	0.07 [d]	5.1	18	8.0	1.9	<1.0	50	4.0	-6.2	583
	09/04/2011	15715	2,750	115 [e]	<6	0.05 [d]	4.7	17	7.8	1.3	<1.0	51	4.2	-6.0	595
	09/04/2011	15716	2,750	113 [e]	<6	0.05 [d]	4.8	17	8.0	1.3	<1.0	50	4.2	-6.8	595
	09/20/2011	15771	2,479–3,002	108 [e]	<6	<0.02	4.7	17	8.0	1.2	<1.0	50 [d]	4.3	-5.2	601
	09/20/2011	15771	2,479–3,002	--	--	--	--	--	--	1.2	<1.0	49 [d]	4.3	--	601
	09/20/2011	15772	2,479–3,002	111 [e]	<6	<0.02	4.6	17	7.9	1.2	<0.01	49	4.2	-6.8	601
	09/20/2011	15772	2,479–3,002	--	--	--	--	--	--	1.2	<0.01	49	4.2	--	601
	09/20/2011	15783	2,479–3,002	--	--	--	--	--	--	1.0	<0.4	53	3.8	--	608
	09/21/2011	15791	2,479–3,002	--	--	--	--	--	--	1.3	0.05	62	4.5	--	606
ER-20-5 #1	06/03/1996	3921	2,300–2,572	149	8.0	<0.25	27	41	11.5	6.0	0.9	107	11	4.7	14
	06/03/1996	12318	2,300–2,572	187 [f]	--	--	26	41	10.3	4.2	0.2	113	6.1	1.4	377
	04/22/1997	3922	2,300–2,572	186	<10	0.10	22	38	8.6	5.7	0.4	105	7.2	2.0	26
	04/22/1997	12317	2,300–2,572	186 [f]	--	<0.05	23	39	10.1	4.5	0.3	104	6.6	-0.8	377
	07/09/1998	5164	2,300–2,356	145	10	<0.25	24	41	9.8	--	--	--	--	--	137
	07/09/1998	12316	2,300–2,572	182 [f]	--	<0.04	25	40	9.6	5.7	0.4	106	7.2	1.0	596
	11/30/2004	13234	--	193 [f]	--	0.07	25	43	10.8	4.6	0.1	118	6.2	1.9	596

Table A.1-5
Major-Ion Data for Wells in the Study Area
(Page 2 of 8)

Site ID	Date	Sample ID [a]	Depth (ft)	HCO_3 (mg/L)	CO_3 (mg/L)	Br (mg/L)	Cl (mg/L)	SO_4 (mg/L)	F (mg/L)	K (mg/L)	Mg (mg/L)	Na (mg/L)	Ca (mg/L)	Charge Balance	Ref_ID [b]
ER-20-5 #3	07/31/1996	3923	3,432–3,881	103	6.4	<0.25	18	35	3.2	6.5	0.6	74	6.1	-6.4	15
	07/31/1996	12322	3,432–3,881	109 [f]	--	--	18	35	3.2	3.0	0.1	73	3.1	3.4	377
	04/22/1997	3924	3,432–3,881	115	<10	0.08	15	31	3.0	6.0	0.2	74	3.4	-6.4	27
	04/22/1997	12321	3,432–3,881	108 [f]	--	0.98	17	35	3.3	3.1	0.1	70	3.2	2.0	377
	04/30/1998	5166	3,432–3,881	--	--	<0.25	16	33	3.4	7.9	0.4	72	4.1	--	139
	04/30/1998	5167	3,432–3,881	--	--	--	--	--	--	4.0	0.2	76	2.7	--	140
	04/30/1998	12320	3,432–3,881	107 [f]	--	<0.02	17	33	3.2	2.1	0.1	68	1.8	0.04	596
	11/15/2001	12319	3,432–3,881	99 [f]	--	0.76	19	35	3.6	3.3	0.1	87	4.4	14	596
	11/29/2004	13235	--	135 [f]	--	0.07	17	35	4.1	3.5	<0.04	80	3.5	1.5	596
ER-20-7	06/30/2009	14912	2,650	183 [e]	<12	0.29	30	50	5.6	4.3	0.2 [d]	97	4.4	-6.4	557
	06/30/2009	14913	2,650	171 [e]	<12	0.28	29	49	5.5	4.3	0.2 [d]	96	4.4	-4.3	557
	07/01/2009	14914	2,535	183 [e]	<12	0.38	29	49	5.5	4.1	0.1 [d]	98	4.1	-5.6	557
	09/24/2010	15470	--	193 [g]	--	<0.05	30	50	6.4	3.9	0.2	118	6.6	1.8	596
	09/24/2010	15383	--	171 [e]	<12	0.15 [d]	30	53	6.3	4.9	--	92	4.9	-7.5	583
	09/24/2010	15384	--	171 [e]	<12	0.15 [d]	31	53	6.3	4.8	--	93	4.8	-7.4	583
	09/24/2010	15457/15458	--	--	--	--	--	--	--	--	<0.4	109	5.0	--	586
	09/24/2010	15459/15460	--	--	--	--	--	--	--	--	<0.4	100	4.4	--	586
ER-20-8 Intermediate (TCA)	08/11/2009	15398	2,700	--	--	0.26	23	43	4.0	2.2 [d]	<1.0	71	3.1	-10.3	559
	08/11/2009	14918	2,700	134 [e]	<12	--	--	--	--	2.5 [d]	<1.0	72	3.1	--	559
	08/11/2009	15399	2,700	--	--	0.22	23	42	4.0	2.2 [d]	<1.0	71	3.0	--	559
	08/11/2009	15397	2,700	146 [e]	<12	--	--	--	--	<3.0	<1.0	72	3.1	--	559
	05/26/2011	15708	2,800	134 [e]	<12	0.10 [d]	26	47	3.7	2.6	0.5 [d]	81	2.3	-4.5	595
	05/26/2011	15709	2,800	134 [e]	<12	0.11 [d]	28	45	3.5	2.4	<0.01	82	1.7	-5.1	595
	06/27/2011	15710	--	--	--	--	--	--	--	2.4	<1.0	79 [d]	2.1	--	595
	06/27/2011	15710	--	122 [e]	<6	0.10 [d]	33	49	3.8	2.4	<1.0	77 [d]	2.1	-8.3	595
	06/27/2011	15711	--	--	--	--	--	--	--	2.4	<1.0	77 [d]	2.1	--	595

Table A.1-5
Major-Ion Data for Wells in the Study Area
(Page 3 of 8)

Site ID	Date	Sample ID [a]	Depth (ft)	HCO_3 (mg/L)	CO_3 (mg/L)	Br (mg/L)	Cl (mg/L)	SO_4 (mg/L)	F (mg/L)	K (mg/L)	Mg (mg/L)	Na (mg/L)	Ca (mg/L)	Charge Balance	Ref_ID [b]
ER-20-8 Intermediate (TCA) (continued)	06/27/2011	15711	--	122 [e]	<6	0.11	28	50	3.8	2.4	<1.0	78 [d]	2.1	-6.2	595
	06/27/2011	15789	--	134 [g]	--	<0.05	28	50	4.3	2.2	0.02	88	2.3	-3.2	606
	06/27/2011	15781	--	--	--	--	--	--	--	2.0	<0.4	89	2.1	--	608
ER-20-8 deep (TSA)	08/11/2009	15396	3,160	--	--	0.24	23	43	4.1	2.2 [d]	<1.0	72	3.5	--	559
	08/11/2009	14917	3,160	146 [e]	<12	--	--	--	--	3.3	<1.0	74	4.5	--	559
	07/22/2011	15712	3,170	134 [e]	<3	0.08 [d]	24	44	4.2 [d]	1.8	<1.0	77	4.4	-5.2	595
	08/08/2011	15713	--	--	--	--	--	--	--	1.8	0.03 [d]	79 [d]	3.4	--	595
	08/08/2011	15713	--	134 [e]	<6	0.08 [d]	23	43	4.2	1.8	<1.0	79	3.4	-4.1	595
	08/08/2011	15714	--	--	--	--	--	--	--	1.7	<0.01	78 [d]	3.3	--	595
	08/08/2011	15714	--	134 [e]	<6	0.08 [d]	24	42	4.1	1.7	<0.01	78 [d]	3.4	-4.8	595
	08/08/2011	15790	--	141 [g]	--	<0.05	24	44	4.7	1.6	0.03	93	3.6	1.3	606
	08/08/2011	15782	--	--	--	--	--	--	--	1.6	<0.4	86	3.4	--	608
ER-20-8 #2	8/31/2009	15312/15314	1,710	134 [e]	<12	0.92	23	36	2.8	3.5	0.02 [d]	66	1.9	-10	573
	8/31/2009	15313/15315	1,710	134 [e]	<12	0.95	22	37	2.9	3.3	0.02 [d]	70	1.7	-7.7	573
	8/31/2009	15317	2,200	--	--	4.0	24	45	3.3	5.3	0.2 [d]	100	4.9	5.7	573
	8/31/2009	15316	2,200	134 [e]	<12	--	--	--	--	6.4	0.4	100	5.3	--	573
	12/03/2009	15185	2,100	146	<12	--	--	--	--	2.8	0.1[d]	82	2.5	-7.9	571
	12/03/2009	15186	2,100	146	<12	--	--	--	--	2.9	0.2 [d]	82	2.7	-7.7	571
	12/03/2009	15187	2,100	--	--	0.12 [d]	27	49	4.6	2.9	<0.01	82	2.2	--	571
	12/03/2009	15188	2,100	--	--	0.12 [d]	27	49	4.6	2.9	<0.01	84	2.3	--	571
	12/18/2009	15189/15191	--	134	<6	0.12 [d]	26	49	4.5	2.5	<0.01	80	1.8	-8.3	571
	12/18/2009	15190	--	134	<6	--	--	--	--	2.5	<0.01	80	1.8	--	571
	12/18/2009	15192	--	--	--	0.12 [d]	26	49	4.5	2.5	0.01[d]	81	1.9	--	571
	12/18/2009	15406	--	141	--	--	29	52	5.4	2.2	0.03	96	1.8	-2.3	607

Table A.1-5
Major-Ion Data for Wells in the Study Area
(Page 4 of 8)

Site ID	Date	Sample ID [a]	Depth (ft)	HCO_3 (mg/L)	CO_3 (mg/L)	Br (mg/L)	Cl (mg/L)	SO_4 (mg/L)	F (mg/L)	K (mg/L)	Mg (mg/L)	Na (mg/L)	Ca (mg/L)	Charge Balance	Ref_ID [b]
ER-EC-1	02/01/2000	8459	2,298–4,750	158 [e]	<6	--	--	--	--	8.2	0.5	120	19	--	243
	02/01/2000	8459.4	2,298–4,750	--	--	0.46	95	120	2.6	8.3	0.5	120	20	--	243
	02/01/2000	7441/7441.21	2,298–4,750	148 [f]	--	1.1	97	145	2.4	6.0	0.4	154	19	-3.1	246, 596
	06/03/2003	12402	2,298–4,750	102 [e]	--	0.45	88	121	2.7	6.2	0.5	153	20	6.9	398
	06/03/2003	12383	2,298–4,750	149 [f]	--	1.4	97	119	2.3	4.9	0.4	144	19	-3.2	596
	06/03/2003	12368	2,298–4,750	146 [e]	<6	0.44	95	120	2.6	8.1 [d]	0.4 [d]	150	19	-0.03	388
	06/03/2003	12368	2,298–4,750	--	--	--	--	--	--	8.0 [d]	0.4 [d]	150	19	--	388
	06/03/2003	12368.5	2,298–4,750	146 [e]	<6	0.42	92	110	2.6	7.9 [d]	0.4 [d]	150	19	1.9	388
	06/03/2003	12368.5	2,298–4,750	--	--	--	--	--	--	8.4 [d]	0.4 [d]	150	19	--	388
	04/02/2009	15200/15202	2,298–4,750	158 [e]	<12	0.53	97	120	2.5	7.3 [d]	0.4 [d]	140	20	-4.3	571
	04/02/2009	15201/15203	2,298–4,750	158 [e]	<12	0.39	100	120	2.5	7.2 [d]	0.4 [d]	140	20	-4.9	571
	04/03/2009	15407	2,298–4,750	159 [e]	--	--	94	118	1.7	5.5	0.4	155	18	-0.3	596
ER-EC-6 (1,581–5,000 ft)	02/10/2000	8475/8475.4	1,628–4,904	146	<3	0.32	52	77	3.1	3.2	<1.0	130	4.2	3.4	243
	02/10/2000	8475.4	1,628–4,904	--	--	--	--	--	--	3.1	<1.0	140	4.1	--	243
	02/10/2000	7434	1,628–4,904	153 [f]	--	0.84	44	56	3.1	2.0	<0.02	128	4.0	6.7	596
ER-EC-6 (1,581–3,820 ft)	06/10/2003	12406	--	134	ND	0.25	50	79	3.0	2.0	0.03	128	4.9	3.8	402
	06/10/2003	12387	--	147 [f]	--	0.90	52	75	2.7	1.8	0.2	120	4.6	-1.2	596
	06/10/2003	12372	--	146	<6	0.24	53	79	2.8	3.1	1.0 [d]	120	4.2	-0.8	388
	06/10/2003	12372	--	--	--	--	--	--	--	3.2	1.0 [d]	120	4.1	--	388
	06/10/2003	12372.5	--	146	<6	0.25	53	79	2.9	2.9	1.0 [d]	120	4.1	-1.0	388
	06/10/2003	12372.5	--	--	--	--	--	--	--	2.9	1.0 [d]	120	4.2	--	388
	04/09/2009	15408	--	163 [f]	--	--	47	73	2.0	1.9	0.01	132	4.1	3.0	596
	04/09/2009	15209/15210	--	158	<12	0.24	53	78 [d]	2.6	2.8	<1.0	120	4.5	-2.2	571
	04/09/2009	15208/15211	--	158	<12	0.21	54	79 [d]	2.5	2.6	<1.0	110	4.3	-6.8	571
ER-EC-11 deep	05/02/2010	15448	3,750	158 [e]	<12	0.17	42	66	2.9	0.7 [d]	0.2 [d]	95	7.3	-7.9	583
	05/02/2010	15446	3,750	158 [e]	<12	0.17	49	68	2.9	0.6 [d]	0.1 [d]	94	5.8	-12	583
ER-EC-11 intermediate	05/02/2010	15450	3,300	158 [e]	<12	0.17	47	67	2.9	0.8 [d]	1.8	95	30	2.9	583

Table A.1-5
Major-Ion Data for Wells in the Study Area
(Page 5 of 8)

Site ID	Date	Sample ID [a]	Depth (ft)	HCO_3 (mg/L)	CO_3 (mg/L)	Br (mg/L)	Cl (mg/L)	SO_4 (mg/L)	F (mg/L)	K (mg/L)	Mg (mg/L)	Na (mg/L)	Ca (mg/L)	Charge Balance	Ref_ID [b]
ER-EC-11 main	10/09/2009	15318	2,450	171 [e]	<12	0.78	56	86	3.6	3.9	0.02 [d]	110	2.4	-12	573
	10/09/2009	15318	2,450	--	--	--	--	--	--	4.0	0.04 [d]	110	2.4	--	573
	10/10/2009	15321	2,750	171 [e]	<12	0.94	56	86	2.9	2.8	<0.01	110	3.8	-11	573
	10/10/2009	15321	2,750	--	--	--	--	--	--	2.9	0.01 [d]	110	3.8	--	573
	10/10/2009	15324	3,150	171 [e]	<12	1.1	57	83	2.7	2.2	<0.01	110	3.9	-10	573
	10/10/2009	15324	3,150	--	--	--	--	--	--	2.4	<0.01	110	4.1	--	573
	10/17/2009	15327	3,285	146 [e]	<12	1.1	38	63 [d]	2.5	5.4	0.01	100	4.1 [d]	-6.3	573
	10/17/2009	15328	3,285	146 [e]	<12	1.1	38	62 [d]	2.5	4.7	<0.01	100	4.4 [d]	-7.1	573
	10/17/2009	15328	3,285	--	--	--	--	--	--	5.5	0.01	100	4.2	--	573
	10/17/2009	15327	3,285	--	--	--	--	--	--	4.7	<0.01	100	4.5	--	573
	10/17/2009	15332	3,755	158 [e]	<12	0.61	42	64 [d]	2.9	1.4	0.05 [d]	96 [d]	4.5 [d]	-8.6	573
	10/17/2009	15332	3,755	--	--	--	--	--	--	1.7	0.03 [d]	97 [d]	4.3	--	573
	05/18/2010	15454	--	146 [e]	<6	<0.02	42	70	3.0	0.7	<0.01	95	3.9	-8.1	583
	05/18/2010	15452	--	146 [e]	<6	0.21	43	70	3.1	0.8	<0.01	95	4.0	-8.3	583
	05/18/2010	15405	--	--	--	--	--	--	--	0.7	0.01	110	3.9	--	596
	05/18/2010	15455	--	--	--	--	--	--	--	--	--	--	3.9	--	585
PM-3	10/27/1988	3153	1,654	165	--	0.7	95	122	--	12	1.4	141	35	2.2	593
	10/27/1988	3153	1,654	155	--	0.6	97	123	--	11	1.4	138	34	1.7	593
	10/28/1988	3154	--	153	--	0.6	98	124	--	11	1.4	137	34	1.2	593
	10/28/1988	3158	1,455	150	--	0.5	98	130	2.4	10	1.5	130	36	-2.0	593
	05/17/1989	3155	1,490	159	--	0.5	93	125	2.5	11	0.6	137	28	-1.7	63
	03/17/1992	3157	1,305	158	--	7.4	84	92	2.5	12	4.0	124	19	-1.0	63
PM-3-1	07/19/2005	14226	1,994 [c]	112	<1.2	--	112	114	2.7	7.4	5.0	114	17		519
	06/12/2007	14834	1,993 [c]	108	<0.6	--	94	106	2.5	6.9	5.2 [d]	101	15	-8.0	550
	06/12/2007	14834.5	1,993 [c]	--	--	--	96	114	3.6	--	--	--	--	--	550
	04/29/2009	15464	1,993 [c]	99	--	--	93	103	2.4	8.8	3.8	130	17	3.9	587

Table A.1-5
Major-Ion Data for Wells in the Study Area
(Page 6 of 8)

Site ID	Date	Sample ID [a]	Depth (ft)	HCO_3 (mg/L)	CO_3 (mg/L)	Br (mg/L)	Cl (mg/L)	SO_4 (mg/L)	F (mg/L)	K (mg/L)	Mg (mg/L)	Na (mg/L)	Ca (mg/L)	Charge Balance	Ref_ID [b]
PM-3-2	10/12/2000	8501	--	142	0.0	--	95	114	--	15	4.4	125	22	1.0	594
	12/10/2003	13411	1,560 [c]	117	<0.3	--	93	116	3.7 [d]	14	4.9	114	21	-2.6	481
	05/25/2004	13270	1,560 [c]	119	<0.7	--	93	114	3.6	16	5.5	119	22	0.1	481
	06/12/2007	14835	1,560 [c]	114	<0.6	--	94	109	3.8	12	4.3	88	18	-13	550
	04/29/2009	15465	1,560 [c]	113	--	--	89	110	3.7	15	5.1	125	21	3.0	587
	04/29/2009	15466	1,560 [c]	--	--	--	92	112	3.8	15	5.2	126	21	--	587
U-20 Water Well	05/23/1987	3233	--	111	--	--	12	31	--	1.7	0.3	57	6.4	0.6	441
	04/16/1990	3234	--	113	--	--	12	29	--	1.8	0.2	58	5.7	1.2	441
	08/02/1990	3235	--	111	--	--	11	31	--	1.8	0.7	58	5.4	1.7	441
	09/11/1990	3236	--	107	1.1	--	11	31	--	1.7	0.4	57	6.2	2.1	441
	05/31/1995	5160	--	88	<5	<0.25	11	27	2.4	1.3	0.6	60	7.6	12	133
	05/31/1995	3238	--	92 [f]	--	--	12	--	--	2.1	0.3	59	6.2	23	171
	11/05/1997	4950.22	--	101	6.1	--	12	32	--	1.6	0.3	59	7.8	2.6	106
	11/05/1997	4950.27	--	93	--	0.1	11	31	2.2	1.4	0.3	61	6.8	7.2	128
	11/05/1997	5130	--	95	--	0.1	11	31	2.4	1.4	0.3	59	6.7	5.4	128
U-20a #2 Water Well	10/14/1964	3162	--	108	ND	--	11	28	2.6	1.9	<0.1	58	5.9	1.0	592
	10/14/1964	3163	--	108	ND	--	11	28	2.6	1.9	--	58	5.9	0.8	61
	03/10/1966	3164	--	106	ND	--	11	27	2.7	0.2	0.1	55	6.1	-1.2	592
	03/21/1971	3165	--	113	ND	--	11	29	2.7	2.2	<0.1	57	5.9	-1.4	61
	10/06/1971	3166.21	--	110	ND	--	10	28	2.8	2.2	0.2	55	5.9	-1.2	61
	04/16/1973	3167	--	122 [e]	--	--	12	29	3.1	1.9	0.02	47	1.5	-18	64
	07/03/1973	3170	--	116 [e]	--	--	11	30	2.7	2.6	0.05	58	0.1	-6.8	64
	01/16/1975	3173	--	113 [e]	--	--	15	28	2.4	2.2	0.1	70	1.0	2.7	64
	07/08/1975	3178	--	118 [e]	--	--	10	28	2.7	3.8	0.1	62	1.2	-1.2	64
	04/01/1988	3184	--	111	--	--	12	33	--	1.7	0.2	59	6.2	1.8	441
	04/10/1988	3185	--	112	--	--	11	38	--	2.3	0.2	63	6.3	2.4	441
U-20ao	12/10/1984	3144	--	114	--	--	3.2	8.1	--	1.9	1.2	38	8.8	2.1	441

Table A.1-5
Major-Ion Data for Wells in the Study Area
(Page 7 of 8)

Site ID	Date	Sample ID [a]	Depth (ft)	HCO_3 (mg/L)	CO_3 (mg/L)	Br (mg/L)	Cl (mg/L)	SO_4 (mg/L)	F (mg/L)	K (mg/L)	Mg (mg/L)	Na (mg/L)	Ca (mg/L)	Charge Balance	Ref_ID [b]
U-20c	09/14/1967	3143	--	140	39	--	6.8	10	5.9	0.9	<0.1	95	0.9	-1.1	61
	09/14/1967	3142	--	130	37	--	8.1	18	6.4	1.4	<0.1	95	2.8	0.1	61
U-20n PS#1 DD-H	09/21/1998	12188	4,101–4,111	109 [f]	--	0.40	11	28	4.0	1.7	0.1	61	2.9	-0.9	369
	09/21/1998	5184	--	107	<6	0.40	13	34	4.8	1.3	<0.1	62	3.0	3.4	152
	09/21/1998	5184	--	--	--	--	--	--	--	2.0	<0.1	61	3.0	--	152
	10/12/1999	12187	--	108 [f]	--	<0.03	11	28	3.6	2.5	0.2	65	4.8	4.1	372
	07/09/2003	12394	--	90 [f]	--	0.60	11	28	3.6	1.9	0.1	61	3.8	5.4	596
	11/15/2005	14016	--	94 [f]	--	<0.01	12	33	4.4	1.7	0.1	62	2.0	0.8	596
UE-20bh #1	12/08/1999	6627.23	2,770	81	--	<0.1	3.5	8.3	--	0.7	<0.1	36	0.5	0.5	217
UE-20d	03/08/1966	3195	2,920	122	ND	--	23	40	3.1	0.2	--	81	1.4	-0.9	592
	03/08/1966	3196	3,200	120	ND	--	24	42	3.1	0.1	0.1	83	1.4	-0.2	592
	07/27/1966	3198	2,446–4,500	137	ND	--	23	44	2.8	1.7	0.1	88	4.3	1.7	592
	07/28/1966	3199	2,446–4,500	143	5.0	--	8.8	53	2.4	0.5	0.1	68	21	3.7	592
	08/12/1966	3200	2,446–4,500	192	4.0	--	24	40	3.0	2.6	0.1	107	8.5	2.0	592
UE-20n #1	06/23/1987	12263	2,850	97	--	0.6	13	31	4.4	--	0.2	75	7.8	13	381
	06/30/1987	9007	2,850	93	--	0.55	13	31	4.4	--	0.2	75	7.8	--	283
	06/30/1987	9007.5	2,850	101	--	--	12	31	4.4	--	0.2	75	7.9	--	283
	07/07/1987	12261	2,850	--	--	--	13	34	4.5	3.8	0.3	76	12	--	381
	07/07/1987	12255	2,850	--	--	--	13	33	4.5	2.9	0.2	96	11	--	381
	07/07/1987	12260	2,850	--	--	--	14	34	4.7	--	--	--	--	--	381
	07/07/1987	9008	2,850	--	--	--	13	34	4.5	3.8	0.3	76	12	--	283
	07/07/1987	9010	--	--	--	--	13	33	4.5	2.9	0.2	96	11	--	283
	07/08/1987	9012	2,850	--	--	--	13	35	4.5	2.8	0.2	95	9.6	--	283
	07/08/1987	12244	2,850	--	--	--	13	35	4.5	2.8	0.2	95	9.9	--	381
	07/08/1987	9012.5	--	--	--	--	13	35	4.5	2.8	0.2	95	10	--	283
	07/09/1987	12240	2,850	--	--	0.3	12	36	4.5	3.8	0.2	80	8.8	--	381
	07/22/1987	12223	2,750	--	--	0.1	13	36	4.2	3.1	0.2	96	8.8	--	381

Table A.1-5
Major-Ion Data for Wells in the Study Area
(Page 8 of 8)

Site ID	Date	Sample ID [a]	Depth (ft)	HCO_3 (mg/L)	CO_3 (mg/L)	Br (mg/L)	Cl (mg/L)	SO_4 (mg/L)	F (mg/L)	K (mg/L)	Mg (mg/L)	Na (mg/L)	Ca (mg/L)	Charge Balance	Ref_ID [b]
UE-20n #1 (continued)	07/22/1987	12229	2,750	--	--	--	16	37	4.6	2.8	0.2	94	8.7	--	381
	07/22/1987	9020.5	2,850	--	--	0.04	13	35	4.3	3.1	0.2	97	8.9	--	283
	07/22/1987	9019	2,850	--	--	--	16	37	4.6	2.8	0.2	95	8.7	--	283
	07/22/1987	9020	2,850	--	--	0.06	14	37	4.1	3.0	0.2	95	8.7	--	283
	07/23/1987	9022.11	2,600	--	--	--	12	37	3.5	2.4	0.17	88	9.6	--	283
	07/23/1987	12220	2,600	--	--	--	12	37	3.5	2.4	0.2	88	9.6	--	381
	08/06/1987	12217	2,750	--	--	0.2	13	34	4.3	2.7	0.2	97	9.7	--	381
	08/06/1987	12215	2,750	--	--	0.2	13	34	4.3	3.0	0.2	88	7.8	--	381
	10/28/1987	12214	2,750	--	--	0.2	--	76	--	1.8	0.2	65	5.7	--	380
	02/09/1988	12213	2,750	--	--	--	--	--	--	1.9	0.2	64	6.3	--	380
	05/10/1988	12212	2,750	--	--	--	--	--	--	2.9	0.7	68	6.1	--	380

[a] UGTA Geochemistry Database sample identification number (N-I, 2012).
[b] UGTA Geochemistry Database reference identification number (N-I, 2012).
[c] Depth is from top of the casing.
[d] Value is considered an estimate as a result of failure to meet specific QC criteria.
[e] Data were converted from mg/L $CaCO_3$ units to mg/L HCO_3 units by multiplying times 1.219.
[f] Data were reported as dissolved inorganic carbon in mg/L HCO_3 units.
[g] Data were converted from dissolved organic carbon in mg/L C units by multiplying times 5.081.

ND = Not detected
-- = Not analyzed

Table A.1-6
Environmental-Isotope Data for Wells in the Study Area
(Page 1 of 2)

Site ID	Date	Sample ID [a]	Depth (ft)	$\delta^{18}O$ (‰)	δD (‰)	$\delta^{13}C$ (‰)	^{14}C (pmc)	$^{36}Cl/Cl$ (ratio)	Ref_ID [b]
ER-20-5 #1	06/03/1996	10463	2,300–2,572	-14.8	-116	-3.8	--	--	327
	06/03/1996	12318	2,300–2,572	-14.9	-114	-2.3	28,169	3.94E-09	377, 382
	04/04/1997	3915	2,300–2,572	-14.9	-115	-3.4	--	--	3
	04/22/1997	12317	2,300–2,572	-15.0	--	-2.8	33,600	3.81E-09	377, 383
	07/09/1998	5164	2,300–2,356	-14.8	-114	-3.9	--	--	164
	07/09/1998	12316	2,300–2,572	-14.9	--	-2.5	81,657	4.11E-09	596
	11/30/2004	13234	--	-14.9	-115	-4.7	96,300	4.39E-09	596
ER-20-5 #3	07/31/1996	10464	--	-15.2	-115	-6.7	--	--	327
	07/31/1996	12322	3,432–3,881	-15.1	-114	-5.7	1,450	1.73E-11	377, 382
	04/04/1997	3919	3,432–3,881	-15.1	-113	-6.5	--	--	3
	04/22/1997	12321	3,432–3,881	-15.1	--	-5.8	1,462	1.68E-11	377, 383
	04/30/1998	5166	3,432–3,881	-15.1	-113	-6.8	--	--	163
	04/30/1998	12320	3,432–3,881	-15.1	-114	-5.6	1,346	1.93E-11	596
	11/15/2001	12319	3,432–3,881	-15.0	-114	-4.0	--	--	596
	11/29/2004	13235	--	-15.1	-114	-9.3	1,680	2.27E-11	586
	4/26/2011	15719	--	-15.7	-118	--	--	--	596
ER-20-7	09/24/2010	15470	--	-15.4	-113	-3.1	69,900	2.46E-09	596
ER-20-4	09/21/2011	15788	--	-14.9	-114	-8.6	--	--	605
	09/21/2011	15791	--	--	-116	--	--	--	606
ER-20-8 (TCA)	06/27/2011	15786	2,486–2,912	-15.0	-115	-7.5	--	--	605
	06/27/2009	15789	2,486–2,912	-15.4	-118	-2.7	122	--	606
ER-20-8 (TSA)	08/08/2011	15787	3,127–3,298	-15.1	-115	-7.2	--	--	605
	08/08/2011	15790	3,127–3,298	-15.5	-116	-2.6	37.6	--	606
ER-20-8 #2	12/18/2009	15400	--	-15.2	-115	-5.4	--	--	578
	12/18/2009	15406	--	-15.4	-117	-2.0	79.1	2.19E-12	607
ER-EC-1	02/01/2000	7441.21	2,298–4,749	-14.8	-114	-4.3	--	--	236
	02/01/2000	7441	2,298–4,749	-14.8	-116	-4.0	5.9	5.46E-13	591, 596
	06/03/2003	12402	2,298–4,749	-14.9	-116	-3.8	--	--	402
	06/03/2003	12383	2,298–4,749	-14.9	-116	-3.1	7.2	5.14E-13	596
	04/02/2009	15380	2,298–4,749	-14.9	-116	-4.6	--	--	576
	04/03/2009	15407	2,298–4,749	-15.0	-116	-2.9	15.2	5.54E-13	596
ER-EC-11 main	05/18/2010	15401	--	-15.2	-115	-4.7	--	--	578
	05/18/2010	15405	--	-15.3	-117	-2.5	24.1	5.55E-13	596
ER-EC-6 (1,581–5,000 ft)	02/10/2000	7434.21	1,628–4,904	-14.9	-114	-4.4	--	--	236
	02/10/2000	7434	1,628–4,904	-15.0	-116	-3.4	5.4	5.41E-13	596
ER-EC-6 (1,581–3,820 ft)	06/10/2003	12406	--	-15.2	-116	-3.4	--	--	398, 402
	06/10/2003	12387	--	-15.0	-117	-2.7	6.6	5.07E-13	596
	04/09/2009	15408	--	-15.3	-116	-2.6	16.3	5.62E-13	596
	04/11/2009	15381	--	-15.1	-116	-4.3	--	--	576

Table A.1-6
Environmental-Isotope Data for Wells in the Study Area
(Page 2 of 2)

Site ID	Date	Sample ID [a]	Depth (ft)	$\delta^{18}O$ (‰)	δD (‰)	$\delta^{13}C$ (‰)	^{14}C (pmc)	$^{36}Cl/Cl$ (ratio)	Ref_ID [b]
PM-3 (3,019 ft)	10/27/1988	3153	1,655	-15.1	-116	-6.8	--	--	63
	10/27/1988	3153	1,655	-15.0	-116	-6.3	--	--	63
	10/28/1988	3154	1,655	-15.0	-116	-6.7	--	--	63
	05/17/1989	10453	1,490	-14.8	-116	--	--	--	327
	05/17/1989	10455	1,780	-14.7	-114	--	--	--	327
	05/17/1989	10457	1,950	-14.8	-115	--	--	--	327
PM-3-2	10/12/2000	8501	--	-14.8	-115	-6.8	--	--	594
U-20 Water Well	05/31/1995	3238	--	--	--	--	9.1	5.67E-13	171
	11/05/1997	4950.21	--	-14.7	-113	-7.2	--	--	105, 106
	11/05/1997	4950.23	--	--	--	-6.2	8.6	--	108
U-20a #2 Water Well	--	3186	--	-14.8	-114	-13.5	15.3	--	99
U-20n PS#1 DD-H	09/21/1998	12188	--	-14.9	-113	-5.7	160,450	1.09E-09	369
	10/12/1999	12187	--	-15.0	-113	-6.0	153,900	1.60E-09	372
	07/09/2003	12394	--	-15.0	-114	-4.0	169,000	2.22E-09	596
	11/15/2005	14016	--	-14.9	-114	-6.4	158,000	1.20E-09	596
UE-20bh #1	06/20/1993	4423	--	-14.7	-109	-9.2	21.0	6.45E-13	171
	12/08/1999	6627.23	2,770	-14.7	-110	-10.5	--	--	217
	12/08/1999	6627.21	2,770	--	--	-9.7	22.4	--	202
UE-20n #1	05/26/1987	8998	2,407	-14.8	-111	--	--	--	283
	05/26/1987	8998.5	2,407	-14.7	--	--	--	--	283
	05/30/1987	8999	3,003	-14.9	-110	--	--	--	381
	05/31/1987	9000	3,294	-15.0	-110	--	--	--	381

[a] UGTA Geochemistry Database sample identification number (N-I, 2012).
[b] UGTA Geochemistry Database reference identification number (N-I, 2012).

A.1.0 REFERENCES

N-I, see Navarro-Intera, LLC.

Navarro-Intera, LLC. 2012. Written communication. Subject: "UGTA Geochemistry Database," UGTA Technical Data Repository Database Identification Number UGTA-4-129. Las Vegas, NV. As accessed on 1 August.

Appendix B

Water-Level Response to Earthquakes

B.1.0 WATER-LEVEL RESPONSE TO EARTHQUAKES

This section describes the water-level responses observed at the NNSS to seismic signals caused by earthquakes. N-I conducts a long-term water-level monitoring (LTWLM) program in the Pahute Mesa area of the NNSS. The pressure transducers (PXDs) used (Instrumentation Northwest model PT12 absolute gauge PXDs) are accurate to within ± 0.06 percent of full scale. For a typical 30-pounds per square inch absolute (psia) PXD, the implied accuracy of the data collected at 20°C is to within ± 0.04 ft.

The number of wells in the LTWLM network varies somewhat based on the availability of calibrated PXDs and the investigation activities at the site. As of the summer of 2012, some 13 wells were in the network. The monitoring of multiple HSUs at a number of the wells brought the total number of records available to around 24.

Although the LTWLM program is designed to capture water-level trends and potential responses to well testing in the Pahute Mesa area and not to monitor for responses to seismic events, responses to earthquakes are noted in the data. With the current program, the responses to seismic events are captured after minutes—not seconds, as may be more useful in a program specifically monitoring for earthquake responses.

The LTWLM pressure records were reviewed for seismic responses and to investigate whether or not there are patterns in the monitoring well network regarding wells that show response to seismic events and those that do not. The response data for several earthquakes were selected to show the effect of these events on water levels at the NNSS. Table B.1-1 lists the earthquakes selected with the dates, times, estimated travel times, magnitudes, and epicenter locations. Arrival of the seismic signals from the various earthquakes at the NNSS is corroborated by the records from the Topopah Springs, Nevada, seismic station operated by the USGS survey. Plots of the station's daily records for the earthquakes shown in Table B.1-1 are included as Figures B.1-1 and B.1-2.

Figure B.1-3 shows where water-level responses were observed to the 8.2 and 8.6 magnitude earthquakes off the west coast of northern Sumatra on April 11, 2012. To aid the visualization, the

Table B.1-1
Example Seismic Events Observed in the Monitoring Well Pressure Records at the NNSS

Date	Time of Seismic Event (PST)	Time Observed (PST)	Estimated Travel Time	Magnitude	Location of Epicenter
03/20/2012	10:02:48	10:19:00	16 min 12 sec	7.4	Oaxaca, Mexico
04/11/2012	00:38:37	01:19:20	44 min 43 sec	8.6	Off the west coast of northern Sumatra
04/11/2012	02:43:09	03:24:10	41 min 01 sec	8.2	Off the west coast of northern Sumatra
04/11/2012	23:15:48	23:21:20	05 min 32 sec	6.9	Gulf of California

Source: USGS, 2012

PST = Pacific Standard Time

same data are shown from two different angles. The direct view at the top does not include the fault traces; the oblique view at the bottom does. Reference to the figure shows the data divided into categories of “Response” and “No Response.” Wells for which no record is available are not shown. In addition to the green (“Response”) and red (“No Response”) rings on the well bores, the well bores are colored according to the HSU the well or completion zone within a well represents. By way of example, a response to the earthquakes was observed at Well ER-EC-13, which is completed in the Fortymile Canyon composite unit (FCCM). At Well ER-20-4, no response was seen in the CHZCM completion, but a response was observed in the CFCU. Table B.1-2 shows the results in tabular fashion.

Figure B.1-4 shows the responses observed at Well ER-EC-11 to the earthquakes near Sumatra and in the Gulf of California on April 11, 2012. The pressure record in the well has been reduced to a head change in feet of water. The record shown does not begin with zero feet of head change because this is simply a portion of a much longer record. As can be seen on Figure B.1-4, the arrival of the pressure wave from the 8.6 magnitude earthquake near Sumatra caused a total change in head of more than 0.6 ft. By comparison, the 6.9 magnitude earthquake in the Gulf of California produced a response in head of a little more than 0.1 ft.

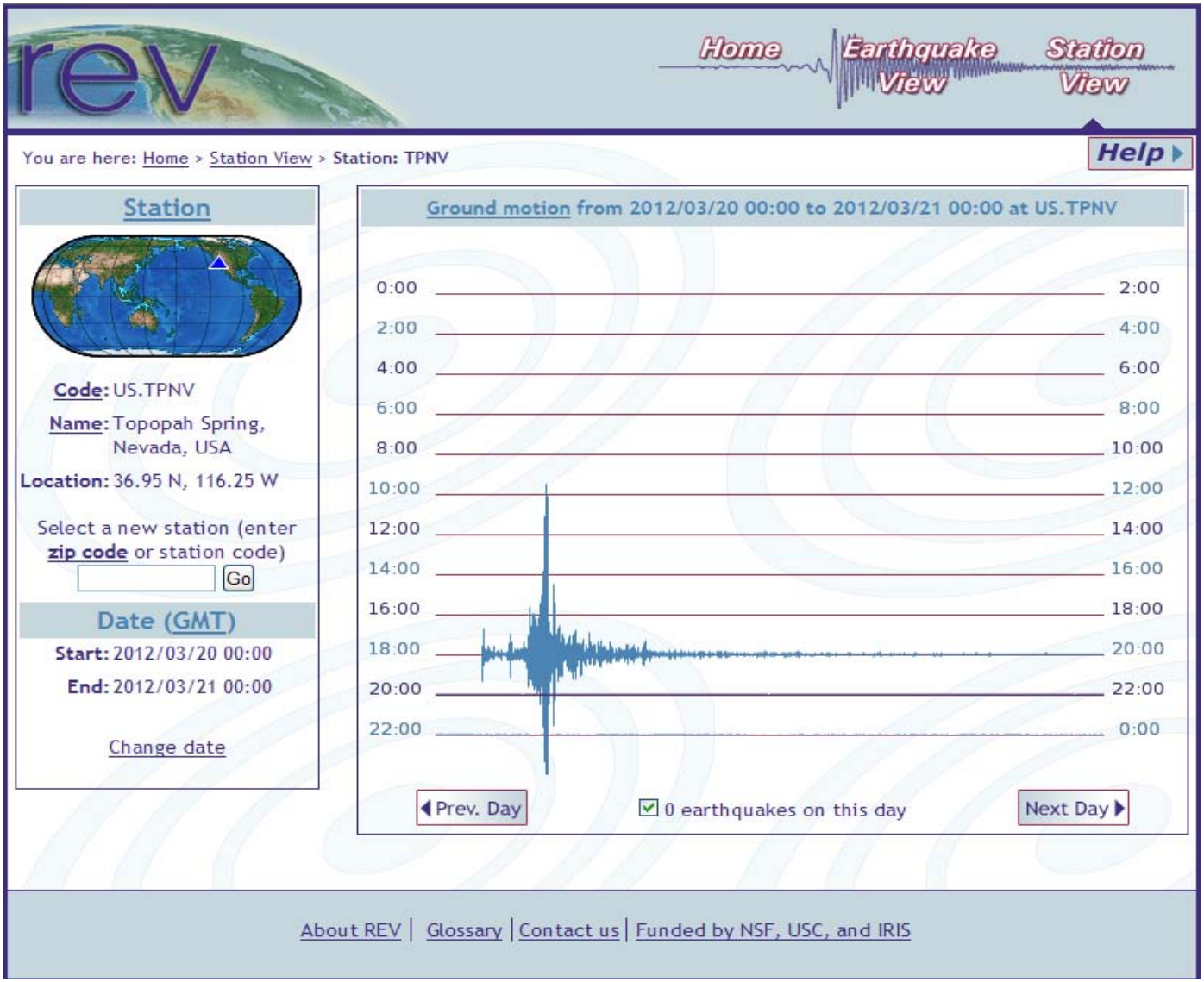

Figure B.1-1
Topopah Spring, Nevada, Seismic Station Record for March 20, 2012
Source: SEIS, 2012a

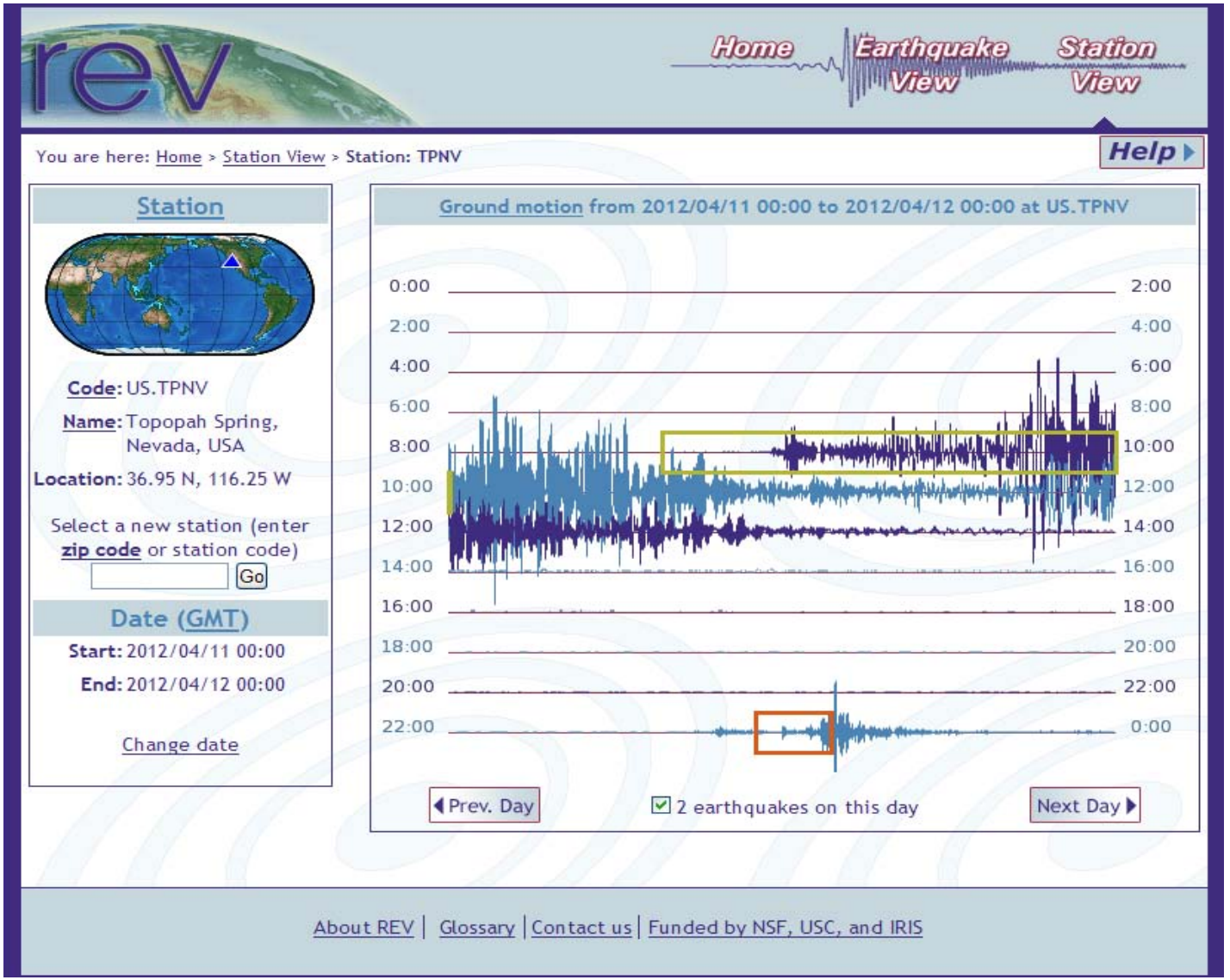

Figure B.1-2
Topopah Spring, Nevada, Seismic Station Record for April 11, 2012
Source: SEIS, 2012b

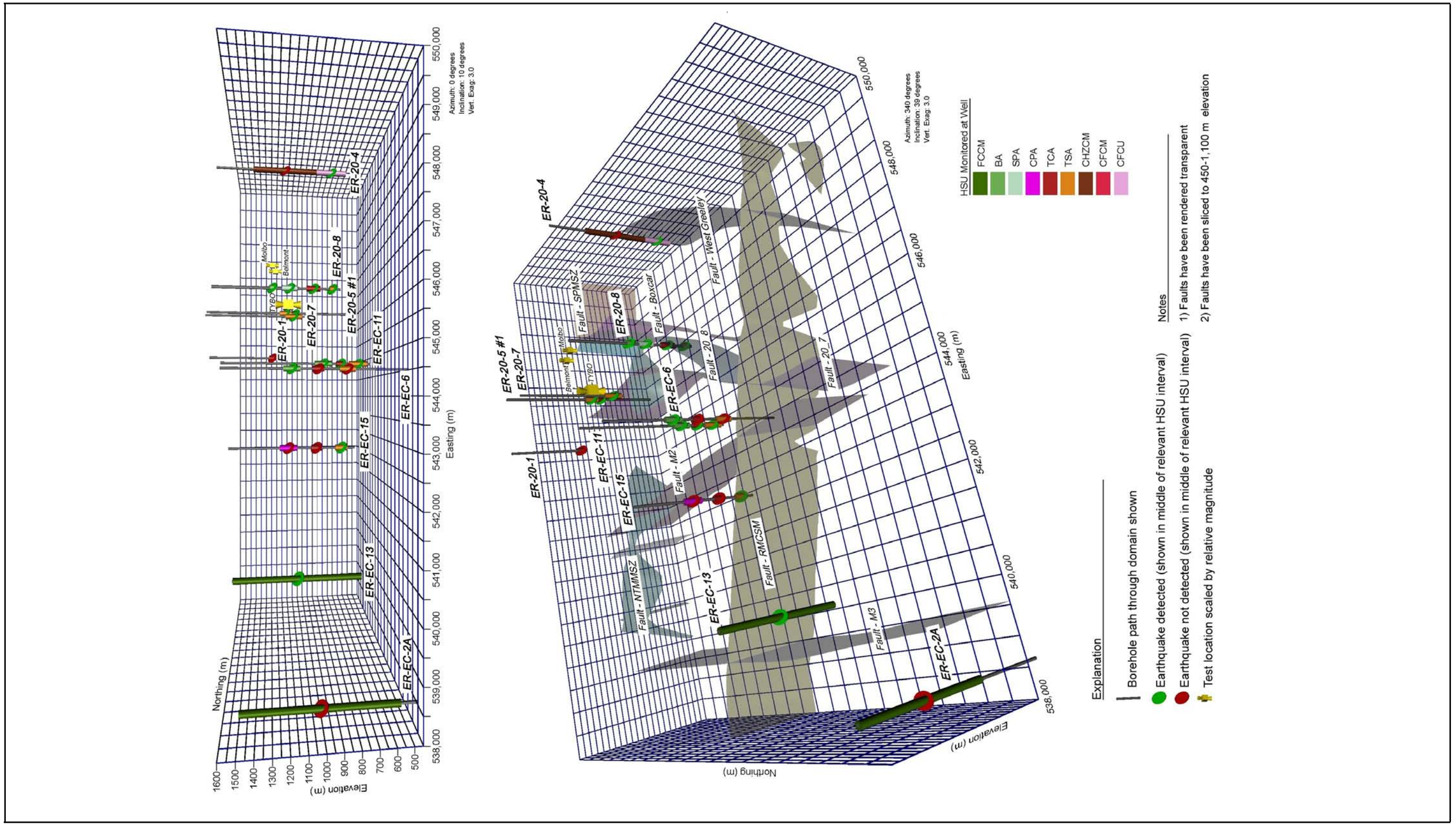

Figure B.1-3
Plot of Responses to the Earthquakes off Sumatra on April 11, 2012

Table B.1-2
Summary of Pressure Responses
(Page 1 of 2)

Well	Principal HSU	Minor HSU	Mag. 7.4, Oaxaca, Mexico (18:02:48 UTC)	Estimated Seismic Wave Initial Arrival [a]	Estimated Time to Pahute Mesa	Mag. 8.6, Off the West Coast of Northern Sumatra (08:38:37 UTC)	Estimated Seismic Wave Initial Arrival [b]	Estimated Time to Pahute Mesa	Mag. 8.2, Off the West Coast of Northern Sumatra (10:43:09 UTC)	Estimated Seismic Wave Initial Arrival [b]	Estimated Time to Pahute Mesa	Mag. 6.9, Gulf of California (04/12/12 07:15:48 UTC)	Estimated Seismic Wave Initial Arrival [b]	Estimated Time to Pahute Mesa
			10:02:48 PST	10:19:00 PST	16 min 12 sec	00:38:36 PST	01:19:20 PST	44 min 43 sec	02:43:09 PST	03:24:10 PST	41 min 01 sec	23:15:48 PST	23:21:20 PST	5 min 32 sec
			03/20/2012			04/11/2012			04/11/2012			04/11/2012		
ER-20-1	TCA		--	--	--	--	--	--	--	--	--	--	--	--
ER-20-4 (S)	CHZCM		--	--	--	--	--	--	--	--	--	--	--	--
ER-20-4 (D)	CHZCM	CFCU	--	--	--	X	X	X	X	X	X	--	--	--
ER-20-5 #1	TSA	CHZCM	X	X	X	X	X	X	X	X	X	--	--	--
ER-20-5 #3	CHZCM		--	--	--	X	X	X	X	X	X	--	--	--
ER-20-7	TSA	LPCU/CHZCM	--	--	--	X	X	X	X	X	X	--	--	--
ER-20-8 (S)	BA/SPA	UPCU	NR	NR	NR	X	X	X	X	X	X	X	X	X
ER-20-8 (I)	TCA	MPCU	--	--	--	X	X	X	X	X	X	X	X	X
ER-20-8 (D)	TSA	LPCU/CHZCM	X	X	X	X	X	X	X	X	X	X	X	X
ER-EC-1	BA/TCA/TSA/CFCM	UPCU/LPCU/CHCU	--	--	--	NR	NR	NR	NR	NR	NR	NR	NR	NR
ER-EC-2A	FCCM	TMCM	--	--	--	--	--	--	--	--	--	--	--	--
ER-EC-6 (S)	BA		X	X	X	X	X	X	X	X	X	--	--	--
ER-EC-6 (I)	TCA	UPCU	--	--	--	--	--	--	--	--	--	--	--	--
ER-EC-6 (D)	TSA	CHCU	--	--	--	--	--	--	--	--	--	--	--	--
ER-EC-11 (S)	BA	FCCU	--	--	--	X	X	X	X	X	X	X	X	X

Table B.1-2
Summary of Pressure Responses
(Page 2 of 2)

Well	Principal HSU	Minor HSU	Mag. 7.4, Oaxaca, Mexico (18:02:48 UTC)	Estimated Seismic Wave Initial Arrival [a]	Estimated Time to Pahute Mesa	Mag. 8.6, Off the West Coast of Northern Sumatra (08:38:37 UTC)	Estimated Seismic Wave Initial Arrival [b]	Estimated Time to Pahute Mesa	Mag. 8.2, Off the West Coast of Northern Sumatra (10:43:09 UTC)	Estimated Seismic Wave Initial Arrival [b]	Estimated Time to Pahute Mesa	Mag. 6.9, Gulf of California (04/12/12 07:15:48 UTC)	Estimated Seismic Wave Initial Arrival [b]	Estimated Time to Pahute Mesa
			10:02:48 PST	10:19:00 PST	16 min 12 sec	00:38:36 PST	01:19:20 PST	44 min 43 sec	02:43:09 PST	03:24:10 PST	41 min 01 sec	23:15:48 PST	23:21:20 PST	5 min 32 sec
			03/20/2012			04/11/2012			04/11/2012			04/11/2012		
ER-EC-11 (I)	TCA	UPCU	--	--	--	X	X	X	X	X	X	X	X	X
ER-EC-11 (D)	TSA	CHCU	--	--	--	X	X	X	X	X	X	X	X	X
ER-EC-13 (S)	FCCM		--	--	--	--	--	--	--	--	--	--	--	--
ER-EC-13 (I)	FCCM		X	X	X	X	X	X	X	X	X	X	X	X
ER-EC-13 (D)	FCCM		X	X	X	X	X	X	X	X	X	X	X	X
ER-EC-15 (S)	UPLFA	FCCU/PBPCU	--	--	--	--	--	--	--	--	--	--	--	--
ER-EC-15 (I)	TCA	LPCU	--	--	--	--	--	--	--	--	--	--	--	--
ER-EC-15 (D)	TSA	CHCU/CFCU	--	--	--	X	X	X	X	X	X	--	--	--

[a] Estimated from water-level response observed at Well ER-20-5 #1
[b] Estimated from water-level response observed at Well ER-20-8

S = Shallow
I = Intermediate
D = Deep

Notes:
PST is 8 hours behind Coordinated Universal Time (UTC)
Arrival times are only accurate to within several minutes

-- = No response
X = Response
NR = No record available

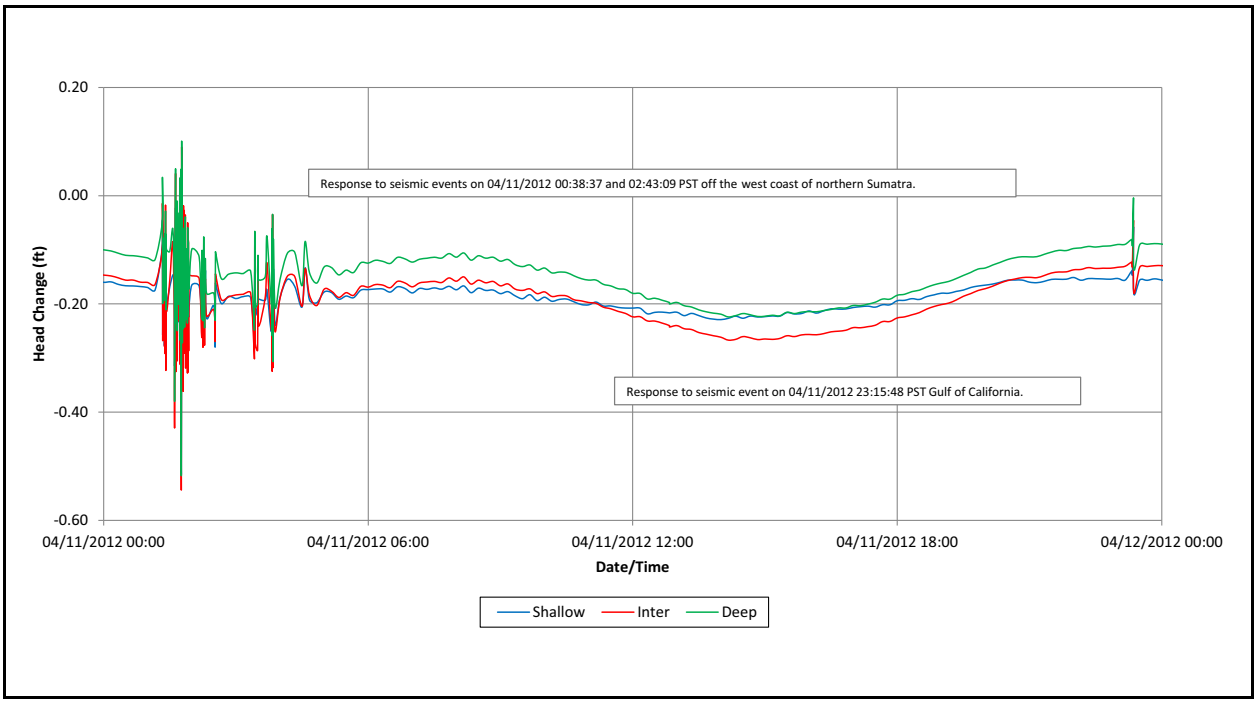

Figure B.1-4
Water-Level Responses Observed at Well ER-EC-11 on April 11, 2012

Figure B.1-5 is an example of a water-level record classified as not exhibiting a response. The figure shows the change in head observed at Well ER-EC-2A on April 11, 2012. Reference to the figure shows no obvious change in head due to either of the earthquakes which occurred that morning off the northern coast of Sumatra or that night in the Gulf of California.

The conclusion drawn from examining the data is that the principal factor in determining whether or not a response is observed is the degree to which a completion zone is hydraulically connected to a fault. In spite of the arrival of a strong seismic signal, wells such as ER-20-1 and ER-EC-2A did not respond because they are not hydraulically well connected to a fault. Well ER-20-8, which is in close proximity to a fault and shown by testing to be in good hydraulic communication with it, showed a response in every completion zone.

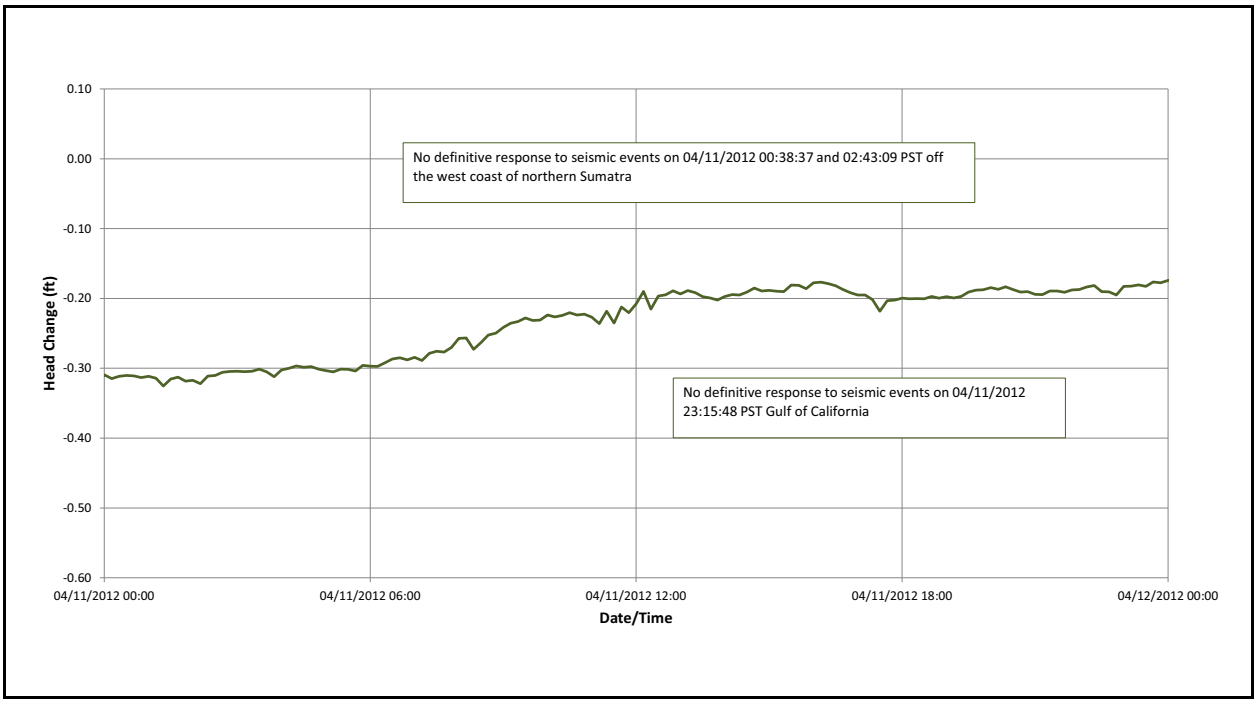

Figure B.1-5
Change in Head at Well ER-EC-2A on April 11, 2012

B.2.0 REFERENCES

SEIS, see University of South Carolina Seismology.

USGS, see U.S. Geological Survey.

University of South Carolina Seismology. 2012a. ”Rapid Earthquake Viewer (REV): Ground motion from 2012/03/20 00:00 to 2012/03/21 00:00 at US.TPNV.” As accessed at http://rev.seis.sc.edu/stations/US/TPNV?year=2012&month=3&day=20&hour=0 on 1 August.

University of South Carolina Seismology. 2012b. ”Rapid Earthquake Viewer (REV): Ground motion from 2012/04/11 00:00 to 2012/04/12 00:00 at US.TPNV.” As accessed at http://rev.seis.sc.edu/stations/US/TPNV?year=2012&month=4&day=11&hour=0 on 1 August.

U.S. Geological Survey. 2012. “Earthquake Hazards Program: 2012 Significant Earthquake and News Headlines Archive.” As accessed at http://earthquake.usgs.gov/earthquakes/eqinthenews/2012 on 1 August.

Appendix C

Radial Flow Model Analysis of Well ER-20-4 Responses

C.1.0 RADIAL FLOW MODEL ANALYSIS OF WELL ER-20-4 RESPONSES

C.1.1 Motivation and Conceptual Model

A radially symmetric flow model for Well ER-20-4 was created with FEHM (Zyvoloski et al., 1997) to investigate whether hydraulic parameters could be estimated for the tuff confining units and pumiceous lavas, in addition to the parameters already obtained for the lavas adjacent to the pumping zone via standard analytic well test methods. The conceptual model suggests that pumiceous lavas are more similar to zeolitic tuff confining units due to the ability of pumice to absorb some of the thermal stress that causes fractures in non-pumiceous lavas during cooling. Consequently, pumiceous lavas are lumped together with the zeolitic tuff confining units in the models presented in the following section as conceptualized by National Security Technologies, LLC (NSTec) (NNSA/NSO, 2011).

C.1.2 Model Setup

A radially symmetric flow model was created for the Well ER-20-4 WDT analysis that extends from -1,250 to -450 m depth in the vertical direction and 0 to 5,000 m in the radial direction. Grid spacing in the vertical direction was 5 m. Grid spacing in the radial direction was variable, and increased with distance from the pumping well: Δr = 0.1 m between r = 0 m and r = 5 m, Δr = 0.5 m between r = 5 m and r = 10 m, Δr = 1.0 m between r = 10 m and r = 50 m, and Δr = 10 m between 50 m and 5,000 m. There were a total of 95,956 nodes and 95,200 elements in the grid. The hydrostratigraphy included alternating lava and lumped zeolitic tuff/pumiceous lava HSUs that were assumed to extend outward to 5,000 m (Figure C.1-1). Layers of similar lithology were assumed to have the same hydrologic properties.

The highly resolved grid near the well bore allowed details of the well completion to be included in the simulation as described by NSTec (NNSA/NSO, 2011). This included (a) the well screen between depths of -916 m and -754 m; (b) the surrounding gravel pack between depths of -1,066 m and -744 m; (c) upper and lower cement plugs between depths of -747 m and -712 m and between -952 m and -930 m, respectively; and (d) open hole between the top of the upper cement plug and the water

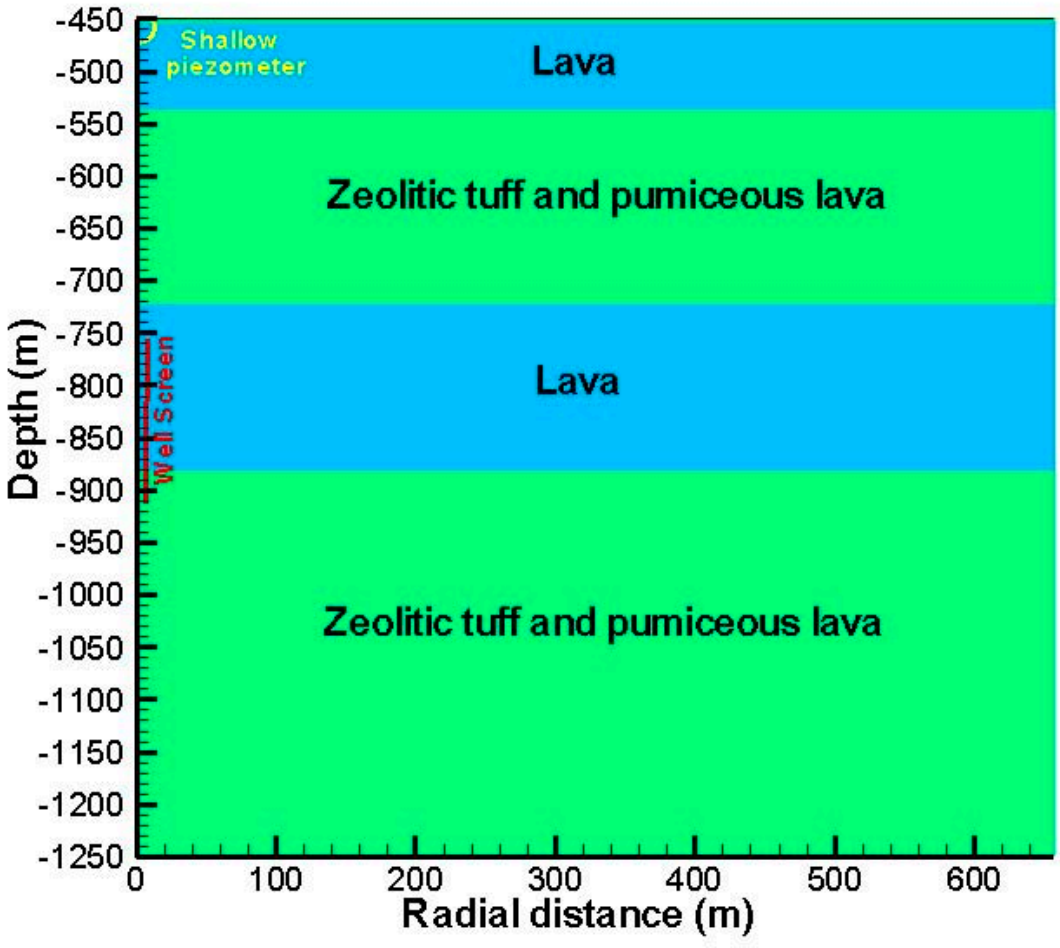

Note: Only the inner 675 m of the 5,000-m radius flow domain is shown.

Figure C.1-1
Inner Part of the Model Domain Showing the Hydrostratigraphic Layers in the Model along with the Depth of the Well Screen and Shallow Piezometer

table (-450 m). The open hole and well-screen segments were assigned permeabilities of 10^{-5} square meters (m^2), and the gravel pack was assigned a permeability of 10^{-11} m^2 to minimize head losses within these parts of the model domain. The open hole and screened interval were also assigned unique values of $S_s = 10^{-4}$ m^{-1} and $S_s = 2 \times 10^{-3}$ m^{-1}, respectively, to simulate borehole storage. The cement plugs were assigned permeabilities of 10^{-18} m^2 to hydraulically isolate the upper and lower parts of well from the pumped interval.

Initial conditions consisted of uniform hydraulic heads of 1,288 m throughout the model domain. Specified hydraulic heads of 1,288 m were imposed along the outer boundary of the model at

r = 5,000 m throughout the simulation. Specified groundwater withdrawals totaling 283 gpm (the average pumping rate) were taken from nodes within the screened interval beginning at t = 0 days and ending at t = 8 days. Water levels were allowed to recover between 8 days and the final simulation time of 13 days.

C.1.3 Parameter Estimation

The parameter estimation code PEST (Doherty, 2010) was used to estimate the permeability of the non-pumiceous lava (*k-lava*), the permeability of the lumped zeolitic tuffs and pumiceous lavas (*k-tuff*), the specific storage coefficient of all HSUs (S_s), the specific yield (S_y) at the water table nodes, and a resistance factor (f_s). The resistance factor represents the damage to the formation adjacent to the borehole wall and was applied to the interface between gravel pack and lavas adjacent to the screened interval (the skin effect in well-testing terminology), and is implemented by altering the harmonic mean permeability between elements. As described in Section 5.2.3, a skin factor of 30 was necessary to explain the observed drawdown in the deep piezometer at Well ER-20-4.

PEST estimates the optimal parameters required to minimize difference between observations and simulated values. In this application, observations consisted of measured drawdowns at both the shallow and deep piezometers at 0.1-day intervals between 0 and 13 days, for a total of 262 observations (131 for each piezometer). The shallow piezometer data were corrected for barometric pressure fluctuations and earth tides using the method of Halford (2006). The observed drawdowns were compared against simulated drawdowns at nodes closest to the midpoints of the shallow piezometer (r = 0.24 m, z = 457.4 m) and the deep piezometer (r = 0.24 m, z = -835.2 m).

To provide additional constraints on the problem and reduce the non-uniqueness of the parameter estimates, a value of 10^{-12} m^2 for *k-lava* was supplied as prior information with a weight of 100 (the value from type-curve analysis was about 2×10^{-12} m^2). This forced PEST to search for optimal parameter combinations that involved values of *k-lava* close to this value without over-constraining the search. Due to the much larger drawdowns at the deep piezometer relative to the shallow piezometer, it was necessary to apply much larger weights (w) to the observations from the shallow piezometer (w = 25.0) compared with those from the deep piezometer (w = 1.0) to ensure that data from both piezometers influenced the calibration. Early parameter optimization attempts also

indicated that the model showed no sensitivity to the value of S_y, so this parameter was fixed at $S_y = 10^{-6}$ to focus PEST on optimizing the remaining parameters.

Estimated parameter values are given in Table C.1-1 along with the linear 95 percent confidence intervals provided by PEST. Although these confidence intervals are only approximate in that they are based on model sensitivities in the vicinity of final estimated parameters, they do indicate that the dataset (supplemented by the prior estimates of *k-lava* provided by fitting an analytical solution) constrains the parameter estimates reasonably well. The results indicate that the combined zeolitic tuff/pumiceous lava units are more permeable than would be thought from core analysis alone, although less permeable than the non-pumiceous lavas. For instance, based on 293 measurements, Flint (1998) gives a mean log permeability for zeolitic tuff from the Calico Hills of $log\ k = -17.34 \pm 1.31$ (1 σ) m^2. This implies substantial fracturing of the combined zeolitic tuff/pumiceous lava units in the vicinity of the well. This is consistent with the image log data that showed more fracturing in the pumiceous lava and bedded tuff intervals than the lavas, possibly from faulting (Prothro, 2011).

Table C.1-1
Results of PEST Optimization

Parameter	Estimated Value	Confidence Interval	
		Lower 95%	Upper 95%
k-lava (m^2)	1.03E-12	9.16E-13	1.16E-12
k-tuff (m^2)	5.61E-13	4.12E-13	7.65E-13
Resistance factor f_s	4.46E-03	4.07E-03	4.88E-03
S_s (m^{-1})	9.19E-06	7.11E-06	1.19E-05

The fit of the numerical model to the data from the shallow piezometer is shown in Figure C.1-2, and the fit to the data from the deep piezometer is shown in Figure C.1-3. The linear plots shown in Figures C.1-2a and C.1-3a indicate the data provide a good overall match to the water-level decline and recovery portions of the data in both piezometers. The log-log plots shown in Figures C.1-2a and C.1-3a show some deviations at early time. In the deep piezometer, these data are irrelevant for estimating formation parameters. In the shallow piezometer, the reasonable fit at later times (when the flow regime is more fully developed) does not invalidate the conceptual model.

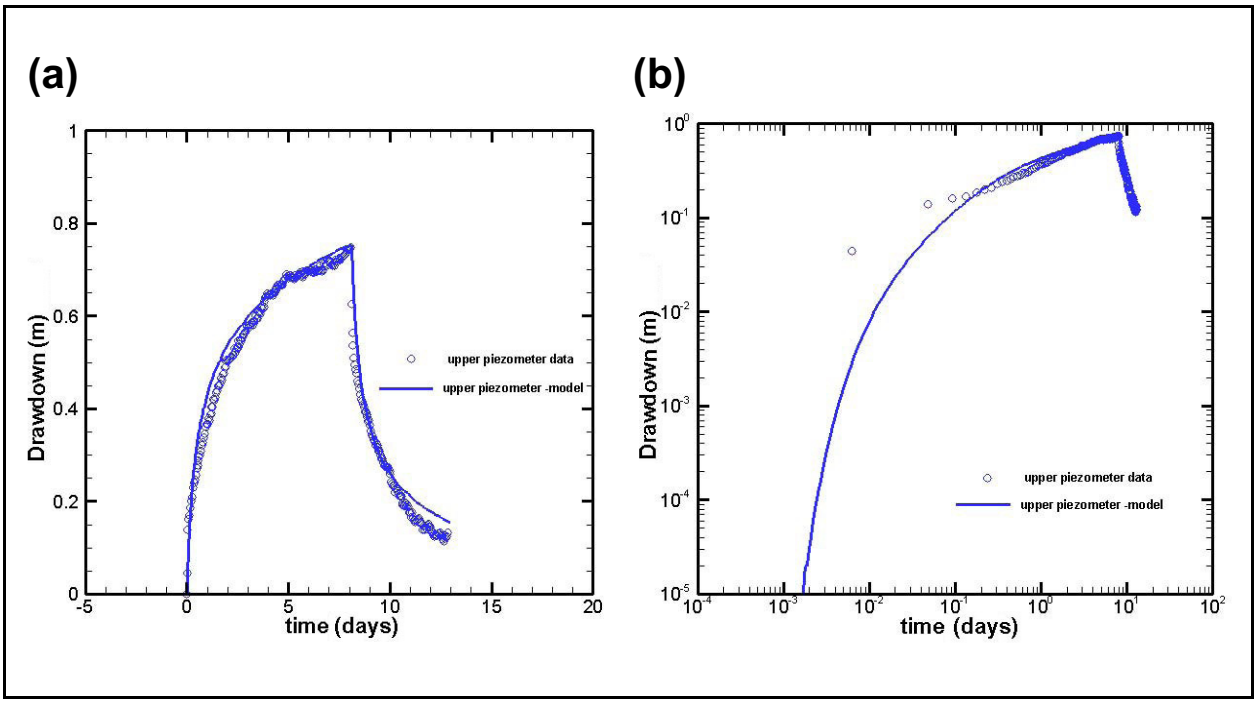

Figure C.1-2
Comparison of Measured and Simulated Water-Level Changes in the Shallow Piezometer of Well ER-20-4: (a) Linear-Linear Plot, and (b) Log-Log Plot

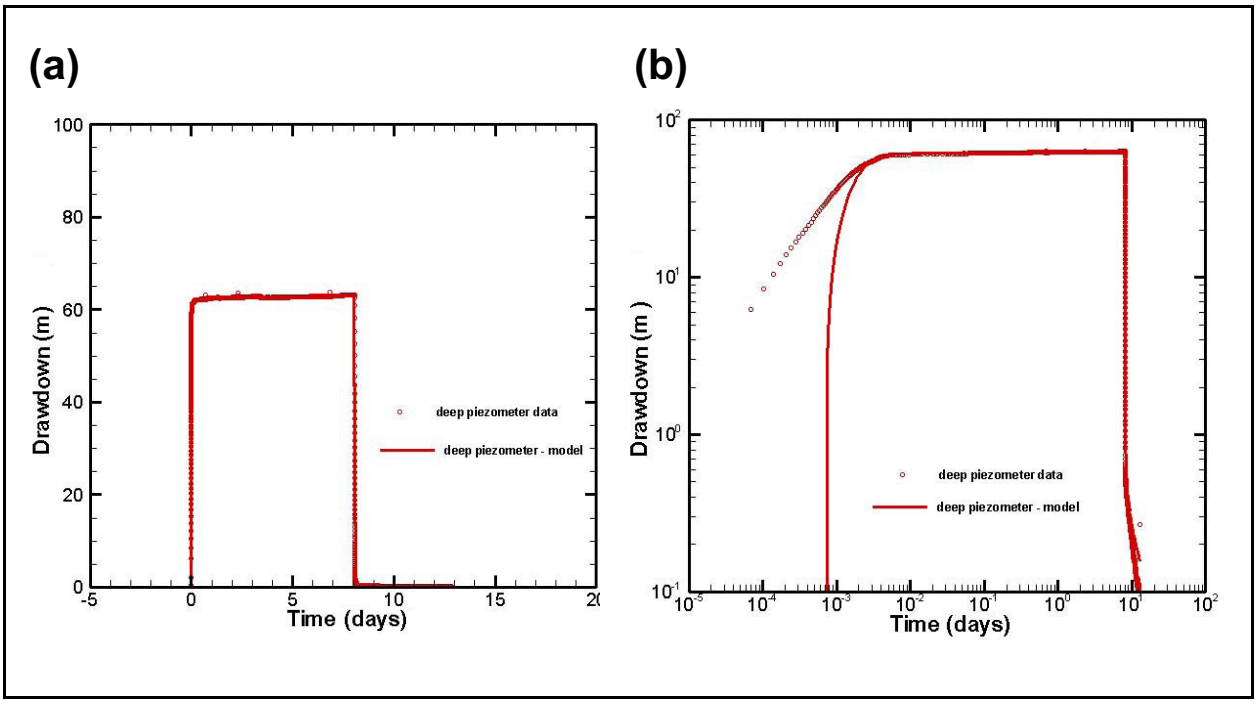

Figure C.1-3
Comparison of Measured and Simulated Water-Level Changes in the Deep Piezometer of Well ER-20-4: (a) Linear-Linear Plot, and (b) Log-Log Plot

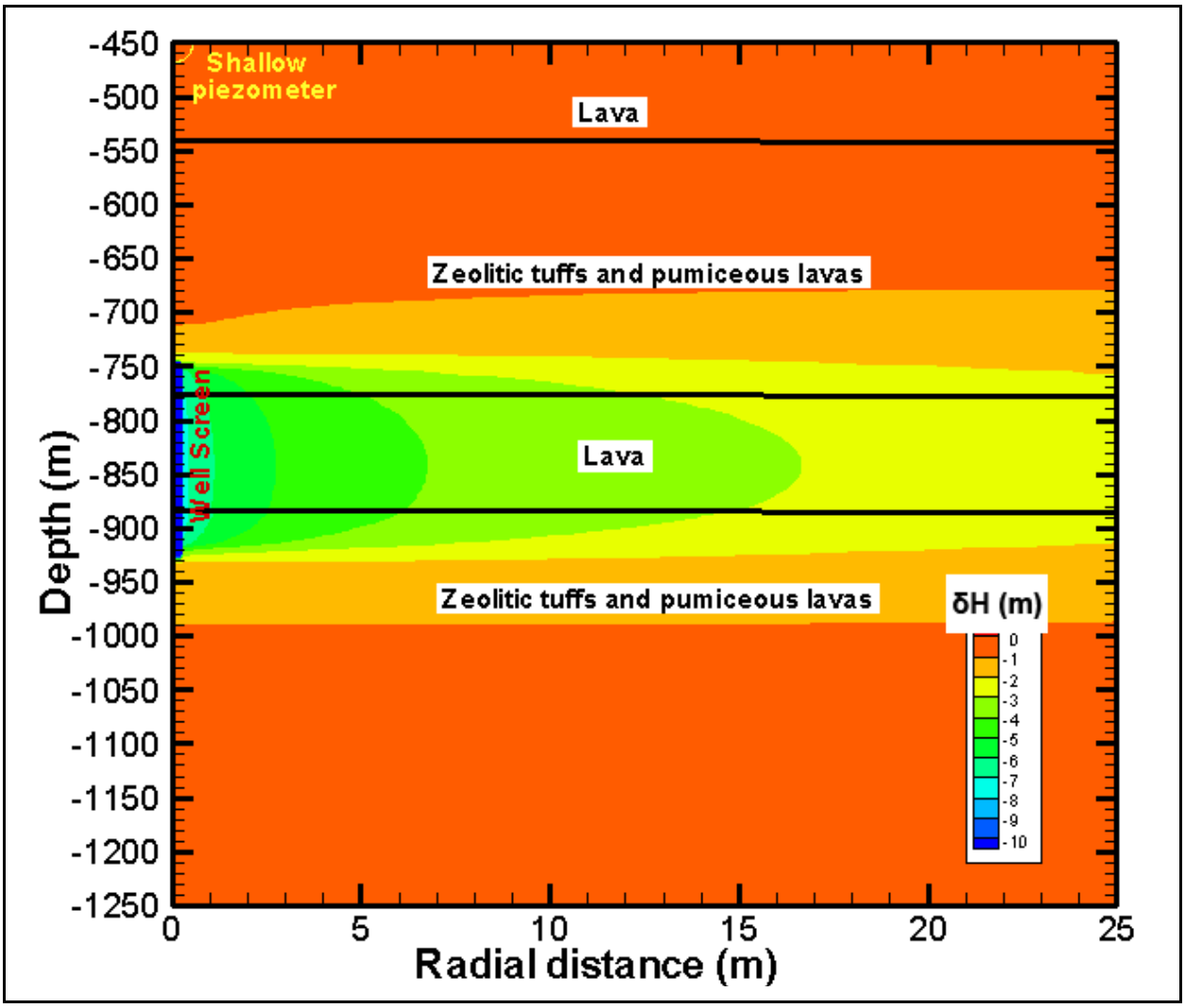

Figure C.1-4
Water-Level Changes after 8 Days of Pumping at 283 gpm

Figure C.1-4 shows the drawdowns after 8 days of pumping in the vicinity of the screened interval. The drawdowns of just a few meters in the vicinity of the borehole, combined with the 63 m of drawdown measured at the lower piezometer (Figure C.1-3), are consistent with the concept that a skin near the borehole wall has significantly affected drawdowns measured in the lower piezometer.

C.2.0 REFERENCES

Doherty, J. 2010. *PEST: Model-Independent Parameter Estimation & Uncertainty Analysis*. Brisbane, Australia: Watermark Numerical Computing. (Available at http://www.pesthomepage.org.)

Flint, L.E. 1998. *Characterization of Hydrogeologic Units Using Matrix Properties, Yucca Mountain, Nevada,* Water-Resources Investigations Report 97-4243. Denver, CO: U.S. Geological Survey.

Halford, K.J. 2006. *Documentation of a Spreadsheet for Time-Series Analysis and Drawdown Estimation*, Scientific Investigations Report 2006-5024. Carson City, NV: U.S. Geological Survey.

NNSA/NSO, see U.S. Department of Energy, National Nuclear Security Administration Nevada Site Offic.e

Prothro, L.B. 2011. Written communication. Subject: *Analysis and Interpretation of Borehole Image Logs from Well ER-20-4*. June. Las Vegas, NV: National Security Technologies, LLC.

U.S. Department of Energy, National Nuclear Security Administration Nevada Site Office. 2011. *Completion Report for Well ER-20-4, Corrective Action Units 101 and 102: Central and Western Pahute Mesa*, DOE/NV--1447. Prepared by National Security Technologies, LLC. Las Vegas, NV.

Zyvoloski, G.A., B.A. Robinson, Z.V. Dash, and L.L. Trease. 1997. *Summary of Models and Methods for the FEHM Application - A Finite-Element Heat and Mass-Transfer Code*, LA-13307-MS. Los Alamos, NM: Los Alamos National Laboratory.

Appendix D

Estimating Aquifer Storage for Well ER-20-8 Using Earth-Tide Analysis

D.1.0 INTRODUCTION

The motion of the sun and the moon causes expansion and contraction of subsurface formations. The strain due to such earth tides induces periodic water-level fluctuations in monitoring wells. These fluctuations in water levels will have the same periodicity as the earth tides, but may be damped or phase-lagged depending on the formation characteristics of the aquifer.

Over the years, multiple techniques have been developed to estimate aquifer properties based on the response of water levels to earth-tide-induced strains. Estimated properties include specific storage, porosity, matrix compressibility (or bulk-modulus), and transmissivity. These methods typically rely on analyzing the periodic signal in earth tides and water levels, and estimating the aquifer properties based on the amplitude ratio and phase lag between dominant frequencies in the earth-tide time series and the water-level time series.

This analysis focuses on estimating specific storage, defined as the volume of water that an aquifer releases from storage, per volume of aquifer, per unit decline in hydraulic head (Freeze and Cherry, 1979). Bredehoeft (1967) showed that the fluctuations in head in an open well produced by tidal dilatation were a function of the specific storage of the aquifer. This analysis assumed incompressible grains, a simplifying assumption that was later relaxed by various authors. For example, Van Der Kamp and Gale (1983) developed expressions for specific storage that included the effects of matrix compressibility. Both these approaches assumed that tidal strains were induced predominantly in the vertical direction. The assumption of only vertical deformation was later relaxed by Rojastaczer and Agnew (1989), who derived expressions relating porosity and specific storage to the amplitude ratio of earth-tide-induced areal strain and the corresponding water-level response. Hsieh et al. (1987) derived theoretical relations for transmissivity and storage based on amplitude ratio and phase lags for harmonic components of earth tides and water levels. Another approach, given by Bernard and Delay (2008), relied on spectral analysis of the auto- and cross-correlation function between barometric, water level, and earth-tide time series. A more empirical approach for estimating specific storage for fractured rock systems was used by Burbey (2010), who estimated specific storage as the slope of the hysteretic curve between volumetric (earth-tide-induced) strain and water levels.

This analysis uses the relationship derived by Bredhoeft (1967) to estimate specific storage of the aquifer. The model assumes incompressible solid grains and only vertically acting tidal stresses. Such an assumption may or may not be valid depending on the type of rock matrix. Cutillo and Bredehoeft (2011) point out that such an assumption may not be "very good for aquifers in competent rocks, especially those where the porosity is small." The assumptions for compressibility and vertical strains will be relaxed in subsequent analysis that will follow this preliminary work.

Time-frequency analysis was conducted on water-level data gathered through the Pahute Mesa long-term head monitoring program (N-I, 2011). Because no direct measurements of earth tides were available, theoretical models were used to generate synthetic earth-tide time series that were also analyzed in the time-frequency domain. Comparison of the time-frequency spectrum of the water-level data and the earth-tide time series allows the calculation of amplitude ratios for specific frequencies in the earth-tide spectrum, which are then used to estimate specific storage for the different monitoring locations.

D.1.1 Methodology

Before conducting spectral analysis on the water-level data, any long-term trends can be removed by using a low-pass filter to isolate low frequencies (less than 1/day) and subtracting the low-frequency signal from the original time series to yield records that have only high frequency (greater than 1/day) periodic signals that represent earth tides. The low-pass filter used for this analysis is based on Godin (1972) and is recommended by Hsieh et al. (1987) and Kilroy (1992). The low pass filter consists of a series of moving averaging operations and can be written mathematically as $A_{24}A_{24}A_{25}/(24\times24\times25)$ where A_n/n is a moving average that takes the average of n consecutive data points and assigns it to time $k + (n\text{-}1)/2$, where k is the time of the first data point considered. For this analysis, the data were resampled at uniform 1-hour intervals. The Godin filter was then used to go through the three averaging steps with 24 hours, 24 hours, and 25 hours averaging windows.

Bredehoeft (1967) related the dilatation of the aquifer material to the specific storage (S_s) of the aquifer and the tide-generating potential[1] (W):

$$S_s = -\left[\left(\frac{1-2\nu}{1-\nu}\right)\left(\frac{2\bar{h}-6\bar{l}}{ag}\right)\right]\frac{dW}{dh} \qquad (D\text{-}1)$$

where

ν = the Poisson ratio of the aquifer material (dimensionless)
$\bar{h}$ and $\bar{l}$ = Love numbers at the surface of the earth (dimensionless)
a = the radius of the earth (L)
g = the gravitational acceleration at the surface of the earth (L/T^2)

The Poisson's ratio is defined as the ratio between the latitudinal and longitudinal strain due to stretching or compressing of a given material. A value of 0.25 is typically used in most analyses (Merritt, 2004; Cutillo and Bredehoeft, 2011). The Love numbers depend on the elastic properties of the earth and relate theoretical tidal potential to actual displacement at the surface of the earth. Typical values recommended in the literature are $\bar{h}$ = 0.6 and $\bar{l}$ = 0.07 (Munk and MacDonald, 1960). The last term in Equation (D-1) can be thought of as the inverse of the unit change in head induced by a unit change in tidal potential. This term can be estimated by the amplitude ratio of the harmonic component of the tidal potential and the same harmonic component of the water level for a given frequency in the tidal spectrum (Merritt, 2004; Cutillo and Bredehoeft, 2011) as

$$\frac{dW}{dh} \approx \frac{A_2(f)}{A_W(f)} \qquad (D\text{-}2)$$

where

$A_2(f)$ = the amplitude of the harmonic component with frequency f of tidal potential
$A_w(f)$ = the amplitude of the harmonic component of the water level with the same frequency

The above relation assumes the soil grains to be incompressible. Van Der Kamp and Gale (1983) argued that such a relation may not adequately represent storage for aquifers with very low compressibility and/or low porosity. They derived a relation that also accounted for matrix compressibility as

$$S_s = -\left[\left(1-\frac{K}{K_s}\right)\left(\frac{1-2\nu}{1-\nu}\right)\left(\frac{2\bar{h}-6\bar{l}}{ag}\right)\right]\frac{dW}{dh} \qquad (D\text{-}3)$$

where

K = the bulk modulus (inverse of compressibility) of the formation
K_s = the bulk modulus of the solid fraction

1. The tidal acceleration (g) is related to tidal potential (W) as $g = -\nabla W$. W has units L^2/T^2.

For incompressible grains, $1/K_s \approx 0$ and the above expression becomes identical to the Bredehoeft (1967) Equation (D-1). Merritt (2004) prefer to use the earlier form of the specific storage expression due to the difficulty in getting site specific values for K and K_s. They note that including compressibility would lead to lower specific storage in general (the term $1 - K/K_s$ would always be less than 1). Similar to the approach applied by Merritt (2004), this study uses the first form S_s expression (Equation [D-1]) as given by Bredehoeft (1967).

Given Equations (D-1) and (D-2), the only two terms that need to be calculated are $A_2(f)$ and $A_w(f)$, i.e., the amplitudes of the harmonic components of tidal potential and water levels. Tidal signals comprise a spectrum of waves with distinct and known frequencies. Table D.1-1 shows the dominant frequencies found in tidal signals.

Table D.1-1
Angular Frequencies and Periods of Five Dominant Tidal Constituents

Name of Constituent	Angular Frequency (degree/hour)	Period (hour)
O_1	13.943	25.819
K_1	15.041	23.934
N_2	28.440	12.658
M_2	28.984	12.421
S_2	30.000	12.00

Source: Hsieh et al., 1987

From Table D.1-1, it is evident that two (K_1 and S_2) of the five tidal constituents have periodicities of 12 and (almost) 24 hours. In practice, these signals can be difficult to analyze because barometric variation also has 12- and 24-hour periodicities. Thus water-level response for these periodic perturbations will be due to the combined effect of earth tides and barometric fluctuations. The other three constituents (O_1, N_2, and M_2) have distinct periodicities from barometric variation and can thus be analyzed in isolation. Of the three, N_2 typically has a poor signal to noise ratio, leaving only O_1 and M_2 signals remaining. Most studies (Hsieh et al., 1987; Merritt, 2004; Cutillo and Bredehoeft, 2011) analyze only these two frequencies when estimating aquifer properties from water-level response to earth-tide forcings. Thus, this analysis was also based only on the O_1 and M_2 signals, ignoring the K_1, S_2, and N_2 frequencies.

Fourier transforms can be used to generate the amplitude and phases of constituent spectra in the respective residual time series (with long-term trend removed). In this work, the TSOFT software (Van Camp and Vauterin, 2005) was used to evaluate the Fourier spectrum of the various time series.

In the presence of noise, the Fourier spectrum obtained may be noisy. Thus, Hsieh et al. (1987) and Cutillo and Bredehoeft (2011) recommend using regression to estimate amplitudes and phases of exact frequencies. The time series may be represented as a summation of cosines as

$$x(t) = \sum_{k=1}^{N} A_k Cos(2\pi f_k t + \varphi_k) + e\,(t) \qquad \textit{(D-4)}$$

where

$x(t)$ = the value (of head or tidal potential) at time t
N = the number of constituent frequencies to be included
f_k = the frequency
A_k = the amplitude of the frequency
φ_k = the phase of component k

The residual error term, $e(t)$, is what remains after fitting all constituent frequencies. The amplitude and phase of given frequencies may be estimated using a least square fitting approach. Cutillo and Bredehoeft (2011) used a linear form of the equation given by

$$h(t) = \sum_{k=1}^{N} [c_0 + c_1 Cos(2\pi f_k t) + c_2 Sin(2\pi f_k t)] \qquad \textit{(D-5)}$$

Because f_k is known (Table D.1-1), the relation becomes linear with respect to c_0, c_1, and c_2, which may then be estimated using linear regression analysis. The amplitude and phase of k^{th} tidal component can then be given by

$$A_k = \sqrt{{c_1}^2 + {c_2}^2} \qquad \textit{(D-6)}$$

$$\varphi_k = atan\left(-\frac{c_2}{c_1}\right) \qquad \textit{(D-7)}$$

D.1.2 Data

Water-level and barometric pressure data were collected through the Pahute Mesa 2010 long-term head monitoring program (N-I, 2011). For this analysis, data for Well ER-20-8 were considered.

The data consist of water levels as measured by pressure transducers (located below the free water surface in the monitoring access casing or tubing) and atmospheric pressure as measured by surface barometers. Only vented pressure transducers were considered for this analysis, as they directly measure gauge pressure. Non-vented pressure transducers (which measure absolute pressure) were not considered, as they require the pressure readings to be corrected for barometric effects, assuming a barometric efficiency of one. It was not clear whether such an assumption was necessarily true for pressure transducers located at depths, where atmospheric pressure variations may get lagged and damped. For Well ER-20-8, two of the depths (deep and intermediate depths) used vented pressure transducers, while the shallow depth used a non-vented pressure transducer. Thus, only the deep (average screen depth of 788 m amsl) and intermediate (average screen depth of 980 m amsl) pressure transducers were considered. The pressure transducers and barometers employ an adaptive sampling scheme with non-uniform sampling intervals. To simplify analysis for this report, all readings were resampled at the 1-hour interval. (See Table D.1-1, which shows that the tidal constituents of interest all have periodicities greater than 12 hours.) For this analysis, a continuous period of record (without any gaps in data) is required. Moreover, it is ideal that water-level data correspond to periods when there were not strong anthropogenic effects (such as pumping). Based on these requirements, a subset of the original time series, spanning from May 11 to August 25, 2010, was used for this analysis.

No measurements of earth tides were available. Thus, a theoretical model was used to generate synthetic earth-tide time series for tidal potential. This was done using the scientific code ETGTAB (Wenzel, 1996). ETGTAB generates various earth-tide components (e.g., earth-tide potential, tidal acceleration, tidal displacement, tidal strain). Required inputs include latitude, longitude, and elevation of location; time (year, month, day, and hour) and duration of tidal signal; choice from four theoretical earth-tide models (Tamura, 1987 was used for this analysis); and information on wave groups to include in the simulation (the default for Tamura [1987] is 14 wave groups). ETGTAB was run for each monitoring well location, thus generating site-specific earth tide potentials. Fourier series analysis was then used to estimate the amplitude A_2 of various wave groups, in the same way as for the water-level time series.

As a validation step, a theoretical model given by Merritt (2004) and Cutillo and Bredehoeft (2011) was used to estimate A_2 (amplitude of the earth-tide potential harmonic) in Equation (D-2).

Merritt (2004) and Cutillo and Bredehoeft (2011) give the following equations to calculate the A_2 for the M_2 and O_1 tidal components:

$$A_2(M_2) = 0.5gK_m b\cos^2(\theta) \quad \textit{(D-8)}$$

$$A_2(O_1) = gK_m b\sin(\theta)\cos(\theta) \quad \textit{(D-9)}$$

where

g = the acceleration due to gravity (L/T^2)
K_m = the general lunar coefficient (equal to 0.537 m)
b = the amplitude factor (0.908 for M_2 and 0.377 for O_1)
θ = the latitude

Both the synthetic earth tide and the model given by Equations (D-8) and (D-9) were used to calculate the amplitude for earth tide potentials

As discussed previously, a low-pass filter (consisting of diurnal moving average) was used to remove any long-term trends from all the data.

D.1.3 Analysis and Results

Figures D.1-1 and D.1-2 show the water-level data for Wells ER-20-8 (D) and ER-20-8 (I). The hourly raw data are juxtaposed on the daily averaged (using the Godin filter discussed earlier), as well as the residual water-level time series. Figure D.1-3 shows the earth-tide potential for this location (the synthetic earth tide model does not consider depth; hence, the same earth tide is used for both well depths).

Figures D.1-4 through D.1-6 show the amplitudes for various spectra for the ER-20-8 (D) water levels, ER-20-8 (I) water levels, and the earth-tide potential, respectively.

Table D.1-2 shows all parameters used in the calculation of specific storage for the two depths. Specific storage estimates for the wells and screens analyzed are shown in Table D.1-3. Results indicate that the spectral analysis and theoretical/regression-fitting approaches give similar S_s estimates. Because the M_2 signal is much stronger than the O_1 signal, the results for the M_2 frequency are more robust (difference in the spectral and theoretical/regression-fitting approaches is negligible).

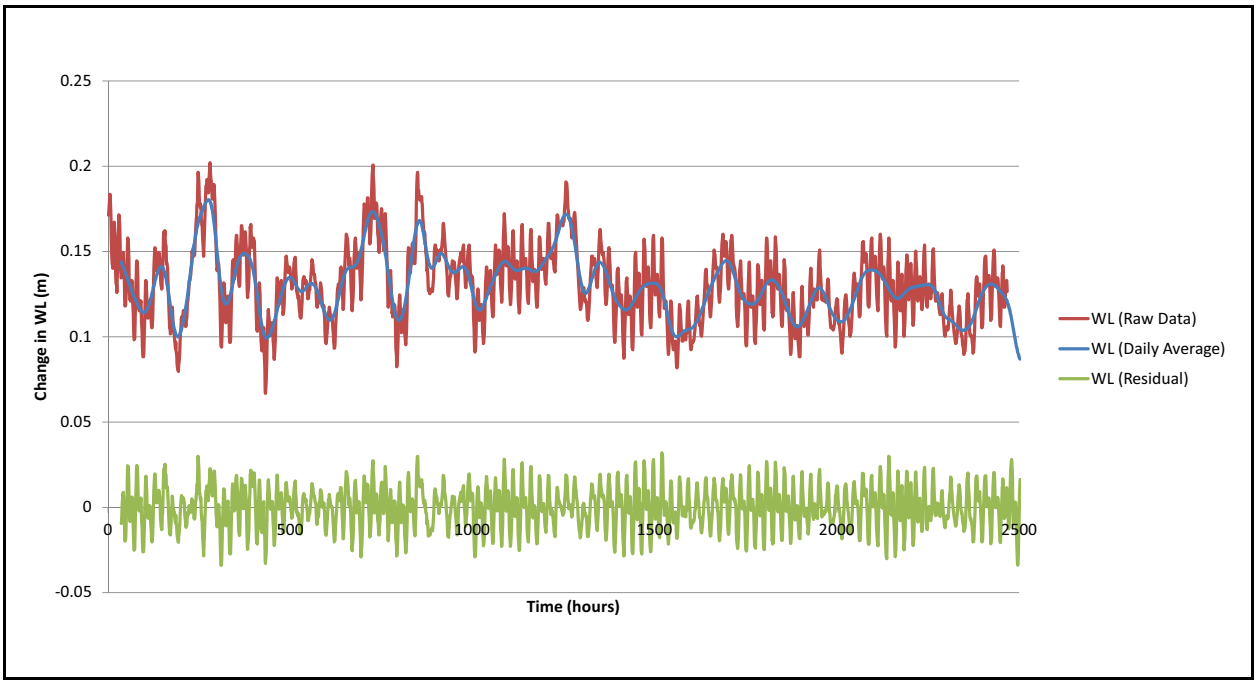

Figure D.1-1
Water-Level Data for Well ER-20-8 (D) (Raw, Daily Average, and Residual)

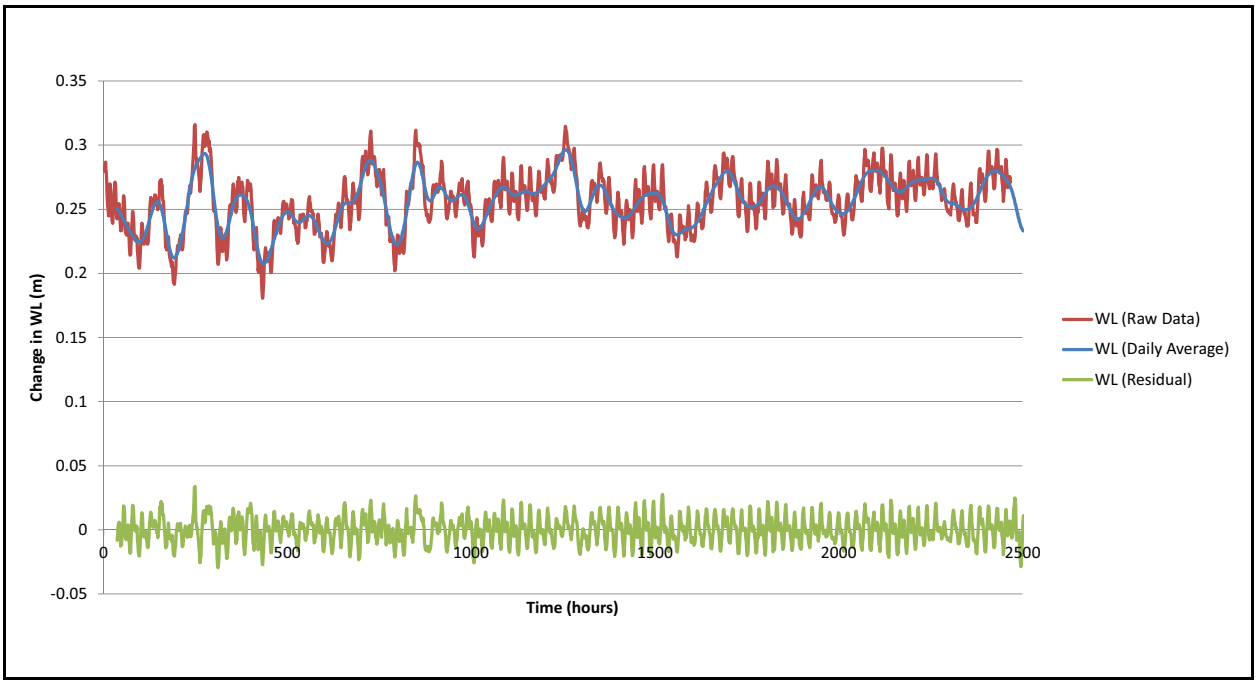

Figure D.1-2
Water-Level Data for Well ER-20-8 (I) (Raw, Daily Average, and Residual)

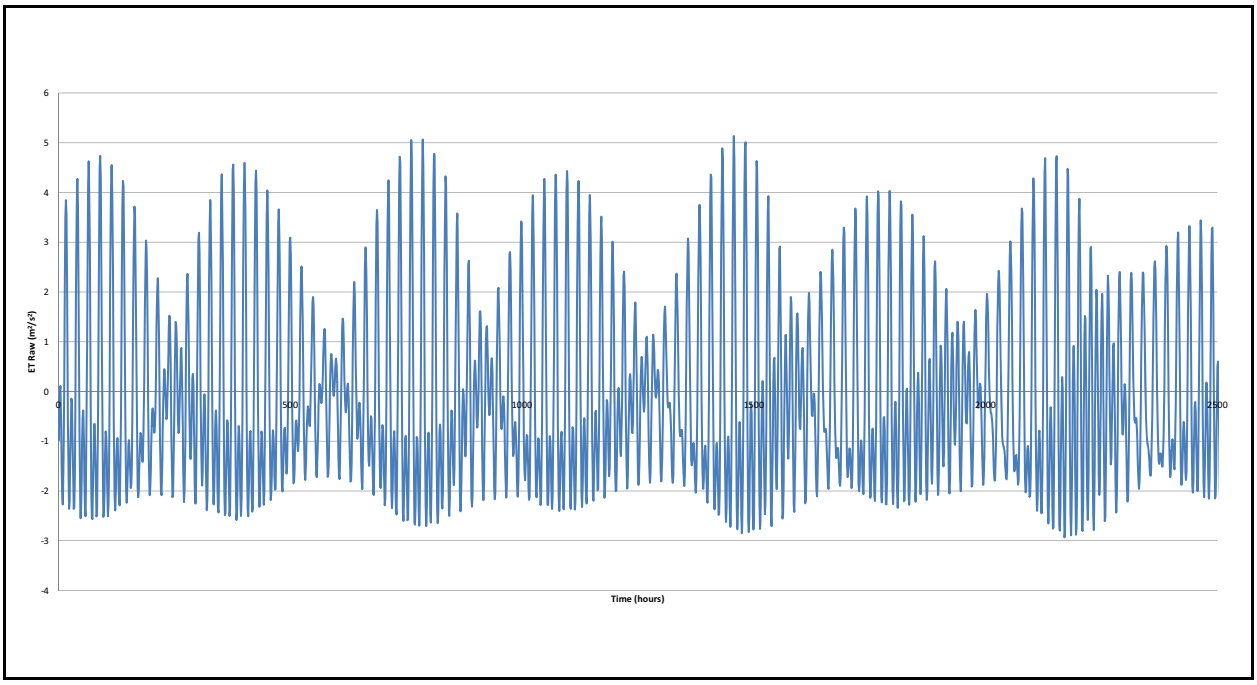

Figure D.1-3
Synthetic Earth-Tide Potential for Well ER-20-8

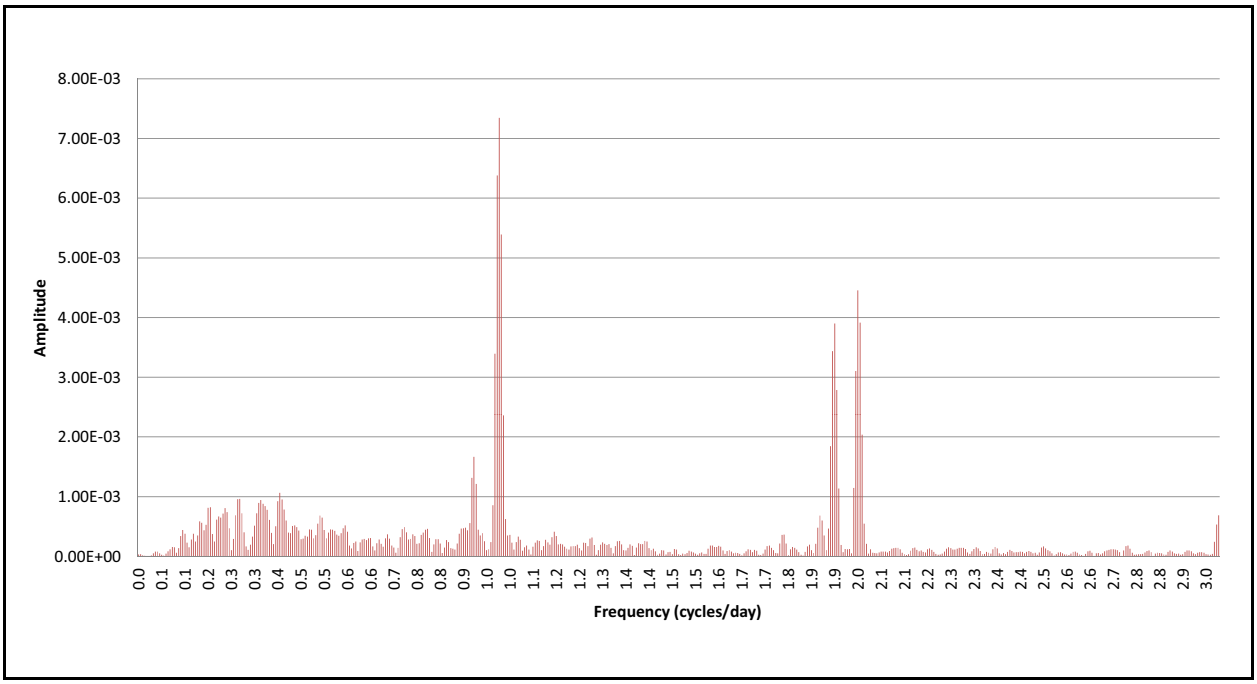

Figure D.1-4
Amplitude Spectra Obtained from Fourier Transform of Well ER-20-8 (D) Water-Level Residuals

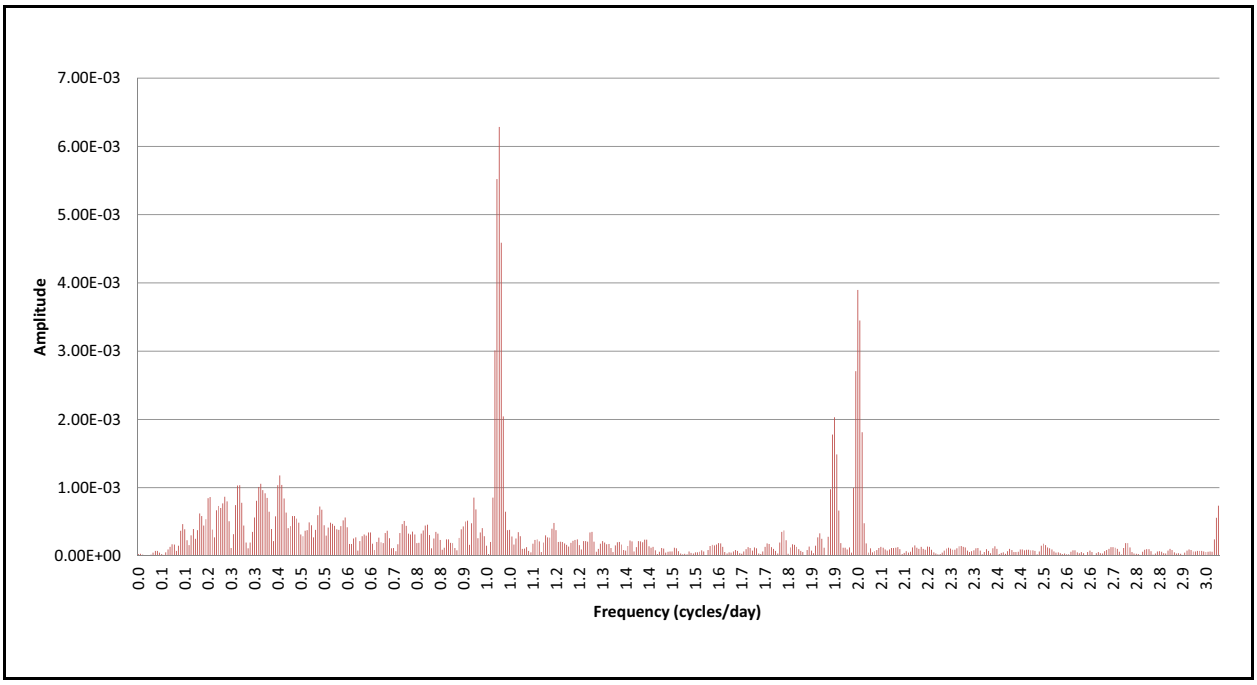

Figure D.1-5
Amplitude Spectra Obtained from Fourier Transform of Well ER-20-8 (I) Water-Level Residuals

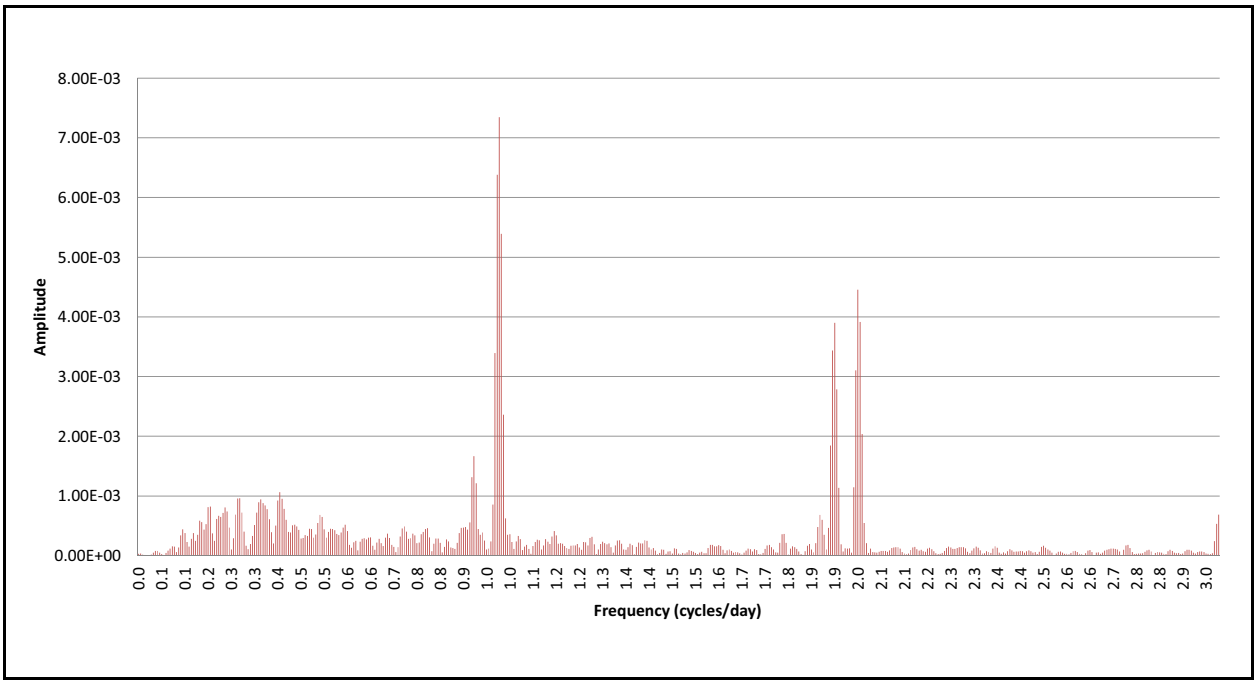

Figure D.1-6
Amplitude Spectra Obtained from Fourier Transform of Earth-Tide Potential at Well ER-20-8

Table D.1-2
Parameters Used for Specific Storage Calculations for Well ER-20-8

Parameter	Value
K (Pa)	0
K_s (Pa)	1
Poisson's Ratio	0.25
$\bar{h}$	0.6
$\dot{l}$	0.07
a (m)	6.37E+06
g (m/s^2)	9.823704
K_m (m)	0.53699664
b, M_2	0.908
b, O_1	0.377
Latitude (degrees north)	37.193032

Table D.1-3
Specific Storage Estimated from Earth-Tide Effects
for Selected Wells on Pahute Mesa

Well ID	Screen ID	S_s (1/m) using M_2	S_s (1/m) Using O_1
ER-20-8	D (Deep)	Using Theoretical/Fit Amplitudes: 2.03E-06 Using Spectral Amplitudes: 2.02E-06	2.55E-06 3.10E-06
ER-20-8	I (Intermediate)	Using Theoretical/Fit Amplitudes: 3.96E-06 Using Spectral Amplitudes: 3.87E-06	4.55E-06 6.05E-06

D.2.0 REFERENCES

Bernard, S., and F. Delay. 2008. "Determination of Porosity and Storage Capacity of a Calcareous Aquifer (France) by Correlation and Spectral Analyses of Time Series." In *Hydrogeology Journal*, Vol. 16(7): pp. 1299–1309.

Bredehoeft, J.D. 1967. "Response of Well-Aquifer Systems to Earth Tides." In *Journal of Geophysical Research*, Vol. 72(12): pp. 3,075–3,087.

Burbey, T.J. 2010. "Fracture Characterization Using Earth Tide Analysis." In *Journal of Hydrology*, Vol. 380(3–4): pp. 237–246.

Cutillo, P.A., and J.D. Bredehoeft, 2011. "Estimating Aquifer Properties from the Water Level Response to Earth Tides." In *Ground Water,* Volume 49(4): pp. 600–610.

Freeze, R.A., and J.A. Cherry. 1979. *Groundwater*. Englewood Cliffs, NJ: Prentice Hall.

Godin, G. 1972. *The Analysis of Tides.* Toronto, Canada: University of Toronto Press.

Hsieh, P.A., J.D. Bredehoeft, and J.M. Farr. 1987. "Determination of Aquifer Transmissivity from Earth Tide Analysis." In *Water Resources Research*, Vol. 23(10): p. 1824–1832.

Kilroy, K.C. 1992. *Aquifer Storage Characteristics of Paleozoic Carbonate Rocks in Southwestern Nevada Estimated from Harmonic Analysis of Water-Level Fluctuations.* University of Nevada at Reno, Ph.D. dissertation.

Merritt, M.L. 2004. *Estimating Hydraulic Properties of the Floridan Aquifer System by Analysis of Earth-Tide, Ocean-Tide, and Barometric Effects, Collier and Hendry Counties, Florida,* Water-Resources Investigations Report 03-4267. Tallahassee, FL: U.S. Geological Survey.

Munk, W.H., and G.J.F. MacDonald. 1960. *The Rotation of the Earth: A Geophysical Discussion.* Cambridge, UK: Cambridge University Press.

N-I, see Navarro-Intera, LLC.

Navarro-Intera, LLC. 2011. Written communication. Subject: *Pahute Mesa Fiscal Year 2010 Long-Term Head Monitoring Data Report.* February. Las Vegas, NV.

Rojstaczer, S., and D.C. Agnew. 1989. "The Influence of Formation Material Properties on the Response of Water Levels in Wells to Earth Tides and Atmospheric Loading." In *Journal of Geophysical Research*, Vol. 94(B9): pp. 12,403–12,411.

Tamura. Y. 1987. "A Harmonic Development of the Tide-Generating Potential. In *Bulletin d'Information des Marées Terrestres,* Vol. 99: pp. 6813–6855.

Van Camp, M., and P. Vauterin. 2005. "Tsoft: Graphical and Interactive Software for the Analysis of Time Series and Earth Tides." In *Computer & Geosciences,* Vol. 31(5): pp 631–640.

Van Der Kamp, G., and J.E. Gale. 1983. "Theory of Earth Tide and Barometric Effects in Porous Formations with Compressible Grains." In *Water Resources Research,* Vol. 19(2): pp. 538–544.

Wenzel, H.-G. 1996. "The Nanogal Software: Earth Tide Data Processing Package ETERNA 3.30." In *Bulletin d'Information des Marées Terrestres,* Vol. 124: pp. 9425–9439. Available at www.bfo.geophys.uni-stuttgart.de/etgtab.html.

Appendix E

Estimating Aquifer Storage for Well ER-EC-11 Using Earth-Tide Analysis

E.1.0 INTRODUCTION

This appendix presents results for spectral analysis using earth-tide response data for water levels measured in Well ER-EC-11 at three screen depths. The methodology is identical to the one used to analyze Well ER-20-8 (Appendix D). As before, data for this analysis were obtained from the Pahute Mesa 2010 long-term head monitoring program (N-I, 2011).

The data consist of water levels as measured by pressure transducers (located below the free water surface in the monitoring access casing or tubing) and atmospheric pressure as measured by surface barometers. Vented pressure gauges were used at all three depths for Well ER-EC-11. The pressure transducers and barometers employ an adaptive sampling scheme with non-uniform sampling intervals. To simplify analysis for this report, all readings were resampled at the 1-hour interval. (See Table E.1-1, which shows that the tidal constituents of interest all have periodicities greater than 12 hours.) For this analysis, a continuous period of record (without any gaps in data) is required. Moreover, it is ideal that water-level data correspond to periods when there were not strong anthropogenic effects (such as pumping). Based on these requirements, a subset of the time series, spanning from June 29 to November 15, 2010, was used for Well ER-EC-11.

A theoretical model was used to generate synthetic earth-tide time series for tidal potential. This was done using the scientific code ETGTAB (Wenzel, 1996).

As with the previous analysis, a low-pass filter (consisting of diurnal moving average) was used to remove any long-term trends from all the data.

E.1.1 Analysis and Results

Figures E.1-1 through E.1-3 show the water-level data for Wells ER-EC-11 (D), ER-EC-11 (I), and ER-EC-11 (S), respectively. The hourly raw data are juxtaposed on the daily averaged (using the Godin filter discussed in Appendix D), as well as the residual water-level time series.

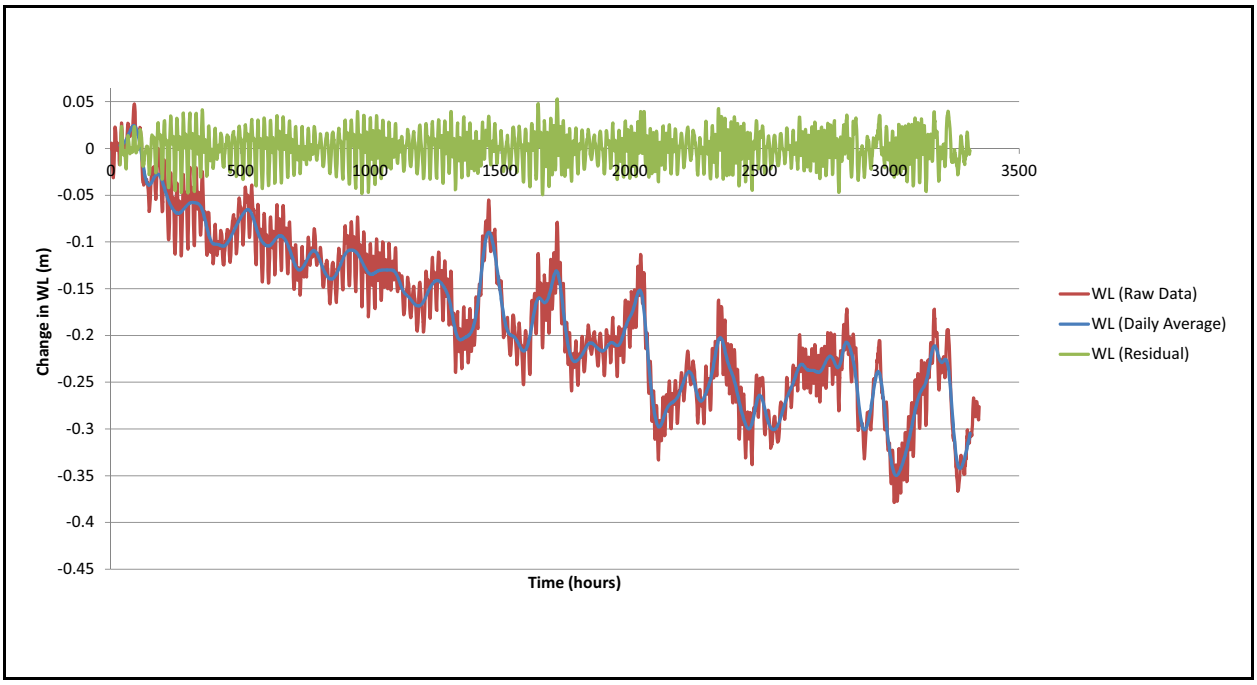

Figure E.1-1
Water-Level Data for Well ER-EC-11 (D) (Raw, Daily Average, and Residual)

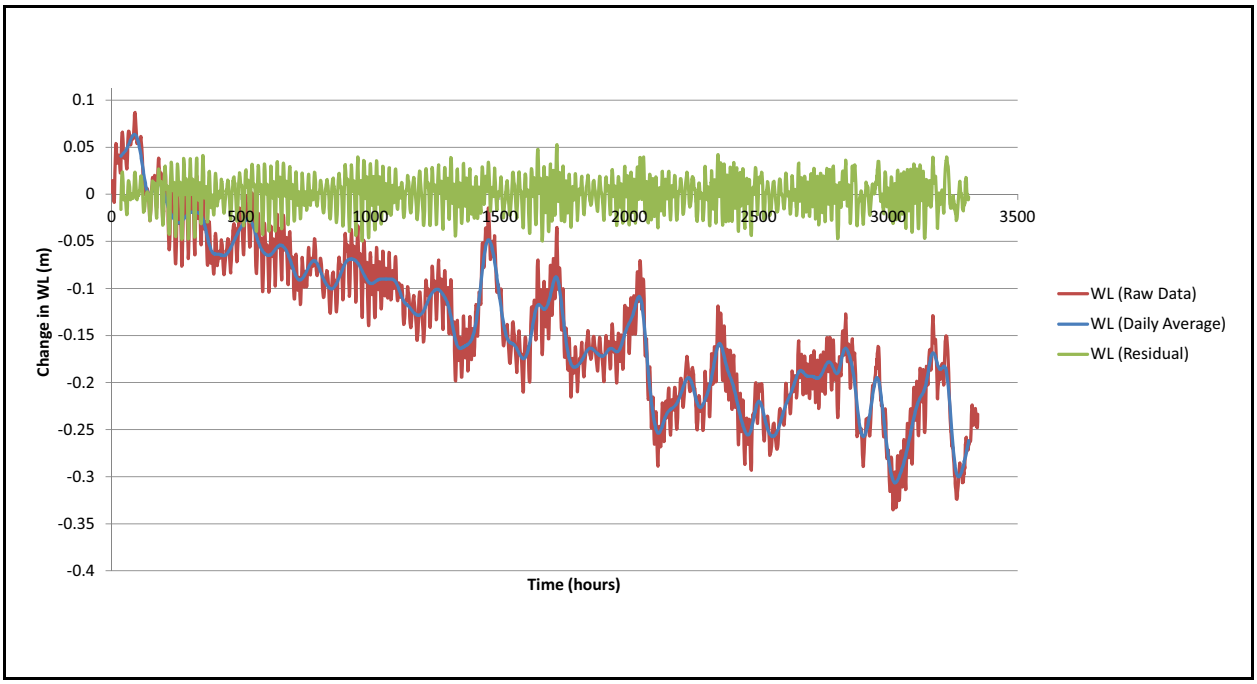

Figure E.1-2
Water-Level Data for Well ER-EC-11 (I) (Raw, Daily Average, and Residual)

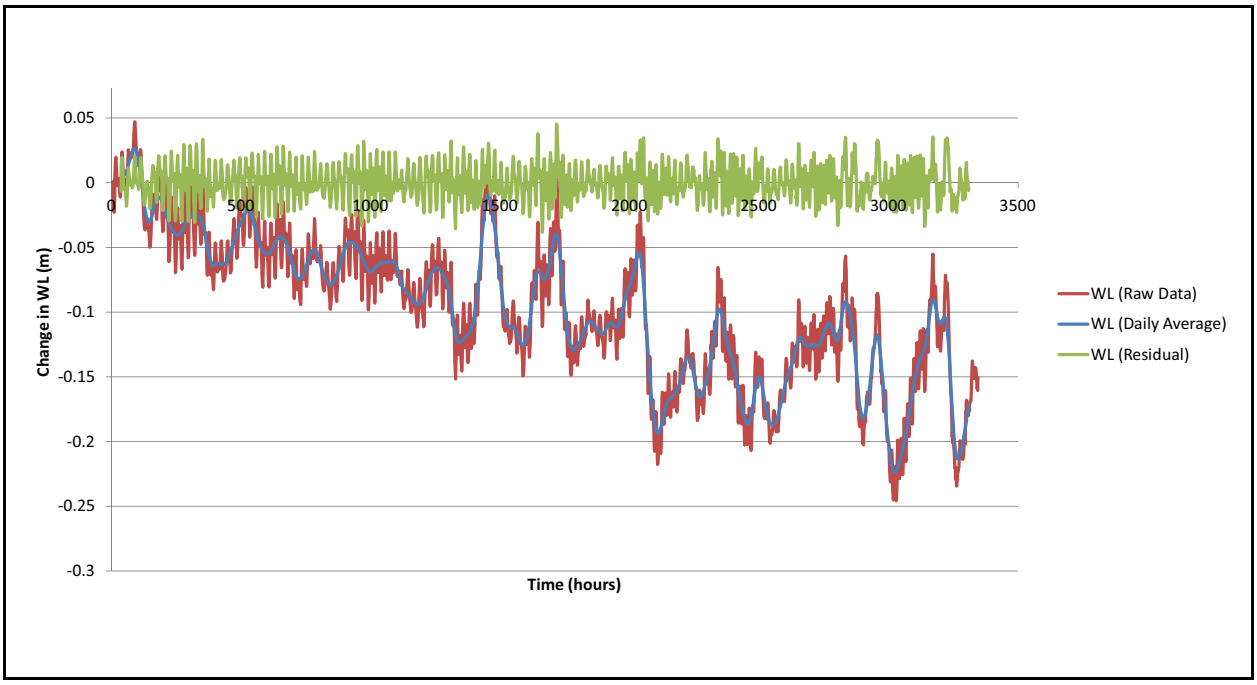

Figure E.1-3
Water-Level Data for Well ER-EC-11 (S) (Raw, Daily Average, and Residual)

Figure E.1-4 shows the earth-tide potential for Well ER-EC-11 (the synthetic earth-tide model does not consider depth; hence, the same earth tide is used for all well depths).

Figures E.1-5 through E.1-8 show the amplitudes for various spectra for the ER-EC-11 (D) water levels, ER-EC-11 (I) water levels, ER-EC-11 (S) water levels, and the earth tide potential, respectively.

Table E.1-1 show all parameters used in the calculation of specific storage for the well.

Specific storage estimates for the wells and screens analyzed are shown in Table E.1-2. Results indicate that the spectral analysis and theoretical/regression-fitting approaches give similar S_s estimates. Because the M_2 signal is much stronger than the O_1 signal, the results for the M_2 frequency are more robust (difference in the spectral and theoretical/regression-fitting approaches is negligible).

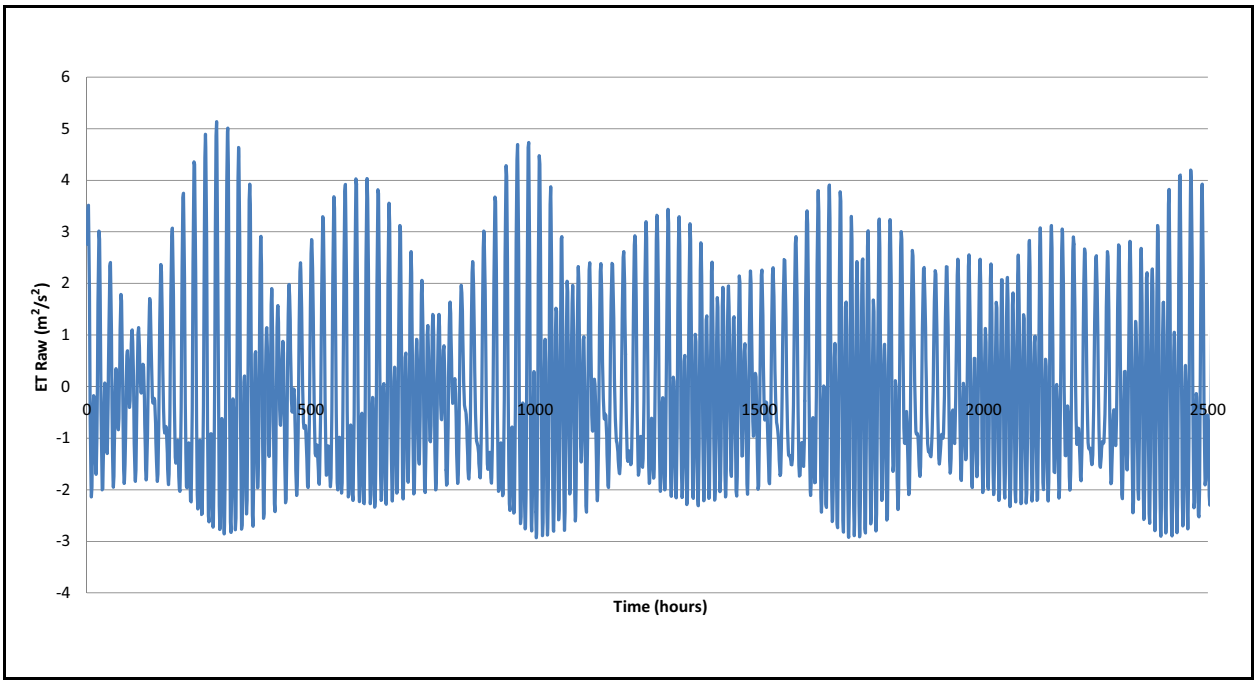

Figure E.1-4
Synthetic Earth-Tide Potential for Well ER-EC-11

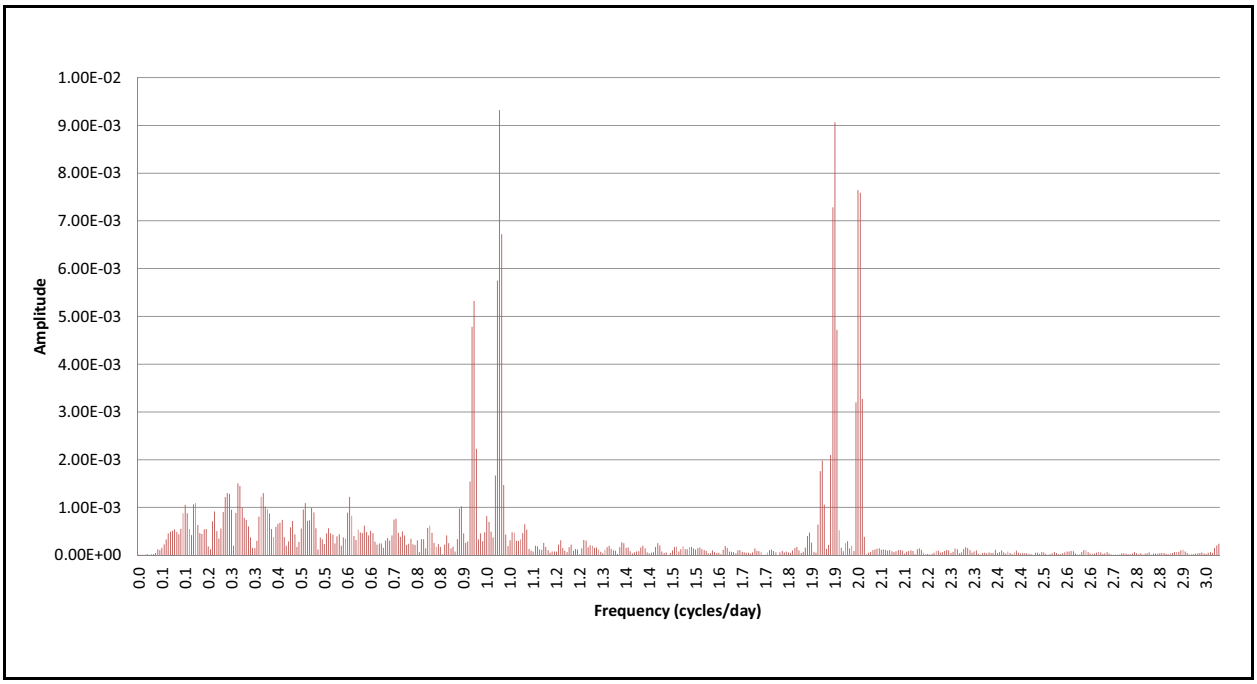

Figure E.1-5
Amplitude Spectra Obtained from Fourier Transform of Well ER-EC-11 (D) Water-Level Residuals

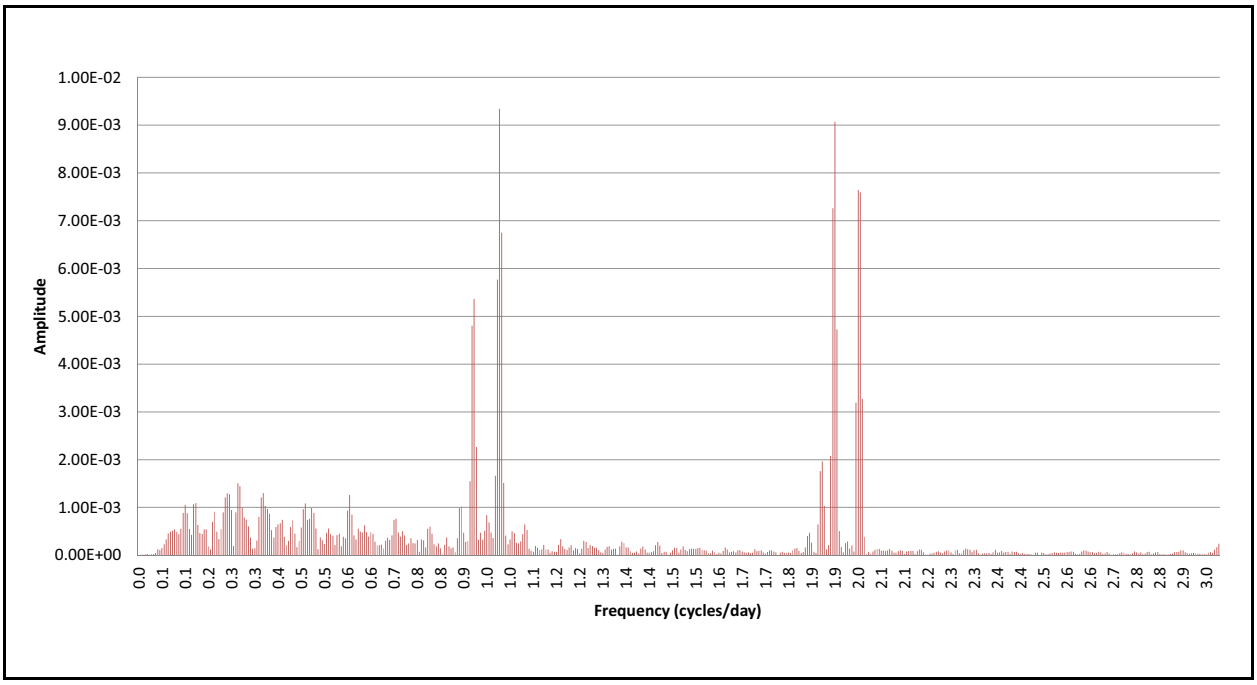

Figure E.1-6
Amplitude Spectra Obtained from Fourier Transform of Well ER-EC-11 (I) Water-Level Residuals

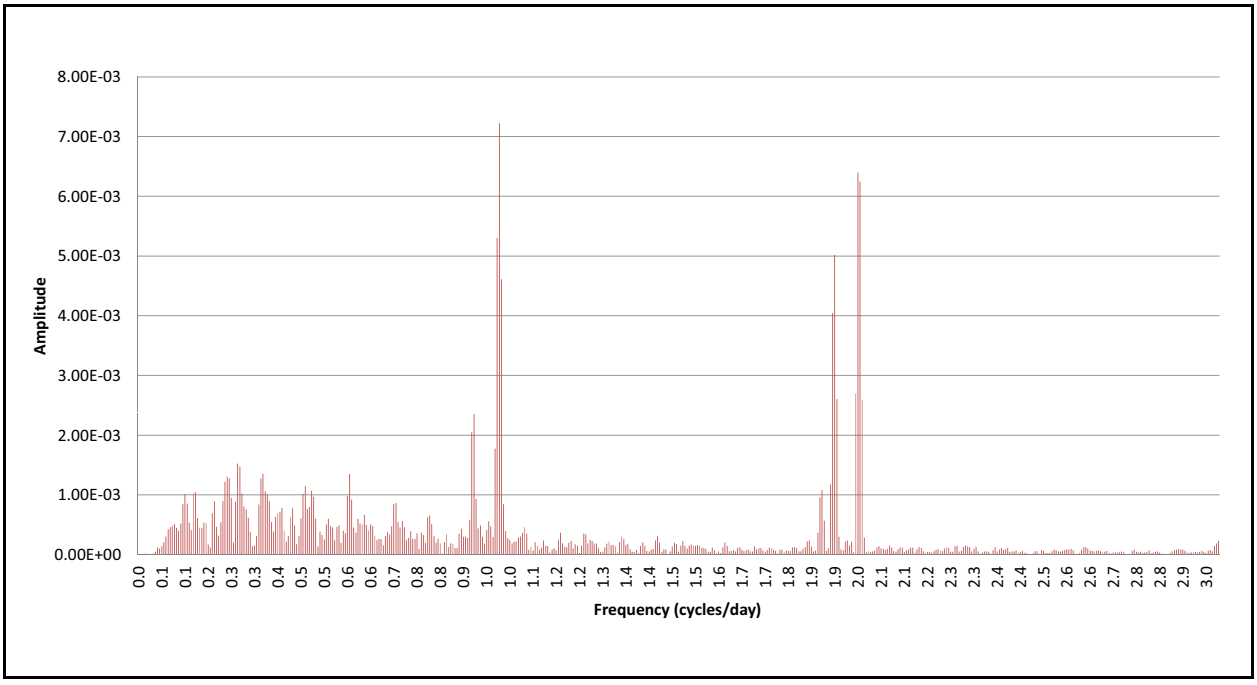

Figure E.1-7
Amplitude Spectra Obtained from Fourier Transform of Well ER-EC-11 (S) Water-Level Residuals

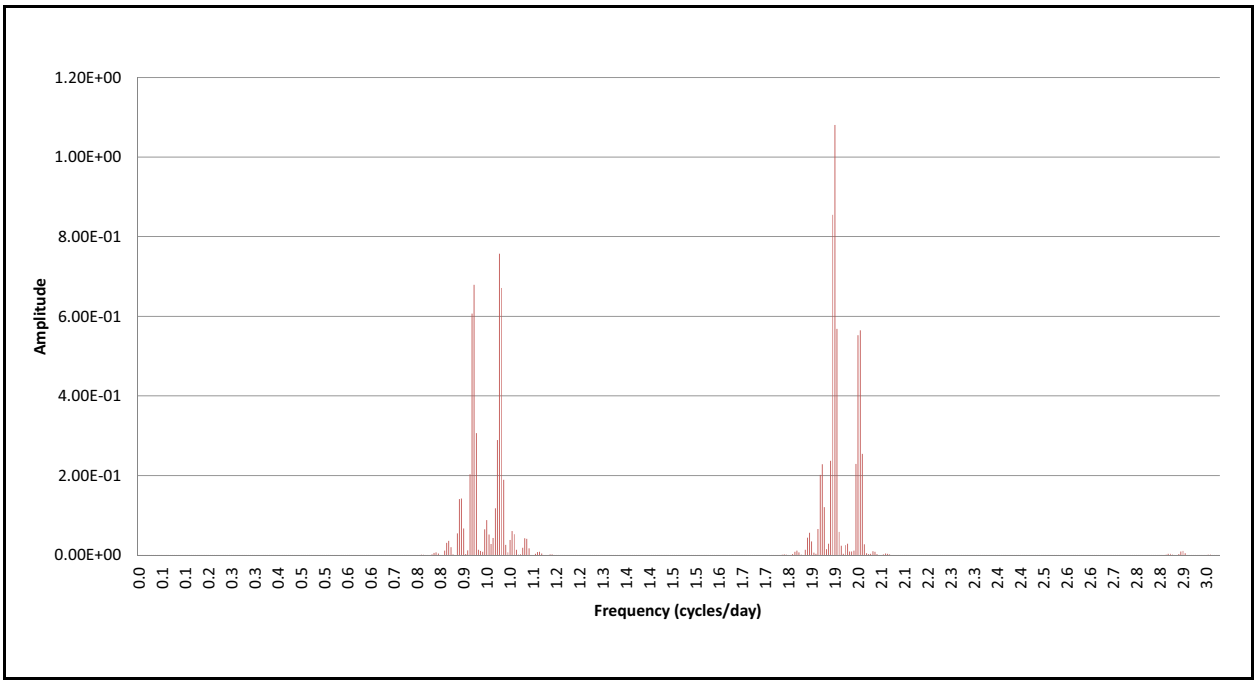

Figure E.1-8
Amplitude Spectra Obtained from Fourier Transform of Earth-Tide Potential at Well ER-20-8

Table E.1-1
Parameters Used for Specific Storage Calculations for Well ER-EC-11

Parameter	Value
K (Pa)	0
K_s (Pa)	1
Poisson's Ratio	0.25
$\bar{h}$	0.6
$\dot{l}$	0.07
a (m)	6.37E+06
g (m/s^2)	9.823704
K_m (m)	0.53699664
b, M_2	0.908
b, O_1	0.377
Latitude (degrees north)	37.197492

Table E.1-2
Specific Storage Estimated from Earth-Tide Effects for Selected Wells on Pahute Mesa

Well ID	Screen ID	S_s (1/m) using M_2	S_s (1/m) using O_1
ER-EC-11	D (Deep)	Using Theoretical/Fit Amplitudes: 1.09E-06 Using Spectral Amplitudes: 9.90E-07	9.66E-06 1.06E-06
ER-EC-11	I (Intermediate)	Using Theoretical/Fit Amplitudes: 1.09E-06 Using Spectral Amplitudes: 9.90E-07	9.75E-07 1.05E-06
ER-EC-11	S (Shallow)	Using Theoretical/Fit Amplitudes: 1.90E-06 Using Spectral Amplitudes: 1.79E-06	2.33E-06 2.40E-06

E.2.0 REFERENCES

N-I, see Navarro-Intera, LLC.

Navarro-Intera, LLC. 2011. Written communication. Subject: *Pahute Mesa Fiscal Year 2010 Long-Term Head Monitoring Data Report.* February. Las Vegas, NV.

Wenzel, H.-G. 1996. "The Nanogal Software: Earth Tide Data Processing Package ETERNA 3.30." In *Bulletin d'Information des Marées Terrestres*, Vol. 124: pp. 9425–9439. Available at www.bfo.geophys.uni-stuttgart.de/etgtab.html.

DISTRIBUTION

	Copies
W.R. Wilborn Environmental Management Operations Activity U.S. Department of Energy National Nuclear Security Administration Nevada Site Office P.O. Box 98518, M/S 505 Las Vegas, NV 89193-8518	2 hard copies w/electronic media
Bimal Mukhopadhyay Environmental Management Operations Activity U.S. Department of Energy National Nuclear Security Administration Nevada Site Office P.O. Box 98518, M/S 505 Las Vegas, NV 89193-8518	1 electronic media
Ken Ortego National Security Technologies, LLC P.O. Box 98521 MS/NLV 082 Las Vegas, NV 89193	UGTA Website
Charles Russell Desert Research Institute 755 E. Flamingo, M/S 433 Las Vegas, NV 89132-0040	UGTA Website
Walt McNab Lawrence Livermore National Laboratory 7000 East Avenue, L-231 Livermore, CA 94550	UGTA Website
Gayle Pawloski Lawrence Livermore National Laboratory 7000 East Avenue, L-231 Livermore, CA 94550	UGTA Website

	Copies
Naomi Becker Los Alamos National Laboratory Hydrology, Geochemistry, and Geology Group, EES-6 Earth and Environmental Sciences Division SM-30 Bikini Atoll Rd., MS F665 Los Alamos, NM 87545	UGTA Website
Ed Kwicklis Los Alamos National Laboratory Hydrology, Geochemistry, and Geology Group, EES-6 Earth and Environmental Sciences Division SM-30 Bikini Atoll Rd., MS T003 Lo Alamos, NM 87545	UGTA Website
Bonnie Thompson U.S. Geological Survey WRD 160 N. Stephanie St. Henderson, NV 89074	UGTA Website
Sam Marutzky Navarro-Intera, LLC P.O. Box 98952, NSF 167 Las Vegas, NV 89193-8952	UGTA Website
Robert Andrews Navarro-Intera, LLC P.O. Box 98952, NSF 167 Las Vegas, NV 89193-8952	UGTA Website
Nate Bryant Navarro-Intera, LLC P.O. Box 98952, NSF 167 Las Vegas, NV 89193-8952	UGTA Website
Bruce Crowe Navarro-Intera, LLC P.O. Box 98952, NSF 167 Las Vegas, NV 89193-8952	UGTA Website
Irene Farnham Navarro-Intera, LLC P.O. Box 98952, NSF 167 Las Vegas, NV 89193-8952	UGTA Website

	Copies
John Londergan Navarro-Intera, LLC P.O. Box 98952, NSF 167 Las Vegas, NV 89193-8952	UGTA Website
Gregory Ruskauff Navarro-Intera, LLC P.O. Box 98952, NSF 167 Las Vegas, NV 89193-8952	UGTA Website
Jeffrey Wurtz Navarro-Intera, LLC P.O. Box 98952, NSF 167 Las Vegas, NV 89193-8952	UGTA Website
Navarro-Intera, LLC Central Files P.O. Box 98952, NSF 156 Las Vegas, NV 89193-8952	1 hard copy w/electronic media
EM Records U.S. Department of Energy National Nuclear Security Administration Nevada Site Office P.O. Box 98518, M/S 505 Las Vegas, NV 89193-8518	1 hard copy w/electronic media